Imperial College London

Doctoral Thesis

Molecular Modelling and Statistical Thermodynamics of Semi-Crystalline Polymers: Network Constraints, Fluid Sorption and Surface Melting

Author:
Michele Valsecchi

Supervisors:
Prof. Amparo Galindo
Prof. George Jackson

A thesis submitted in fulfilment of the requirements for the degree of Doctor of Philosophy

Molecular Systems Engineering Group
Department of Materials

July 24, 2023

Declaration of Authorship

I, Michele Valsecchi, declare that the work presented in this thesis titled "Molecular Modelling and Statistical Thermodynamics of Semi-Crystalline Polymers: Network Constraints, Fluid Sorption and Surface Melting" is my own. Where I have used the works of others, it is stated and referenced accordingly.

Copyright Declaration

Abstract

Accurately predicting gas and liquid solubility in semi-crystalline polymers is crucial for optimizing their production, performance, and degradation behaviour. In this thesis a novel statistical-mechanical model for semi-crystalline polymers is proposed. The amorphous domains are divided into two portions: the semi-rigid inter-lamellar domains and the melt-like "free" amorphous domains. Solubility in the inter-lamellar domains is reduced due to the presence of tie-molecules, which are polymer chains connecting different crystals. By incorporating reversible mass exchange at the crystal/amorphous interface, the model predicts variations in lamellar thickness and solubility with temperature.

According to our model, the equilibrium solubility in each polymer sample is determined by its crystallinity (ω_c), the fraction of tie-molecules at the crystal/amorphous interface (p_T), and the fraction of free amorphous domains (ψ). While crystallinity can be easily measured, p_T and ψ are adjusted to minimize differences between the model's predictions (made in conjunction with the SAFT-γ Mie equation of state) and experimental sorption isotherms of pure fluids in polyethylene (PE), polypropylene (PP), and polyethylene glycol (PEG) samples. The model accurately reproduces the solubility of all solutes considered after the assignment of unique p_T and ψ values to each sample. A meta-analysis of literature data reveals that in PE, ψ decreases with crystallinity and p_T is in the range 0.2 – 0.4.

The model's predictions of solubility of binary mixtures of short hydrocarbons in PE are in good agreement with experimental data. The model also accurately captures the temperature dependence of solubility in most of the polymer samples considered, except for those with low crystallinity where changes in ψ with temperature may need consideration. Additionally, the model is applied to study the moisture uptake by PEG. By employing simple thermodynamic considerations, the model qualitatively predicts the humidity at which deliquescence occurs and describes the moisture uptake at each relative humidity after adjusting p_T.

Acknowledgements

First of all, this work would not have been possible without my indefatigable partner, Zoe. Her love, patience and kindness have been my strongest driving force during the many months I spent writing. I am also grateful to my family for supporting in me at every step along the way. I will never feel alone as long as I have you.

I would like to thank my close friends for sharing all of these years with me in London. Jack, for the innumerable rides on the Mini. Dani, for keeping me company in long study days. Alvi, my beloved flatmate, for making me feel at home. And thank you Marco, Marta, Giulia, Ali, Edo, Trilli, for being great friends and making my time here special.

Of the MSE Group and CPSE members, I am particularly indebted to Tom, Maz and Sakhr for first making me feel part of the team. And then, in no particular order, to Malak, Matthias, Fabian, Tanuj, Isaac, Lauren, Harry, Thomas, Felipe, Griffin, Saher, Ahmed, Gustavo, Shubhani and all the other present and past members for the fun times and memories.

I am particularly grateful to my supervisors, Prof. Amparo Galindo and Prof. George Jackson, for the time dedicated to me these past four years, as well as for all the insight and guidance. I owe all of my professional growth to them. I would also like to thank Dr. Andrew Haslam for mentoring me and for the hours spent playing music together. Thank you Prof. Daryl Williams for interviewing me, writing me letters of recommendation and helping me decide on my next steps. Last but not least, I would like to extend my gratitude to Procter & Gamble Company for funding my PhD work and David Eike in particular for the valuable feedback received in the past years.

Contents

List of Figures

List of Tables

1. Introduction

Polymers are a class of substances composed of macro-molecules and characterized by a number of well-defined repeating units called monomers.[1] Contrarily to materials made of small constituents, upon cooling polymers cannot fully crystallize and invariably display a micro-structure that is a combination of the ordered crystalline state and the "disordered" *amorphous* state typical of fluids – hence the adjective "semi-crystalline". Due to the abundance of macro-molecules in nature, many biological materials are semi-crystalline. Animal hair and vegetable fibres are two examples of naturally occurring semi-crystalline polymers made mostly of keratin (a protein) and cellulose (a polysaccharide), respectively. Early humans valued these materials due to their availability, physical/chemical stability and insulating properties: some findings suggest that linen fibre weaving might have started as early as the 30^{th} millennium B.C.,[2] while evidence of selective breeding of woolly sheep dates back to the 6^{th} millennium B.C.[3] Nowadays, about 32 million tonnes of natural fibre[4] and about 2 million tonnes of wool[5] are harvested worldwide each year.

In addition to bio-molecules, a long list of synthetic polymers – i.e., polymers synthesized starting from petrochemical products – are semi-crystalline at ambient conditions. For example, common synthetic semi-crystalline polymers include polyethylene (PE), polypropylene (PP), polyvinyl chloride (PVC) and polyethylene terephtalate (PET) – although the last two are often produced in almost fully amorphous, glassy form. In

contrast to bio-polymers, the production of synthetic polymers can be easily scaled up as it does not require breeding animals or growing crops. Nowadays, about 400 million tonnes of synthetic plastic are produced each year worldwide, with semi-crystalline PE and PP alone accounting for about 50% of the total figure.[6]

The widespread production and use of semi-crystalline polymers can be traced back to their low average cost, their chemical stability and a number of unique material properties. Since the most commonly used polymers are carbon-based organic molecules, semi-crystalline polymers generally have a much lower density at ambient conditions than the other most common types of solids – i.e., metals and ceramics. At the same time, even though polymers form molecular crystals held together by weak inter-molecular interactions – orders of magnitude weaker than the metallic, covalent and ionic bonding typical of metals and ceramics – they possess much better mechanical properties than, e.g., ice and waxes. This peculiar behaviour is the result of the presence of *tie-molecules*,[7] i.e., un-crystallized polymer sections spanning the amorphous regions and linking different crystals. These chain segments partially restrict the relative motion of the crystalline domains, thereby making semi-crystalline polymers both flexibile and tough while being lightweight.

Another quality for which semi-crystalline polymers are valued is their excellent barrier performance with respect to the solubility and diffusivity of gases and liquids. Around 42% of the total plastic production is destined to packaging,[8] whose purpose is protecting its content from the external environment by preventing fluid permeation. Moreover, thanks to their chemical resistance and barrier properties semi-crystalline polymers like high-density PE (HDPE), PVC, polyamide (PA), polyether ether ketone (PEEK), polytetrafluoroethylene (PTFE) and polyvinylidine fluoride (PVDF) are used extensively for fluid transport either as pipe materials[9,10] or as liners to protect metal surfaces from corrosion and embrittlement.[11,12] Minimizing the fluid uptake of semi-crystalline polymers is also critical to ensure the integrity of a wide range of polymer-containing

products. For example, the moisture uptake by hydrophilic polymers like polyetyhylene glycol (PEG) in humid environment can threaten the stability of certain pharmaceutical formulations.[13] Similarly, the mechanical properties of semi-crystalline polymers can be dramatically altered if the concentration of solutes becomes too high, in a phenomenon known as *plasticisation*.[14–16]

In some applications, however, promoting fluid solubility in semi-crystalline polymers can be desirable. During PE production, greater concentrations of ethylene in the growing polymer near the catalyst sites increases the reaction rate and yield.[17,18] In the detergent and perfume industry, ensuring the persistence of certain ingredients in hair or fibres can lead to longer lasting freshness and softness.[19,20] Perhaps more importantly, the ability of oxidising agents to diffuse within semi-crystalline polymer is one of the factors affecting their degradation rate when left in the environment.[21,22] This is particularly relevant today, as the sheer amount of synthetic plastic produced combined with its short usage lifespan (about 40% of all plastic produced is single-use[8]) and long degradation times (up to thousands of years[23]) has led to serious concerns on its environmental impact, with activist groups and global agencies alike calling for strong regulatory actions on the plastics market. Engineering packaging materials to provide sufficient barrier performance while selectively allowing certain oxidants to diffuse might help diminish their lifetime in the environment.[24]

From a theoretical perspective, predicting the barrier properties of semi-crystalline polymers requires determining the equilibrium solubility and permeation constants of simple fluids in these materials at given thermodynamic conditions. Accurate solubility models are needed in all applications in which semi-crystalline samples are in contact with fluids for a long time, and can also help provide estimates of intrinsically out-of-equilibrium properties like permeation constants. For example, according to the widely employed solution– diffusion model reviewed by Wijmans and Baker[25] permeation of a fluid through a polymeric membrane proceeds first by dissolution of a molecule in the surface layers

of the polymer in contact with the fluid, and then by diffusion driven by the gradient in chemical potential across the membrane. Equilibrium models can provide estimates of both the solute concentration on the surface layers* and the solute's chemical potential as a function of its concentration in the polymer. It must be noted, however, that diffusion constants and overall permeation rates are significantly influenced by microstructural features such as the average tortuosity[26,27] of the inter-connected amorphous domains, defined as the ratio between the length the shortest path between two points divided by their euclidean distance. The investigation of these effects is outside of the scope of the present work, in which the focus is kept on equilibrium solubility.

The development of equilibrium theories describing the interaction of fluids with semi-crystalline polymers presents an important challenge. Contrarily to liquid polymer melts or perfect molecular crystals, semi-crystalline polymers are metastable systems due to the very slow dynamics of the macromolecules they are composed of. For example, the ratio of crystalline polymer over the total polymer mass (known as the crystallinity) of semi-crystalline polymer samples can increase over time as the chains reorganise in configurations corresponding to their equilibrium crystal structure – a phenomenon known as recrystallization.[28,29] Furthermore, when cooling a sample below the glass transition temperature T_g – which is a function of many factors such as the polymer type and cooling rate – its amorphous domains become kinetically trapped in local minima of the free energy forming a glass.[30–33] High temperatures, solvent uptake and external loads can accelerate recrystallization or induce plasticisation of glassy amorphous domains, resulting in dramatic changes of the macroscopic properties of a polymer sample (*physical aging*[34,35]).

The metastable nature of semi-crystalline polymers seems to suggest that their thermodynamic properties cannot be described accurately by employing equilibrium theories. Nevertheless, in many cases the dynamic phenomena discussed are slow enough

*Assuming these are locally in equilibrium with the fluid

that these materials can be considered to be in a *pseudo*-equilibrium state.[36] Whereas "true" equilibrium states of bulk materials can be characterised only by a small number of variables (e.g., temperature, pressure and composition), the pseudo-equilibrium state of a polymeric material must be specified by additional sample-specific, production history-dependent features which can vary in the event of plasticisation or recrystallisation.

In the most prominent solubility models developed to date, the pseudo-equilibrium methodology applied to semi-crystalline polymers relies on two key approximations. Firstly, the crystalline domains can in most cases be considered impermeable filler particles for the purpose of calculating fluid solubility due to their dense packing.[26,37] Crystallinity is therefore an important sample-specific parameter when modelling fluid solubility in semi-crystalline polymers, as it is shown in Section 3.2. On the other hand, due to the lack of long-range structure the amorphous domains can be modelled as equilibrium liquids (or, more precisely, subcooled polymer melts) subject to a certain "perturbation" or set constraints imposed by the presence of the crystalline domains.[38–45]

Critically, the underlying equilibrium theory for the amorphous domains does not depend on the production history of the polymeric material and is effectively decoupled from the sample-specific properties which only affect the perturbation. As a result, the composite model can leverage the accurate representation of polymer mixtures' properties offered by equilibrium theories of the liquid state and in many cases also inherit their model parameters – which normally carry information on the inter-molecular interaction between the polymer and solute molecules and are optimised to reproduce fluid phase equilibrium data. On the other hand, while some sample-specific properties such as crystallinity can be directly measured others (such as the topological features of polymer chains in the amorphous domains) are more elusive and are usually found by minimisation of the difference between the composite model's predictions and experimental solubility and

swelling data in semi-crystalline polymers.

Such methodologies can therefore yield indirect estimates of micro-structural features of the polymer samples. It is of particular interest to choose as free parameters of a given model a set of sample-specific properties that are material constants in the absence of physical aging (i.e., as long as the pseudo-equilibrium state persists), thereby enabling prediction of solubility and swelling data outside of the range of conditions in which the model may be parameterised. The success of the operation hinges on the use of a predictive equilibrium theory of liquid polymer mixtures coupled with accurate models for the perturbation induced by the crystalline structure on the amorphous domains.

Historically, among equilibrium theories lattice models were the first to provide a good description of polymer mixtures. In lattice models polymer chains and solute molecules are arranged in a static 3-dimensional lattice, thereby enabling straightforward calculations of the configurational entropy of polymer chains. The first successful theory of polymer mixtures was the Flory–Huggins–Staverman (FHS) solution theory,[46–48] which is still used extensively in both academic and industrial settings. More recent models – namely, the Sanchez–Lacombe theory[49] and lattice cluster theory of Dudowicz and Freed[50] – improved over the original FHS theory by allowing to investigate pressure effects (via the introduction of lattice vacancies) and to introduce structural details of the monomers. Nevertheless, lattice models have two intrinsic weaknesses. Firstly, the lattice model cannot be directly mapped onto realistic force-fields which are necessary to obtaining transport properties via computer simulation. Secondly, lattice models do not provide an accurate description of the gas state, and therefore require coupling with additional theories to accurately describe vapour-liquid equilibria.

An alternative to lattice fluid models is offered by perturbation theories, which find their roots in the work of van der Waals[51] and saw significant development starting

from the work of Zwanzig in 1954.[52] Perturbation theories are based on the idea that liquid properties are dominated by repulsion and that the attractive contributions can be added perturbatively based on a repulsive reference system. Among these, the family of statistical associating fluid theory (SAFT) equations of state[53,54] – stemming from the thermodynamic perturbation theory of Wertheim[55–59] – has been extensively applied to the description of polymer mixtures.

SAFT-type equations of state possess a number of advantages over lattice-based models like the FHS theory. One of them is their ability to predict the thermodynamic properties of a system of molecules starting from detailed molecular models (including realistic inter-molecular potentials and hydrogen bonding), enabling the investigation of out-of-equilibrium properties like viscosity and diffusivity via direct comparison with molecular dynamics (MD) simulations.[60,61] Furthermore, SAFT equations of state provide an accurate representation of both liquids and gases, resulting in a comprehensive description of fluid-phase properties (such as vapour-liquid equilibrium, critical points *etc.*).

Among the various versions of SAFT,[62–67] the SAFT-γ Mie equation of state[66,67] employs a group-contribution (GC) methodology that combines the rigorous theoretical foundation of SAFT with simplicity of use and predictive power. The SAFT-γ Mie EoS has been successfully employed to describe the fluid-phase thermodynamic properties of various compounds of industrial interest,[67–70] active pharmaceutical ingredients,[71] salts[72] and polymers such as PE, PP, PS and PVC.[67,73,74] Updated parameter databases include over 60 different groups,[72] allowing for predictions of the fluid properties of many organic and inorganic compounds of practical interest. In this work the SAFT-γ Mie EoS is therefore chosen as the equilibrium theory due to its ability to provide a unified description of simple fluid and equilibrium polymer mixtures, combined with its predictive capabilities enabled by the group-contribution framework.

The level of detail and complexity offered by modern fluid-phase EoS is however not found in state-of-the art models for the perturbation induced by the crystalline polymer on the amorphous domains. The most prominent physical-based models in the literature[38–41] employ very crude approximations such as assuming that the amorphous domains are isotropic – a condition violated between crystalline lamellae – or that amorphous chain segments follow the Gaussian statistics typical of polymer liquids. More recent developments[43–45] have not added physical insight, despite the wealth of new evidence on the thermodynamics of semi-crystalline polymers across length and time scales gained in the past 60 years. Inaccurate models of the impact of the crystalline domains can hinder the usefulness of the overall theory by diminishing its predictive power and preventing direct comparison with experiments and computer simulation.

Therefore, the following objectives are set in the current work:

- develop and test SAFT-γ Mie models for a set of industrially relevant polymers, with a particular emphasis on PE – chosen due to the simplicity of its repeating unit;
- increase the level of detail of the description of the amorphous domains for use in solubility models;
- bridge the understanding of semi-crystalline polymers by unifying different solubility models under the same framework and by incorporating insight from other experimental evidence;
- utilize the resulting compound model in conjunction with equilibrium solubility measurements to produce indirect estimates of sample-specific properties of semi-crystalline polymers;

- predict solvent uptake and polymer melting in a number of model systems that are of industrial and scientific interest.

Thesis overview

In order to reflect the objectives outlined, this thesis is structured as follows.

In Chapter 2 an overview of the SAFT-γ Mie equation of state is presented. After establishing the theoretical foundation of the equation of state, various approaches to parameter estimation are discussed. Original results of the parameterisation procedure for the series of linear aldehydes and for a set of unlike interaction parameters relevant to the mixtures of polymers with target solutes are presented.

In Chapter 3 a novel model describing the influence of sample-specific properties of semi-crystalline samples on their thermodynamic properties is presented. A general model is developed in order to allow for use with equations of state different than SAFT-γ Mie. In Section 3.1 an overview of the relevant experimental evidence regarding crystallization and microstructure of semi-crystalline polymers is discussed. In Section 3.2 after a review of state-of-the-art solubility models, the new theory is formally derived with an in-depth discussion of all the assumptions and approximations. Emphasis is placed on unifying disparate models under the same formalism – the constraint pressure formalism (*cf.* Section 3.2.3).

Chapter 4 is dedicated to the comparison of the model with available experimental data. In Section 4.1 the predictions of the model regarding the variation of the crystallinity, inter-lamellar distance and other properties with temperature are compared with experimental data, where available. In Section 4.2 the model is applied to reproduce the sorption isotherm of *n*-hexane, *n*-heptane, cyclohexane and toluene in semi-crystalline PE and PP samples. In Section 4.3 a systematic study of single-solute sorption isotherms

in PE is performed in order to understand the dependendence of the tie-molecule fraction parameter on crystallinity. In Sections 4.2.4, 4.3.5 and 4.3.4 the model's predictions regarding the variation of solubility with temperature and the solubility of mixtures (i.e., co-solubility effects) in the samples parameterized previously are shown together with experimental data. Finally, in Section 4.4 the model is applied to the study of moisture uptake in semi-crystalline PEG.

In Chapter 5 the results presented are critically reviewed and potential avenues of improvement are discussed. This thesis concludes with a series of Appendices containing mathematical derivations and a more in-depth analysis of certain aspects of the model.

2. The SAFT-γ Mie EoS

Chapter Overview

In this Chapter the SAFT-γ Mie EoS is reviewed, where "EoS" stands for equation of state. Here and in the rest of the present work the term is used to identify any analytical expression that expresses the free energy of a system (either the Helmholtz or the Gibbs free energy) in terms of temperature, volume (or pressure) and composition, i.e., $A(T, V, \boldsymbol{N})$ or $G(T, P, \boldsymbol{N})$.

In Section 2.2 the theoretical foundations of the SAFT-γ Mie EoS, its molecular models and force fields are reviewed. In Section 2.3 we show how the knowledge of the Helmholtz free energy of a system allows to calculate all the other thermodynamic properties of a system, including chemical potentials and phase behaviour. In Section 2.4 various parameter estimation procedures are discussed. In Section 2.5 the molecular models and SAFT-γ Mie parameters of all the polymers and solutes developed in the present work are presented and the comparison between the SAFT-γ Mie prediction and experimental data used in the parameterisation procedure is presented.

2.1. Force field and molecular model

In the SAFT-γ Mie approach, every molecule is modelled as a fully-flexible heteronuclear chain. Each chain segment of type k represents a distinct functional group and interacts with other segments of type l through a four-parameter Mie potential:

$$u_{kl}^{\text{Mie}}(r_{kl}) = C_{kl}\epsilon_{kl}\left(\left(\frac{\sigma_{kl}}{r_{kl}}\right)^{\lambda_{kl}^{r}} - \left(\frac{\sigma_{kl}}{r_{kl}}\right)^{\lambda_{kl}^{a}}\right), \tag{2.1}$$

where r_{kl} represents the distance between the centers of mass of the two groups and C_{kl} is given by

$$C_{kl} = \frac{\lambda_{kl}^{r}}{\lambda_{kl}^{r} - \lambda_{kl}^{a}}\left(\frac{\lambda_{kl}^{r}}{\lambda_{kl}^{a}}\right)^{\frac{\lambda_{kl}^{a}}{\lambda_{kl}^{r}-\lambda_{kl}^{a}}} \tag{2.2}$$

in order to have $\min_{r\in(0,+\infty)} u_{kl}^{\text{Mie}}(r) = -\epsilon_{kl}$. Here, σ_{kl} is the size parameter which determines the location of the zero of the potential; ϵ_{kl} is the energy well depth; λ_{kl}^{a} and λ_{kl}^{r} are, respectively, the attractive and repulsive exponent. Moreover, each segment k may possess any number $N_{ST,k}$ of types of association sites, with each site a having multiplicity $n_{k,a}$. The interaction potential between site a on group k and site b on group l is given by

$$u_{kl,ab}^{\text{HB}}(r_{kl,ab}) = \begin{cases} -\epsilon_{kl,ab}^{\text{HB}} & \text{if } r_{kl,ab} \leq r_{kl,ab}^{c} \\ 0 & \text{otherwise} \end{cases}, \tag{2.3}$$

where both sites are assumed to be placed at a distance $r_{kl,ab}^{d}$ from the Mie centers. The cut-off radius $r_{kl,ab}^{c}$ and the distance from the dispersion cores $r_{kl,ab}^{d}$ are incorporated via a bonding volume $K_{kl,ab}^{\text{HB}}$.[66,67] In Figure 2.1 we show as an example the SAFT-γ Mie molecular models of three polymers studied in this work: PE, PP and PEG. In Figure 2.2 we show two generic SAFT-γ Mie groups with association sites to clarify the meaning of the distances r_{kl} and $r_{kl,ab}$ entering Equations 2.1 and 2.3.

The interaction between any distinct pair of monomers is then uniquely defined by the

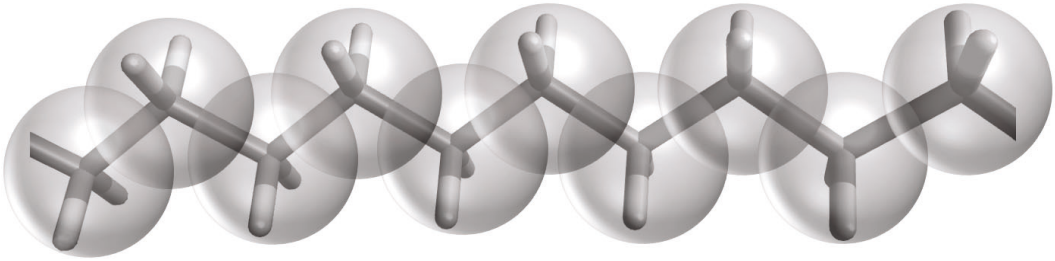

(a) PE

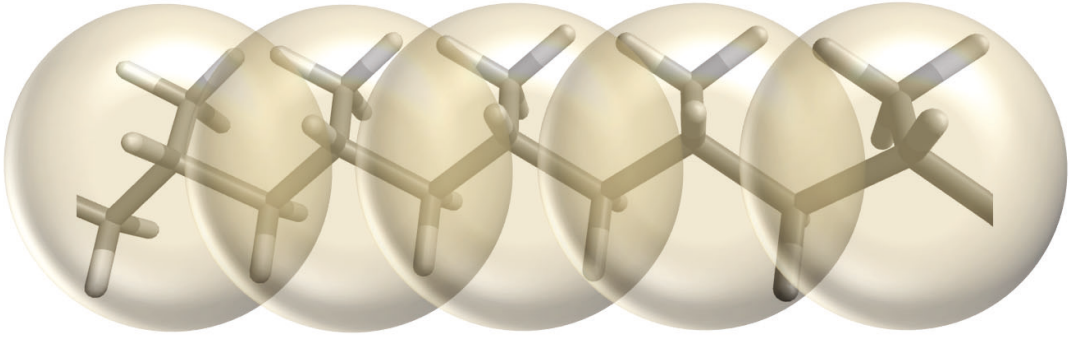

(b) Isotactic PP

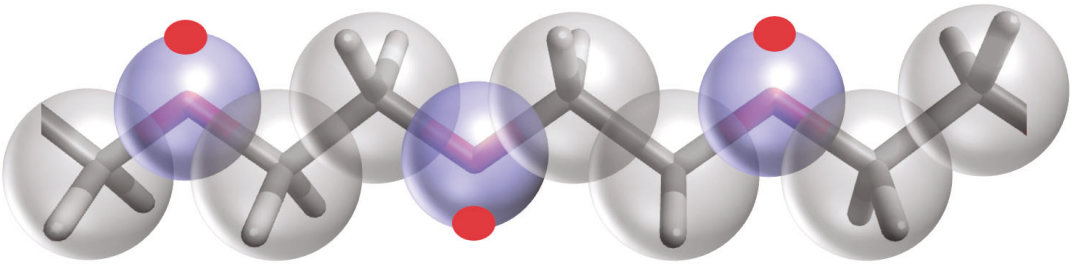

(c) PEG

Figure 2.1.: A schematic depiction of the SAFT-γ molecular models for PE, PP and PEG used in the current work. From top to bottom: united-atom model for PE featuring the CH_2 group; coarse-grained model for (isotactic) PP featuring the $CH_2CH(CH_3)$ group; united-atom model for PEG featuring the second-order CH_2^{OE} group (gray) and the cO group (blue). The red dots represent association sites of type e. All the group parameters can be found in Tables 2.1, 2.2 and 2.3.

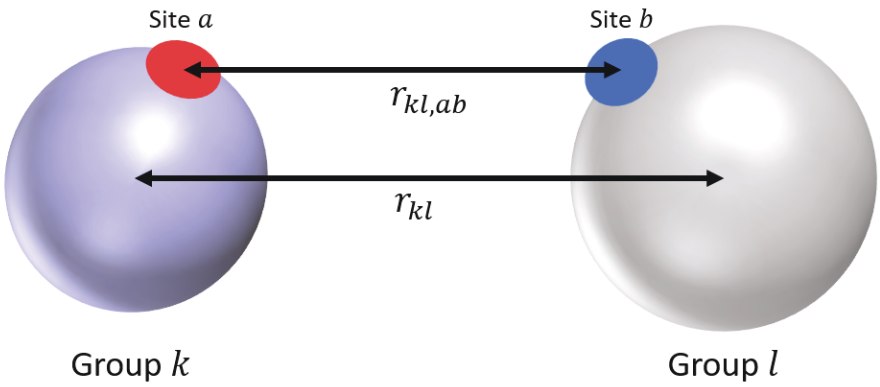

Figure 2.2.: A schematic representation of two SAFT-γ Mie groups with association sites. The interaction between the centers of mass of group k and group l at distance r_{kl} is mediated by a Mie potential (Equation 2.1); the interaction between site a and site b at distance $r_{kl,ab}$ is mediated by a 3-D square-well potential (Equation 2.3).

four dispersion parameters $\sigma_{kl}, \epsilon_{kl}, \lambda_{kl}^r, \lambda_{kl}^a$ and by the eventual $\epsilon_{kl,ab}^{\mathrm{HB}}, K_{kl,ab}^{\mathrm{HB}}$ for every pair (a_k, b_l) of sites. In most cases, however, λ_{kl}^a is set to 6 in order to reflect the form of the induced-dipole interaction (i.e., the London dispersion force[75]) and reduce the dimension of the parameter space. Furthermore, the unlike interaction parameters can be calculated from the corresponding quantities describing the like interactions using a set of combining rules[66,67] which are reported in Appendix A.

Additionally, in the SAFT-γ Mie approach an additional group parameter, the shape factor S_k, is incorporated to account for non-tangential chain segments k[67,76] (see Equation 2.18). The inclusion of the shape factor in SAFT-γ Mie gives rise to a group-contribution approach for molecules formed from different functional groups which are represented by the various segments. In particular, each group k is characterised by the number of identical segments it is made of (ν_k^*), its shape factor S_k, its Mie force-field parameters, and the number and types of association sites present. Each component i in a mixture is uniquely characterized by the type of groups it is composed of $(k = 1, 2 \ldots N_{\mathrm{G}})$ and the number of groups of each type $(\nu_{k,i})$.

2.2. Free energy

In SAFT-γ Mie the Helmholtz free energy of a system of N neutral molecules can be expressed as the sum of four terms which represent the contribution of the translational degrees of freedom (i.e., the ideal-gas term), monomer-monomer interaction, chain formation and association:[66,67]

$$A^{\mathrm{EoS}} = A^{\mathrm{id}} + A^{\mathrm{mono}} + A^{\mathrm{chain}} + A^{\mathrm{assoc}}. \tag{2.4}$$

2.2.1. The ideal gas term

Here and in the rest of this work k_{B} represents Boltzmann's constant and T the thermodynamic (absolute) temperature. As it is customary, we define $\beta = 1/k_{\mathrm{B}}T$. For a system of N molecules of N_{C} distinct components, the ideal gas term is given by[67]

$$\frac{A^{\mathrm{id}}}{NK_{\mathrm{B}}T} = \sum_{i=1}^{N_{\mathrm{C}}} x_i \ln\left(\rho_i \Lambda_i^3\right), \tag{2.5}$$

where x_i is the mole fraction of component i, $\rho_i = x_i\rho = Nx_i/V$ and Λ_i is the thermal de Broglie wavelength of component i:

$$\Lambda_i = \sqrt{\frac{h^2}{2\pi m_i k_{\mathrm{B}} T}}, \tag{2.6}$$

where m_i is the mass of component i and h is Planck's constant.

2.2.2. The monomer term

The monomer term is the residual Helmoholtz free energy of a system of interacting Mie monomers obtained by decomposing every component into its group constituents, and is approximated using a third-order Barker and Henderson high-temperature expansion.[77,78] This theory follows early work from Zwanzig[52] and embodies the observation that the properties of the liquid state are dominated by repulsion. Accordingly, the Mie potential of each pair of groups is split in a repulsive ($u^0_{kl} > 0$) and an attractive ($u^1_{kl} < 0$) contribution such that $u^{\text{Mie}}_{kl}(r) = u^0_{kl}(r) + u^1_{kl}(r)$. The repulsive part is given as

$$u^0_{kl}(r_{kl}) = \begin{cases} u^{\text{Mie}}_{kl} & \text{if } r_{kl} \leq \sigma_{kl} \\ 0 & \text{otherwise} \end{cases}, \tag{2.7}$$

whereas the attractive contribution is

$$u^1_{kl}(r_{kl}) = \begin{cases} 0 & \text{if } r_{kl} \leq \sigma_{kl} \\ u^{\text{Mie}}_{kl} & \text{otherwise} \end{cases}. \tag{2.8}$$

The residual free energy of the Mie fluid mixture is obtained by considering the Mie force field

$$U^{\text{Mie}} = \sum_{\alpha\alpha'} u^{\text{Mie}}_{\alpha\alpha'} \tag{2.9}$$

as a perturbation of the reference purely repulsive force field

$$U_0 = \sum_{\alpha\alpha'} u^0_{\alpha\alpha'}, \tag{2.10}$$

where α and α' are two distinct Mie monomers and the sum runs over all distinct pairs of monomers. The perturbation is simply $U_1 = U^{\text{Mie}} - U_0$. By denoting with $\langle . \rangle_0$ the canonical ensemble average in the reference purely repulsive system and with A_0 the cor-

responding free energy, a central result in perturbation theory is[52]

$$-\beta\left(A^{\text{mono}}-A_0\right)=\ln\langle e^{-\beta U_1}\rangle_0==\sum_{n=1}^{\infty}\frac{(-\beta)^n}{n!}\kappa_n^0\left[U_1\right]. \tag{2.11}$$

The series on the right hand side is obtained by (formal) expansion of the exponential and logarithmic functions in the middle expression, and defines the cumulants $\kappa_n^0\left[U_1\right]$ of the perturbation U_1 in the reference system. This notation highlights the functional dependence of the cumulants on the form of the perturbation. The cumulants can be found as a function of the moments $\mu_m^0=\langle {U_1}^m\rangle_0$ using the following general formula:

$$\kappa_n^0=\sum_{l=1}^{n}(-1)^{l-1}(l-1)!B_{n,l}\left(\mu_1^0,\mu_2^0,\ldots,\mu_{n-l+1}^0\right) \tag{2.12}$$

where the $B_{n,l}$ functions are the incomplete Bell polynomials. For example, the first three cumulants are given by

$$\begin{aligned}\kappa_1^0&=\langle U_1\rangle_0\\ \kappa_2^0&=\langle U_1^2\rangle_0-\langle U_1\rangle_0^2\\ \kappa_3^0&=\langle U_1^3\rangle_0-3\langle U_1^2\rangle_0\langle U_1\rangle_0+2\langle U_1\rangle_0^3\end{aligned}\quad. \tag{2.13}$$

The cumulant expansion of Equation 2.11 is sometimes called "high-temperature" expansion, although the cumulants themselves are functions of temperature due to the underlying temperature-dependence of the probability density function (PDF) of the reference system.

The central idea in the Barker and Henderson theory[77,78] is to map the reference soft repulsive potential to an effective hard-core potential characterised by a temperature-dependent diameter $d(T)$. With perturbation techniques, Barker and Henderson showed that for a one-component fluid, provided that the diameter d of the equivalent hard-

sphere system is chosen so that

$$d(T) = \int_0^\sigma \mathrm{d}r \left[1 - e^{-\beta u^0(r)}\right], \tag{2.14}$$

the free energy of the reference purely repulsive system, A_0, and its distribution functions needed to calculate the cumulants in Equation 2.11 can be approximated by the equivalent hard-sphere free energy and hard-sphere distribution functions:

$$\beta A^{\mathrm{mono}} \approx \beta A^{\mathrm{HS}} + \beta \kappa_1^{\mathrm{HS}}\left[U_1\right] - \frac{\beta^2}{2!}\kappa_2^{\mathrm{HS}}\left[U_1\right] + \ldots \tag{2.15}$$

However, it must be noted that these approximations are only exact at "first order" in the difference between the soft-core and hard-core reference potential;[77–80] the reader is referred to the original work for a formal treatment of this perturbation approach.

This procedure takes advantage of the extensive knowledge of hard-sphere equations of state and pair distribution functions,[81–86] which results in good approximation for $A_0 \approx A^{\mathrm{HS}}$ and the cumulants in Equation 2.11. The success of perturbation theory is due to its ability to provide an accurate description in most thermodynamic conditions. In the limit of high temperature or low density, higher order terms in Equations 2.11 and 2.15 become negligible since they involve powers of β and higher-order density distributions. At the same time, since the higher-than-first-order terms in the series quantify the fluctuations of the attractive potential around its average value the BH approximation is also accurate at high density, where fluctuations are suppressed.[80] Similarly, in the low-temperature limit the need to include more terms in the expansion is balanced by the increased accuracy of the hard-core mapping.

The BH expansion is implemented in SAFT-γ Mie by assigning to each monomer k an

equivalent hard-core diameter d_{kk} given by

$$d_{kk}(T) = \int_0^{\sigma_{kk}} \mathrm{d}r \left[1 - e^{-\beta u_{kk}^{\mathrm{Mie}}(r)}\right]. \tag{2.16}$$

The monomer excess Helmholz free energy to the third order of the expansion is therefore written as

$$\frac{A^{\mathrm{mono}}}{N_s k_{\mathrm{B}} T} = a^{\mathrm{HS}} + \beta a_1 + \beta^2 a_2 + \beta^3 a_3. \tag{2.17}$$

Here we have defined N_s as the effective total number of segments:

$$N_s = \left(\sum_{i=1}^{N_{\mathrm{C}}} x_i \tilde{m}_i\right) N = \left(\sum_{i=1}^{N_{\mathrm{C}}} x_i \sum_{k=1}^{N_{\mathrm{G}}} \nu_{k,i} \nu_k^* S_k\right) N, \tag{2.18}$$

where $\tilde{m}_i = \sum_{k=1}^{N_{\mathrm{G}}} \nu_{k,i} \nu_k^* S_k$ is the effective number of segments of component i. a^{HS} is the (reduced) residual free energy of a mixture of hard-spheres; in SAFT-γ Mie the expression proposed by Boublík[84] and Mansoori[85] is employed:

$$a^{\mathrm{HS}} = \frac{6}{\pi \rho_s} \left[\left(\frac{\zeta_2^3}{\zeta_3^2} - \zeta_0\right) \ln\left(1 - \zeta_3\right) + 3\frac{\zeta_1 \zeta_2}{1 - \zeta_3} + \frac{\zeta_2^3}{\zeta_3 \left(1 - \zeta_3\right)^2}\right], \tag{2.19}$$

where $\rho_s = N_s / V$ is the effective segment density and ζ_m are the m^{th} density moments:

$$\zeta_m = \frac{\pi \rho}{6} \sum_{i=1}^{N_{\mathrm{C}}} \sum_{k=1}^{N_{\mathrm{G}}} x_i \nu_{k,i} \nu_k^* S_k d_{kk}^m. \tag{2.20}$$

The three additional terms in Equation 2.17 are the first three cumulants of u_{kl}^1, ensemble-averaged in the reference hard-sphere system. For example, a_1 is simply the mean attractive energy calculated based on the hard-sphere reference:

$$a_1 = 2\pi \rho_s \int_{\sigma_{kl}}^{+\infty} g_{kl}^{\mathrm{HS}}(r) u_{kl}^{\mathrm{Mie}}(r) r^2 \mathrm{d}r, \tag{2.21}$$

where g_{kl}^{HS} is the radial distribution function (RDF) for the pair (k, l) in the reference hard-sphere system. In practice, in SAFT-γ Mie the integral in Equation 2.21 is approximated by means of the mean-value theorem, expansions of g_{kl}^{HS} around $r = d_{kl}$ (i.e., at contact) and *ad hoc* mixing rules.[66,67] These simplifications provide algebraic expressions for a_1 and do not lead to significant losses in accuracy.

The exact expressions for a_2 and a_3 require the knowledge of particle distribution functions in the reference hard-sphere fluid of order higher than 2, which are notoriously hard to evaluate. For this reason, a_2 is obtained by means of the macroscopic compressibility approximation[77] (MCA) and an empirical correction factor.[66] Lastly, a_3 is calculated by means of an empirical expression fitted to simulation data of Mie fluids and its inclusion in the theory leads to improved accuracy of the predictions near critical points. The interested reader is referred to the original publications[66,67] for the explicit expressions of a_2, a_3 and a more in-depth discussion on the approximations involved.

2.2.3. The chain term

Both the chain and association terms are written using Wertheim's first-order thermodynamic perturbation theory[55–59] (TPT1) using the Mie monomer fluid as reference. The TPT framework allows one to account for the influence of strong directional interactions like hydrogen bonding (or covalent bonding in the case of polymerisation) on fluids of monomers that otherwise only interact via spherically-symmetric potentials. Wertheim showed that the grand-canonical partition function of an associating system can be written as an infinite series of integrals (often represented via graphs) involving the particle density functions of the reference non-associating fluid.

There are two major approximations that characterise the TPT of Wertheim. The first one is the order at which the graph expansion is truncated, which determines the or-

der of the reference monomer distribution functions needed to calculate the integrals. For example, TPT1 includes exclusively two-body effects and therefore only requires the knowledge of the pair radial distribution function (RDF) of the reference monomer fluid, whereas TPT2 and TPT3 need 3- and 4-particle distribution functions.[87,88] The second approximation is the so-called single-chain approximation, whereby only graphs of associating chains surrounded by monomers are considered in the graph sum corresponding to the Helmholtz free energy difference due to monomer association. This approximation is exact in the limit of weak association or in the limit of infinite chain dilution. The reader is referred to a recent pedagogical review of TPT for more details.[88]

The chain term accounts for irreversible bonding between different monomers in the reference Mie fluid. It can be obtained using the TPT1 framework by simultaneously taking the limit of infinitely localised and infinitely strong association. In SAFT-γ Mie the expression is given by[66,67,89]

$$\frac{A^{\text{chain}}}{Nk_{\text{B}}T} = -\sum_{i=1}^{N_{\text{C}}} x_i \left(\tilde{m}_i - 1\right) \ln g_{ii}^{\text{Mie}}\left(\bar{\sigma}_{ii}; \zeta_{\text{x}}\right), \tag{2.22}$$

where $\tilde{m}_i$ is the effective number of segments of component i (*cf.* Equation 2.18) and $g_{ii}^{\text{Mie}}\left(\bar{\sigma}_{ii}; \zeta_{\text{x}}\right)$ is the value of an effective RDF at contact for the monomers of component i evaluated at an effective packing fraction ζ_{x}. The word "effective" is used here for the RDF in the sense that in order to calculate g_{ii}^{Mie} the heteronuclear chain i is replaced by an equivalent homonuclear chain made of identical Mie monomers of diameter $\bar{\sigma}_{ii}$, well depth $\bar{\epsilon}_{ii}$ and repulsive exponent $\bar{\lambda}_{ii}^{r}$ which are determined by appropriate averaging[67] over the respective values of the the monomers of component i. Similarly, the effective packing fraction of the reference hard-sphere mixture ζ_{x} is found using a diameter $\bar{d}$ obtained by appropriate averaging over the BH hard-sphere diameters d_{kl} (*cf.* Equation 2.16 and Appendix A). See the original publications[66,67] for additional details on the

way this averaging is performed.

A close inspection of Equation 2.22 reveals the key approximations of TPT1. Each $\left[(\tilde{m}_i - 1) \ln g_{ii}^{\text{Mie}}\right]$ in the free energy experssion originates from the chemical potential of a single chain composed of $\tilde{m}_i$ effective monomers of type i brought into contact at distance $\bar{\sigma}_{ii}$, where correlation higher than second order between the monomers are neglected; a multiplication by x_i follows in order to obtain the free energy, under the assumption of infinitely dilute chains. Despite the crude approximations, the TPT1 formalism is known to provide an accurate description of polymer properties in the high-density limit, with deviations expected mostly at low and medium density due to the single-chain approximation breaking down.[87] As a result, SAFT models for polymers have managed to accurately describe critical properties (UCST and LCST), compressibility effects and vapour-liquid envelopes for associating and non-associating polymer mixtures.[64,90–94]

2.2.4. The association term

The association term in SAFT-γ Mie accounts for reversible association due to hydrogen bonding or other strong directional inter-molecular interactions. The expression for A^{assoc} is the following:[67]

$$\frac{A^{\text{assoc}}}{N k_{\text{B}} T} = \sum_{i=1}^{N_{\text{C}}} x_i \sum_{k=1}^{N_{\text{G}}} \nu_{k,i} \sum_{a=1}^{N_{\text{ST},k}} n_{k,a} \left(\ln X_{i,k,a} + \frac{1 - X_{i,k,a}}{2} \right). \tag{2.23}$$

In this Equation $N_{\text{ST},k}$ is the number of types of sites on group k, $n_{k,a}$ is the number of sites of type a on group k and $X_{i,k,a}$ is the fraction of molecules of component i not bonded at site a on group k. The latter quantity is found via solution of the mass action

equations[66,67]

$$X_{i,k,a} = \left(1 + \rho \sum_{j}^{N_{\mathrm{C}}} \sum_{l}^{N_{\mathrm{G}}} \sum_{b}^{N_{\mathrm{ST},l}} x_j \nu_{l,j} n_{l,b} X_{j,l,b} \Delta_{ij,kl,ab} \right)^{-1} . \tag{2.24}$$

The association strength $\Delta_{ij,kl,ab}$ is found after angle averaging the square-well association potential (Equation 2.3) and is given by

$$\Delta_{ij,kl,ab} = \bar{\sigma}_{ij}^3 \left[\exp\left(\frac{\epsilon_{kl,ab}^{\mathrm{HB}}}{k_{\mathrm{B}} T} \right) - 1 \right] I_{kl,ab}. \tag{2.25}$$

Whereas the effective unlike Mie diameter $\bar{\sigma}_{ij}$ is calculated using combining rules (as are all unlike diameters in the theory, *cf.* Appendix A), the dimensionless integrals $I_{kl,ab}$ are obtained using the RDF of the reference Mie fluid g_{kl}^{Mie}, the cut-off radius $r_{kl,ab}^{c}$ and the distance of the association sites from the Mie cores $r_{kl,ab}^{d}$. In practice, via additional approximation invoking the equivalence (at zeroth order) $g_{kl}^{\mathrm{Mie}} \approx g_{kl}^{\mathrm{HS}}$ the following expression is obtained:[67]

$$I_{kl,ab} \approx g_{kl}^{\mathrm{HS}} \left(\bar{d}_{kl} \right) K_{kl,ab} \left(\bar{\sigma}_{ij}, \bar{d}_{ij}, r_{kl,ab}^{c}, r_{kl,ab}^{d} \right) . \tag{2.26}$$

Here $K_{kl,ab}$ is the bonding volume and can be calculated with an appropriate integral.[66,67] In order to reduce the dimension of the parameter space, in SAFT-γ Mie the bonding volume $K_{kl,ab}$ is taken as an adjustable parameter.

2.3. Thermodynamic relations and computational details

In this Section the thermodynamic relations between the Helmholtz free energy and other macroscopic variables are established. The superscript "EoS" is added to all functions to indicate that their functional form is determined by the particular equation of state used.

Systems are here implicitly considered to be fluids in equilibrium.

2.3.1. A note on composition

Throughout this work when no polymer is present in a system, the composition is denoted with the vector $\boldsymbol{y} = \{y_1, y_2, \dots y_{N_\mathrm{C}}\}$ containing the number of moles y_i of each of the N_C components. In mixtures containing polymers, a distinction is implemented between "small" molecules (or solutes) and polymers by specifying composition with the vector $\boldsymbol{n}_\mathrm{s} = \{n_{\mathrm{s},1}, n_{\mathrm{s},2} \dots n_{\mathrm{s},N_\mathrm{C}}\}$ of moles of solutes and with the vector $\boldsymbol{\nu} = \{\nu_1, \nu_2 \dots\}$ of moles ν_i of the polymer molecules of type i. We do not specify the exact number of types of polymer molecules as in most polymer systems branching and polydispersity can lead to a huge number of structurally different polymer molecules in the same system.

2.3.2. Derivatives of the Helmholtz free energy

In this work the SAFT-γ Mie Helmholtz free energy of a system at given $T, V, \boldsymbol{n}_\mathrm{s}, \boldsymbol{\nu}$ conditions is computed using Clapeyron.jl,[95] an open-source package for the calculation of thermodynamic properties of fluids written in Julia.[96] Additionally, all the derivatives of the the Helmholtz free energy discussed here are obtained via symbolic differentiation of the Helmholtz free energy enabled by Julia.

The chemical potential of a component in a mixture is defined as the partial derivative of the system's Helmholtz free energy with respect to the number of moles of that component at constant temperature, volume and moles of all the other components. For a generic polymer + solutes mixture, the chemical potential $\mu_{\mathrm{s},i}^{\mathrm{EoS}}$ of a solute i is thus

obtained as

$$\mu_{\mathrm{s},i}^{\mathrm{EoS}} = \left(\frac{\partial A^{\mathrm{EoS}}}{\partial n_{\mathrm{s},i}}\right)_{T,V,\boldsymbol{n}_{\mathrm{s}}\setminus\{n_{\mathrm{s},i}\},\boldsymbol{\nu}}, \tag{2.27}$$

where the notation $\boldsymbol{n}_{\mathrm{s}} \setminus \{n_{\mathrm{s},i}\}$ indicates that the moles of components $j \neq i$ are kept constant. Similarly, the chemical potential of the polymer molecule of type i, $\mu_{\mathrm{p},i}$, is obtained via

$$\mu_{\mathrm{p},i}^{\mathrm{EoS}} = \left(\frac{\partial A^{\mathrm{EoS}}}{\partial \nu_i}\right)_{T,V,\boldsymbol{n}_{\mathrm{s}},\boldsymbol{\nu}\setminus\{\nu_i\}}. \tag{2.28}$$

In particular, if the polymer mixture is monodisperse (i.e., if only one well-defined type of polymer molecule is present in the system) the polymer chemical potential μ_{p} is given by

$$\mu_{\mathrm{p}}^{\mathrm{EoS}} = \left(\frac{\partial A^{\mathrm{EoS}}}{\partial \nu}\right)_{T,V,\boldsymbol{n}_{\mathrm{s}}}. \tag{2.29}$$

The pressure the mixture is obtained by taking the partial derivative of its Helmholtz free energy with respect to volume at constant temperature and composition:

$$P^{\mathrm{EoS}} = -\left(\frac{\partial A^{\mathrm{EoS}}}{\partial V}\right)_{T,\boldsymbol{n}_{\mathrm{s}},\boldsymbol{\nu}}. \tag{2.30}$$

2.3.3. Thermodynamic potentials

There are various thermodynamic potentials that can be defined by Legendre transformation of the Helmholtz free energy of a polymer + solutes mixture, A^{EoS}, which is usually written as a function of $T, V, \boldsymbol{n}_{\mathrm{s}}, \boldsymbol{\nu}$. For example, by keeping the pressure P instead of the volume V constant, we can define the function

$$G^{\mathrm{EoS},*}(T, P, \boldsymbol{n}_{\mathrm{s}}, \boldsymbol{\nu}; V) = A^{\mathrm{EoS}}(T, V, \boldsymbol{n}_{\mathrm{s}}, \boldsymbol{\nu}) + PV, \tag{2.31}$$

and require that it is minimum with respect to V at fixed $T, P, \boldsymbol{n}_\mathrm{s}, \boldsymbol{\nu}$:

$$\min_V G^{\mathrm{EoS},*}(T, P, \boldsymbol{n}_\mathrm{s}, \boldsymbol{\nu}; V) = G^{\mathrm{EoS}}(T, P, \boldsymbol{n}_\mathrm{s}, \boldsymbol{\nu}), \tag{2.32}$$

where

$$\begin{gathered} V = V^{\mathrm{EoS}}(T, P, \boldsymbol{n}_\mathrm{s}, \boldsymbol{\nu}) \\ \Updownarrow \\ \left(\frac{\partial G^{\mathrm{EoS},*}}{\partial V}\right)_{T,P,\boldsymbol{n}_\mathrm{s},\boldsymbol{\nu}} = P + \left(\frac{\partial A}{\partial V}\right)_{T,\boldsymbol{n}_\mathrm{s},\boldsymbol{\nu}} = 0 \end{gathered} . \tag{2.33}$$

In particular, $G^{\mathrm{EoS}}(T, P, \boldsymbol{n}_\mathrm{s}, \boldsymbol{\nu})$ is defined as the Gibbs free energy of the system. Due to the property of the Legendre transform, we have

$$V^{\mathrm{EoS}}(T, P, \boldsymbol{n}_\mathrm{s}, \boldsymbol{\nu}) = \left(\frac{\partial G^{\mathrm{EoS}}}{\partial P}\right)_{T,\boldsymbol{n}_\mathrm{s},\boldsymbol{\nu}} . \tag{2.34}$$

Similarly, if the pressure and the chemical potential of each of the solutes are specified we can define the osmotic free energy $\Omega_\mathrm{s}^{\mathrm{EoS},*}$ via

$$\Omega_\mathrm{s}^{\mathrm{EoS},*}(T, P, \boldsymbol{\mu}_\mathrm{s}, \boldsymbol{\nu}; \boldsymbol{n}_\mathrm{s}) = G^{\mathrm{EoS}}(T, P, \boldsymbol{n}_\mathrm{s}, \boldsymbol{\nu}) - \sum_{i=1}^{N_\mathrm{C}} \mu_{\mathrm{s},i} n_{\mathrm{s},i}. \tag{2.35}$$

Minimisation of $\Omega_\mathrm{s}^{\mathrm{EoS},*}$ with respect to the number of moles of each solute yields the equilibrium number of solute molecules $n_{\mathrm{s},i}^{\mathrm{EoS}}(T, P, \boldsymbol{\mu}_\mathrm{s}, \boldsymbol{\nu})$ – which can also be found by differentiation of $\Omega_\mathrm{s}^{\mathrm{EoS}} = \min_{\boldsymbol{n}_\mathrm{s}} \Omega_\mathrm{s}^{\mathrm{EoS},*}$ as in 2.34. One should note that at equilibrium we have

$$\Omega_\mathrm{s}^{\mathrm{EoS}}(T, P, \boldsymbol{\mu}_\mathrm{s}, \boldsymbol{\nu}) = \sum_i \nu_i \mu_{\mathrm{p},i}^{\mathrm{EoS}}(T, P, \boldsymbol{\mu}_\mathrm{s}, \boldsymbol{\nu}) \tag{2.36}$$

due to the extensivity of the system, where the index i runs over all the chemically and structurally distinct types of polymer molecules in the system.

2.3.4. Pure-component saturation properties

Let us consider a fluid made of a single component. Thermodynamic stability requires that at fixed temperature T, volume V and number of molecules N the Helmholtz free energy of the system must be at a global minimum with respect to any variation of the system's properties compatible with the constraints T, V, N. In particular, if the system is stable in a single homogeneous phase partitioning its volume and particles in two homogenous sub-systems must lead to an increase in Helmholtz free energy, i.e.,

$$A^{\mathrm{EoS}}(T,V,N) \leq A^{\mathrm{EoS}}(T,V_1,N_1) + A^{\mathrm{EoS}}(T,V_2,N_2) \tag{2.37}$$

for each pair of (N_1, N_2) and (V_1, V_2) such that $V_1 + V_2 = V$ and $N_1 + N_2 = N$. A necessary condition that follows from Equation 2.37 is that if a system is stable at T, V, N conditions the Hessian matrix H_A of its Helmholtz free energy

$$\mathrm{H}_A(T,V,N) = \begin{bmatrix} \frac{\partial^2 A^{\mathrm{EoS}}}{\partial V^2}(T,V,N) & \frac{\partial^2 A^{\mathrm{EoS}}}{\partial V \partial n}(T,V,N) \\ \frac{\partial^2 A^{\mathrm{EoS}}}{\partial n \partial V}(T,V,N) & \frac{\partial^2 A^{\mathrm{EoS}}}{\partial n^2}(T,V,N) \end{bmatrix} \tag{2.38}$$

must be positive semi-definite, a condition that is called "local stability". Since the matrix is symmetrical due to Schwarz's theorem*, it is sufficient that

$$\begin{cases} \left(\frac{\partial^2 A^{\mathrm{EoS}}}{\partial V^2}\right)_{T,N} & = -\left(\frac{\partial P^{\mathrm{EoS}}}{\partial V}\right)_{T,N} \geq 0 \\ \left(\frac{\partial^2 A^{\mathrm{EoS}}}{\partial N^2}\right)_{T,V} & = \left(\frac{\partial \mu^{\mathrm{EoS}}}{\partial N}\right)_{T,V} \geq 0 \end{cases} \tag{2.39}$$

*A sufficient condition for Schwarz's theorem to hold is that all second partial derivatives of A^{EoS} are continuous.

for the system to be locally stable. By defining $\rho = N/V$ as the particle density and noticing that at constant temperature the Gibbs–Duhem relation imposes

$$-N\mathrm{d}\mu^{\mathrm{EoS}} + V^{\mathrm{EoS}}\mathrm{d}P = 0 \Leftrightarrow \rho\left(\frac{\partial\mu^{\mathrm{EoS}}}{\partial\rho}\right)_{T,V} = \left(\frac{\partial P^{\mathrm{EoS}}}{\partial\rho}\right)_{T,V} \tag{2.40}$$

both the conditions expressed in Equation 2.39 can be restated by the single equation

$$\left(\frac{\partial P^{\mathrm{EoS}}}{\partial\rho}\right)_{T} \geq 0, \tag{2.41}$$

where we have used the fact that pressure and the chemical potential of a pure compound only depend on density and temperature. At fixed temperature T, if the system is locally stable (Equation 2.41) at all densities ρ it is also globally stable (Equation 2.37).

There exists a temperature T_{c} – known as the critical temperature[†] – above which homogeneous fluids are thermodynamically stable at all (V, n) and therefore do not phase separate in a gas and liquid phase. Fluids above their critical temperature are deemed "supercritical". In the present work, the critical temperature is found using the Clapeyron.jl package[95] via solution of the following pair of non-linear equations:

$$\left(\frac{\partial^2 A^{\mathrm{EoS}}}{\partial V^2}\right)_{T,N} = \left(\frac{\partial^3 A^{\mathrm{EoS}}}{\partial V^3}\right)_{T,N} = 0 \tag{2.42}$$

for the critical temperature T_{c} and volume V_{c}.

At all temperatures lower than T_{c} there exists a range of densities in which the system can lower its Helmholtz free energy by separating in a gas phase with density ρ_{g} and a liquid phase with density $\rho_{\mathrm{l}} > \rho_{\mathrm{g}}$. At each temperature T, since the total Helmholtz free energy of the system must be stationary with respect to exchanges of volume and

[†]To be precise, the critical temperature of liquid-gas coexistence

particles between the two phases we must have

$$\begin{cases} P^{\mathrm{EoS}}(T, \rho_{\mathrm{g}}) = P^{\mathrm{EoS}}(T, \rho_{\mathrm{l}}) = P_{\mathrm{sat}}(T) \\ \mu^{\mathrm{EoS}}(T, \rho_{\mathrm{g}}) = \mu^{\mathrm{EoS}}(T, \rho_{\mathrm{l}}) = \mu_{\mathrm{sat}}(T) \end{cases}, \tag{2.43}$$

where $P_{\mathrm{sat}}(T)$ is referred to as saturation pressure or vapour pressure. Solution of this pair of non-linear equations yields the density of the gas ($\rho_{\mathrm{g}}(T)$) and liquid ($\rho_{\mathrm{l}}(T)$) in equilibrium at temperature T. In this work, the saturation pressure and densities of sub-critical fluids are calculated using the Clapeyron.jl package which implements non-linear solvers with appropriate guesses to solve the pair of equations in 2.43.

2.3.5. Phase equilibrium in mixtures

At fixed temperature T and pressure P, a mixture of N_{C} components can phase separate in a number $\mathcal{N}_{\mathrm{p}}$ of phases bounded by the Gibbs phase rule:

$$\mathcal{N}_{\mathrm{p}} \leq N_{\mathrm{C}} + 2. \tag{2.44}$$

At equilibrium at fixed temperature, pressure and overall composition, the chemical potential of each component must be equal in all phases and the Gibbs free energy of the overall system must be at a global minimum. In this work, the Helmholtz free energy Langrangian dual (HELD) algorithm[97] is used to find the number and composition of each phase at equilibrium once temperature T, pressure P and overall system composition are specified – the so-called TP flash calculation. The algorithm ensures that the chemical potential of each species is the same in each phase but does not ensure

convergence to a global minimum[‡].

Dew and bubble point calculations

The dew pressure can be defined as the pressure at which the first droplet of liquid forms upon increasing pressure of a homogeneous gas mixture at fixed temperature and overall composition. Similarly, the bubble pressure P_{bub} can be defined at each temperature and overall composition as the pressure at which the first bubble of gas phase forms upon decreasing the pressure of a homogeneous liquid mixture. In this work, both the bubble pressure and dew pressure of a systems are calculated using the Clapeyron.jl package and the solutions are checked for consistency using the HELD algorithm.

A semi-open perspective for nonvolatile components

Polymers possess extremely low volatility, meaning that their concentration in gas phases can normally be neglected. For similar reasons, polymer + solutes mixtures are expected to have an infinitesimally small dew pressure at most temperatures as long as the amount of polymer is not also negligible. As a consequence, performing a TP flash calculation for a polymer + solutes mixture at given temperature, composition and sufficiently low pressure results in the equilibrium between a liquid polymer-rich phase and an external gas phase that can be considered devoid of any polymer molecules. Furthermore, in many applications the fluids in contact with polymer samples can be considered to be effectively infinite in extension.

In order to simplify calculations, it is therefore convenient to force the concentration of the polymer in the gas phase to be zero. At fixed temperature, pressure and composition

[‡]However, as noted by the authors,[97] it is quite unlikely that the algorithm terminates on a local minimum.

$\boldsymbol{y}$ the chemical potential of the solutes $\boldsymbol{\mu}_{\mathrm{s}} = \boldsymbol{\mu}_{\mathrm{s}}^{\mathrm{EoS}}(T, P, \boldsymbol{y})$ is thus fixed by the gas phase and we can consider the polymer a semi-open system allowing exchanges of solute molecules only. The equilibrium number of particles of solute i in the polymer – $n_{\mathrm{s},i}^{\mathrm{EoS}}$ – can thus be found as a function of $T, P, \boldsymbol{\mu}_{\mathrm{s}}, \boldsymbol{\nu}$ via minimisation of the osmotic free energy $\Omega_{\mathrm{s}}^{\mathrm{EoS},*}$ (Section 2.3.3).

2.4. Parameter estimation

It is customary in SAFT-γ Mie to employ a top-down parametrization procedure, which involves optimising a set of like and unlike group parameters in order to reproduce experimental measurements of macroscopic properties of systems containing the target groups. Fully-predictive bottom-up parameterisation with *ab initio* methods is possible for quasi-spherical molecules and dimers[98] but large deviations between predictions and experimental data are expected for associating compounds and highly asymmetric components (such as polymers). Therefore, in the present work all SAFT-γ Mie parameters are found by minimisation over the free parameter space of an appropriate objective function:

$$f_{\mathrm{obj}} = \sum_{i=1}^{N_{\mathrm{obj}}} \omega_i \sum_{j=1}^{N_{S_i}} \sum_{k=1}^{N_{D_{ij}}} \left[\frac{u_{ijk}^{\mathrm{exp}} - u_{ijk}^{\mathrm{calc}}}{\mathcal{S}_{ijk}} \right]^2 , \tag{2.45}$$

where $i = 1, ..N_{\mathrm{obj}}$ iterates over macroscopic thermodynamic properties described by the experimental data, $j = 1, ..N_{S_i}$ over the systems that exhibit the property i and $k = 1, ..N_{D_{ij}}$ over the experimental data points for the property i and the system j; additionally, each property i can be assigned – arbitrarily or through a Pareto optimization – an appropriate weight ω_i in order to give more or less importance to different properties. u_{ijk}^{exp} and u_{ijk}^{calc} are, respectively, the k^{th} experimental value of property i of system j and the corresponding calculated one as a function of the thermodynamic conditions and of the parameter set. The parameter $\mathcal{S}_{ijk}^2$ accounts for the uncertainty in the ex-

perimental data and can be set to "constant" or "constant-relative", i.e. $\mathcal{S}_{ijk}^2 = (0.01)^2$ or $\mathcal{S}_{ijk}^2 = \left(0.01 \cdot u_{ijk}^{\text{exp}}\right)^2$, respectively. In this work the weights are chosen so that each data point has the same weight in the objective function (i.e., $w_i = 1$ for all i), while the uncertainties are set to "constant-relative" which corresponds to assuming a uniform distribution in the relative uncertainty of the experimental data.

Normally, pure-component properties such as saturation densities and vapour pressure are included in the parameterisation whenever the like interaction parameters of a group are missing. These parameters are the "identity card" of SAFT-γ Mie groups and must always be found via a parameter estimation procedure. The unlike interaction parameters of a group pair can be estimated by using combining rules (*cf.* Appendix A) or by including pure component and/or mixture properties – such as the fluid phase behaviour or excess properties – of systems containing the target groups in the parameterisation.

2.5. Optimized SAFT-γ Mie parameters

In this Section all the SAFT-γ Mie parameters of the groups used in this work are listed. For original like and unlike group parameters the comparison between SAFT-γ Mie predictions and the experimental data used in the parameterisation procedure of Section 2.4 is shown.

2.5.1. Solute models

This subsection contains the SAFT-γ Mie molecular models and corresponding group parameters of the solutes – i.e., small molecules – considered in the present work. All the parameters are reported in Tables 2.1, 2.2 and 2.3.

Table 2.1.: SAFT-γ Mie like interaction parameters and molecular model for all the groups used in the present work. All the symbols are defined in Section 2.1. TW indicates that the molecular model and/or parameter set has been developed in this work. The bottom rows are groups that in the present work only appear as part of polymers (i.e., PP and PEG).

Group k	ν_k^*	S_k	σ_{kk} (Å)	ϵ_{kk}/k_B (K)	λ_{kk}^a	λ_{kk}^r	$N_{\mathrm{ST},k}$	$n_{k,H}$	n_{k,e_1}	Ref
CH_3	1	0.57255	4.0772	256.77	6.0000	15.050				67
CH_2	1	0.22932	4.8801	473.39	6.0000	19.871				67
CH	1	0.07210	5.2950	95.621	6.0000	8.0000				68
C	1	0.04072	5.6571	50.020	6.0000	8.0000				68
aCH	1	0.32184	4.0578	371.53	6.0000	14.756	1	0	1	68
CH_2=	1	0.44887	4.3175	300.90	6.0000	20.271				68
CH_2^{eth}=	1	0.44887	4.3175	300.90	6.0000	20.271				TW
CH=	1	0.20037	4.7488	952.54	6.0000	15.974				68
cCH_2	1	0.24751	4.7852	477.36	6.0000	20.386				68
H_2O	1	1.00000	3.0063	266.68	6.0000	17.020	2	2	2	99
CH_4	1	1.00000	3.7370	152.58	6.0000	12.504				100
$aCCH_3$	1	0.31655	5.4874	651.41	6.0000	23.627				101
CH_2OH	2	0.58538	3.4054	407.22	6.0000	22.699	2	1	1	101
CHO	2	0.61331	3.0900	311.36	6.0000	8.1793				TW
CH_2^{OE}	1	0.22932	4.8801	473.39	6.0000	19.871				94
cO	1	0.47500	3.0000	586.52	6.0000	26.870	1	0	1	94
PP_{mono}	1	1.00000	4.1030	276.21	6.0000	10.938				73

Table 2.2.: SAFT-γ Mie unlike potential well depth ϵ_{kl} and repulsive exponent λ^r_{kl} for all the pairs of groups needed to model systems considered in the present work. CR indicates the use of combining rules (*cf.* Appendix A). TW indicates parameters developed in this work.

Group k	Group l	ϵ_{kl}/k_B (K)	λ^r_{kl}	Ref	Group k	Group l	ϵ_{kl}/k_B (K)	λ^r_{kl}	Ref
CH_3	CH_2	350.77	CR	67	CH_2	CH4	243.13	12.642	70
CH_3	CH	387.48	CR	68	CH_2	CHO	313.00	CR	TW
CH_3	C	339.91	CR	68	CH_2	$CH_2{}^{OE}$	CR	CR	94
CH_3	aCH	305.81	CR	68	CH_2	PP_{mono}	359.34	CR	TW
CH_3	CH_2=	333.48	CR	68	CH_2=	CH	426.76	CR	68
CH_3	CH_2^{eth} =	333.48	CR	TW	CH_2=	CH_2^{eth} =	CR	CR	TW
CH_3	CH=	252.41	CR	68	CH_2=	CH=	275.75	CR	68
CH_3	cCH2	355.95	CR	68	CH_2^{eth} =	CH	426.76	CR	TW
CH_3	CHO	238.23	CR	TW	$CH_2{}^{OE}$	cO	325.94	10.054	94
CH_3	PP_{mono}	CR	CR	73	$CH_2{}^{OE}$	CH_2OH	404.74	CR	94
CH_2	CH	506.21	CR	68	$CH_2{}^{OE}$	H_2O	283.38	11.885	94
CH_2	C	300.07	CR	68	cO	CH_2OH	606.80	CR	94
CH_2	aCH	415.64	CR	68	cO	H_2O	350.09	14.872	94
CH_2	CH_2=	386.80	CR	68	CH_2OH	H_2O	353.37	CR	94
CH_2	CH_2^{eth} =	362.79	CR	TW	CH_2^{eth} =	CH=	275.75	CR	TW
CH_2	CH=	459.40	CR	68	CH_2	cCH2	471.85	CR	TW
CH_2	$aCCH_3$	525.13	CR	TW	$aCCH_3$	PP_{mono}	374.72	CR	TW
aCH	PP_{mono}	CR	CR	TW	cCH_2	PP_{mono}	359.53	CR	TW

Table 2.3.: SAFT-γ Mie association energy $\epsilon^{HB}_{kl,ab}$ and bonding volume $K^{HB}_{kl,ab}$ for all the pairs of groups needed to model systems considered in the present work.

Group k	Group l	site a	site b	$\epsilon^{HB}_{kl,ab}/k_B$ (K)	$K^{HB}_{kl,ab}$ (Å^3)	Ref
cO	CH_2OH	e	H	1472.5	433.15	TW
cO	H_2O	e	H	2193.2	50.01	TW
H_2O	CH_2OH	e	H	621.7	425.00	101
		H	e	2153.2	147.40	
H_2O	H_2O	e	H	1985.4	101.69	99
CH_2OH	CH_2OH	e	H	2097.9	62.31	101

Linear alkanes

Linear n-alkanes are modelled as composed of two united-atom methyl groups CH_3 and a variable number of united-atom methylene groups CH_2. For example, n-butane is modelled as composed of two CH_3 and two CH_2 groups. The like and unlike parameters of the two groups were optimised by Papaioannou and coworkers[67] to reproduce pure component and mixture properties of linear alkanes. Methane is modelled as a single CH_4 group following Burger and coworkers.[70]

Branched alkanes

Depending on their topology, branched alkanes are modelled with a variable number of methyl and methylene groups in addition to a variable number of the ternary united-atom sp^3 carbon group (CH) and quaternary carbon group (C). For example, isopentane is composed of three CH_3 groups, one CH_2 group and one CH group. The SAFT-γ Mie parameters of the CH and C groups were developed by Dufal *et al.*[68] to reproduce pure component and mixture properties of systems containing branched alkanes.

We stress that SAFT-γ Mie does not distinguish between components with the same groups but different group connectivity due to the TPT1 approximation of the chain term (*cf.* Section 2.2). For example, 2-methylhexane and 3-methylhexane cannot be distinguished if only the four groups mentioned are used. In general, molecules possessing the same functional groups but different spatial arrangement and group connectivity can only be separated by defining *ad hoc* second-order groups that account for the local environment of each group in different molecules.[102]

Alk-1-enes

Alk-1-enes are modelled in SAFT-γ Mie using the aforementioned methyl, methylene groups and two additional united-atom sp^2 carbon groups: the CH_2= group and the CH= group. For example, 1-hexene is modelled using three CH_2 groups, one CH_3 group, one CH_2= group and one CH= group. The like and unlike SAFT-γ Mie parameters for these groups were proposed by Dufal *et al.*[68] and are optimized to reproduce pure component and VLE data of the series of 1-alkenes and mixtures of alkanes and alkenes. The C= group developed by the same authors can be used to model branched alkanes, which however are not studied in this work.

It is questionable whether the same SAFT-γ Mie parameter set can describe both long 1-alkenes and its shortest representatives like ethylene and propylene. For example, the electronic environment around the two sp^2 carbons of ethylene should be noticeably different than in longer alkenes resulting in a different effective dispersion potential around the CH_2= group. In general, we expect that if a sufficiently high number of series members (labelled by n) are included in a parameterisation procedure (*cf.* Section 2.4) in which the same groups are used for all members, the parameters become biased to reproduce the properties of the longer molecules[67,68] due to the limiting behaviour of many thermodynamic properties as $n \to \infty$. After comparison with literature data, it was found that the solubility of ethylene in tetracontane (i.e., the n-alkane with 40 carbons) is over-predicted using the current parameter set (*cf.* Figure 2.3a) whereas the agreement is much better (*cf.* Figure 2.4) for mixtures of longer 1-alkenes (propylene and 1-butene) and n-alkanes (n-hexane and n-heptane).

In order to adjust the least number of parameters, we define here the new second-order group CH_2^{eth} = to model ethylene. This group possesses the same like and unlike interaction parameters as its previously-defined counterpart (CH_2 =), with the exception of its unlike dispersion energy ϵ_{kl} with the methylene group (CH_2) which is optimised

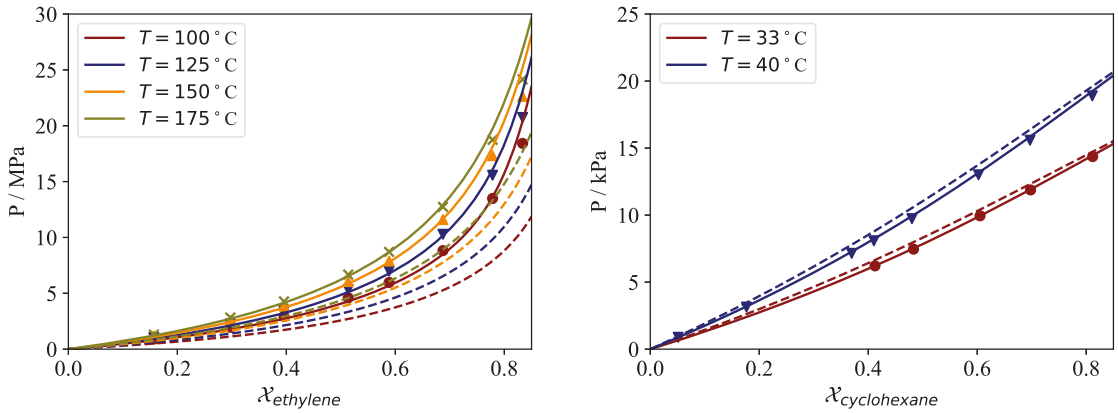

(a) (b)

Figure 2.3.: Bubble pressure curves of ethylene + tetracontane (a) and cyclohexane + eicosane (b) mixtures. The solid curves represent SAFT-γ Mie calculations with the updated unlike interaction well-depths between the CH_2 group and two groups composing ethylene and cyclohexane (CH_2^{eth} = and cCH_2, respectively – see Table 2.2), while the dashed curves calculations with the parameter set developed by Dufal and coworkers.[68] Experimental data are shown with markers and are taken from de Loos and coworkers[103] and Gomez and coworkers.[104]

to reproduce the solubility of ethylene in tetracontane (Figure 2.3a). This ensures that this modification only affects the properties of ethylene-containing mixtures and not of all the other compounds containing the CH_2 and CH_2 = groups. The optimal value for the unlike dispersion energy is found to be 362.79 K, as opposed to the value of 386.80 K used for the CH_2= group of longer alk-1-enes (Table 2.2).

Ring molecules

Similarly, due to the approximations of TPT1 SAFT-γ Mie cannot properly account for the formation of rings from a monomer fluid as all components are assumed to be linear chains. Though some effort has been recently made to include ring formation in SAFT,[107] the version implemented here does not account for these effect. As a result, the methylene group of linear alkanes (CH_2) cannot be used to model cyclohexane, for which a different group (cCH_2) must be defined. Cyclohexane is therefore modelled as

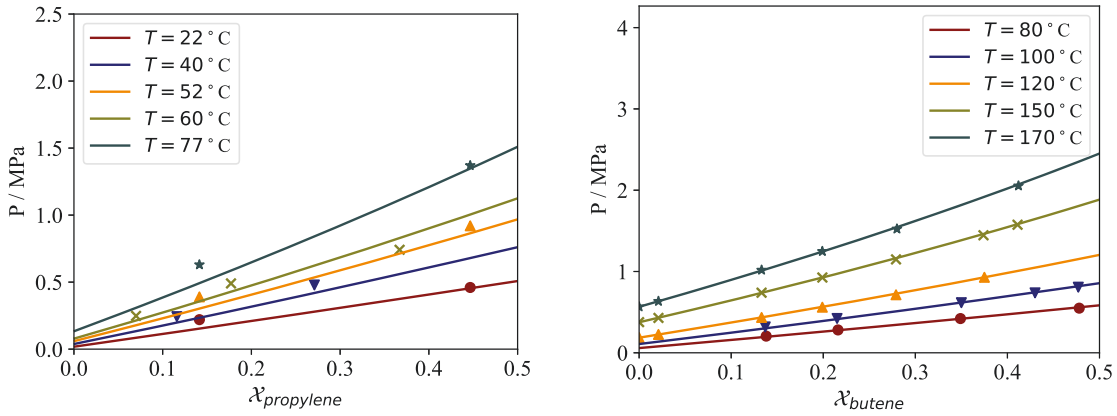

(a) (b)

Figure 2.4.: Bubble pressure curves of (a) 1-propylene + *n*-hexane and (b) 1-butene / *n*-heptane mixtures. The solid curves represent SAFT-γ Mie calculations, while markers experimental data from Mallepally and coworkers[105] and Thoedtmann and coworkers,[106] respectively. Notice that propylene and longer alk-1-enes are modelled using the original CH_2= group as opposed to the newly-defined CH_2^{eth}= group which is used only for ethylene.

a collection of 6 united-atom cCH_2 groups, whereas benzene as a collection of 6 united-atom aromatic carbon groups (aCH) and toluene as 5 aCH groups and one coarse-grained $aCCH_3$ group.

The like and unlike SAFT-γ Mie parameters of the cCH_2 and aCH groups were developed by Dufal and coworkers[68] to model pure component and mixture properties of cyclohexane, benzene and their mixtures with a variety of organic compounds. After comparison with experimental data it was found that the interaction between the cCH_2 and CH_2 had to be modified slightly from 469.67 K to 471.85 K to reproduce the solubility of cyclohexane in eicosane (see Figure 2.3b). The like SAFT-γ Mie parameters involving the $aCCH_3$ group were proposed by Papaioannou and coworkers[100] to reproduce the pure component properties of toluene. Some of its unlike parameters have been proposed later by Hutacharoen and coworkers[101] to reproduce pure component and mixture properties of various alkanes and alkanols.

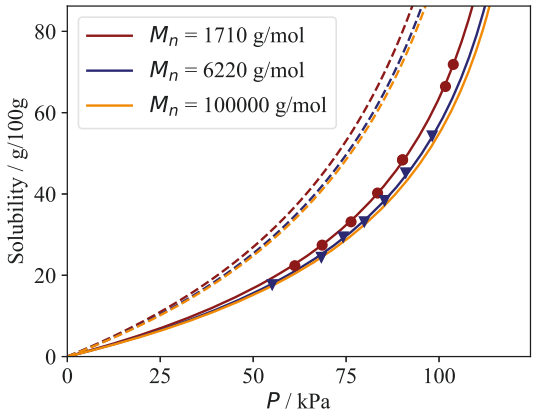

Figure 2.5.: Solubility of toluene in molten polyethylene of mean molecular weight $M_n = 1710$ g/mol, $M_n = 6220$ g/mol and $M_n = 100,000$ g/mol at 120 °C. Solid curves are SAFT-γ Mie calculations for monodisperse PE with the optimised ϵ_{kl} between toluene's aCCH$_3$ group and PE's CH$_2$ group (*cf.* Table 2.2), while dashed curves represent calculations with the parameter proposed by Hutacharoen and coworkers.[101] Symbols are experimental data from Wohlfarth and coworkers.[108]

However, no reference is made regarding the inclusion of mixture properties of toluene and alkanes in the parameterisation procedure. As shown in Figure 2.5, the SAFT-γ Mie predictions overestimate the solubility of toluene in molten PE using the unlike energy well depth $\epsilon_{kl}/k_B = 569.18$ K between the aCCH$_3$ group and the CH$_2$ group developed by Hutacharoen and coworkers (dashed curves). This parameter is therefore changed to 525.18 K (solid curves in Figure 2.5; *cf.* Table 2.2). These modifications ensure that the fluid-phase behaviour or cyclohexane + PE and toluene + PE mixtures is predicted accurately by our SAFT-γ Mie model (*cf.* Section 2.5.2).

Water

Water is modelled as a single Mie monomer (H$_2$O) decorated with two association sites of type e and two sites of type H representing the two lone electron pairs on the oxygen and the two hydrogens, respectively. All of its like dispersion and association parameters

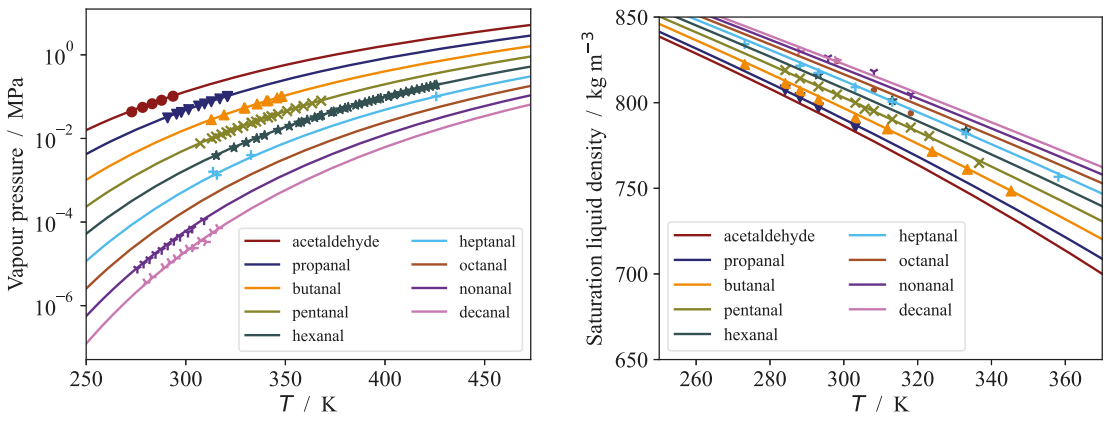

(a) (b)

Figure 2.6.: Pure component properties of the series of linear aldehydes. Solid curves represent SAFT-γ Mie calculations with the original parameter set reported in Tables 2.1 and 2.2, while symbols experimental data.[109–126] a) Vapour pressure b) Liquid density at saturation

(Tables 2.1, 2.2 and 2.2) were developed by Dufal and coworkers.[99]

Linear aldehydes

Linear aldehydes are modelled as linear chains made of a methyl group CH_3, a variable number of methylene groups CH_2 and a newly-defined terminal carbonyl group CHO. For example, pentanal is modelled as one methyl group, three methylene groups and a terminal carbonyl group. The group CHO is modelled as made of two identical segments ($\nu_k^* = 2$). As an example of a "standard" SAFT parameterisation procedure, the like SAFT-γ Mie parameters of the newly-defined CHO group and its unlike energy parameters with the CH_2 and CH_3 group are optimised to reproduce vapour pressure and saturation liquid density of the series of aldehydes, as well as the binary VLE properties of mixtures of linear aldehydes and *n*-alkanes. As seen in Figures 2.6 and 2.7, the optimal parameter set provides an accurate representation of the experimental data included in the parameterisation procedure.

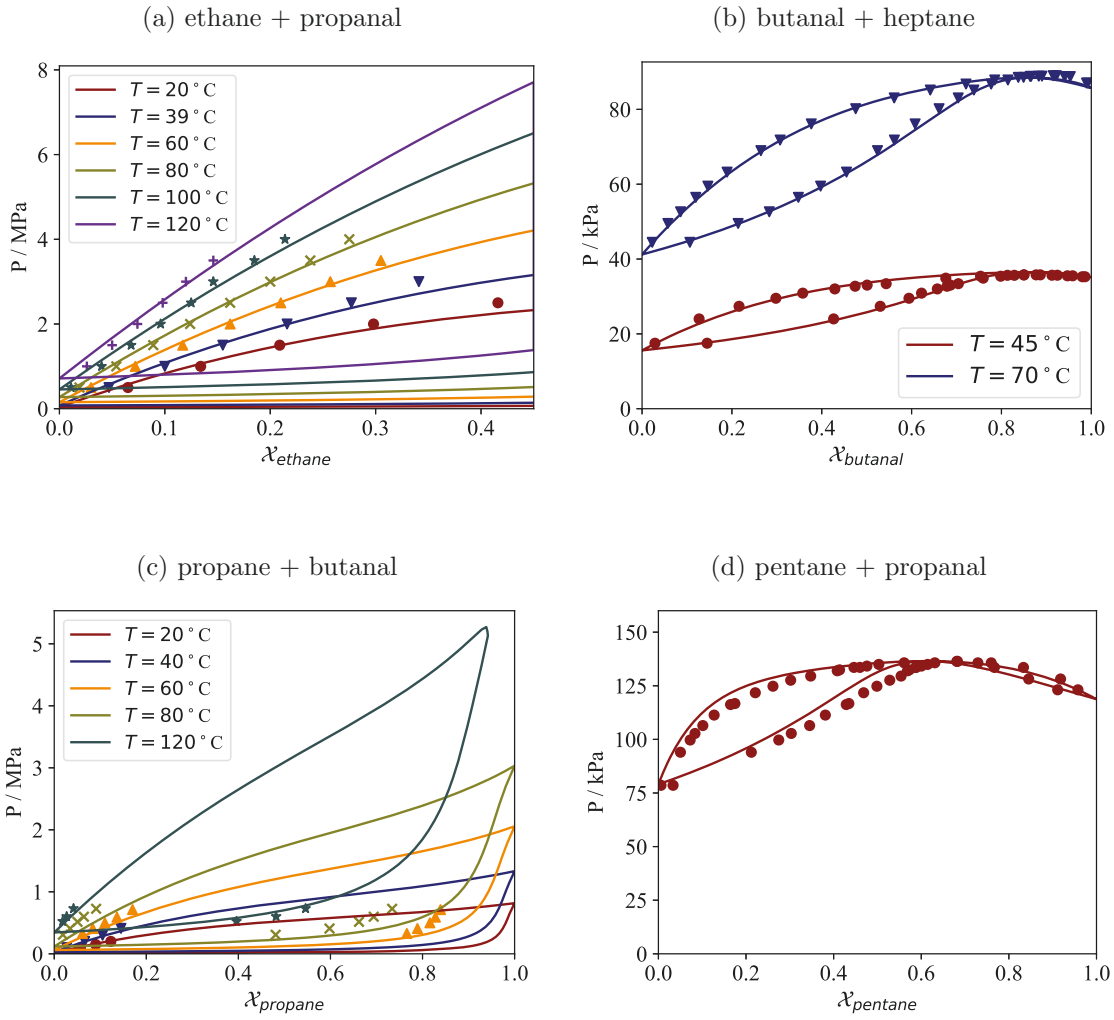

Figure 2.7.: Isothermal vapour-liquid diagram of mixtures of linear aldehydes and n-alkanes. Solid curves represent SAFT-γ Mie calculations, while symbols experimental data.[127–129]

2.5.2. Polymer models

This subsection contains the SAFT-γ Mie models of the polymers considered in the present work, i.e., PE, PEG and PP. All the relevant parameters are reported in Tables 2.1, 2.2 and 2.3. Due to the inability of SAFT-γ Mie to deal with random branching, every polymer considered here is a linear chain of well-defined repeating units which can be supplemented by two end units. Both the repeating and end units are simply defined in terms of the number and types of SAFT-γ Mie groups they are composed of. Therefore, by calling $\nu^{\mathrm{R}}_{k,\mathrm{p}}, \nu^{\mathrm{E}}_{k,\mathrm{p}}$ the number of groups of type k in the polymer's repeating and end units we can write

$$\nu_{k,\mathrm{p}} = 2\nu^{\mathrm{E}}_{k,\mathrm{p}} + n\nu^{\mathrm{R}}_{k,\mathrm{p}}, \tag{2.46}$$

where $\nu_{k,\mathrm{p}}$ is the number of groups of type k that defines the polymer molecule in the SAFT-γ Mie framework and n is the degree of polymerisation. Furthermore, in this work the polydispersity of the polymer samples is entirely neglected. Systems containing a given polymer are therefore assumed to be composed of polymer molecules with the same degree of polymerisation n. Given the mean molecular weight of a polymer M_n, the degree of polymerisation is thus found via

$$n = \left[\frac{M_n - 2\sum_k w_k \nu^{\mathrm{E}}_{k,p}}{\sum_k w_k \nu^{\mathrm{R}}_{k,p}} \right], \tag{2.47}$$

where $[x]$ denotes the nearest integer of x and w_k the molar mass of group k and the sum runs over all the distinct types of SAFT-γ Mie groups in the system.

Neglecting random branching and polydispersity should have a limited effect on the vapour-liquid equilibrium properties of polymer mixtures at fixed mass fraction fraction of polymer.[94,108,130,131] For example, as Figure 2.5 suggests the solubility of toluene in molten monodisperse PE quickly approaches a master curve for increasing M_n. In general, we expect that the VLE properties of polymer mixtures should depend only

slightly on the polymer's molecular weight distribution as long as the concentration of chain ends remains low – i.e., at moderate to high M_n.

Branching and polydispersity can however strongly influence liquid-liquid phase separation in polymer + solute mixtures, as seen both experimentally and confirmed by theoretical calculations and computer simulation.[73,94,132] Furthermore, these features affect out-of-equilibrium properties of polymer systems such as their melt viscosity and crystallisation rates.[60,133–135] Different molecular weight distributions or branching can therefore lead to very different crystallinity and microstructure in semi-crystalline polymer samples. This is exemplified by the family of polyethylenes, whose crystallinity at room temperature can vary from about 20% for highly branched samples (LDPE) up to around 80 % for non-branched samples (HDPE).[136] Therefore, in the present work all of these effects are neglected at the EoS level but indirectly influence the fluid solubility in semi-crystalline polymers by determining their sample-specific properties (*cf.* Chapter 3).

It is critical to ensure that the equation of state and its parameters properly represent the vapour-liquid equilibrium properties of each polymer + solute mixture. An inaccurate model at the EoS level can introduce systematic errors in the solubility predictions in semi-crystalline polymers, as the properties of the amorphous domains are written in terms of those of a subcooled polymer melt described by the EoS (*cf.* Chapter 3). In turn, this can lead to systematic bias in the sample-specific parameters of a semi-crystalline polymer, which are also optimised to reproduce solubility data. For each polymer listed below, the accuracy of the SAFT-γ Mie predictions for molten polymer + solute mixtures must therefore be tested before using the composite model described in Chapter 3.

PE

Polyethylene (PE) is modelled as a linear sequence of CH_2 groups (i.e., as a long *n*-alkane; Figure 2.1). The end units, when present, are two CH_3 groups. Although the transferability of groups developed for short molecules to long polymers is not guaranteed in SAFT-γ Mie due to the approximations of TPT1 (*cf.* Section 2.2), using the same model for short *n*-alkanes and PE provides semi-quantitative predictions for the solubility of pentane in PE (bubble curves) and the UCST of propane + hexacontane mixtures.[67] In addition, the SAFT-γ Mie parameters between the CH_2 group and all of other SAFT-γ Mie groups needed to model solute + polyethylene mixtures in the present work have been explicitly optimised to reproduce properties of systems containing *n*-alkanes and/or PE (*cf.* Section 2.5.1). We note that this procedure can be avoided by defining a second order polymer group $CH_2{}^{PE}$ and separately develop part of its parameter set by including only polymer properties in the parameterisation procedure. This is what was done for the PP and the PEG groups (see below).

It is important to note that no distinction is made between randomly branched PE – e.g., low- and medium-density PE (LDPE and MDPE, respectively) – , regularly branched PE copolymers – i.e., linear low-density PE (LLDPE), obtained by copolimerisation of ethylene with other alk-1-enes – and linear PE – i.e., high-density PE (HDPE). It could be possible to model LLDPEs such as polyethylene-*co*-butene or polyethylene-*co*-hexene by considering bigger repeating units including a variable number of CH_2 groups, a CH group and a CH_3 group. However, we expect that the effect of these branches on fluid-phase VLE properties should be minor as they normally constitute only a fraction of the repeating units[137,138] and their chemical nature is very close to that of the backbone.

PP

In this work, polypropylene (PP) is modelled as a homonuclear chain – i.e., composed of a single repeating monomer – of coarse-grained groups $CH_2CH(CH_3)$ which are hereafter named PP_{mono} (Figure 2.1). This molecular model and its parameters were proposed by Fayaz-Torshizi and Müller[73] to reproduce the saturation liquid density and vapour pressure of short, branched alkanes. However, the authors did not propose any unlike interaction parameters. Since in Chapter 3 the solubility of *n*-hexane, *n*-heptane, cyclohexane and toluene in semi-crystalline PP is predicted, it is important to ensure that the SAFT-γ Mie model accurately reproduces the VLE properties of fluid mixtures of these solutes and polypropylene.

To this end, the SAFT-γ Mie predictions are compared with experimental solubility data of the four compounds in atactic PP (aPP). This PP isomer lacks regular sterochemical configuration of the side-chain methyl groups and is practically fully amorphous at all temperatures. In particular, at room temperature this polymer does not form a glass but rather an equilibrium subcooled melt – as confirmed by its waxy appearance[139] – and therefore constitutes an ideal system for EoS testing in that temperature range (where stereoregular PP samples would invariably be semi-crystalline). The experimental data was kindly provided by Dr. J. Ramadani and Prof. D. Williams. (Imperial College London, Department of Chemical Engineering). The unlike energy well depths ϵ_{kl} between the PP_{mono} group and the CH_2 group (*n*-hexane, *n*-heptane), the cCH_2 group (cyclohexane) and the $aCCH_3$ group (toluene) are therefore optimised (via minimisation of 2.45) to reproduce the solubility of the respective compounds in aPP. The optimised parameters can be found in Tables 2.2, whereas comparison with experimental data is shown in Figure 2.8. Notice that the unlike dispersion energies reported in previously published work[139] are wrong due to a bug in the code calculating combining rules. Errata corrige was submitted to the Journal of Physical Chemistry B to amend

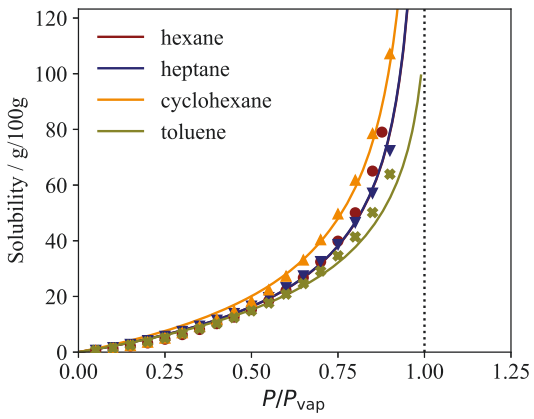

Figure 2.8.: Solubility of n-hexane, n-heptane, cyclohexane and toluene at 25 °C in atactic PP as a function of the ratio of pressure and the partial pressure of each respective substance. The calculations shown use the optimised unlike energy well depths reported in Table 2.2 instead of combining rules. aPP is a fully amorphous, waxy solid at room temperature and should therefore be described accurately by a fluid-phase EoS such as SAFT-γ Mie.

the inaccuracy.

PEG

Polyethylene glycol (PEG) is a polymer characterised by the oxyethylene repeating unit (CH_2CH_2O). The name polyethylene oxide (PEO) is sometimes given to high-molecular weight PEG molecules. By employing a united-atom modelling approach, in the present work the oxyethylene repeating unit is split in two "oxyethylene" methylene groups $CH_2{}^{OE}$ and an oxygen group cO (Figure 2.1). Both of these groups were defined by the present author in his MSc work recently submitted for publication.[94] The $CH_2{}^{OE}$ group is a second-order group accounting for the presence of the electronegative oxygen on the polarisability and therefore dispersion potential of the CH_2 group found on n-alkanes. Therefore, the $CH_2{}^{OE}$ has the same like SAFT-γ Mie parameters of the CH_2 group but potentially different unlike parameters with other groups.

The oxygen group cO represents instead the oxygens in linear polyethers located more

than one carbon away from chain ends and is decorated by one association site of type *e*. Depending on the polymerisation conditions, the ends of PEG can be hydroxil (OH) or methyl (CH_3) groups. For hydroxy-terminated PEG molecules two CH_2OH groups are added to the polymer's definition. This group was developed by Hutacharoen and cowokers[101] to represent pure component and mixture properties of primary alcohols. Methyl-terminated PEGs are not considered here but can be modelled using the methyl CH_3 end group.

The like SAFT-γ Mie parameters of the $CH_2{}^{OE}$ and cO groups and their unlike parameters with the H_2 and CH_2OH group are reported in Tables 2.1, 2.2 and 2.3 and have been optimised to reproduce the closed-loop miscibility gap observed in the orthobaric phase diagrams of PEG + water mixtures.[94] In Figure 2.9 the model's predictions for the solubility of water vapour in molten PEG as a function of the water pressure (bubble pressure curves) are compared to experimental data by Malcolm and Rowlinson[140] and Herskowitz and Gottlleb.[141] The agreement between the predictions and the experimental data is excellent, especially considering that these properties were not included in the parameterisation procedure. In the present work, the parameter set developed previously is used without modifications since only mixtures of water and PEG are considered.

Concluding remarks

In this Chapter the SAFT-γ Mie equation of state has been presented. In Sections 2.2 and 2.3 the formal aspects of theory and its link to equilibrium thermodynamic properties of fluids have been discussed. In Sections 2.4 and 2.5 we have shown how a top-down parameterisation procedure can be employed to develop transferable SAFT-γ Mie group parameters that allow prediction of a range of fluid-phase properties of

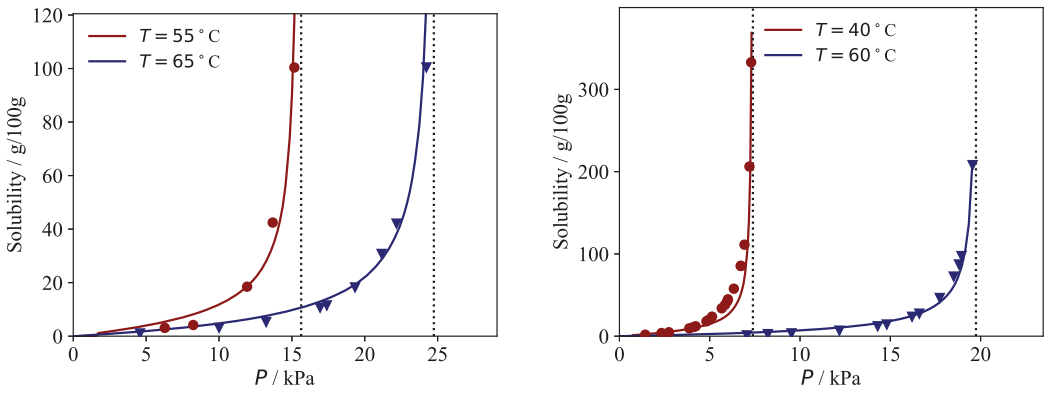

(a) (b)

Figure 2.9.: Solubility of water vapour in molten PEG (symbols) and corresponding SAFT-γ Mie theoretical calculations (solid curves) using the parameters provided in Tables 2.1, 2.2 and 2.3 as a function of pressure. The vertical dashed curves correspond to the vapour pressure of water at the respective temperatures. (a) Data from Malcolm and Rowlinson[140] ($M_n = 3,000$ g/mol) (b) Data from Herskowitz and Gottlleb[141] at 40 °C ($M_n = 600$ g/mol) and 60 °C ($M_n = 6,000$ g/mol).

both small molecules and polymers. In particular, we have presented molecular models and corresponding optimised SAFT-γ Mie parameters for solutes (n-alkanes, 1-alkenes, cyclohexane, toluene, aldehydes and water) and polymers (PE, PP, PEG) that will be further investigated in the current work. In Chapter 4, the accurate description of mixtures of small molecules and liquid polymer melts provided by SAFT-γ Mie is coupled with a methodology developed in Chapter 3 to describe fluid sorption and a range of other thermodynamic properties of semi-crystalline polymers.

3. Statistical-Thermodynamics of Semi-Crystalline Polymers

Chapter overview

This Chapter is structured as follows. In Section 3.1 the latest experimental evidence on the microstructure and thermodynamic properties of semi-crystalline polymers is reviewed, forming the basis of our subsequent discussion. In Section 3.2, a general formalism to describe the equilibrium between small-molecule fluids and semi-crystalline polymers is presented after a review of previous literature. Finally, in Section 3.3 a new thermodynamic model is developed to address incompatibilities between state-of-the-art theories of fluid sorption in semi-crystalline polymers and our current understanding of their structure and thermodynamics.

3.1. Structure and thermodynamics

This Section opens with an overview of the morphology and thermodynamic stability of polymer crystals (Section 3.1.1). In Section 3.1.2, the microstructural features of semi-crystalline polymers and basics of crystallisation theory are discussed. Section 3.1.3 is

dedicated to the description of polymer chain topology in the inter-lamellar domains, supplemented by a survey of relevant theoretical and computational work. In Sections 3.1.4 and 3.1.5 the concepts of crystal-fixed *vs* crystal-mobile polymers and of free *vs* constrained amorphous domains are introduced. The Section concludes with an overview of experimental methods to determine the crystallinity of a sample.

3.1.1. Stability of polymer crystals

Elementary thermodynamic considerations suggest that a melt of monodisperse and stereoregular homopolymers at fixed pressure P should freeze at a temperature $T_{\mathrm{m}}^{0} > 0$ K called the freezing point – in principle a function of molecular weight and pressure – in a well-defined crystalline phase. For polymer melts, the equilibrium crystalline structure is an extended-chain crystal[142,143] in which polymer chains are aligned along the [001] crystallographic axis*. Preparing such crystal structures however requires high temperatures and pressures, an isothermal crystallisation and sufficiently flexible polymers. For example, extended-chain PE crystals with an hexagonal unit cell were first prepared by Wunderlich and coworkers[145] at pressures up to 5.3 katm. At lower (i.e., ambient) pressures, the stable crystal structure of PE was later found to be orthorombic,[146,147] which is the same structure observed in semi-crystalline PE. Aside from PE, other polymers such as PEO,[148–152] PTFE[153] and PET[154] are known to form extended-chain crystals under the right conditions.

Nevertheless, under most crystallisation conditions homopolymers do not form extended-chain crystals. Rather, by regularly folding several times they form *quasi*-2D crystalline structures called *lamellae* whose lateral dimensions (of the order of micrometers) are much bigger than their thickness l_{c} – known as the lamellar thickness –, which can vary

*One should note that the polymer chains can form helices around the [001] axis such as in the monoclinic α form of isotactic PP[144]

from a few to tens of nanometers depending on the polymer considered.[155,156] Since chain folding occurs entirely on the two major surfaces of the lamellae, we denote the latter "fold surfaces". Conversely, the remaining surfaces are denoted "lateral lamellar surfaces".

The first strong evidence that chain folding was the preferential mechanism of polymer crystallisation came in 1957[157–159] with the successful observation of solution-grown PE crystals formed by individual polymer molecules. However, the formation of these structures was expected as single-chain extended-chain crystals cannot be formed. On the other hand, it was initially thought that crystals in melt-crystallised samples were formed by bundles of different polymer chains rather than by a smaller number of chains folded multiple times – the so-called "fringed-micelle" morphology. In the 1960s, theoretical analysis by Flory,[160] Keller[161] and others found the fringed-micellar configuration to be thermodynamically unfavourable, leading to widespread recognition that semi-crystalline polymers possess a folded lamellar morphology.

We shall here apply simple thermodynamic considerations to establish the range of stability of pure lamellar crystals. At fixed temperature T and pressure P, the sign of the Gibbs free energy difference ΔG between a lamella of thickness l_c and an equivalent mass of molten polymer[†] determines whether the lamella is thermodynamically stable ($\Delta G < 0$) or whether it melts ($\Delta G > 0$). This quantity can be written as a sum of a bulk term and a surface term:[28,162]

$$\Delta G = \Delta G_{\text{crys}} + \Delta G_{\text{surface}}. \tag{3.1}$$

Here, ΔG_{crys} is the Gibbs free energy difference between equivalent masses of extended-chain crystalline polymer and molten polymer. By using the fact that the Gibbs free

[†]It is more convenient to reason in terms of mass as individual polymer molecules are in general part of multiple lamellae.

energy G of the extended-chain crystal and of the melt is the Legendre transform of their respective enthalpy H, the following holds:

$$\left(\frac{\partial\left(\Delta G_{\mathrm{crys}} \,/\, T\right)}{\partial\left(1 \,/\, T\right)}\right)_{P} = \Delta H_{\mathrm{crys}}. \tag{3.2}$$

Since at the equilibrium melting point T_{m}^{0} we have $\Delta G_{\mathrm{crys}}(T_{\mathrm{m}}^{0}) = 0$, by expanding $\Delta G_{\mathrm{crys}}/T$ around $T = T_{\mathrm{m}}^{0}$ at first order in powers of $1/T$ we then obtain

$$\Delta G_{\mathrm{crys}}(T, P) \approx \Delta H_{\mathrm{crys}}^{0}(P)\left(1 - \frac{T}{T_{\mathrm{m}}^{0}}\right), \tag{3.3}$$

where $\Delta H_{\mathrm{crys}}^{0}(P) = \Delta H_{\mathrm{crys}}(T_{\mathrm{m}}^{0}, P)$. Due to the similarity between the density of the crystalline and molten polymer, pressure has a negligible influence on these quantities at low to moderate pressure and is therefore neglected in the following development.

Conversely, $\Delta G_{\mathrm{surface}}$ represents the interfacial free energy contribution due to the existence of the fold surfaces and the lateral lamellar surfaces. Since the lateral dimensions of the lamellae are generally much bigger than the lamellar thickness, the surface free energy is dominated by the contribution of the fold surface:

$$\Delta G_{\mathrm{surface}} \approx 2\sigma_{\mathrm{e}} A_{\Sigma}. \tag{3.4}$$

Here, A_{Σ} represent the area of one of the two fold surfaces of the lamella. The fold surface free energy per unit area, σ_{e}, originates from the entropic and energetic penalties to chain folding[28,142,160,163–167] as well the accumulation of topological defects such as chain ends and entanglements in the amorphous domains[168–172] (See Section 3.2).

By combining 3.4 with the preceding equations and dividing by the polymer mass, we

obtain

$$\Delta g(T) \approx -\Delta h_{\mathrm{m}}^{0}\left(1-\frac{T}{T_{\mathrm{m}}^{0}}\right)+\frac{2\sigma_{\mathrm{e}}}{\rho_{\mathrm{c}} l_{\mathrm{c}}}, \tag{3.5}$$

where ρ_{c} is the crystal density, Δg the specific Gibbs free energy of formation of a lamella and $\Delta h_{\mathrm{m}}^{0} = -\Delta h_{\mathrm{crys}}^{0}$ the specific enthalpy of fusion of an extended chain crystal at its melting point. We have also used the fact that the volume V_{c} of the lamella can be approximated by $V_{\mathrm{c}} \approx A_{\Sigma} l_{\mathrm{c}}$. A lamella of thickness l_{c} will therefore melt at temperature T_{m} given by

$$T_{\mathrm{m}} = T_{\mathrm{m}}^{0}\left(1-\frac{2\sigma_{\mathrm{e}} T_{\mathrm{m}}^{0}}{\rho_{\mathrm{c}} \Delta h_{\mathrm{m}}^{0} l_{\mathrm{c}}}\right). \tag{3.6}$$

This is sometimes referred to as Gibbs–Thompson equation,[156] even though the term more appropriately refers to equations relating the free energy and the curvature of interfaces.[173,174] In Equation 3.6:

- the crystal density ρ_{c} does not vary significantly with temperature or pressure;
- $\Delta h_{\mathrm{m}}^{0}$ and T_{m}^{0} depend weakly on pressure and approach well-defined limits as the molecular weight increases;[169]
- the fold free energy is approximately constant for a given polymer at fixed stereochemical arrangement.[156,162,165]

As a result, the melting point of lamellar crystals of a given polymer sample lies on a straight line in the T_{m} versus l_{c}^{-1} plot which intersect the y axis ($l_{\mathrm{c}} \to +\infty$) at $T_{\mathrm{m}} = T_{\mathrm{m}}^{0}$. Similarly, at every temperature $T < T_{\mathrm{m}}$ only lamellae with thickness greater than a minimum l_{c}^{*} given by

$$l_{\mathrm{c}}^{*}(T) \approx \frac{2\sigma_{\mathrm{e}} T_{\mathrm{m}}^{0}}{\Delta h_{\mathrm{m}}^{0} \rho_{\mathrm{c}}\left(T_{\mathrm{m}}^{0}-T\right)}. \tag{3.7}$$

are stable with respect to the molten state. One should note that although this argument was initially made for the crystallisation of homopolymers, copolymers that containing non-crystallisable units (such as polyethylene-co-octene[156]) display a similar behaviour

with the caveat that the melting point of the extended-chain crystal, T_{m}^{0}, is lowered by the presence of non-crystallisable monomers.[170,175]

3.1.2. Microstructure and crystallisation

While melting of lamellar crystals can be described with reasonable accuracy by the methods just described, the molecular mechanisms that determine the typical value of l_{c} after crystallisation of semi-crystalline polymers have been at the center of much debate in the scientific community in the past decades.

Typically, isothermal crystallisation of homopolymer melts proceeds first by heterogeneous nucleation of primary (dominant) lamellae on pre-existing seeds (impurities, seeding agents or pre-formed nuclei), followed by a growth of secondary (subsidiary) lamellae in the uncrystallised mass between primary lamellae according to an in-filling mechanism.[156,176] Depending on the crystallization conditions, primary and secondary lamellae organise into bigger mesostructures such as *spherulites* or *shish-kebab* structures.[135,177] The lamellae usually stack on top of each other sandwiching layers of amorphous material in between, which are referred to as *inter-lamellar* amorphous domains. Although these alternating structures (the so-called "lamellar stacks") lack perfect order, they can be characterised by the average inter-lamellar distance l_{a} and the lamellar thickness l_{c} (or, equivalently, by the long period $LP = l_{\mathrm{a}} + l_{\mathrm{c}}$).

As a result, semi-crystalline polymer samples can be characterised by the mass fraction crystallinity ω_{c}, defined as the ratio between the crystalline polymer mass $m_{\mathrm{p}}^{\mathrm{c}}$ and the total polymer mass $m_{\mathrm{p}}^{\mathrm{tot}}$:

$$\omega_{\mathrm{c}} = \frac{m_{\mathrm{p}}^{\mathrm{c}}}{m_{\mathrm{p}}^{\mathrm{tot}}}. \tag{3.8}$$

The persistence of uncrystallised amorphous mass can be heuristically justified by realizing that the time needed for a macro-molecule to rearrange in configurations compatible

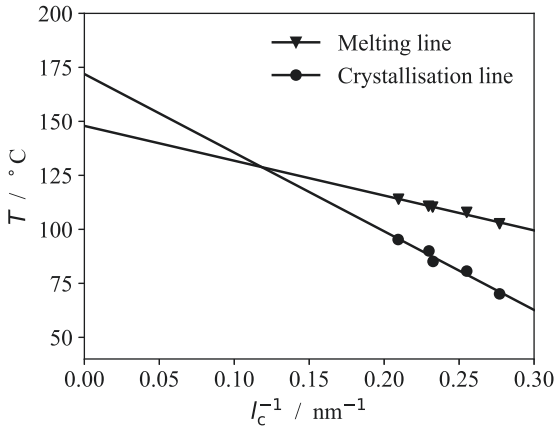

Figure 3.1.: Melting and crystallisation lines for a sample of syndiotactic polypropylene-co-octene (sPPcO15). The markers represent experimental measurements of the average lamellar thickness at various temperatures obtained using SAXS by Hauser and coworkers.[179] The polymer sample was first crystallised isothermally at the five temperatures indicated (circles) and then heated until melting occured (triangles). Note that the average lamellar thickness is not altered upon heating in sPPcO15 due to the absence of intra-crystalline chain dynamics (*cf.* Section 3.1.4). The solid lines represent linear fits of the experimental data.

with the formation of extended-chain structures far exceeds the characteristic timescale at which individual sections of the polymer are incorporated in different growing crystalline nuclei.[178] In general, the resulting lamellar and inter-lamellar size distribution is a function of the crystallisation temperature T_c and the polymer considered. Hoffman and Lauritzen[28,162] (HL) first conjectured using classical nucleation theory that the lamellar thickness of a growing crystal is kinetically selected by balancing nucleation and growth rates of individual crystalline folds with the thermodynamic driving force of crystallisation[‡].

In the HL theory, the average crystal thickness of the formed crystals $\langle l_c \rangle$ can be written as

$$\langle l_c \rangle \approx l_c^* + \delta l, \tag{3.9}$$

[‡]Essentially Equation 3.5 with the addition of lateral surface free energy terms

where l_c^* is given by Equation 3.7 and $\delta l > 0$ is directly proportional to the crystallisation temperature T_c at low to moderate undercooling.[142] The crystallisation line – obtained by plotting the T_c against $\langle l_c \rangle^{-1}$ – thus lies below the melting line (Equation 3.6 with $l_c = \langle l_c \rangle$). In particular, it is observed that the extrapolated lines intersect at a temperature $T_{crit} < T_m^0$ below which nucleation rates plummet due to the high free energy barriers to the formation of stable crystalline nuclei[156] (Figure 3.1). Although the HL theory has received a lot of attention since its original formulation, some authors have suggested that physical mechanisms other than kinetic ones are at the basis of the observed crystal size distribution. Strobl,[156] for example, has suggested a thermodynamic multiphasic scheme according to which lamellar thickness is selected by successive crystal reorganisations between polymorphic mesophases. The reader is referred to a recent review by Zhang and coworkers[143] for an in-depth account of the state of the art in polymer crystallisation theory.

3.1.3. Fold surface and chain topology in the inter-lamellar domains

After crystallisation, amorphous chains trapped in the inter-lamellar domains can be divided in five categories based on topological arguments (see Figure 3.2):

- bridges, i.e., chain segments that cross the inter-lamellar amorphous domains and "bridge" two adjacent lamellae;
- un-entangled loops, i.e., chain segments that start and end in the same lamella without being entangled with other loops;
- entangled loops, i.e., loops entangled with one or more loops on the opposite lamella;
- tails, i.e., polymer chain ends excluded by the crystal structure and tethered to one lamella;

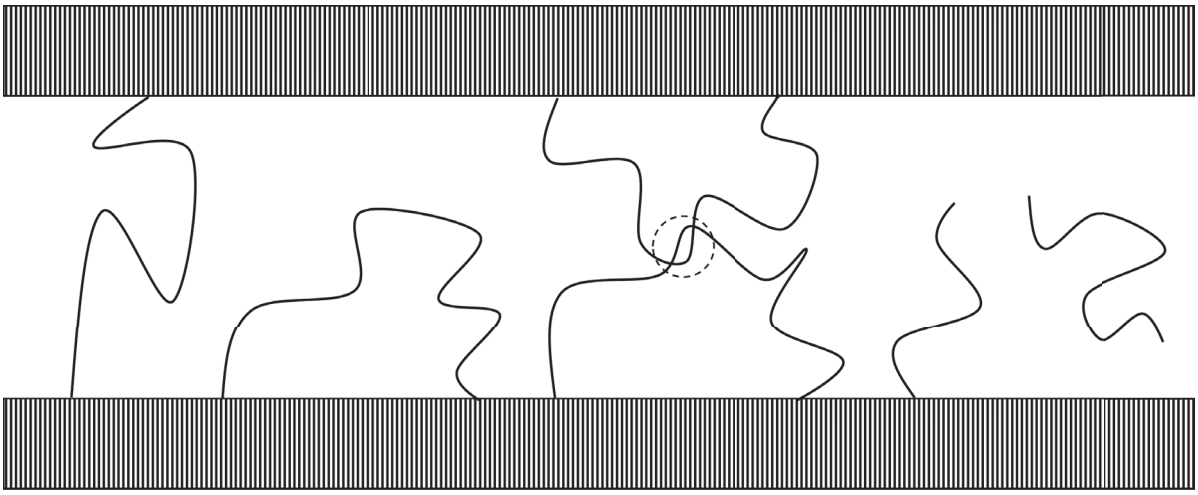

Figure 3.2.: A schematic representation of the five types of polymer chains that can be found in the amorphous domains. From left to right: bridges, un-entangled loops, entangled loops, tails, and free chains.

- free chains, i.e. entire polymer molecules able to diffuse in the inter-lamellar domains.

Both bridges and entangled loops are here collectively referred to as "tie-molecules" and are considered elastically effective upon deformation of the amorphous domains since they link mechanically two opposing lamelle,[7] in contrast to un-entangled loops and tails.

Tight-folds

As part of his argument against the fringed-micellar morphology, Flory[160] pointed out that due to the dissipation of the crystalline order in the amorphous phase and the continuity of the polymer molecules, a considerable number of loops had to remain confined in the crystal/amorphous interface – the so-called "tight-folds". Tight-folds can be discriminated by whether they perform adjacent or non-adjacent re-entry in the lamella they originate from[135,180] (i.e., in one of the neighboring crystal sites or not).

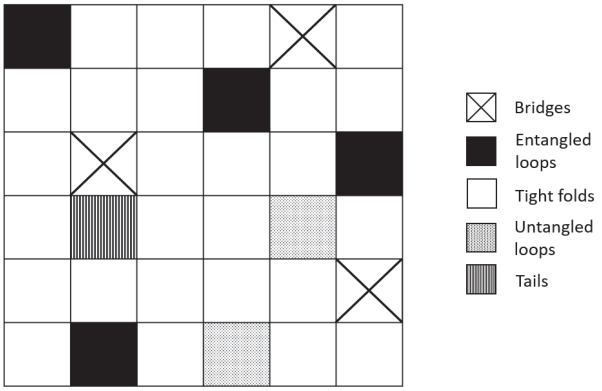

Figure 3.3.: A schematic representation of the (001) crystal plane of a hypothetical polymer crystal with a square 2D lattice section. The direction of the chain segments in the lamellae is perpendicular to this plane. The empty white squares represent tight-fold sites on the lamellar surface; the filled black squares represent stems connected to entangled loops; the crossed squares, bridges; the striped squares, tails; and the dotted squares, loose loops. The surface fraction of tie-molecules p_{T} is the ratio of the number of black and crossed sites to the total number of sites; in this illustration $p_{\mathrm{T}} = 7/36$, $p_{\mathrm{NT}} = 3/36$ and $p_{\mathrm{TF}} = 1 - p_{\mathrm{T}} - p_{\mathrm{NT}} = 26/36$. If a is the lattice parameter, for this square 2D lattice $\rho_{\mathrm{A}} = 1/a^2$.

The amorphous mass at sufficient distance from the interface is therefore only composed of tie-molecules, "loose" loops (i.e., un-entangled loops that are not tight folds) and tails.

By counting the number of crystalline stems crossing the crystal/amorphous interface, we denote with p_{TF} the fraction that perform tight-folds, with p_{T} the fraction connected to tie-molecules and with p_{NT} the fraction connected to loose loops and tails (Figure 3.3). Note that $p_{\mathrm{TF}} + p_{\mathrm{T}} + p_{\mathrm{NT}} = 1$. By calling ρ_{A} the cross-section of a chain in the crystal (obtained by counting the number of stems per unit area on the (001) plane), the surface density of stems performing tight folds ($\rho_{\mathrm{A,TF}}$), connected to tie-molecules ($\rho_{\mathrm{A,T}}$) and to loose loops and tails ($\rho_{\mathrm{A,NT}}$) on the crystal/amorphous interface is therefore given

by

$$\begin{aligned} \rho_{\mathrm{A,TF}} &= p_{\mathrm{TF}}\rho_{\mathrm{A}}\cos\gamma \\ \rho_{\mathrm{A,T}} &= p_{\mathrm{T}}\rho_{\mathrm{A}}\cos\gamma \quad , \\ \rho_{\mathrm{A,NT}} &= p_{\mathrm{NT}}\rho_{\mathrm{A}}\cos\gamma \end{aligned} \tag{3.10}$$

where γ is the chain-tilt angle between the [001] crystallographic axis (i.e., the chain direction) and the normal to the crystal/amorphous interface.[135] Although generally the chain-tilt angle is small, in PE it can vary between 20°and 40°.[181,182]

Even though direct experimental evidence of the existence of tie-molecules in semi-crystalline polymers has been available since the seminal work of Keith and coworkers,[183] quantities like p_{T} or p_{TF} have never been measured due to the challenge posed by resolving the contour of polymer strands in experiments.[184] As a consequence, a great body of work in the literature is dedicated to modelling the topology of inter-lamellar amorphous domains due to its great influence on the mechanical[7,185–194] and thermodynamic[39,195–200] properties of semi-crystalline polymers.

Soon after the establishment of chain-folding as the preferential mechanism of formation of polymer crystals, the relative amount of tight-folds performing adjacent *vs* non-adjacent re-entry became a subject of intense scientific debate. Flory was a proponent of the "random switchboard" model, according to which most of the tight folds should perform non-adjacent re-entry in the crystal. In 1984, Flory, Yoon and Dill[165] claimed using a 3D lattice model that p_{TF} should be approximately 0.7 and that only one every five tight-folds performed adjacent re-entry. In their model, calculations were performed by approximating the configurational partition function of loops in a semi-infinite 3D cubic lattice.

However, the previous year Monte Carlo (MC) simulation by Mansfield[164] using a similar lattice model had indicated that adjacent re-entry should be favoured unless explicit

energy penalty terms for their formation were included in MC transition probabilities. Their findings were supported by another theoretical investigation of the 3D lattice model of Marqusee and Dill,[166] who argued that adjacent tight folding should dominate even in the absence of energetic effects. Both works found that the fraction of tight folds should be about 0.72-0.75 when their formation is not penalised. Kumar and Yoon[167] then revisited the calculations of Flory, Yoon and Dill and found that both energetic penalty terms and chain-tilt influence significantly the probability of occurrence of tight-folds of both kinds. In particular, their calculations indicate that in the in the absence of energy penalties the fraction of tight-folds in PE with a realistic tilt angle ($\gamma = 40°$) should be approximately 0.5.

Bridges

Guttman, DiMarzio and Hoffman's[201,202] Gambler's Ruin (GR) model was one of the first theories to include the finite extension of the amorphous domains in the description. In the GR model, polymer chains are assumed to perform a 3D random walk in the inter-lamellar domains starting from one of the two lamellae. Chains that start and end in the same lamella are categorised as loops, whereas chains that end in the opposite lamella as bridges. In the limit of high-molecular weight, the GR model predicts that the fraction of bridges should be inversely proportional to the inter-lamellar spacing l_a and that at zero chain tilt ($\gamma = 0$, Equation 3.10) the fraction of tight folds should be about 2/3 to avoid density anomalies[184,201,202]

In later theoretical work, Huang and Brown[190] (HB) proposed another approach based on the observed dependence of slow crack growth rates in semi-crytalline PE. The HB model assumes that bridges can only be formed if the end-to-end distance of the polymer molecules in the melt is bigger than the sum of the inter-lamellar distance l_a and double the lamellar thickness l_c. This hypothesis leads to the fraction of bridges in the inter-

lamellar domains depending on the lamellar thickness, crystallinity and the polymer's molecular weight.[190] More recently, Adikhari and Muthukumar[184] improved upon the HB model by accounting for the ability of individual polymer chains to form links with multiple lamellae. Their analytical model predicts that the fraction of bridges should decrease with decreasing molecular weight and increasing inter-lamellar distance and be smaller than about 0.06 for realistic parameter combinations.

Entanglements

The models just mentioned only provide predictions for the fraction of bridges but neglect entangled loops, even though a high concentration of entanglements is expected in the amorphous domains. In fact, the entanglements between polymer chains in the melt are mostly segregated during the crystallisation process and accumulate in the amorphous domains due to the timescale mismatch between crystal accretion rates and reptation dynamics.[172,178,203–205] Various modifications to the Huang and Brown theory have been proposed to account for the effects of entanglements,[188,191] which were reviewed by Seguela.[7] However, analytical models predicting the amount of entanglements that persists in the inter-lamellar domains as a function of crystallisation conditions are missing.

The question has been instead addressed via computer simulation. A lattice Monte Carlo study by Lacher, Bryant and Howard[206] showed that increasing the inter-lamellar distance l_a decreases the bridge fraction, whereas the number of entangled loops stays constant or increases. More recently, Nilsson and coworkers[207] predicted using a 3D random-walk model that the fraction of tie-molecules p_T (bridges and entangled loops) should not exceed 0.1 and that in most conditions the number of entangled loops is about double the number of bridges. In their work, the configurations of polymer molecules between two plates were generated using the rotational isomeric state model.[207]

Limits of our current understanding

Despite their differences, all theories and computer simulation models described invariably assume that the resulting chain topology after crystallization can be obtained by using the chain statistics valid in the melt. As a result, these models cannot account for the chain reorganization on the mesoscale that happens during crystallization[7,156] or the increase in entanglement density in the inter-lamellar domains compared to the melt caused by crystallisation.[172]

There are some exceptions to this trend. In the past three decades Rutledge and coworkers[182,208–215] have used a combination of a realistic united-atom force fields and a topology-altering Monte Carlo scheme to predict the thermo-mechanical response (i.e. elastic moduli, shear stress) of the inter-lamellar domains of PE, PE copolymers and PP. Since the chain topology is allowed to vary during the simulation, the inter-lamellar domains display an "equilibrium" distribution of loops, bridges and tails determined by the various simulation parameters. It is also worth mentioning the contribution of Uneyama and coworkers,[216] who proposed a self-consistent field-theoretical model allowing to obtain various statistical properties of the inter-lamellar polymer chains by minimisation of an appropriate free energy functional.

Nonetheless, there is no evidence that the topology of the inter-lamellar domains should conform to the distributions proposed by these authors either – although arguably these methodologies represents more closely the pseudo-equilibrium state of the inter-lamellar domains compared to the theories using unperturbed chain statistics. More work is therefore needed to predict chain statistics directly from crystallisation conditions or from sample-specific properties such as crystallinity and molecular weight distribution.

3.1.4. Crystal-fixed and crystal-mobile polymers

A large class of flexible semi-crystalline polymers such as PE, isotactic PP, PEO and PTFE display variation of crystallinity and lamellar thickness with temperature, an effect deemed premelting or partial melting.[156,217] This phenomenon highlights the presence of mass exchanges between the crystalline regions and the amorphous domains in these polymers, showing that the crystal size distribution is not only determined by kinetic effects during crystallisation. In particular, electron microscopy,[218] small-angle X-ray scattering[155,200] and temperature-modulated DSC[219–221] measurements have shown that this mass exchange is partially or entirely reversible, indicating the existence of a local equilibrium at the crystal/amorphous interface.

In the past decades, time-domain nuclear magnetic resonance (TD-NMR) analysis of semi-crystalline samples has contributed significantly to the current understanding of the molecular mechanisms at the basis of this exchange equilibrium.[205,217,222–229] TD-NMR can shed insight on the relaxation dynamics of the molecular strands polymer chains both in melts and in semi-crystalline polymers by measuring the recovery time of nuclear spin polarisation after a radio-frequency pulse.[229] In particular, analysis of the so-called T_2 relaxation decay – also known as the "transverse" relaxation time, caused by nuclear spin-spin coupling – indicates the presence of various relaxation processes (or "modes") characteristic of semi-crystalline polymers.[222,230] Among these, the α_c-relaxation mode is associated with the presence of intra-crystalline chain dynamics (ICD)[205,228] – i.e. the longitudinal sliding motion of chains in the polymer crystal.

Boyd[222] first noted that polymers with active α_c-relaxation mode displayed on average higher crystallinity due to annealing of the lamellar crystals during and after isothermal crystallisation. Building on Boyd's intuition, Hu and Schmidt-Rohr[223] postulated that polymers can be categorised in "crystal-fixed" and "crystal-mobile" depending on whether they display the characteristic α_c-relaxation mode. Examples of crystal-

fixed polymers are copolymers of ethylene with long 1-alkenes such as polyethylene-co-octene,[231] syndiotactic PP (sPP)[156] and poly(ϵ-caprolactone).[232] Conversely, PE homopolymers, isotactic PP, PEO, PTFE, and polybutadiene (PBD) are all crystal-mobile at room temperatures.[156] Since Hu and Schmidt-Rohr, various authors have systematically applied this concept to differentiate the phenomenological behaviour of these two classes of polymers.[156,205,228]

In crystal-fixed polymers the size distribution of the lamellae is determined at crystallisation (as discussed in Section 3.1.2) and is quite narrow.[156] Upon increasing temperatures, the smallest lamellae become unstable (*cf.* Equation 3.7) leading to continuous crystal melting and recrystallisation,[205] whereas the bigger lamellae maintain their size due to the absence of ICD. On the other hand, in crystal-mobile polymers the lamellae spontaneously thicken already during crystallisation due to the crystal/amorphous exchange equilibrium enabled by the α_c-relaxation. In particular, the lamellae can undergo reversible partial melting at temperatures T smaller than their melting point (Equation 3.6). This process leads to a size selection of the inter-lamellar domains in the case of crystal-mobile polymers as the crystal thickening is balanced by entropy loss in the inter-lamellar domains caused by an increase in entanglement density and decrease in chain flexibility.[156,164,172,200] In the following, this assumption is deemed "local-equilibrium hypothesis".

Roe, Krigbaum and Smith[195,196] first used this idea to describe the reversible variation of crystallinity observed in semi-crystalline polyethylene (i.e., premelting). Their model assumed an isotropic crystalline morphology resembling the "fringed-micelle" model and predicted that the crystallinity at each temperature was a function of the number of statistical links N_c of amorphous chains that first deposit on growing crystals. The local-equilibrium hypothesis was later used by Fischer[197] and Zachmann and Peterlin[198] to predict the variation of inter-lamellar distance with temperature. These authors assumed that the inter-lamellar amorphous domains are composed only of un-entangled

loops and the resulting empirical parameters of the models needed to fit melting data – in this case, related to the average length of loops at crystallisation, N_0 – had unphysical values.[200]

More recently, Mansfield and Rieger[199,233] and Albrecht and Strobl[200] assumed, by contrast, that these domains are only composed of a network of entangled segments. This hypothesis is more compatible with the local-equilibrium hypothesis, as un-entangled loops should be eventually absorbed in the lamellae due to ICD. Mansfield and Rieger reasoned that the entangled chain segments in the inter-lamellar mass orient anisotropically upon increasing the inter-lamellar distance due to their anchoring points being fixed on the lamellar surface. Albrecht and Strobl noted that Mansfield and Rieger's model led to a conservation of the anisotropic features of the inter-lamellar domains at melting, which was deemed unphysical. Even though there is no indication that the entangled state of the inter-lamellar domains can be reversibly relaxed until complete melting, Albrecht and Strobl managed to obtain the correct limit by adding a term to the free energy accounting for the mobility of the entangled network junctions.

Both of these models managed to correctly capture the variation of the inter-lamellar distance with temperature after adjusting the average number of statistical segments in the loops at crystallistation (N_0) to reproduce experimental premelting data, with Albrecht and Strobl's model leading to more physically meaningful values. Nevertheless, both models contain a severe inconsistency as they assume that the end-to-end distribution of the polymer chains in the inter-lamellar domains can be described by Gaussian statistics. This approximation is only valid when the fractional extension of the chain segments (i.e., the ratio between their end-to-end distance and the one in their extended configuration) is small, whereas the local-equilibrium hypothesis predicts that chain segments should be very taut at temperatures sufficiently below the melting point[7,39,195,205] – as it is shown later in the current work (Section 4.1).

3.1.5. Free and constrained amorphous domains

In most experimental and theoretical works, semi-crystalline polymers are approximately described by the lamellar stack or "2-domain" model, which stipulates that all amorphous mass lies between crystalline lamellae. Although this model is accurate for homopolymers with high crystallinity, samples cooled at very low temperatures or whose molecules possess enough defects (i.e., comonomers and branching) display a fringed-micellar / nodular morphology in which "islands" of lamellar stacks are surrounded by amorphous mass.[176] A transition must therefore occur upon decreasing crystallinity between the lamellar stack morphology and the fringed-micellar one.

Measurements of the T_2 transverse relaxation time in low-field ^{1}H TD-NMR experiments suggest[224,234–238] that two populations of amorphous chains exist in semi-crystalline polymers: the mobile amorphous fraction (MAF) and the rigid amorphous fraction (RAF). While the small transverse relaxation time of the RAF implies that polymer chains producing that signal are taut and/or constrained, the longer relaxation times of the MAF indicates unconstrained, melt-like behaviour of the respective polymer strands.

In order to reconcile this observation with the 2-domain model, most authors assume that the RAF is composed of amorphous chains with limited mobility at the crystal/amorphous interface and that the MAF is all the remaining inter-lamellar amorphous mass. As recently noted by Chmelař and coworkers,[238] this assignment cannot be correct at lower crystallinity. The authors suggested instead that for PE samples with low-to-medium crystallinity the "constrained", rigid portion (RAF) is presumably the inter-lamellar amorphous mass whereas the "free", unconstrained portion (MAF) corresponds to amorphous mass outside of the lamellar stacks or in contact with the lateral lamellar surfaces. Using a spherulite reconstruction technique, Chmelař and coworkers also demonstrated that such free amorphous domains are expected at crystallinity lower

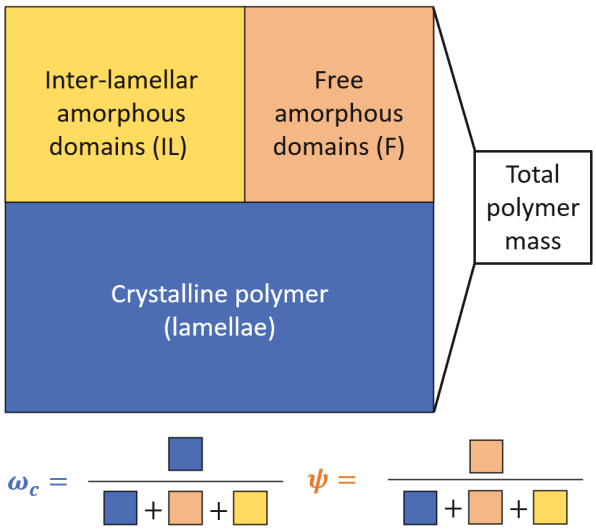

Figure 3.4.: A schematic representation of the "three-domain" model. The entire square represents the total polymer mass, whereas the coloured regions the mass of polymer in each of the respective domains.

than about 60%.

As shown in Figure 3.4, we can define ψ as the ratio between the free amorphous mass, $m_{\mathrm{p}}^{\mathrm{F}}$, and the total polymer mass $m_{\mathrm{p}}^{\mathrm{tot}}$ in a manner analogous to Equation 3.8:

$$\psi = \frac{m_{\mathrm{p}}^{\mathrm{F}}}{m_{\mathrm{p}}^{\mathrm{tot}}}. \tag{3.11}$$

As expected, NMR,[224,234–238] PALS[239] and a combination of DSC and WAXS[240] studies have found that ψ tends to zero at high crystallinity (lamellar stack morphology) and to one at low crystallinity (fringed-micellar / nodular morphology[176]). To the list of evidence provided by Chmelař and coworkers, we add that tie-molecules in the inter-lamellar domains should be fairly taut (and therefore semi-rigid) both due to the high entanglement density[7,172,178,205] and, in the case of crystal-mobile polymers, local-equilibrium effects at the crystal/amorphous interface (*cf.* Section 3.1.4). In the current work we adopt this morphological model, as seen in Section 3.3.

3.1.6. Crystallinity measurements

Various measures of crystallinity can be defined by assuming that some extensive properties of semi-crystalline polymers are simply the sum of the respective properties of the crystalline and amorphous domains. All of these procedures require knowledge of the respective quantities for the "pure" domains, which can be obtained via correlation of experimental data or using a theoretical description. It is important to note that these domains are implicitly taken to be homogeneous. The different assumptions and techniques employed for the calculation of ω_c often yield slightly different measures for the crystallinity, thus making this quantity somewhat ill-defined.

Density measurements

For example, by considering density measurements under the assumption that a unique specific volume v_c can be assigned to the crystalline domains and a unique specific volume v_a to the amorphous domains, it is straightforward to show that the mass fraction of crystallinity ω_c of a polymer sample is given by[131]

$$\omega_c = \frac{v_a - v}{v_a - v_c}, \tag{3.12}$$

where v is the overall specific volume of the sample.

Differential scanning calorimetry (DSC)

Another measure of crystallinity can be obtained using differential scanning calorimetry (DSC). According to this methodology, a sample is heated at a constant heat rate and its specific enthalpy of fusion Δh_m is compared to that of an ideal extended-chain crystal,

$\Delta h_{\mathrm{m}}^{0}$, obtained by extrapolation of experimental melting enthalpy data or theoretical considerations:[241]

$$\omega_{\mathrm{c}} = \frac{\Delta h_{\mathrm{m}}}{\Delta h_{\mathrm{m}}^{0}}. \tag{3.13}$$

It is important to point out that this procedure neglects heat capacity changes in the crystalline and amorphous domains.

SAXS/WAXS

Small and wide-angle X-ray scattering (SAXS and WAXS, respectively) can be used to provide another measure of crystallinity. In WAXS diffraction spectra, the crystalline regions appear as definite peaks at specific angles whereas amorphous regions appear as a diffuse halo. The crystallinity can therefore be estimated by taking the ratio between the integrated intensity of the crystalline peaks and the integrated intensity of the entire diffraction trace.[242,243] Conversely, in SAXS the volume fraction of crystallinity of the lamellar stack $\phi_{\mathrm{c}}^{\mathrm{LS}}$ can be obtained by analysis of the interface distribution function (IDF) obtained by Fourier transformation of the scattering profile.[156,200,244] If one assumes that all the polymer is organised in lamellar stacks ($\psi = 0$), this crystallinity corresponds to the overall (volume fraction) crystallinity of the sample.

3.2. Solubility of small molecules in semi-crystalline polymers

We will now develop a statistical thermodynamic formalism aimed at modelling fluid solubility in semi-crystalline polymers. After a survey of experimental evidence and previous theoretical work (Sections 3.2.1 and 3.2.2), different theories are unified under the constraint-pressure formalism (Section 3.2.3) which elucidates the effect of network

constraints on the chemical potentials of the solutes and on the overall density in compressible polymer systems. The local-equilibrium hypothesis is then stated rigorously in terms of the equality of the monomer chemical potential of the lamellae and the amorphous domains in order to model crystal-mobile polymers (Section 3.2.4). In Section 3.2.5, the problem of finding the equilibrium solubility and polymer mass in the amorphous domains of crystal-mobile polymers is shown to be equivalent to minimising an appropriate thermodynamic potential.

Let us consider a homogeneous fluid of N_{C} components at temperature T, pressure P and composition $\boldsymbol{y} = \{y_1, y_2 \dots y_{N_{\mathrm{C}}}\}$ in contact with a semi-crystalline polymer sample. We denote with $\boldsymbol{S} = \{S_1, S_2 \dots S_{N_{\mathrm{C}}}\}$ the vector of solubilities of each of the fluid components in the sample, defined as the ratio between the mass of component i retained in the polymer ($m_{\mathrm{s},i}$) and the total polymer mass ($m_{\mathrm{p}}^{\mathrm{tot}}$):

$$S_i = \frac{m_{\mathrm{s},i}}{m_{\mathrm{p}}^{\mathrm{tot}}}. \tag{3.14}$$

The solubility $\boldsymbol{S}$ is in principle the sum of an *adsorption* term on the surfaces of the polymer sample and a bulk *absorption* term:

$$\boldsymbol{S} = \boldsymbol{S}^{(\mathrm{ad})} + \boldsymbol{S}^{(\mathrm{ab})}. \tag{3.15}$$

In practice, however, unless the sample has a very high specific surface or the absorption is insignificant it can be assumed that the total sorption is almost entirely represented by absorption, i.e. $\boldsymbol{S} \approx \boldsymbol{S}^{(\mathrm{ab})}$. In the following analysis only absorption is considered, and the term solubility and absorption will be used interchangeably.

When a dry (i.e., pure) semi-crystalline sample is placed in contact with the fluid, the solubility of each component increases until it reaches an apparent plateau after a characteristic time that we denote with $\tau \sim \tau_D$, determined by the diffusion kinetics of each

solute in the polymer matrix.[26,245] However, since semi-crystalline polymers are out-of-equilibrium systems, irreversible changes in the microstructure due to melting of small lamellae and recrystallisation (*cf.* Section 3.1.2) can in principle change the amount of solutes dissolved over a typical timescale $\tau \sim \tau_R$. In the following, it is implicitly assumed that the characteristic timescale over which irreversible recrystallisation phenomena (or, more generally, physical and chemical aging) take place is much bigger than the characteristic time of diffusion-limited phenomena, i.e.,

$$\tau_D << \tau_R. \tag{3.16}$$

This corresponds to assuming that on the timescales of solute diffusion the lamellar structure of the material is preserved.

For $\tau > \tau_D$, semi-crystalline polymers swollen by a fluid are therefore considered to be in a pseudo-equilibrium "state" in which some of their characteristic out-of-equilibrium features (such as their inter-crystalline chain topology, *cf.* Section 3.1.3) act as fixed constraints. Note that we are not excluding the existence of faster local chain reorganisation effects compatible with such constraints, which could give rise to reversible melting due to intra-crystalline chain dynamics (*cf.* Section 3.1.4) over a timescale $\tau_{\mathrm{ICD}} \approx \tau_D << \tau_R$.

The equilibrium solubility $\boldsymbol{S}$ is therefore intended as a function of the fluid temperature, pressure and composition $(T, P, \boldsymbol{y})$ and of a set of material constraints $\boldsymbol{\Gamma}_{\mathrm{c}}$ that define the polymer's pseudo-equilibrium state:

$$\boldsymbol{S} = \boldsymbol{S}\left(T, P, \boldsymbol{y}; \boldsymbol{\Gamma}_{\mathrm{c}}\right) \tag{3.17}$$

The presence of irreversible transformations leads to a time-dependence of the constraints $\boldsymbol{\Gamma}_{\mathrm{c}}$, which can be tested consistently during sorption measurements by looking

for hysteresis in sorption/desorption cycles.

3.2.1. Experimental evidence and thermodynamic modelling

One of the most common starting assumptions employed to model $\boldsymbol{S} \approx \boldsymbol{S}^{(\mathrm{ab})}$ at given temperature T, pressure P and composition $\boldsymbol{y}$ of the external fluid is that the crystalline domains are essentially impermeable to the solutes relatively to the amorphous ones; mathematically, this translates into

$$\boldsymbol{S} \approx \omega_{\mathrm{a}} \boldsymbol{S}_{\mathrm{a}} = (1 - \omega_{\mathrm{c}}) \boldsymbol{S}_{\mathrm{a}}, \tag{3.18}$$

where both $\boldsymbol{S}_{\mathrm{a}}$ – the solubility in the amorphous domains only – and the crystallinity ω_{c} (Equation 3.8) are in principle functions of $T, P, \boldsymbol{y}$ and of the sample-specific constraints $\boldsymbol{\Gamma}_{\mathrm{c}}$. Here and in the following, equations between vectors are intended as element-by-element equations; the scalar factor $(1 - \omega_{\mathrm{c}})$ in Equation 3.18 thus multiplies all the N_{C} equations for the individual solutes.

Experimental evidence supporting the idea that crystalline domains are impermeable to the solute molecules has been available since the studies of Richards[37] and Michaels and co-workers[26,245,246] on the solubility of small hydrocarbons in polyethylene. Heuristically, this behaviour can be explained by comparing the high enthalpy of formation of a defect in the crystalline phase with the enthalpy of solution in the amorphous domains; it is energetically unfavourable for a solute to deform a dense, ordered lattice rather than mixing in the less dense and already disordered amorphous domains.

It should be noted, however, that there are some notable exceptions to this general trend. Polymers with very bulky monomers and with high stereoregularity (such as syndiotactic polystyrene, s-PS) can form crystal structures which can accommodate solute particles as interstitials without deforming the crystal architecture significantly,

thereby reducing the enthalpy of formation of a defect up to the point where *ad*sorption in the interstitial sites becomes favourable.[247–249] Another exception might arise when the particles absorbing are very small, as it is the case for molecular hydrogen (H_2) and helium (He). In the ensuing discussion we will focus on systems for which the approximation embodied in Equation 3.18 is justified.

From a thermodynamic perspective, the equilibrium between an external fluid and amorphous domains with respect to exchanges of solute particles is realized through the equality of the chemical potentials $\boldsymbol{\mu}_\mathrm{s}$ of the N_C solutes in the external fluid and in the amorphous domains:

$$\boldsymbol{\mu}_\mathrm{s} = \boldsymbol{\mu}_\mathrm{s}^\mathrm{a} = \boldsymbol{\mu}_\mathrm{s}^\mathrm{f} \tag{3.19}$$

Here, the subscript s indicates the solute, and the superscripts a and f the amorphous domain and external fluid phase, respectively. Note the absence of a corresponding equation for the the exchange of polymer molecules involving the polymer chemical potential μ_p, as we assume for simplicity that no polymer is present in the external fluid. This approximation should be very accurate for medium to high-molecular weight polymers[131] and exact when the external fluid is gaseous or much larger than the polymer sample. At temperature T, pressure P and composition $\boldsymbol{y}$ the chemical potentials in the fluid can be calculated directly with a fluid equation of state like SAFT-γ Mie (Section 2.3 and Equation 2.27):

$$\boldsymbol{\mu}_\mathrm{s}^\mathrm{f} = \boldsymbol{\mu}_\mathrm{s}^\mathrm{EoS}\left(T, P, \boldsymbol{y}\right). \tag{3.20}$$

As in Section 2.3, the superscript EoS indicates that the functional form of the chemical potentials is imposed by the choice of a given equation of state. Note that in this equation the polymer composition is implicitly fixed to zero, and that phase stability must be checked for example via TP flash calculations (Section 2.3.5).

Under the assumption that no polymer is present in the fluid phase it can be particularly helpful to treat the polymer sample as a semi-open system allowing exchanges

of solute particles but not of polymer molecules with the fluid (the so-called "osmotic ensemble"[44]). By combining Equations 3.19 and 3.20, the solubility $\boldsymbol{S}_\mathrm{a}$ can therefore be considered as a function of T, P, the N_C chemical potentials $\boldsymbol{\mu}_\mathrm{s} = \boldsymbol{\mu}_\mathrm{s}^\mathrm{f} = \boldsymbol{\mu}_\mathrm{s}^\mathrm{EoS}(T, P, \boldsymbol{y})$ and the constraints $\boldsymbol{\Gamma}_\mathrm{c}$:

$$\boldsymbol{S}_\mathrm{a} = \boldsymbol{S}_\mathrm{a}(T, P, \boldsymbol{\mu}_\mathrm{s}; \boldsymbol{\Gamma}_\mathrm{c}) \iff \boldsymbol{\mu}_\mathrm{s}^\mathrm{a}(T, P, \boldsymbol{S}_\mathrm{a}; \boldsymbol{\Gamma}_\mathrm{c}) = \boldsymbol{\mu}_\mathrm{s}. \tag{3.21}$$

In order to solve Equation 3.21 for the solubility $\boldsymbol{S}_\mathrm{a}(T, P, \boldsymbol{\mu}_\mathrm{s}; \boldsymbol{\Gamma}_\mathrm{c})$ it is necessary to specify the functional form of the solute chemical potentials $\boldsymbol{\mu}_\mathrm{s}^\mathrm{a}(T, P, \boldsymbol{S}_\mathrm{a}; \boldsymbol{\Gamma}_\mathrm{c})$ in the amorphous domains.

Michaels and Bixler's hypothesis

The simplest approach is to assume that these domains behave as subcooled polymer melts due to their disordered, "liquid-like" structure:

$$\boldsymbol{\mu}_\mathrm{s}^\mathrm{a} \approx \boldsymbol{\mu}_\mathrm{s}^\mathrm{EoS}(T, P, \boldsymbol{S}_\mathrm{a}). \tag{3.22}$$

By combining this with Equations 3.19 and 3.20, the value of $\boldsymbol{S}_\mathrm{a}$ can thus be obtained directly from a VLE calculation in which no polymer is allowed in the gas phase (*cf.* Section 2.3).

Note that the composition of the amorphous domains is specified with the solubility $\boldsymbol{S}_\mathrm{a}$ instead of the mole fractions of all components since the solution of Equation 3.22 should not depend significantly on the molecular weight of the polymer or polydispersity at medium to high molecular weights (*cf.* Section 2.5.2). The calculations can therefore be performed for a monodisperse polymer of high molecular weight (e.g., $n_0 = 1000$ repeating units). In the following analysis, the amorphous solubility calculated via the combination of Equations 3.19, 3.20 and 3.22 is denoted with

$$\boldsymbol{S}_{\mathrm{a}} = \boldsymbol{S}_{\mathrm{a}}^{\mathrm{EoS}}(T, P, \boldsymbol{\mu}_{\mathrm{s}}).$$

This is approach was originally proposed by Michaels and Bixler,[26] who used the Flory-Huggins-Staverman theory[46–48] to model the liquid polymer + solute mixture. More recently, Paricaud and coworkers[131] improved on Michaels and Bixler's work by coupling a more advanced equation of state (i.e., the SAFT-VR Mie EoS – a "primitive" version of SAFT-γ Mie) with a model predicting the variation of crystallinity with temperature taken from Flory.[175] The authors managed to provide a satisfactory description of the solubility at various temperatures of short hydrocarbons in semi-crystalline PE.

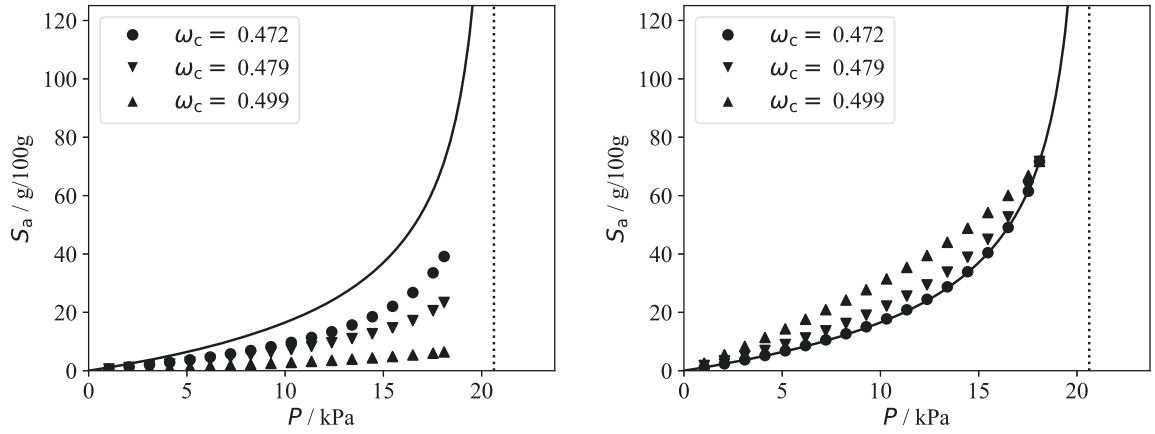

(a) (b)

Figure 3.5.: Solubility of n-hexane in amorphous PE at 25 °C. The continuous curves represent SAFT-γ Mie predictions using the n-hexane model defined in Section 2.5.1; PE is modelled as a homonuclear chain of $n_0 = 1000$ methylene monomers (Section 2.5.2). The symbols represent experimental data[139] (uncertainty smaller than the marker size), while the vertical dotted lines represent the vapour pressure P_{vap} of n-hexane at 25 °C. a) Comparison of the theoretical prediction $S_{\mathrm{a}}^{\mathrm{EoS}}$ and the apparent amorphous solubility $S_{\mathrm{a}}^{\mathrm{exp}}$ in the three samples calculated using Equation 3.23. b) Comparison of the theoretical prediction and the scaled solubility in the three samples; the linear scaling is performed by enforcing that the apparent solubility in the three samples at $P = 0.9P_{\mathrm{vap}}$ matches the theoretical predictions.

Constrained amorphous domains

Despite the apparent success of Michaels and Bixler's approach, a large amount of experimental and theoretical studies[38–45,194,250–258] have shown that if the crystallinity $\omega_{\mathrm{c}}^{\mathrm{exp}}$ of a sample and the solubility S_i^{exp} of a given solute are separately measured, the apparent solubility in the amorphous domains $S_{\mathrm{a},i}^{\mathrm{exp}}$ obtained by inverting Equation 3.18 is lower than $S_{\mathrm{a},i}^{\mathrm{EoS}}$ regardless of the equation of state used, i.e.,

$$S_{\mathrm{a},i}^{\mathrm{exp}} = S_i^{\mathrm{exp}} / \left(1 - \omega_{\mathrm{c}}^{\mathrm{exp}}\right) \leq S_{\mathrm{a},i}^{\mathrm{EoS}}. \tag{3.23}$$

We provide experimental evidence of this fact with sorption data measured by Dr. J. Ramandani and Prof. D. Williams (Imperial College London, Department of Chemical Engineering) as part of a joint study[139] – see Section 4.2 or the publication for more details on the experimental procedure. In Figure 3.5 the apparent solubility of pure *n*-hexane in the amorphous domains of three semi-crystalline PE samples – LDPE, MDPE and HDPE – measured at 25 °C is compared with $S_{\mathrm{a}}^{\mathrm{EoS}}$ (the index i is here omitted since the external fluid is pure hexane) calculated using the SAFT-γ Mie models for *n*-alkanes and PE developed in Section 2.5.2. Note that PE is modelled here as a homonuclear chain of $n_0 = 1000$ CH_2 monomers.

One can see from Figure 3.5a that $S_{\mathrm{a}}^{\mathrm{exp}} < S_{\mathrm{a}}^{\mathrm{EoS}}$ for all the semi-crystalline PE samples. Furthermore, the apparent amorphous solubility is found to decrease with increasing crystallinity. One can justify these findings while retaining the assumption that $S_{\mathrm{a}} = S_{\mathrm{a}}^{\mathrm{EoS}}$ by either assuming that the calculated crystallinity greatly underestimates the true value or that only a fraction of the amorphous domains is available for sorption, resulting in an "effective" crystallinity which is higher than the calculated value.

Fortunately, it is possible to test the validity of these assumptions. If either of these

hypotheses are correct, a linear scaling of $S_{\mathrm{a}}^{\mathrm{exp}}$ at each pressure so that the apparent amorphous solubilities in different polyethylene samples match at a given pressure should result in three overlapping experimental curves. Physically, the linear scaling is equivalent to assuming that the calculated crystallinity used in Equation 3.23 is underestimated. In Figure 3.5b, the three experimental data sets are scaled so that the amorphous solubility measured at the highest pressure (i.e., 90% of the vapour pressure of *n*-hexane at 25 °C) matches the theoretical calculations. It can be seen that the scaled experimental data sets do not match, and that the curvature decreases with increasing crystallinity.

These findings clearly indicate that the solubility in the amorphous domains of the three different PE samples is different. In particular, if the measured values of crystallinity are accepted as being correct, it follows that $S_{\mathrm{a}}^{\mathrm{exp}} < S_{\mathrm{a}}^{\mathrm{EoS}}$ for all samples and that $S_{\mathrm{a}}^{\mathrm{exp}}$ decreases with increasing crystallinity.

3.2.2. Elastic models

In cross-linked polymer networks (such as rubbers and gels) the bulk solubility of gases and liquids is lower than the one measured for the corresponding un-crosslinked polymers. It is now well understood[134,178,259–263] that this phenomenon can be traced back to the increase in the free energy (mainly of entropic origin) of the chain segments between cross-links following the expansion (or "swelling") of the network caused by the introduction of a solute. By analogy, the most prominent solubility models in the literature assume that the solubility reduction in the amorphous domains of semi-crystalline polymers originates from the elastic forces exerted by the tie-molecules (*cf.* Section 3.1.3) upon swelling.

Theories for swelling in rubbers and semi-crystalline polymers – here colloquially referred to as "elastic" models – aim to derive approximations for the excess chemical

potential $\Delta\mu^{\mathrm{c}}_{\mathrm{s},i}$, intended as the difference between the chemical potential of a solute in the swollen amorphous polymer network ($\mu^{\mathrm{a}}_{\mathrm{s},i}$) and the corresponding chemical potential in a subcooled polymer + mixture at the same temperature, pressure and composition:

$$\Delta\mu^{\mathrm{c}}_{\mathrm{s},i}\left(T, P, \boldsymbol{S}_{\mathrm{a}}; \boldsymbol{\Gamma}_{\mathrm{c}}\right) = \mu^{\mathrm{a}}_{\mathrm{s},i}\left(T, P, \boldsymbol{S}_{\mathrm{a}}; \boldsymbol{\Gamma}_{\mathrm{c}}\right) - \mu^{\mathrm{EoS}}_{\mathrm{s},i}\left(T, P, \boldsymbol{S}_{\mathrm{a}}\right). \tag{3.24}$$

In practice, however, all the theories discussed in this subsection are derived using the Flory–Huggins–Staverman theory[47,48,264] in which pressure is undefined since the molecules occupy the sites of an incompressible lattice. According to this theory, in a mixture of ν linear and monodisperse polymer molecules and n_{s} solute molecules of a single type the solute chemical potential can be expressed as[259]

$$\mu^{\mathrm{FHS}}_{\mathrm{s}}(T, n_{\mathrm{s}}, \nu) = k_{\mathrm{B}}T\left[\ln(1-\phi_{\mathrm{p}}) + \left(1 - \frac{1}{Z}\right)\phi_{\mathrm{p}} + \chi\phi^2_{\mathrm{p}}\right], \tag{3.25}$$

where $Z = \bar{V}_{\mathrm{p}}/\bar{V}_{\mathrm{s}}$ is the ratio between the (partial) molar volume of the polymer and the solute (assumed constant in lattice models) and the volume fraction of the polymer is given by

$$\phi_{\mathrm{p}} = \frac{\nu\bar{V}_{\mathrm{p}}}{\nu\bar{V}_{\mathrm{p}} + n_{\mathrm{s}}\bar{V}_{\mathrm{s}}} = \frac{Z\nu}{Z\nu + n_{\mathrm{s}}}. \tag{3.26}$$

The term $k_{\mathrm{B}}T\chi\phi^2_{\mathrm{p}}$ in Equation 3.25 is the (partial molar) heat of mixing[§] derived from a mean-field treatment of the interactions between the solute and the polymer's monomers. When suitably extended to deal with multiple solutes and polydisperse polymer mixtures,[265] the expression in Equation 3.25 thus constitutes the reference "EoS" term in the sense of Equation 3.24 for all the elastic models discussed in this subsection. It is noteworthy that in some works the factor $1/Z$ is omitted;[39,41] this approximation is certainly valid for most polymer/solute pairs but leads to small differences in the formulae that are reported here.

[§]More appropriately, an excess mixing free energy if χ is allowed to vary with temperature

Flory-Rehner theory

Due to the similarity between the chemical cross-links in rubbers and the physical cross-links between tie-molecules and lamellae in semi-crystalline polymers, the Flory-Rehner theory[259] – a model originally developed to describe swelling in rubbers – and its modifications have been applied extensively to semi-crystalline polymers. According to the FR theory, the elastic chemical potential of a solute in a cross-linked network is given by

$$\frac{\Delta\mu^{\mathrm{c}}_{\mathrm{s},i}}{RT} \approx \frac{\rho_{\mathrm{a}}\bar{V}_{\mathrm{s},i}}{\bar{M}_{\mathrm{c}}}\left(\phi_{\mathrm{p}}^{1/3} + \left(1 - \frac{2}{f_{\mathrm{N}}}\right)\phi_{\mathrm{p}}\right), \tag{3.27}$$

where ρ_{a} is the pure amorphous polymer density, f_{N} the functionality of the network (i.e., the number of chains emanating from each cross-link) and $\bar{M}_{\mathrm{c}}$ the average molecular weight of polymer chains between cross-links. Whereas the term in $\phi_{\mathrm{p}}^{1/3}$ in Equation 3.27 is due to the stretching entropy of the chains, the "ideal gas" term proportional to ϕ_{p} is due to the loss of translational degrees of freedom due to the chain ends being grouped in f_{N}-functional cross-links.

Rogers and coworkers[38] first applied directly the Flory-Rehner (FR) theory to describe the sorption of organic vapors in polyethylene. Since the cross-links in semi-crystalline polymers (i.e., the crystalline lamellae) have a very high functionality, for $f_{\mathrm{N}} \to \infty$ we obtain the expression derived by Rogers:[38]

$$\frac{\Delta\mu^{c}_{\mathrm{s},i}}{RT} \approx \frac{\rho_{\mathrm{a}}\bar{V}_{\mathrm{s},i}}{\bar{M}_{\mathrm{c}}}\left(\phi_{\mathrm{p}}^{1/3} + \phi_{\mathrm{p}}\right) \tag{3.28}$$

The theory was later extended by Brown and coworkers[40] to take into account that swelling of the interlamellar amorphous mass is one-dimensional. Their modification resulted in the elastic term depending on ϕ_p^{-1} instead of $\phi_p^{1/3}$, a very significant difference from the original FR theory. Building on their work, Liu and Neogi[41] then proposed modifications to the ideal-gas term due to the discrepancies between the stretching

behaviour of real polymer networks and the idealised affine network model of the FR theory.[259,261,266–268] Their expression for $\Delta\mu_{\mathrm{s},i}$ thus reads

$$\frac{\Delta\mu^{\mathrm{c}}_{\mathrm{s},i}}{RT} \approx \frac{\rho_{\mathrm{a}}\bar{V}_{\mathrm{s},i}}{\bar{M}_{\mathrm{c}}}\left(\phi_{\mathrm{p}}^{-1} + \frac{1}{2}\phi_{\mathrm{p}}\right). \tag{3.29}$$

Normally, for all of the theories derived from the FR theory the amorphous density ρ_{a} and the partial molar volumes of the solutes $\bar{V}_{\mathrm{s},i}$ are assumed known, whereas the mean molecular weight of chains between cross-link $\bar{M}_{\mathrm{c}}$ is adjusted to reproduce sorption data. This procedure has been successfully applied to model the solubility of organic vapours in PE[38,40,41] and PP[251] and of CO_2 in PTFE, MFA and PVDF,[269] with the most recent iterations of the theory performing better at higher solute concentrations.[40,41]

Michaels and Hausslein theory

Michaels and Hausslein[39] were among the first authors to notice that the excess elastic activity

$$a^{\mathrm{c}}_{\mathrm{s},i} = \exp\left(\Delta\mu^{\mathrm{c}}_{\mathrm{s},i}/RT\right) \tag{3.30}$$

of various penetrants in polyethylene – found by comparing experimental solubility data to the the Flory–Huggins–Staverman theory for the equilibrium polymer mixtures – depends markedly on temperature at constant composition (i.e., ϕ_{p}), with a reversible behaviour below about 100 °C. In order to explain this phenomenon using the Flory–Rehner theory the molecular weight of the polymer chains between cross-links must vary with temperature as seen in Equations 3.27, 3.28 and 3.29. Michaels and Hausslein then proposed that (in polyethylene) each tie-molecule is in equilibrium with the crystalline lamellae with respect to exchanges of monomers. This phenomenon makes the tension of the tie-molecules temperature dependent, as it is the result of a local equilibrium between

the entropic forces that "loosen" the chains and the driving force of crystallization which, by contrast, makes the chains taut by removing monomers from them (see Figure 3.6).

Using the local-equilibrium hypothesis, Michaels and Hausslein developed a model for the excess chemical potential of a solute featuring the mass fraction f_{T} of elastically effective chains (i.e., bridges and entangled loops) in the amorphous domains as a free parameter:

$$\Delta\mu_{\mathrm{s},i}^{\mathrm{c}} = \frac{\bar{V}_{\mathrm{s},i}}{\bar{V}_{\mathrm{p}}} \frac{\Delta\bar{h}_{\mathrm{m}}^{0}\left(1-\frac{T}{T_{\mathrm{m}}^{0}}\right)+\Delta\mu_{p}^{\mathrm{EoS,res}}}{\frac{3}{2f_{\mathrm{T}}\phi_{p}}-1}. \tag{3.31}$$

Here, $\bar{V}_{\mathrm{p}}$ is the partial molar volume of the polymer whereas $\Delta\bar{h}_{\mathrm{m}}^{0}$ and T_{m}^{0} are the melting enthalpy (per mole of polymer) and melting temperature of a perfect polymer crystal. The quantity $\Delta\mu_{\mathrm{p}}^{\mathrm{EoS,res}}$ is the difference in polymer chemical potential between a polymer mixture swollen at volume fraction ϕ_{p} and a pure polymer liquid. The resulting MH theory has been applied extensively to model the sorption of various compounds in PE,[39,42,43,251–257] PE copolymers[270] and isotactic PP.[251]

Despite the different application, it is clear that Michaels and Hausslein's theories relies on the local-equilibrium hypothesis described in Section 3.1.4. In fact, the MH theory was actually inspired by the early models of Roe and Krigbaum.[39,195,196] This implies that for crystal-mobile polymers (e.g., PE, isotactic PP, PEO, PTFE[156,217]) we expect to observe both reversible changes in the lamellar thickness and an increase in the activity of solutes dissolved due to the same phenomenon – i.e., the presence of the α_{c} relaxation mode. In particular, in Section 3.2.4 we show that both phenomena can be described under the same unified theory.

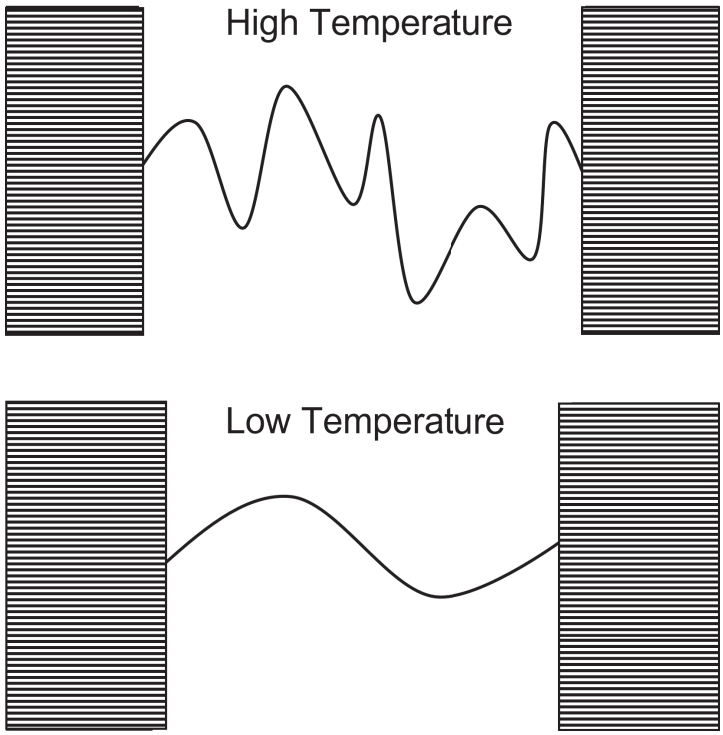

Figure 3.6.: A schematic illustration of the effect of the local-equilibrium hypothesis on tie-molecules. The tie-molecules are shorter and more taut at low temperatures due to the increase in the driving force of crystallization. The lamellae (rectangles) are thicker at lower temperatures due to the inclusion of more tie monomers.

3.2.3. The constraint pressure formalism (This work)

Using compressible EoS in solubility calculations

In order to use compressible equations of state (i.e., EoS in which pressure can be specified) in Equation 3.24 to calculate $\mu_{\mathrm{s},i}^{\mathrm{EoS}}$ in combination with expressions for $\Delta\mu_{\mathrm{s}}^{\mathrm{c}}$ derived by the elastic models reported, one of two strategies must be implemented. The first requires calculating at fixed temperature T, pressure P and composition $\boldsymbol{S}_{\mathrm{a}}$ the volume fraction of the polymer ϕ_{p} via the partial molar volumes $\bar{V}_{\mathrm{s},i}$:

$$\begin{aligned} \phi_{\mathrm{s},i} &= \frac{n_{\mathrm{s},i}\bar{V}_{\mathrm{s},i}}{V} \\ \phi_{\mathrm{p}} &= 1 - \sum_{i} \phi_{\mathrm{s},i} \end{aligned} \tag{3.32}$$

where the partial molar volumes and the volume can be calculated as appropriate derivatives of the EoS Gibbs free energy (*cf.* Section 2.3.3):

$$\begin{aligned} \bar{V}_{\mathrm{s},i}^{\mathrm{EoS}} &= \left(\frac{\partial V^{\mathrm{EoS}}}{\partial n_{\mathrm{s},i}}\right)_{T,P,\boldsymbol{n}_{\mathrm{s}}\setminus\{n_{\mathrm{s},i}\},\nu} \\ \bar{V}_{\mathrm{p}}^{\mathrm{EoS}} &= \left(\frac{\partial V^{\mathrm{EoS}}}{\partial \nu}\right)_{T,P,\boldsymbol{n}_{\mathrm{s}}} \\ V^{\mathrm{EoS}} &= \left(\frac{\partial G^{\mathrm{EoS}}}{\partial P}\right)_{T,\boldsymbol{n}_{\mathrm{s}},\nu} \end{aligned} \quad . \tag{3.33}$$

Here the polymer has been assumed to be monodisperse to simplify the notation – ν represent the moles of polymer molecules. Banaszak and coworkers[43] adapted the MH theory in this fashion to be used with the PC-SAFT EoS.[64,65] However, the expressions for $\Delta\mu_{\mathrm{s},i}^{\mathrm{c}}$ derived above assume incompressibility in the first place. A rigorous treatment starting from Helmholtz free energy of the system is instead required to precisely transfer the assumptions of lattice-based elastic models to compressible theories (see our approach in Section 3.3).

A semi-empirical approach

Recently, Memari and co-workers[44,271,272] showed with Monte Carlo simulation in the osmotic $(T, P, \boldsymbol{\mu}_\mathrm{s})$ ensemble that the solubility reduction of small molecules in the amorphous domains of PE can be captured by assuming that they behave like a subcooled liquid subject to an extra isotropic stress, the "constraint pressure" P_c, which increases the effective thermodynamic pressure in those domains from the external pressure P to $P + P_\mathrm{c}$. The same idea was employed by Minelli and co-workers[45] to calculate the solubility of simple gases in PE, PP, and PEO, using the Sanchez-Lacombe (SL) equation of state[49] which, like SAFT theories, allows the pressure to be specified in the calculations.

In these works, the chemical potential of the solutes in the amorphous domains is written as

$$\mu_{\mathrm{s},i}^{\mathrm{a}} \approx \mu_{\mathrm{s},i}^{\mathrm{EoS}}(T, P + P_\mathrm{c}, \boldsymbol{S}_\mathrm{a}). \tag{3.34}$$

By combining Equations 3.19, 3.20 and 3.34, the solubility $\boldsymbol{S}_\mathrm{a}$ can be intended as a function of T, P, the N_C chemical potentials $\boldsymbol{\mu}_\mathrm{s}$ of the fluid components and the constraint pressure P_c:

$$\boldsymbol{S}_\mathrm{a} = \boldsymbol{S}_\mathrm{a}(T, P, \boldsymbol{\mu}_\mathrm{s}; P_\mathrm{c}) \iff \boldsymbol{\mu}_\mathrm{s}^{\mathrm{EoS}}(T, P + P_\mathrm{c}, \boldsymbol{S}_\mathrm{a}) = \boldsymbol{\mu}_\mathrm{s} \tag{3.35}$$

It can be shown under mild assumptions (*cf.* Appendix B) that increasing P_c at fixed $T, P, \boldsymbol{\mu}_\mathrm{s}$ decreases the equilibrium solubility in the amorphous domains at low to moderate solubility, i.e.,

$$\left(\frac{\partial S_{\mathrm{a},i}}{\partial P_\mathrm{c}}\right)_{T,P,\boldsymbol{\mu}_\mathrm{s}} < 0. \tag{3.36}$$

Both Memari and coworkers[44] and Minelli and coworkers[45] found that the typical values of P_c needed to correctly describe the sorption isotherms ranged between 10 and 80 MPa, a very significant pressure compared to the typical external pressure. Furthermore, P_c was found to decrease with increasing temperature and decreasing crys-

tallinity.

Fischlschweiger and coworkers[273] have proposed that the P_c could be of a mechanical origin, either due to potential residual stresses in the polymer following crystallization or due to the formation of the cavities needed to accommodate the solute particles in the amorphous domains. In the current work, neither of these hypotheses are considered as the constraining effect can be simply explained by considering the swelling restriction induced by the tie-molecules – as the elastic models discussed in Section 3.2.2 have shown. However, elastic models have invariably been developed using incompressible fluid theories such as the Flory–Huggins–Staverman theory in which pressure is undefined. We will now show for the first time that the concept of constraint pressure naturally emerges naturally when compressible polymer mixtures are subject to network constraints.

Formal derivation (This work)

Let $T, V, \boldsymbol{n}_s, \boldsymbol{\nu}, \boldsymbol{\Gamma}_c$ be respectively temperature, volume, the solute(s) composition vector (in moles of solutes), the polymer composition vector (i.e., the molecular weight distribution) and the vector of variables specifying the network constraints (e.g. chemical or physical cross-links) acting on a polymer network. The free energy of the swollen network A can be written as

$$A(T, V, \boldsymbol{n}_s, \boldsymbol{\nu}; \boldsymbol{\Gamma}_c) = A^{\mathrm{EoS}}(T, V, \boldsymbol{n}_s, \boldsymbol{\nu}) + \Delta A^c(T, V, \boldsymbol{n}_s, \boldsymbol{\nu}; \boldsymbol{\Gamma}_c), \tag{3.37}$$

where A^{EoS} is the free energy of a liquid polymer-solute mixture at the same temperature, volume and concentration and ΔA^c the free energy difference due to the formation of network constraints (e.g. chemical or physical cross-links). We anticipate that this free energy difference is mostly entropic in origin and due to the reduced configuration space

available to polymer chains upon cross-linking and deformation.[134,265] Assuming that these constraints are irreversible, pressure is obtained as

$$\begin{aligned} P\left(T,V,\boldsymbol{n}_{\mathrm{s}},\boldsymbol{\nu},\boldsymbol{\Gamma}_{\mathrm{c}}\right) &= -\left(\frac{\partial A}{\partial V}\right)_{T,\boldsymbol{n}_{\mathrm{s}},\boldsymbol{\nu},\boldsymbol{\Gamma}_{\mathrm{c}}} = -\left(\frac{\partial A^{\mathrm{EoS}}}{\partial V}\right)_{T,\boldsymbol{n}_{\mathrm{s}},\boldsymbol{\nu}} - \left(\frac{\partial \Delta A^{\mathrm{c}}}{\partial V}\right)_{T,\boldsymbol{n}_{\mathrm{s}},\boldsymbol{\nu},\boldsymbol{\Gamma}_{\mathrm{c}}}, \\ &= P^{\mathrm{EoS}}(T,V,\boldsymbol{n}_{\mathrm{s}},\boldsymbol{\nu}) - P_{\mathrm{c}}(T,V,\boldsymbol{n}_{\mathrm{s}},\boldsymbol{\nu},\boldsymbol{\Gamma}_{\mathrm{c}}) \end{aligned} \tag{3.38}$$

where P^{EoS} is the pressure of the reference unconstrained liquid (*cf.* Section 2.3) and we have defined

$$P_{\mathrm{c}}(T,V,\boldsymbol{n}_{\mathrm{s}},\boldsymbol{\nu},\boldsymbol{\Gamma}_{\mathrm{c}}) = \left(\frac{\partial \Delta A^{\mathrm{c}}}{\partial V}\right)_{T,\boldsymbol{n}_{\mathrm{s}},\boldsymbol{\nu},\boldsymbol{\Gamma}_{\mathrm{c}}}. \tag{3.39}$$

This quantity is positive for polymer networks since the configurational entropy of the network chains decreases upon increases in volume. By rearranging Equation 3.38, we see that at constant pressure P the equilibrium volume $V(T,P,\boldsymbol{n}_{\mathrm{s}},\boldsymbol{\nu},\boldsymbol{\Gamma}_{\mathrm{c}})$ is a solution of

$$P^{\mathrm{EoS}}(T,V(T,P,\boldsymbol{n}_{\mathrm{s}},\boldsymbol{\nu},\boldsymbol{\Gamma}_{\mathrm{c}}),\boldsymbol{n}_{\mathrm{s}},\boldsymbol{\nu}) = P + P_{\mathrm{c}}(T,V(T,P,\boldsymbol{n}_{\mathrm{s}},\boldsymbol{\nu},\boldsymbol{\Gamma}_{\mathrm{c}}),\boldsymbol{n}_{\mathrm{s}},\boldsymbol{\nu},\boldsymbol{\Gamma}_{\mathrm{c}}). \tag{3.40}$$

By inverting[¶],the functional relationship between P^{EoS} and V (Equation 3.40) we then have

$$V(T,P,\boldsymbol{n}_{\mathrm{s}},\boldsymbol{\nu},\boldsymbol{\Gamma}_{\mathrm{c}}) = V^{\mathrm{EoS}}(T,P+P_{\mathrm{c}},\boldsymbol{n}_{\mathrm{s}},\boldsymbol{\nu}), \tag{3.41}$$

where V^{EoS} is the equilibrium volume of the reference liquid and P_{c} is a function of state via Equation 3.39. Simultaneous solution of Equations 3.39 and 3.41 yields the equilibrium values of V and P_{c} at fixed $T,P,\boldsymbol{n}_{\mathrm{s}},\boldsymbol{\nu},\boldsymbol{\Gamma}_{\mathrm{c}}$.

In all the elastic models discussed in Section 3.2.2[38–41,259] the polymer chain statistics in the reference polymer liquid is assumed to be unperturbed by the presence of the solute

[¶]One should note that in theory we must account for phase transitions when inverting $P^{\mathrm{EoS}}(V)$. In solubility calculations – where $T,P,\boldsymbol{\mu}_{\mathrm{s}}$ are fixed – these issues can be avoided by using as first guess the equilibrium volume and composition of a swollen polymer melt.

– the so-called phantom-chain statistics[265] –, resulting in ΔA^{c} not depending explicitly on the number of moles of solute $\boldsymbol{n}_{\mathrm{s}}$:

$$A(T, V, \boldsymbol{n}_{\mathrm{s}}, \boldsymbol{\nu}, \boldsymbol{\Gamma}_{\mathrm{c}}) \approx A^{\mathrm{EoS}}(T, V, \boldsymbol{n}_{\mathrm{s}}, \boldsymbol{\nu}) + \Delta A^{\mathrm{c}}(T, V, \boldsymbol{\nu}, \boldsymbol{\Gamma}_{\mathrm{c}}). \tag{3.42}$$

It must be stressed that this hypothesis is not justified for highly swollen networks (e.g. gels) far from their θ temperature.[134,259] Under this approximation, the chemical potential $\mu_{\mathrm{s},i}$ of a solute i is given by

$$\begin{aligned} \mu_{\mathrm{s},i}\left(T, V, \boldsymbol{n}_{\mathrm{s}}, \boldsymbol{\nu}, \boldsymbol{\Gamma}_{\mathrm{c}}\right) &= \left(\frac{\partial A}{\partial n_{\mathrm{s},i}}\right)_{T,V,\boldsymbol{n}_{\mathrm{s}}\setminus\{n_{\mathrm{s},i}\},\boldsymbol{\nu},\boldsymbol{\Gamma}_{\mathrm{c}}} \\ &\approx \left(\frac{\partial A^{\mathrm{EoS}}}{\partial n_{\mathrm{s},i}}\right)_{T,V,\boldsymbol{n}_{\mathrm{s}}\setminus\{n_{\mathrm{s},i}\},\boldsymbol{\nu}} \\ &= \mu_{\mathrm{s},i}^{\mathrm{EoS}}(T, V, \boldsymbol{n}_{\mathrm{s}}, \boldsymbol{\nu}) \end{aligned} . \tag{3.43}$$

At fixed pressure P, exploiting now the invertibility of the function $\mu_{\mathrm{s},i}^{\mathrm{EoS}}(V)$ and using Equation 3.41 we finally obtain

$$\mu_{\mathrm{s},i}(T, P, \boldsymbol{n}_{\mathrm{s}}, \boldsymbol{\nu}, \boldsymbol{\Gamma}_{\mathrm{c}}) = \mu_{\mathrm{s},i}^{\mathrm{EoS}}(T, P + P_{\mathrm{c}}, \boldsymbol{n}_{\mathrm{s}}, \boldsymbol{\nu}). \tag{3.44}$$

Notice the similarity to Equation 3.34, aside from the difference in how composition is specified ($\boldsymbol{S}_{\mathrm{a}}$ versus $\boldsymbol{n}_{\mathrm{s}}, \boldsymbol{\nu}$). The combination of Equations 3.41 and 3.44 elucidates how for systems in which $\Delta A^{\mathrm{c}} \approx \Delta A^{\mathrm{c}}(T, V, \boldsymbol{\nu}, \boldsymbol{\Gamma}_{\mathrm{c}})$ the effect of constraints is *formally* equivalent to the addition of a (state-dependent) pressure P_{c} to an otherwise unconstrained liquid polymer-solute mixture.

Since the "liquid-like" amorphous domains have a very low compressibility, the increase in chemical potential of a solute i due to the presence of network constraints can be

expressed as

$$\Delta\mu^{\mathrm{c}}_{\mathrm{s},i} = \mu^{\mathrm{EoS}}_{\mathrm{s},i}(T, P + P_{\mathrm{c}}, \boldsymbol{n}_{\mathrm{s}}, \boldsymbol{\nu}) - \mu^{\mathrm{EoS}}_{\mathrm{s},i}(T, P, \boldsymbol{n}_{\mathrm{s}}, \boldsymbol{\nu}) \approx \bar{V}_{\mathrm{s},i} P_{\mathrm{c}}, \tag{3.45}$$

where $\bar{V}_{\mathrm{s},i} = \bar{V}^{\mathrm{EoS}}_{\mathrm{s},i}(T, P, \boldsymbol{n}_{\mathrm{s}}, \boldsymbol{\nu})$ is the partial molar volume of solute i in the bulk rubber or amorphous domains (Equation 3.33)[‖]. All the elastic models discussed can thus be unified under the formalism just developed. The magnitude of the constraint pressure can be calculated with the help of Equation 3.45 by simply dividing the excess chemical potential obtained with these models by $\bar{V}_{\mathrm{s},i}$. Finally, we note that the approach of Memari and coworkers[44,271,272] and of Minelli and coworkers[45] – who used a constant P_{c} – corresponds to setting $\Delta A^{\mathrm{c}} \approx P_{\mathrm{c}} V$

3.2.4. Formal statement of the local equilibrium hypothesis (This work)

We will now develop a general formalism to explore the consequences of the local-equilibrium hypothesis on the thermodynamic properties of the amorphous domains of crystal-mobile polymers (*cf.* Section 3.1.4). Let us assume again that the free energy of a constrained polymer system satisfies Equation 3.42. Furthermore, for simplicity let us assume that the system is made of ν identical chains of n monomers each. The arguments below can be extended to polydisperse chain distributions. Since n can change it is hereon included in the variables characterizing A. We will further write $A = A(T, V, \boldsymbol{n}_{\mathrm{s}}, n; \nu, \boldsymbol{\Gamma}_{\mathrm{c}})$ to emphasize that the constraints $\boldsymbol{\Gamma}_{\mathrm{c}}$ and therefore ν cannot vary.

Equilibrium with respect to exchanges of chain monomers between the system and a reservoir – in our case, the crystalline lamellae – at fixed $T, V, \boldsymbol{n}_{\mathrm{s}}, \nu, \boldsymbol{\Gamma}_{\mathrm{c}}$ can be treated

[‖] for a formal justification of 3.45, see Equation B.4 in Appendix B

formally by considering the swollen network as a semi-open system allowing exchanges of chain monomers but not of entire polymer molecules with the reservoir. In this framework, the lamellae are thus assumed to fix the "monomer chemical potential" $\mu_{\mathrm{p,mono}}$, defined as the change in Gibbs free energy (at fixed T, P) of the lamella due to the incorporation of one mole of monomers. By using similar arguments to those leading to Equation 3.4, in the limit of high molecular weight ($n \to +\infty$) the Gibbs free energy G_{lamella} of a lamella with n monomers can be written as

$$G_{\mathrm{lamella}}(T, P, n, A_\Sigma) \approx n\mu^{\mathrm{EoS}}_{\mathrm{p,mono}}(T, P) - nM_0\Delta h^0_{\mathrm{m}}\left(1 - \frac{T}{T^0_{\mathrm{m}}}\right) + 2\sigma_{\mathrm{e}}A_\Sigma \tag{3.46}$$

where M_0 is the molar mass of a monomer and $\mu^{\mathrm{EoS}}_{\mathrm{p,mono}}$ the chemical potential *per monomer* of the pure liquid polymer in the limit of high molecular weight (*cf.* Appendix C). In the limit of high molecular weight both the melting temperature T^0_{m} and specific melting enthalpy Δh^0_{m} of the extended chain crystal should not depend on the molecular weight**. Local equilibrium at the fold surface leads to a change in the number of crystalline monomers at constant fold surface area A_Σ:

$$\begin{aligned}\mu_{\mathrm{p,mono}} &= \left(\frac{\partial G_{\mathrm{lamella}}}{\partial n}\right)_{T,P,A_\Sigma} \\ &\approx \mu^{\mathrm{EoS}}_{\mathrm{p,mono}}(T, P) - M_0\Delta h^0_{\mathrm{m}}\left(1 - \frac{T}{T^0_{\mathrm{m}}}\right) + 2A_\Sigma\left(\frac{\partial \sigma_{\mathrm{e}}}{\partial n}\right)_{T,P,A_\Sigma}\end{aligned} . \tag{3.47}$$

Since the interfacial free energy of the fold surface per unit area (σ_{e}) can be a function of parameters such as the inter-lamellar distance[156] – which varies during partial melting –, in general its partial derivative with respect to n should be computed. However, in the current work this term is neglected for simplicity, leading to the following

**As pointed out in Section 3.1.1, however, the melting point T^0_{m} can change due to presence of non-crystallisable units

expression:

$$\mu_{\mathrm{p,mono}} \approx \mu^{\mathrm{EoS}}_{\mathrm{p,mono}}(T,P) - M_0 \Delta h^0_{\mathrm{m}} \left(1 - \frac{T}{T^0_{\mathrm{m}}}\right). \tag{3.48}$$

Since all the network chains are identical, an increase of one monomer per chain corresponds to a decrease of ν monomers in the lamellae. Equilibrium between the lamella and the inter-lamellar domains is therefore expressed by the following equation:

$$\begin{aligned} \mu_{\mathrm{p,mono}} &= \frac{1}{\nu}\left(\frac{\partial A}{\partial n}\right)_{T,V,\boldsymbol{n}_{\mathrm{s}},\nu,\boldsymbol{\Gamma}_{\mathrm{c}}} = \left(\frac{\partial \tilde{A}}{\partial n}\right)_{T,V,\boldsymbol{n}_{\mathrm{s}},\nu,\boldsymbol{\Gamma}_{\mathrm{c}}} \\ &= \frac{1}{\nu}\left(\frac{\partial A^{(n),\mathrm{EoS}}}{\partial n}\right)_{T,V,\boldsymbol{n}_{\mathrm{s}},\nu} + \frac{1}{\nu}\left(\frac{\partial \Delta A^{\mathrm{c}}}{\partial n}\right)_{T,V,\nu,\boldsymbol{\Gamma}_{\mathrm{c}}} \end{aligned} \tag{3.49}$$

Here, the reduced Helmholtz free energy $\tilde{A}$ is obtained by $\tilde{A} = A/\nu$ and we have used Equation 3.42. The superscript (n) has been added to the Helmholtz free energy of the unconstrained liquid A^{EoS} to emphasize that it must be calculated for chains of n monomers each.

Taking derivatives with respect to n amounts to treat this quantity as a continuous variable; in the current work, this procedure is justified by the fact that the polymer strands possess a large number of individual monomers. Details on how these derivatives are calculated for our model are given in Section 3.3.3.

3.2.5. Solubility calculations in the $T, P, \boldsymbol{\mu}_{\mathbf{s}}, \mu_{\mathbf{p,mono}}$ ensemble (This work)

Since for crystal-mobile polymers at fixed temperature T, pressure P and composition $\boldsymbol{y}$ of the external fluid both the chemical potential of the solutes (Equation 3.20) and the monomer chemical potential of the polymer (Equation 3.48) are fixed, we can treat solubility calculation formally by calculating thermodynamic properties in the

$T, P, \boldsymbol{\mu}_\mathrm{s}, \mu_\mathrm{p,mono}$ ensemble. Crystal-fixed polymers can be treated instead in the corresponding $T, P, \boldsymbol{\mu}_\mathrm{s}$ ensemble where the number of polymer's monomers in the amorphous domains is not allowed to change.

By noticing that the number of polymer molecules ν and the constraints $\boldsymbol{\Gamma}_\mathrm{c}$ are constants we can define in the same spirit of Section 2.3.3 the function

$$\begin{aligned}\Phi^*(T, P, \boldsymbol{\mu}_\mathrm{s}, \mu_\mathrm{p,mono}; V, \boldsymbol{n}_\mathrm{s}, n; \nu, \boldsymbol{\Gamma}_\mathrm{c}) &= A(T, V, \boldsymbol{n}_\mathrm{s}, n; \nu, \boldsymbol{\Gamma}_\mathrm{c}) + PV \\ &\quad - \sum_{i=1}^{N_\mathrm{C}} \mu_{\mathrm{s},i} n_{\mathrm{s},i} - \nu \mu_\mathrm{p,mono} n\end{aligned} \tag{3.50}$$

and require that at equilibrium it is stationary with respect to variations in the volume V, number of solute particles $\boldsymbol{n}_\mathrm{s}$ and number of chain monomers n :

$$\begin{cases} V = V(T, P, \boldsymbol{\mu}_\mathrm{s}, \mu_\mathrm{p,mono}; \nu, \boldsymbol{\Gamma}_\mathrm{c}) \\ \boldsymbol{n}_\mathrm{s} = \boldsymbol{n}_\mathrm{s}(T, P, \boldsymbol{\mu}_\mathrm{s}, \mu_\mathrm{p,mono}; \nu, \boldsymbol{\Gamma}_\mathrm{c}) \\ n = n(T, P, \boldsymbol{\mu}_\mathrm{s}, \mu_\mathrm{p,mono}; \nu, \boldsymbol{\Gamma}_\mathrm{c}) \end{cases} \Leftrightarrow \begin{cases} \left(\frac{\partial \Phi^*}{\partial V}\right)_{T,P,\boldsymbol{\mu}_\mathrm{s},\mu_\mathrm{p,mono},\boldsymbol{n}_\mathrm{s},n,\nu,\boldsymbol{\Gamma}_\mathrm{c}} = 0 \\ \left(\frac{\partial \Phi^*}{\partial n_{\mathrm{s},i}}\right)_{T,P,\boldsymbol{\mu}_\mathrm{s},\mu_\mathrm{p,mono},V,\boldsymbol{n}_\mathrm{s}\setminus\{n_{\mathrm{s},i}\},n,\nu,\boldsymbol{\Gamma}_\mathrm{c}} = 0 \\ \left(\frac{\partial \Phi^*}{\partial n}\right)_{T,P,\boldsymbol{\mu}_\mathrm{s},\mu_\mathrm{p,mono},V,\boldsymbol{n}_\mathrm{s},\nu,\boldsymbol{\Gamma}_\mathrm{c}} = 0 \end{cases} . \tag{3.51}$$

The $2N_\mathrm{C} + 2$ Equations on the right hand side correspond to the equilibrium conditions previously stated (Equations 3.40, 3.19 and 3.49). In particular, since the number of polymer molecules ν is constant, we note that the same result can be obtained by minimising the reduced potential

$$\begin{aligned}\tilde{\Phi}^*(T, P, \boldsymbol{\mu}_\mathrm{s}, \mu_\mathrm{p,mono}; V, \tilde{\boldsymbol{n}}_\mathrm{s}, n; \nu, \boldsymbol{\Gamma}_\mathrm{c}) &= \Phi^*/\nu \\ &= \tilde{A}(T, V, \boldsymbol{n}_\mathrm{s}, n; \nu, \boldsymbol{\Gamma}_\mathrm{c}) + P\tilde{V} \\ &\quad - \sum_{i=1}^{N_\mathrm{C}} \mu_{\mathrm{s},i} \tilde{n}_{\mathrm{s},i} - \mu_\mathrm{p,mono} n\end{aligned} \tag{3.52}$$

with respect to variations in the reduced volume $\tilde{V} = V/\nu$, number of solute molecules

per polymer molecule $\tilde{\boldsymbol{n}}_{\mathrm{s}} = \boldsymbol{n}_{\mathrm{s}}/\nu$ and number of chain monomers n.

Note that applying simultaneously the four driving forces $T, P, \boldsymbol{\mu}_{\mathrm{s}}$ and $\mu_{\mathrm{p,mono}}$ is not at odds with the Gibbs-Duhem equation for the system as its free energy A is in general not extensive in all the four conjugated variables $S, V, \boldsymbol{n}_{\mathrm{s}}, n$ – where S indicates entropy – due to the presence of ΔA^{c}.

3.3. Development of a new model (This work)

In this Section a new model for predicting the solubility of small molecules in semi-crystalline polymers is developed by applying the formalism developed in Sections 3.2.3, 3.2.4 and 3.2.5.

3.3.1. Improving upon previous theories

All of the solubility models reviewed in Section 3.2 present features that are incompatible with the current understanding of the physics of the amorphous domains. Model parameters such as the mean molecular weight of the chains $\bar{M}_{\mathrm{c}}$ for the FR theory or the fraction of elastically effective polymer f_{T} of the MH theory – obtained via comparison of the model predictions with solubility data – therefore possess only qualitative physical meaning. Furthermore, these approximations can diminish the ability of these models to predict solubility in conditions different from the ones in which the model parameters were obtained.

Non-Gaussian chain stretching

As shown in Section 3.2.2, there is strong support for the idea that the solubility reduction in semi-crystalline polymers is due to the stretching of the tie-molecules upon

swelling. However, all the models reported derive expressions for the excess chemical potential $\Delta\mu^{c}_{s,i}$ (Equation 3.24) by assuming that the end-to-end probability distribution of the polymer chains conforms to Gaussian statistics which is valid only for small end-to-end displacements relative to the extended-chain configuration.[134] This is at odds with the fact that the inter-lamellar domains are highly constrained.[193,205,238] In particular, in crystal-mobile polymers the local-equilibrium between the lamellae and the amorphous mass should make the tie-molecules taut at temperatures sufficiently lower than the melting point[7,39,42,194–196] – as it is show in Section 4.1.

Anisotropic swelling

Another indisputable fact is that due to the rigidity of the crystal structure swelling in the inter-lamellar domains must be essentially one-dimensional. This concept was implemented in the swelling models by Brown[40] and Liu and Neogi,[41] as well as in the premelting studies by Mansfield *et al.*[199] and Albrecht and Strobl.[200] However, all of these models make use of the Gaussian approximation. Moreover, Brown's and Liu and Neogi's models are only applicable to crystal-fixed polymers, whereas Mansfield and Albrecht and Strobl's models only deal with pure polymers.

Limits of the Michaels and Hausslein theory

The Michaels and Hausslein theory[39] is the only solubility model to date to account for the mass exchange at the crystal/amorphous interface, which is a defining characteristic of crystal-mobile polymers. Nevertheless, the model assumes that the amorphous domains are completely isotropic and that the polymer chains conform to Gaussian statistics. Furthermore, the mass fraction of elastically effective chains f_{T} – the main model parameter – should vary with temperature due to the local-equilibrium hypothesis, whereas it has been used as a constant for each polymer sample in most of the

subsequent works that implemented the theory.[39,42,43,251–258] These issues are addressed in Section 3.3.3 with the development of a new model for the Helmholtz free energy of the inter-lamellar domains.

Free and inter-lamellar domains

All the solubility models reviewed are based on the 2-domain model, according to which all the amorphous mass can be considered homogeneous. As mentioned in Section 3.1.5, there is strong evidence for the existence of two populations of amorphous chains in semi-crystalline polymers: one semi-rigid and constrained, and one "loose" and melt-like. In the current work, following Chmelař and coworkers[238] the amorphous domains are divided in constrained inter-lamellar domains (superscript IL) and "free" extra-lamellar amorphous domains (superscript F) that possess approximately the properties of a polymer melt.

If two types of amorphous domains are present, we can define $m_{\mathrm{s},i}^{\mathrm{F}}$ and $m_{\mathrm{s},i}^{\mathrm{IL}}$ as the mass of each solute i in the free and inter-lamellar domains, respectively. The overall solubility S_i of solute i (Equation 3.14) can then be expressed as a function of the solubility in the free ($S_{\mathrm{a},i}^{\mathrm{F}} = m_{\mathrm{s},i}^{\mathrm{F}}/m_{\mathrm{p}}^{\mathrm{F}}$) and inter-lamellar ($S_{\mathrm{a},i}^{\mathrm{IL}} = m_{\mathrm{s},i}^{\mathrm{IL}}/m_{\mathrm{p}}^{\mathrm{IL}}$) amorphous domains:

$$\begin{aligned} S_i &= \frac{m_{\mathrm{s},i}}{m_{\mathrm{p}}^{\mathrm{tot}}} = \frac{m_{\mathrm{s},i}^{\mathrm{F}}}{m_{\mathrm{p}}^{\mathrm{tot}}} + \frac{m_{\mathrm{s},i}^{\mathrm{IL}}}{m_{\mathrm{p}}^{\mathrm{tot}}} \\ &= \frac{m_{\mathrm{p}}^{\mathrm{F}}}{m_{\mathrm{p}}^{\mathrm{tot}}} \frac{m_{\mathrm{s},i}^{\mathrm{F}}}{m_{\mathrm{p}}^{\mathrm{F}}} + \frac{m_{\mathrm{p}}^{\mathrm{LS}}}{m_{\mathrm{p}}^{\mathrm{tot}}} \frac{m_{\mathrm{p}}^{\mathrm{IL}}}{m_{\mathrm{p}}^{\mathrm{LS}}} \frac{m_{\mathrm{s},i}^{\mathrm{IL}}}{m_{\mathrm{p}}^{\mathrm{IL}}} \\ &= \psi S_{\mathrm{a},i}^{\mathrm{F}} + (1-\psi)\left(1-\omega_{\mathrm{c}}^{\mathrm{LS}}\right) S_{\mathrm{a},i}^{\mathrm{IL}} \end{aligned} \quad , \tag{3.53}$$

Here, ψ is the mass fraction of free amorphous domains (Equation 3.11) whereas

$$\omega_{\mathrm{c}}^{\mathrm{LS}} = \frac{m_{\mathrm{p}}^{\mathrm{c}}}{m_{\mathrm{p}}^{\mathrm{LS}}} = \frac{m_{\mathrm{p}}^{\mathrm{c}}}{m_{\mathrm{p}}^{\mathrm{c}} + m_{\mathrm{p}}^{\mathrm{IL}}} = 1 - \frac{m_{\mathrm{p}}^{\mathrm{IL}}}{m_{\mathrm{p}}^{\mathrm{LS}}} \tag{3.54}$$

is the crystallinity of the lamellar stacks (LS) – since all crystalline polymers are considered to be lamellar. This quantity can be related to the total crystallinity ω_{c} and ψ by combining Equations 3.8 and 3.11:

$$\omega_{\mathrm{c}}^{\mathrm{LS}} = \frac{m_{\mathrm{p}}^{\mathrm{c}}}{m_{\mathrm{p}}^{\mathrm{LS}}} = \frac{m_{\mathrm{p}}^{\mathrm{c}}}{m_{\mathrm{p}}^{\mathrm{tot}}} \frac{m_{\mathrm{p}}^{\mathrm{tot}}}{m_{\mathrm{p}}^{\mathrm{LS}}} = \frac{\omega_{\mathrm{c}}}{1-\psi}. \tag{3.55}$$

By comparing Equation 3.53 to Equation 3.18, we can also write

$$S_i = (1-\omega_{\mathrm{c}}) S_{\mathrm{a},i} = (1-\omega_{\mathrm{c}}) \left(\phi S_{\mathrm{a},i}^{\mathrm{F}} + (1-\phi) S_{\mathrm{a},i}^{\mathrm{IL}} \right), \tag{3.56}$$

where

$$\phi = \frac{m_{\mathrm{p}}^{\mathrm{F}}}{m_{\mathrm{p}}^{\mathrm{F}} + m_{\mathrm{p}}^{\mathrm{IL}}} = \frac{\psi}{1-\omega_{\mathrm{c}}} \tag{3.57}$$

is the mass fraction of free amorphous mass relative to the total amorphous mass in the sample; the overall sorption of solute i in the amorphous domains thus satisfies

$$S_{\mathrm{a},i} = \phi S_{\mathrm{a}}^{\mathrm{F}} + (1-\phi) S_{\mathrm{a},i}^{\mathrm{IL}}, \tag{3.58}$$

i.e., it is a weighted average of the solubility in the free and inter-lamellar domains.

3.3.2. Free amorphous domains

We treat the free amorphous domains as subcooled polymer + solutes mixtures:

$$A^{\mathrm{F}}(T, V, \boldsymbol{n}_{\mathrm{s}}, n; \nu, \boldsymbol{\Gamma}_{\mathrm{c}}) \approx A^{(n),\mathrm{EoS}}(T, V, \boldsymbol{n}_{\mathrm{s}}, \nu), \tag{3.59}$$

where the superscript (n) indicates the number of monomers of the polymer chains as in Equation 3.49. Although we can expect inhomogeneities in both the density and stress state to be present in these domains, this assumption reflects the defining property of free amorphous domains – i.e., being composed of "loose" polymer chains with slow, melt-like dynamics.[193,238]

It must be noted that we assume the local equilibrium between the free amorphous mass and the lamellae to be absent; this is a crude simplification, as the persistence of amorphous mass in these domains must be due to local equilibrium on the lateral lamellar surfaces[156,274] or chain ends and defects.[131,150,170,175,275] However, this assumption is necessary if we take $A^{\mathrm{F}} = A^{\mathrm{EoS}}$ since otherwise below the melting point of the polymer all the monomers of the polymer chains would be incorporated in the lamellae due to the absence of constraints. It might be important to relax this approximation if the variation of the free amorphous mass with temperature and concentration needs to be calculated.

Therefore, at fixed $T, P, \boldsymbol{\mu}_{\mathrm{s}}$ the solubility of each component in the free amorphous domains $S^{\mathrm{F}}_{\mathrm{a},i}(T, P, \boldsymbol{\mu}_{\mathrm{s}})$ is simply calculated by using Equation 3.19, 3.20 and 3.22 (i.e., $S^{\mathrm{F}}_{\mathrm{a},i} = S^{\mathrm{EoS}}_{\mathrm{a},i}$). The polymer is modelled as having no ends and a fixed number of monomers $n_0 = 1000$.

3.3.3. Inter-lamellar domains

In this section an expression for the free energy of the inter-lamellar amorphous domains in semi-crystalline polymers is derived, based on a simple statistical-mechanics model. The constraint pressure emerges naturally from this treatment due only to the presence of tie-molecules bridging the two opposing lamellae. The local-equilibrium hypothesis is then applied in order to remove an unknown from the solubility calculations (namely, the

average number of monomers per tie-molecule) in crystal-mobile polymers. The resulting model is characterized by two free parameters: the fraction of stems connected to tie-molecules, p_{T}, and the inter-lamellar distance l_{a}^{*} of the pure semi-crystalline polymer at an arbitrary temperature T^{*} and pressure P^{*}.

This allows one to calculate the dependence of both P_{c} and the the crystallinity of the lamellar stacks $\omega_{\mathrm{c}}^{\mathrm{LS}}$ on temperature, pressure and composition. As a result, the contribution $S_{\mathrm{a},i}^{\mathrm{IL}}(T,P)$ can be calculated either with the combination of with Equations 3.34 and 3.19 or by minimisation of the $\tilde{\Phi}$ potential described in Section 3.2.5. The total sorption S can finally be determined with Equation 3.53. This formalism includes crystal-fixed polymers as a special case in which mass exchanges at the crystal/amorphous surface are not allowed. However, an extra parameter or extra assumptions are needed to quantify the average number of monomer per polymer chain (see below).

Morphological model

For simplicity, the lamellar stacks are modelled as a sequence of alternating layers of crystalline polymer (the lamellae) and amorphous material characterized by a well-defined lamellar thickness l_{c} and inter-lamellar distance l_{a}. Let V be the volume of a region of the amorphous domains included between two parallel crystalline lamellae. The relationship between V and l_{a} is simply

$$V = A_{\Sigma} l_{\mathrm{a}}, \tag{3.60}$$

where A_{Σ} is the area of one lamellar surface facing the inter-lamellar domains (the fold surface). Although this quantity might change with temperature due to mass exchanged between the lateral lamellar surfaces and the free amorphous mass,[156,274] in the current model it must be a constant as the latter phenomenon does not take place (see discussion in Section 3.3.2).

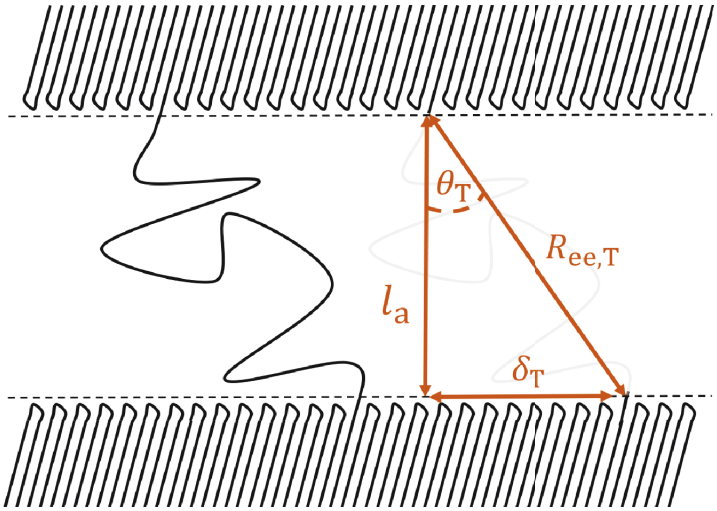

Figure 3.7.: A schematic depiction of a bridge molecule in the inter-lamellar domains. $R_{ee,T}$ is its end-to-end distance, l_a the inter-lamellar distance and δ_T the projection of the end-to-end vector of the bridge on the lamellar surface.

In this model, the constraints $\mathbf{\Gamma}_c$ acting on the inter-lamellar domains are embodied by the rigidity of the crystal structure which prevents the crystalline stems in the lamellae from moving along the plane parallel to the lamellar surfaces[††]. As a consequence, the topology of the inter-lamellar domain – i.e., the fraction of tie-molecules p_T, but more in general of loops etc. – is assumed to be constant. We stress that all of these approximations can break down at temperatures near the melting point, where recrystallization and structural reorganizations on the meso-scale may occur.[156]

In the following development tails and free chains (Figure 3.2) are neglected as their effect should be minimal except for very low-molecular weight samples. Furthermore, we introduce here the major approximation that the inter-lamellar domains are only composed of bridges. This is not realistic, as both entangled and un-entangled loops should be greater in number than bridges.[7,190,201,207] However, at the level of description employed here accounting for the full topological complexity of the inter-lamellar domains would introduce too many free parameters without adding physical insight.

[††]Note that in crystal-mobile polymers longitudinal chain motion is expected (*cf.* Section 3.1.4)

This approximation is inspired by the observation that bridges and entangled loops (i.e., the tie-molecules) should have a similar effect mechanical and swelling properties of the inter-lamellar domains.[7,193,258] As shown in Appendix E, at the level of our description substituting all entangled loops with equivalent bridges with the same average tension and inclination leaves the constraint pressure unchanged. On the other hand, un-entangled loops should not contribute significantly to the solubility reduction as they do not stretch upon swelling. This approximation will be progressively justified at key points of the following discussion; the full treatment accounting for loops is reported in Appendix E.

The equivalent bridges of the current model for the inter-lamellar domains (subscript T) are assigned the same average properties, i.e., the same magnitude of the end-to-end vector $R_{\mathrm{ee,T}}$ and number of monomers n_{T} (Figure 3.7). Introduction of chain length distributions in the theory is possible but not essential to capture the main physical features of the problem, and it requires additional assumptions on the shape of said distribution. Notice that bridges do not have end groups: it is therefore assumed that polymer chains in the inter-lamellar domains are only composed of main-chain monomers.

Due to the rigidity of the crystal structure, the projection of the end-to-end vector of each bridge, $\boldsymbol{R}_{\mathrm{ee,T}}$, on the lamellar surfaces is a constant, hereafter named δ_{T} (Figure 3.7):

$$R_{\mathrm{ee,T}} = \|\boldsymbol{R}_{\mathrm{ee,T}}\| = \sqrt{l_{\mathrm{a}}^2 + \delta_{\mathrm{T}}^2}. \tag{3.61}$$

Furthermore, the number of equivalent bridges ν_{T} must also be a constant. We denote with $\rho_{\mathrm{A,T}} = \nu_{\mathrm{T}}/A_{\Sigma}$ the surface density of equivalent bridges (i.e., of stems connected to tie-molecules, Section 3.1.3) on the fold surface. The free energy of the inter-lamellar domains, A^{IL}, is therefore a function of $T, V, \boldsymbol{n}_{\mathrm{s}}, \nu_{\mathrm{T}}$ but also of the number of equivalent

bridge monomers n_{T} and the lateral displacement δ_{T}:

$$A^{\mathrm{IL}} = A^{\mathrm{IL}}(T, V, \boldsymbol{n}_{\mathrm{s}}, n_{\mathrm{T}}; \nu_{\mathrm{T}}, \delta_{\mathrm{T}}); \tag{3.62}$$

the same convention will be used for the other thermodynamic properties of the inter-lamellar domains.

Helmholtz free energy

In order to calculate the Helmholtz free energy of the inter-lamellar amorphous domains, we employ an approach which is similar to the one used by Flory[259] to derive an expression for the free energy of a swollen polymer network. By physically detaching all the bridges in the amorphous domains from the lamellar surface, a confined polymer-solute mixture is obtained (the "confined fluid" - see Figure 3.8). The free energy of the inter-lamellar amorphous domains A^{IL} can be related to the free energy of the confined fluid $A^{'}$ as follows:

$$A^{\mathrm{IL}} \approx A' - k_{\mathrm{B}}T \ln p_{\mathrm{c}} + \Delta E_{\mathrm{bond}}. \tag{3.63}$$

Here, ΔE_{bond} is the energy gain due to the formation of irreversible chemical bonds between the bridges and the lamellae; p_{c}, on the other hand, represents the probability of finding the detached chain segments in configurations compatible with bonding with the lamellae in the confined fluid.

The probability that a given tie-segment j in the confined fluid has the ends in positions $\mathbf{R}_j^{'}, \mathbf{R}_j^{''}$ can be written as $2\Delta\tau^2 p_{\mathrm{ee}}^{'}\left(\mathbf{R}_j^{'}, \mathbf{R}_j^{''}\right)$, where $p_{\mathrm{ee}}^{'}$ is the end-to-end probability distribution in the confined fluid and $\Delta\tau$ is the average volume in which the ends of the bridges remain confined due to thermal motion and bonding with the lamellae.[259] This volume is in principle (at least) temperature-dependent, but its variations with temperature are small due to the strength of the chemical bonds. Furthermore, one

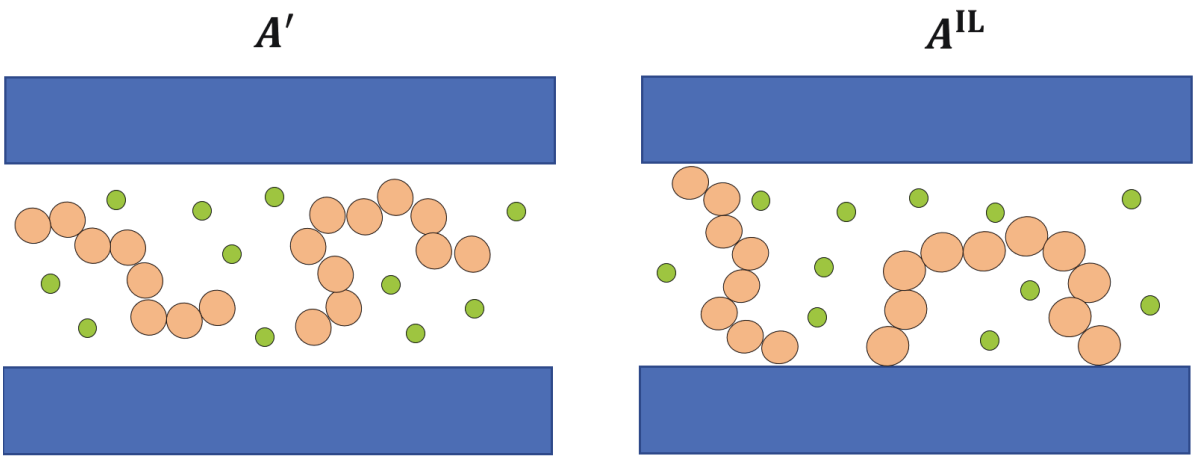

Figure 3.8.: A schematic representation of the systems related by Equation 3.63: the confined polymer-solute mixture (left) and the inter-lamellar domains (right). The orange chains represent polymer segments, the green circles solute molecules, and the blue rectangles lamellae. Notice that in the current model we assume that all the bridges have the same number of monomers and that loops are absent (in contrast to what the picture suggests).

should note that in general p'_{ee} depends on temperature, solute concentration and volume aside from the end-to end distance $\mathbf{R}'_j - \mathbf{R}''_j$ and number of chain monomers n_{T}. These dependencies are kept implicit for now to simplify the notation. The factor 2 comes from the equivalence of the two chain ends.

We then perform the approximation

$$p'_{\mathrm{ee}}\left(\mathbf{R}'_j, \mathbf{R}''_j\right) \approx p_{\mathrm{ee}}\left(\mathbf{R}'_j, \mathbf{R}''_j\right), \tag{3.64}$$

where p_{ee} is the end-to-end probability distribution of a polymer chain with the same number of monomers in a *bulk* polymer mixture characterized by the same temperature, polymer and solute density as the confined fluid.

With this approximation one neglects the fact that the presence of the lamellae breaks the bulk symmetry, meaning that the actual probability for a free chain in the confined fluid of attaining configurations with its ends in the volumes $\Delta\tau$ centered at

$\mathbf{R}_j^{'}, \mathbf{R}_j^{''}$ might be different from $2\Delta\tau^2 p_{\mathrm{ee}}\left(\mathbf{R}_j^{'}, \mathbf{R}_j^{''}\right)$ due for example to the interaction with the crystal surface and the inability of bridge monomers to "cross" the lamellar surface.[276]

Since p_{ee} is a bulk end-to-end distribution, due to translational and rotational invariance we have

$$p_{\mathrm{ee}}\left(\mathbf{R}_j^{'}, \mathbf{R}_j^{''}\right) = \frac{1}{V} p_{\mathrm{ee}}(R_{\mathrm{ee},j}), \tag{3.65}$$

where $R_{\mathrm{ee},j}$ is the magnitude of the end-to-end vector of the j^{th} chain. Since all the chains are assumed to have the same number of monomers n_{T} and (magnitude of the) end-to-end vector $R_{\mathrm{ee,T}}$ (Figure 3.7), we can thus approximate p_{c} with

$$p_{\mathrm{c}} \approx \nu_{\mathrm{T}}! \left(\frac{2\Delta\tau^2 p_{\mathrm{ee}}\left(R_{\mathrm{ee,T}}\right)}{V}\right)^{\nu_{\mathrm{T}}}, \tag{3.66}$$

where the factor $\nu_T!$ accounts for the number of ways to choose chain segments in the confined fluid to fill the ν_T pairs of bonding sites on the lamellae. This approximation amounts to assuming that as the structure of bound chain segments is progressively built from the detached chains, the probability for an unbound chain to attain configurations compatible with its target constrained state is not influenced by the presence of the other constrained segments. At this level we are thus neglecting any pair and higher-order correlations between chains, as it is customary in polymer networks models.[39,259,266]

Equation 3.63 for the Helmholtz free energy can therefore be rewritten as

$$A^{\mathrm{IL}} \approx A' - k_{\mathrm{B}}T\left(\nu_{\mathrm{T}} \ln\left(p_{\mathrm{ee}}\left(R_{\mathrm{ee,T}}\right)\Delta\tau\right) + \nu_{\mathrm{T}} \ln\left(\frac{\Delta\tau}{V}\right) + \zeta(\nu_{\mathrm{T}})\right) + \Delta E_{\mathrm{bond}}. \tag{3.67}$$

Here, $\zeta(\nu_{\mathrm{T}})$ includes all the terms which depend only on the number of segments; since the topology of the inter-lamellar domains is assumed to not change, $\zeta(\nu_{\mathrm{T}})$ is just a

constant in the free energy.

The final approximation that we perform is to assume that the free energy of the confined fluid, $A^{'}$, is the free energy of a bulk polymer-solute mixture at the same temperature, volume and composition:

$$A^{(n_{\mathrm{T}}),'}(T, V, \boldsymbol{n}_s, \nu_{\mathrm{T}}) \approx A^{(n_{\mathrm{T}}),\mathrm{EoS}}(T, V, \boldsymbol{n}_s, \nu_{\mathrm{T}}). \tag{3.68}$$

Here, the superscript (n_{T}) has been added to emphasize that the polymer chains in the confined and bulk mixture have n_{T} monomers (as in Equation 3.49 and following discussion). Approximating $A^{'}$ with A^{EoS} amounts to neglecting finite-size effects on the thermodynamic properties of an unconstrained polymer mixture confined between two lamellae. This approximation is consistent with the assumption $p_{\mathrm{ee}}^{'} \approx p_{\mathrm{ee}}$ discussed earlier. Equation 3.67 is thus now in the form of Equation 3.37, and we can identify ΔA^{c} with

$$\begin{aligned} \Delta A^{\mathrm{c}} &= -\nu_{\mathrm{T}} k_{\mathrm{B}} T \ln\left(p_{\mathrm{ee}}\left(R_{\mathrm{ee,T}}\right)\Delta\tau\right) - \nu_{\mathrm{T}} k_{\mathrm{B}} T \ln\left(\frac{\Delta\tau}{V}\right) + C(T) \\ &= \Delta A^{\mathrm{el}} + \Delta A^{\mathrm{loc}} + C(T) \end{aligned}, \tag{3.69}$$

where the quantity $C(T)$ is volume-independent and contains the bonding energy and the $\zeta(\nu)$ term. ΔA^{el} is the "elastic" contribution to ΔA^{c} due to the stretching of the bridges. ΔA^{loc}, one the other hand, represents an ideal gas term due to the loss of translational degrees of freedom of the constrained chains. It can be shown (*cf.* Appendix E) that under similar assumptions the inclusion of loops in the theory (both entangled and not) would lead to 2 additional stretching term and two additional ideal gas terms to Equation 3.69.

As can be seen in Equation 3.69, in order to calculate ΔA^{c} the functional form of the bulk end-to-end probability distribution $p_{\mathrm{ee}}(R_{\mathrm{ee,T}})$ must be specified. In general, this

distribution is a complicated function of the end-to-end vector $R_{\mathrm{ee,T}}$ since it includes all the effects of the intra-molecular bonding interactions and of the interactions with the other monomers and the solutes. However, it is possible to show[134,260,265] that for long chains in polymer melts or concentrated solutions, the average squared end-to-end distance of a chain with M bonds of length l is given by

$$\langle R_{\mathrm{ee}}^2 \rangle = C_\infty M l^2, \tag{3.70}$$

where C_∞ is the Flory characteristic ratio which is roughly a constant for a given polymer.

In line with the phantom chain model used in most polymer network theories,[38–40,134,199,259] in this work we assume

$$p_{\mathrm{ee}}(R_{\mathrm{ee,T}}; T, V, \boldsymbol{n}_{\mathrm{s}}, n_{\mathrm{T}}, \nu_{\mathrm{T}}) \approx p_{\mathrm{ee}}^{\mathrm{FJ}}(R_{\mathrm{ee,T}}; N_{\mathrm{T}}, b), \tag{3.71}$$

where $p_{\mathrm{ee}}^{\mathrm{FJ}}$ is the end-to-end probability distribution of an *equivalent* freely jointed chain (i.e., $C_\infty^{\mathrm{FJ}} = 1$) with N_{T} monomers and bond length b. This approximations results in p_{ee} depending only on n_{T} and $R_{\mathrm{ee,T}}$, and therefore ΔA^{c} is now composition-independent (in line with Equation 3.42). The two equivalent chain parameters N_{T} and b can be found by enforcing that the contour length and mean square end-to-end distance of the two chains is the same:

$$\begin{cases} \langle R_{\mathrm{ee,T}}^2 \rangle^{\mathrm{FJ}} = \langle R_{\mathrm{ee,T}}^2 \rangle = C_\infty \mathcal{N}_{\mathrm{b}} n_{\mathrm{T}} l^2 \\ R_{\mathrm{max,T}}^{\mathrm{FJ}} = R_{\mathrm{max,T}} = \mathcal{N}_{\mathrm{b}} n_{\mathrm{T}} l \cos\left(\frac{\pi - \theta_{\mathrm{B}}}{2}\right) \end{cases} \rightarrow \begin{cases} N_{\mathrm{T}} &= \frac{\cos^2((\pi-\theta_{\mathrm{B}})/2)}{C_\infty} \mathcal{N}_{\mathrm{b}} n_{\mathrm{T}} \\ b &= \frac{C_\infty}{\cos((\pi-\theta_{\mathrm{B}})/2)} l \end{cases}. \tag{3.72}$$

In the equation above $\mathcal{N}_{\mathrm{b}}$ is the number of main-chain bonds per monomer (e.g., 1 in PE an 3 in PEG), whereas l and θ_{B} are, respectively, the (average) bond length and bond angle of the real chain. Alternatively, by defining $l_{\mathrm{mono}} = l \cos\left((\pi - \theta_{\mathrm{B}})/2\right)$ the

two equations in 3.72 can be expressed as

$$n_{\mathrm{T}}/N_{\mathrm{T}} = b/(\mathcal{N}_{\mathrm{b}} l_{\mathrm{mono}}) = \frac{C_\infty}{\mathcal{N}_{\mathrm{b}} \cos^2((\pi - \theta_{\mathrm{B}})/2)} = \eta, \tag{3.73}$$

where η is a constant. Therefore, the equivalent freely-jointed chain has fewer but longer bonds than the real chain.

Using the accurate Langevin statistics – a rigorous result for freely-jointed chains if the force is imposed instead of a displacement – $p_{\mathrm{ee}}^{\mathrm{FJ}}$ can be approximated by[260,265]

$$\begin{aligned} \ln p_{\mathrm{ee}}^{\mathrm{FJ}}\left(R_{\mathrm{ee,T}}, N_{\mathrm{T}}; b\right) &\approx \ln C(N_{\mathrm{T}}) - \frac{1}{b}\int_0^{R_{\mathrm{ee,T}}} \mathcal{L}^{-1}\left(\frac{R}{N_{\mathrm{T}} b}\right) \mathrm{d}R \\ &= \ln C(N_{\mathrm{T}}) - N_{\mathrm{T}} \int_0^{x_{\mathrm{T}}} \mathcal{L}^{-1}(x')\mathrm{d}x' \\ &= \ln C(N_{\mathrm{T}}) - N_{\mathrm{T}}\left[x_{\mathrm{T}}\mathcal{L}^{-1}(x_{\mathrm{T}}) - \ln \frac{\sinh \mathcal{L}^{-1}(x_{\mathrm{T}})}{\mathcal{L}^{-1}(x_{\mathrm{T}})}\right] \end{aligned}, \tag{3.74}$$

where $\mathcal{L}^{-1}$ is the inverse of the Langevin function $\mathcal{L}(y) = \coth y - 1/y$ and $C(N_{\mathrm{T}})$ is a normalization constant – see Appendix F for its definition. Here, we have defined the fractional extension of the tie-molecules

$$x_{\mathrm{T}} = R_{\mathrm{ee,T}}/(N_{\mathrm{T}} b). \tag{3.75}$$

In the Gaussian approximation ($x_{\mathrm{T}} \to 0$),

$$\begin{aligned} \ln p_{\mathrm{ee}}^{\mathrm{FJ}}\left(R_{\mathrm{ee,T}}, N_{\mathrm{T}}; b\right) &\approx -\frac{3}{2}\ln\left(\frac{2\pi N_{\mathrm{T}} b^2}{3}\right) - N_{\mathrm{T}}\frac{3}{2}x_{\mathrm{T}}^2 \\ &= -\frac{3}{2}\ln\left(\frac{2\pi N_{\mathrm{T}} b^2}{3}\right) - \frac{3R_{\mathrm{ee,T}}^2}{2N_{\mathrm{T}} b^2} \end{aligned}. \tag{3.76}$$

Before proceeding with the discussion, it is useful to summarize the assumptions and approximations that are employed to model the inter-lamellar domains:

- In the current model an equilibrium statistical mechanics treatment of the inter-lamellar domains is employed, which implies that these domains should be rubbery rather than glassy. In the latter case, the system could in fact be trapped in a local minimum of the free energy. It may be possible to extend the theory to semi-crystalline polymers with glassy amorphous domains using non-equilibrium theories such as the Non-Equilibrium Thermodynamics for Glassy Polymers (NET-GP) model originally developed by Doghieri, Sarti, and co-workers.[277,278] The NET-GP theory has been successfully employed to describe sorption isotherms of semi-crystalline polymers such as PTFE and MFA,[269] with glass transitions occurring above room temperature.

- We have assumed that the inter-lamellar domains are only composed of bridges. Despite the crude approximation, in Appendix E it is shown that un-entangled loops do not contribute significantly to the solubility reduction (i.e., P_c), whereas entangled loop have qualitatively the same effect as bridges. The surface density of equivalent bridges in the current model is therefore intended as the surface density of tie-molecules $\rho_{A,T}$ (bridges + entangled loops) in the real system.

- In order to find a simple expression for the free energy, the probability of finding a given chain segment in the confined fluid in configurations compatible with its bonded state is assumed to be independent of the presence of the other constrained chain segments. This assumption means that the molecular environment of the chain segments is not altered significantly upon the formation of the ties. This condition is violated if the chain segments in the inter-lamellar amorphous domains attain configurations that are atypical of the molten state.

- The effects that the surfaces of the lamellae have on the thermodynamics of the amorphous domains are neglected. In particular, the end-to-end probability distributions appropriate for concentrated polymer solutions are here used to approx-

imate the probability of observing the two ends of a given bridge on the surfaces of two opposing lamellae. Furthermore, if the inter-lamellar distance l_a is small, finite size effects[276,279–284] should make the free energy A' of the polymer mixture confined in the inter-lamellar amorphous domains different from the one calculated using an equation of state for bulk fluids, A^EoS.

- Langevin statistics is employed to approximate the end-to-end probability distributions, thus accounting for the finite extensibility of real chain segments. To our knowledge, this is the first time that this approximation has been used instead of the Gaussian approximation in the context of predicting sorption in semi-crystalline polymers. Furthermore, this assumption is consistent with the observation that tie-segments in the amorphous domains should be fairly taut.[7,207,238]

Equilibrium with an external fluid

The equilibrium reduced volume $\tilde{V} = V/\nu_\mathrm{T}$, number of solute particles per equivalent bridge $\tilde{n}_{\mathrm{s},i} = n_{\mathrm{s},i}/\nu_\mathrm{T}$ and chain monomers in the inter-lamellar domains n_T can be found by minimisation of the reduced potential $\tilde{\Phi}^{\mathrm{IL},*}$ of the inter-lamellar domains (Equation 3.52):

$$\begin{aligned}\tilde{\Phi}^{\mathrm{IL},*}(T,P,\boldsymbol{\mu}_\mathrm{s},\mu_\mathrm{p,mono};V,\tilde{\boldsymbol{n}}_\mathrm{s},n;\nu_\mathrm{T},\delta_\mathrm{T}) = \tilde{A}^{(n_\mathrm{T}),\mathrm{EoS}}(T,V,\boldsymbol{n}_\mathrm{s},\nu_\mathrm{T}) \\ + \Delta A^\mathrm{c}(T,V,n_\mathrm{T};\nu_\mathrm{T},\delta_\mathrm{T})/\nu_\mathrm{T} \\ + P\tilde{V} - \sum_{i=1}^{N_\mathrm{C}} \mu_{\mathrm{s},i}\tilde{n}_{\mathrm{s},i} - \mu_\mathrm{p,mono} n_\mathrm{T}\end{aligned} \quad . \tag{3.77}$$

Here, $\tilde{A}^{(n_\mathrm{T}),\mathrm{EoS}} = A^{(n_\mathrm{T}),\mathrm{EoS}}/\nu_\mathrm{T}$. The knowledge of $\tilde{n}_{\mathrm{s},i}$ and n_T yields immediately $S^\mathrm{IL}_{\mathrm{a},i}$ since all the inter-lamellar mass is made of bridges:

$$S^\mathrm{IL}_{\mathrm{a},i} = m^\mathrm{IL}_{\mathrm{s,i}}/m^\mathrm{IL}_\mathrm{p} = \frac{M_{\mathrm{s},i}}{M_0}\frac{\tilde{n}_{\mathrm{s},i}}{n_\mathrm{T}}. \tag{3.78}$$

Here, $M_{s,i}$ and M_0 are the molar mass of the solute and the polymer's monomers, respectively. Similarly, the crystallinity of the lamellar stacks ω_c^{LS} is simply related to the number of equivalent bridge monomers n_T:

$$1 - \omega_c^{LS} = \frac{m_p^{IL}}{m_p^{LS}} = \frac{\nu_T M_0}{m_p^{LS}} n_T = K n_T, \tag{3.79}$$

where K is a constant due to the assumption that there is no mass exchange between the lamellar stacks and the free amorphous mass (i.e., that m_p^{LS} and ψ are a constant). Both Equations 3.78 and 3.79 can be extended straightforwardly to include un-entangled loops by multiplying and dividing (respectively) the right-hand side by the mass fraction of tie-molecules f_T (Appendix D). Neglecting un-entangled loops thus corresponds to setting $f_T = 1$.

ΔA^c is given by Equation 3.69 with the Langevin approximation for p_{ee} (Equation 3.74); it is a function of volume as the end-to-end distance is a function of the inter-lamellar distance l_a (Equation 3.61), which in turns is a function of the (reduced) volume via

$$l_a = V/A_\Sigma = \rho_{A,T} V/\nu_T = \rho_{A,T} \tilde{V}, \tag{3.80}$$

where we have used the definition of the surface density of tie-molecules (i.e., of equivalent bridges) $\rho_{A,T} = \nu_T/A_\Sigma$.

The reduced EoS free energy, $A^{(n_T),EoS}/\nu_T$, can be calculated explicitly using an equation of state of choice. In the current work, however, an approximate expression is used in order to elucidate the physical meaning of this quantity and its derivatives in polymer systems. Since $A^{(n_T),EoS}$ is extensive in the volume V, number of solute molecule $\boldsymbol{n}_s$ and number of polymer molecules ν_T, we can write

$$A^{(n_T),EoS} = \sum_{i=1}^{N_C} n_{s,i} \mu_s^{(n_T),EoS} + \nu_T \mu_p^{(n_T),EoS} - P^{(n_T),EoS} V. \tag{3.81}$$

Dividing by ν_{T}, we obtain

$$\begin{aligned}\tilde{A}^{(n_{\mathrm{T}}),\mathrm{EoS}} &= \sum_{i=1}^{N_{\mathrm{C}}} \tilde{n}_{\mathrm{s},i}\mu_{\mathrm{s},i}^{(n_{\mathrm{T}}),\mathrm{EoS}} + \mu_{\mathrm{p}}^{(n_{\mathrm{T}}),\mathrm{EoS}} - P^{(n_{\mathrm{T}}),\mathrm{EoS}}\tilde{V} \\ &= \sum_{i=1}^{N_{\mathrm{C}}} \tilde{n}_{\mathrm{s},i}\mu_{\mathrm{s}}^{(n_{\mathrm{T}}),\mathrm{EoS}} + n_{\mathrm{T}}\mu_{\mathrm{p,mono}}^{(n_{\mathrm{T}}),\mathrm{EoS}} - P^{(n_{\mathrm{T}}),\mathrm{EoS}}\tilde{V}\end{aligned}, \tag{3.82}$$

where we have defined the monomer chemical potential calculated via the EoS as $\mu_{\mathrm{p,mono}}^{(n_{\mathrm{T}}),\mathrm{EoS}} = \mu_{\mathrm{p}}^{(n_{\mathrm{T}}),\mathrm{EoS}}/n_{\mathrm{T}}$ in the same spirit of Equation 3.48. In Appendix C it is shown that at fixed temperature, pressure and mass fraction of solutes and polymer the monomer chemical potential has a well-defined limit as $n_{\mathrm{T}} \to \infty$.

Similarly, at constant temperature, monomer density and mass fraction of solutes and polymer, the monomer chemical potential $\mu_{\mathrm{p,mono}}^{(n_{\mathrm{T}}),\mathrm{EoS}}$, the chemical potential of the solutes $\mu_{\mathrm{s},i}^{(n_{\mathrm{T}}),\mathrm{EoS}}$ and the pressure $P^{(n_{\mathrm{T}}),\mathrm{EoS}}$ have well-defined limits as $n_{\mathrm{T}} \to \infty$. Therefore, in the current work all the functions in Equation 3.82 are calculated using a reference system in which the number of chain monomers is fixed to an arbitrary high value n_0:

$$\tilde{A}^{(n_{\mathrm{T}}),\mathrm{EoS}} \approx \sum_{i=1}^{N_{\mathrm{C}}} \tilde{n}_{\mathrm{s},i}\mu_{\mathrm{s},i}^{(n_0),\mathrm{EoS}} + n_{\mathrm{T}}\mu_{\mathrm{p,mono}}^{(n_0),\mathrm{EoS}} - P^{(n_0),\mathrm{EoS}}V/\nu_{\mathrm{T}}. \tag{3.83}$$

In order to make sure that the mass fraction of polymer and the overall monomer density is unchanged, the pressure and chemical potentials of the reference polymer + solute mixture must be calculated at a different volume and composition:

$$(T, V, \boldsymbol{n}_{\mathrm{s}}, \nu_{\mathrm{T}}) \to \left(T, \frac{n_0}{n_{\mathrm{T}}}\frac{V}{\nu_{\mathrm{T}}}, \frac{n_0}{n_{\mathrm{T}}}\frac{\boldsymbol{n}_{\mathrm{s}}}{\nu_{\mathrm{T}}}, 1\right) = \left(T, \frac{n_0}{n_{\mathrm{T}}}\tilde{V}, \frac{n_0}{n_{\mathrm{T}}}\tilde{\boldsymbol{n}}_{\mathrm{s}}, 1\right). \tag{3.84}$$

The dependence on n_{T} of the thermodynamic properties of the liquid mixture with n_{T} monomers is now enforced through the composition only. At fixed pressure (instead of volume), the EoS functions of state in the reference mixture are calculated at the same

pressure ($P + P_\mathrm{c}$, *cf.* Section 3.2.3) but different composition:

$$(T, P + P_\mathrm{c}, \boldsymbol{n}_\mathrm{s}, \nu_\mathrm{T}) \rightarrow \left(T, P + P_\mathrm{c}, \frac{n_0}{n_\mathrm{T}} \tilde{\boldsymbol{n}}_\mathrm{s}, 1\right). \tag{3.85}$$

Equilibrium can now be solved by minimisation of $\tilde{\Phi}^{\mathrm{IL},*}$, which corresponds to setting its partial derivatives with respect to $\tilde{V}, \tilde{n}_{\mathrm{s},i}$ and n_T equal to zero (Section 3.2.5). In the next two subsections these derivatives are calculated explicitly since they lead to $2N_\mathrm{C}+2$ equilibrium equations and since their value is useful for numerical implementations of the minimisation problem.

Constraint pressure and equilibrium volume

Setting the partial derivative of $\tilde{\Phi}^{\mathrm{IL},*}$ with respect to volume equal to zero leads to the definition of the equilibrium constraint pressure and equilibrium volume at fixed total pressure P, as shown in Section 3.2.3:

$$\begin{aligned}\left(\frac{\partial\tilde{\Phi}^{\mathrm{IL},*}}{\partial\tilde{V}}\right)_{T,P,\boldsymbol{\mu}_\mathrm{s},\mu_\mathrm{p,mono},\boldsymbol{n}_\mathrm{s},n_\mathrm{T},\nu_\mathrm{T},\boldsymbol{\Gamma}_\mathrm{c}} &= P + \left(\frac{\partial\tilde{A}^{\mathrm{IL}}}{\partial\tilde{V}}\right)_{T,\boldsymbol{n}_\mathrm{s},n_\mathrm{T},\nu_\mathrm{T},\boldsymbol{\Gamma}_\mathrm{c}}, \\ &= P - P^{(n_\mathrm{T}),\mathrm{EoS}} + P_\mathrm{c} = 0\end{aligned} \tag{3.86}$$

where we have used Equation 3.40. While the EoS pressure is approximated with the one calculated in the reference polymer + solute mixture with n_0 monomers (see Equation 3.84), the constraint pressure is found by substituting Equation 3.69 in Equation

3.39:

$$\begin{aligned} P_{\mathrm{c}} &= \left(\frac{\partial \Delta A^{\mathrm{c}}}{\partial V}\right)_{T,\boldsymbol{n}_{\mathrm{s}},n_{\mathrm{T}},\nu_{\mathrm{T}},\boldsymbol{\Gamma}_{\mathrm{c}}} \\ &= \left(\frac{\partial \Delta A^{\mathrm{el}}}{\partial V}\right)_{T,\boldsymbol{n}_{\mathrm{s}},n_{\mathrm{T}},\nu_{\mathrm{T}},\boldsymbol{\Gamma}_{\mathrm{c}}} + \left(\frac{\partial \Delta A^{\mathrm{loc}}}{\partial V}\right)_{T,\boldsymbol{n}_{\mathrm{s}},n_{\mathrm{T}},\nu_{\mathrm{T}},\boldsymbol{\Gamma}_{\mathrm{c}}} \\ &= -\nu_{\mathrm{T}} k_{\mathrm{B}} T \left(\frac{\partial R_{\mathrm{ee,T}}}{\partial V}\right)_{\boldsymbol{\Gamma}_{\mathrm{c}}} \left(\frac{\partial \ln p_{\mathrm{ee}}(R_{\mathrm{ee,T}})}{\partial R_{\mathrm{ee,T}}}\right)_{T,\boldsymbol{n}_{\mathrm{s}},n_{\mathrm{T}},\nu_{\mathrm{T}}} + \frac{\nu_{\mathrm{T}} k_{\mathrm{B}} T}{V} \\ &= \nu_{\mathrm{T}} \left(\frac{\partial R_{\mathrm{ee,T}}}{\partial V}\right)_{\boldsymbol{\Gamma}_{\mathrm{c}}} f_{\mathrm{ee,T}} + \frac{\nu_{\mathrm{T}} k_{\mathrm{B}} T}{V} \end{aligned} \tag{3.87}$$

Here, $f_{\mathrm{ee,T}} = -k_{\mathrm{B}}T\,(\partial \ln p_{\mathrm{ee}}/\partial R_{\mathrm{ee,T}})_{T,\boldsymbol{n}_{\mathrm{s}},n_{\mathrm{T}},\nu_{\mathrm{T}}}$ is the (thermodynamic) force acting on the ends of the bridges under the assumptions of the current model. The constancy of the constraints $\boldsymbol{\Gamma}_{\mathrm{c}}$ in the equation above influences how the partial derivative $(\partial R_{\mathrm{ee,T}}/\partial V)$ is calculated. Recalling $V = A_{\Sigma} l_{\mathrm{a}}$ and $R_{\mathrm{ee,T}} = \sqrt{l_{\mathrm{a}}^2 + \delta_{\mathrm{T}}^2}$ (Equation 3.61) we thus obtain

$$\begin{aligned} \left(\frac{\partial R_{\mathrm{ee,T}}}{\partial V}\right)_{\boldsymbol{\Gamma}_{\mathrm{c}}} &= \frac{1}{A_{\Sigma}} \left(\frac{\partial \sqrt{l_{\mathrm{a}}^2 + \delta_{\mathrm{T}}^2}}{\partial l_{\mathrm{a}}}\right)_{\delta_{\mathrm{T}}}, \\ &= \frac{\cos\theta_{\mathrm{T}}}{A_{\Sigma}} \end{aligned} \tag{3.88}$$

where θ_{T} is the angle formed between $\boldsymbol{R}_{\mathrm{ee,T}}$ and the normal to the lamellar surfaces. This equation enforces one-dimensional swelling of the inter-lamellar domains, in line with other modelling works.[40,41] As mentioned at the beginning of Section 3.3, many of the most utilized models for swelling in semi-crystalline polymers[39,259,285] assume isotropic swelling, which translates into

$$\left(\frac{\partial R_{\mathrm{ee,T}}}{\partial V}\right)_{\mathrm{iso}} = \frac{R_{\mathrm{ee,T}}}{3V}. \tag{3.89}$$

Substitution of Equation 3.88 in Equation 3.87 yields

$$P_{\mathrm{c}} = \rho_{\mathrm{A,T}} f_{\mathrm{ee,T}} \cos\theta_{\mathrm{T}} + \frac{\rho_{\mathrm{A,T}} k_{\mathrm{B}} T}{l_{\mathrm{a}}} = P_{\mathrm{el}} + P_{\mathrm{loc}}, \tag{3.90}$$

where $\rho_{\mathrm{A,T}} = \nu_{\mathrm{T}}/A_{\Sigma}$ is the surface density of the equivalent bridges (i.e., of tie-molecules) on the lamellar surfaces.

This form of P_{c} emphasizes how P_{el} is equivalent to the mechanical pressure that would be exerted on the inter-lamellar domains by substituting each equivalent bridge with a spring at tension $f_{\mathrm{ee,T}}$. On the other hand, P_{loc} originates from the localisation of the center of mass of the bridges. In Appendix E it is shown how the presence of entangled loops gives rise to a contribution to P_{el} that is symmetrical to that of the bridges. Similarly, both entangled and un-entangled loops lead to two additional P_{loc} terms which should however be small.

The force in the Langevin approximation is given by[134]

$$f_{\mathrm{ee,T}} = \frac{k_{\mathrm{B}} T}{b} \mathcal{L}^{-1}\left(x_{\mathrm{T}}\right). \tag{3.91}$$

The key improvement offered by the Langevin approximation over the Gaussian one is that the former leads to a force that diverges as $x_{\mathrm{T}} \to 1$. This is important as tie-molecules should be fairly taut, especially in crystal-mobile polymers and at low temperatures.[7,39,195,196,207,216] Furthermore, it is shown later (*cf.* Section 4.1) that in order to comply with the local equilibrium hypothesis the Gaussian approximation leads to unphysical values of x_{T}.

By substituting the expression for the force of Equation 3.91 into Equation 3.90 and expressing $\rho_{\mathrm{A,T}}$ in mol/m^2, the constraint pressure then becomes

$$P_{\mathrm{c}} \approx \frac{RT\rho_{\mathrm{A,T}}}{b} \left(\mathcal{L}^{-1}(x_{\mathrm{T}}) \cos\theta_{\mathrm{T}} + \frac{b}{l_{\mathrm{a}}} \right). \tag{3.92}$$

As $x_{\mathrm{T}} \to 0$, the Gaussian approximation yields

$$P_{\mathrm{c}} \approx \frac{RT\rho_{\mathrm{A,T}}}{b}\left(3x_{\mathrm{T}}\cos\theta_{\mathrm{T}} + \frac{b}{l_{\mathrm{a}}}\right). \tag{3.93}$$

In the equations above k_{B} has been substituted by R – the universal gas constant – by expressing $\rho_{\mathrm{A,T}}$ in mol m^{-2}.

The equilibrium volume of the inter-lamellar amorphous domains is instead given by Equation 3.41:

$$\begin{aligned} V^{\mathrm{IL}}(T,P,\boldsymbol{n}_{\mathrm{s}},n_{\mathrm{T}};\nu_{\mathrm{T}},\delta_{\mathrm{T}}) &= V^{(n_{\mathrm{T}}),\mathrm{EoS}}(T,P+P_{\mathrm{c}},\boldsymbol{n}_{\mathrm{s}},\nu_{\mathrm{T}}) \\ &= m_{\mathrm{p}}^{\mathrm{IL}}\bar{v}_{\mathrm{p}}^{\mathrm{IL}} + \sum_{i=1}^{N_{\mathrm{C}}}\bar{v}_{\mathrm{s},i}^{\mathrm{IL}}m_{\mathrm{s},i} \\ &= m_{\mathrm{p}}^{\mathrm{IL}}\left(\bar{v}_{\mathrm{p}}^{\mathrm{IL}} + \sum_{i=1}^{N_{\mathrm{C}}}\bar{v}_{\mathrm{s},i}^{\mathrm{IL}}S_{\mathrm{a},i}^{\mathrm{IL}}\right) \end{aligned}. \tag{3.94}$$

Here, the extensivity of $V^{(n_{\mathrm{T}}),\mathrm{EoS}}$ has been used to express the volume in terms of the (state-dependent) partial *specific* volumes of the solutes and the polymer in the inter-lamellar amorphous domains, calculated by dividing the partial molar volume of each component (Equation 3.33) by its molar mass:

$$\begin{cases} \bar{v}_{\mathrm{s},i}^{\mathrm{IL}} &= \bar{V}_{\mathrm{s},i}^{(n_{\mathrm{T}}),\mathrm{EoS}}\left(T,P+P_{\mathrm{c}},\boldsymbol{n}_{\mathrm{s}},\nu_{\mathrm{T}}\right)/M_{\mathrm{s},i} \\ \bar{v}_{\mathrm{p}}^{\mathrm{IL}} &= \bar{V}_{\mathrm{p}}^{(n_{\mathrm{T}}),\mathrm{EoS}}\left(T,P+P_{\mathrm{c}},\boldsymbol{n}_{\mathrm{s}},\nu_{\mathrm{T}}\right)/M_{\mathrm{p}} \end{cases}. \tag{3.95}$$

One should note that here the partial specific volumes are calculated using the reference polymer mixture with n_0 monomers, which means (*cf.* Equation 3.85)

$$\begin{cases} \bar{v}_{\mathrm{s},i}^{\mathrm{IL}} &\approx \bar{v}_{\mathrm{s},i}^{(n_0),\mathrm{EoS}}\left(T,P+P_{\mathrm{c}},\frac{n_0}{n_{\mathrm{T}}}\tilde{\boldsymbol{n}}_{\mathrm{s}},1\right) \\ \bar{v}_{\mathrm{p}}^{\mathrm{IL}} &\approx \bar{v}_{\mathrm{p}}^{(n_0),\mathrm{EoS}}\left(T,P+P_{\mathrm{c}},\frac{n_0}{n_{\mathrm{T}}}\tilde{\boldsymbol{n}}_{\mathrm{s}},1\right) \end{cases} \tag{3.96}$$

The quantity

$$\rho^{\mathrm{IL}}_{\mathrm{p,eff}}(T, P, \boldsymbol{n}_{\mathrm{s}}, n_{\mathrm{T}}; \nu_{\mathrm{T}}, \delta_{\mathrm{T}}) = \frac{m^{\mathrm{IL}}_{\mathrm{p}}}{V^{\mathrm{IL}}} = \left(\bar{v}^{\mathrm{IL}}_{\mathrm{p}} + \sum_{i=1}^{N_{\mathrm{C}}} \bar{v}^{\mathrm{IL}}_{\mathrm{s},i} S^{\mathrm{IL}}_{\mathrm{a},i} \right)^{-1} \tag{3.97}$$

can be identified as the effective polymer density in the inter-lamellar domains. We note that in the absence of penetrant molecules $\rho^{\mathrm{IL}}_{\mathrm{p,eff}} = \rho^{(n_{\mathrm{T}}),\mathrm{EoS}}(T, P + P_{\mathrm{c}}, 0, \nu_{\mathrm{T}})$ is simply the (mass) density of the pure inter-lamellar domains which in the current model is slightly higher then the density of a pure polymer liquid – and consequently higher then the density of the free amorphous domains – due to the action of P_{c}.

A simple mass balance (Appendix D) shows that the inter-lamellar distance l_{a} is related to the effective polymer density via

$$l_{\mathrm{a}} = \frac{M_0 \rho_{\mathrm{A,T}} n_{\mathrm{T}}}{f_{\mathrm{T}} \rho^{\mathrm{IL}}_{\mathrm{p,eff}}}. \tag{3.98}$$

Here, f_{T} is the mass fraction of tie-molecules in the inter-lamellar domains. Therefore, the inter-lamellar distance increases approximately linearly with the number of monomers n_{T} at fixed f_{T}. A manipulation of Equation 3.98 leads to

$$f_{\mathrm{T}} = \frac{M_0 \rho_{\mathrm{A,T}}}{\rho^{\mathrm{IL}}_{\mathrm{p,eff}} x_{\mathrm{T}} \cos\theta_{\mathrm{T}} l_{\mathrm{mono}} \mathcal{N}_{\mathrm{b}}} \rightarrow x_{\mathrm{T}} \cos\theta_{\mathrm{T}} = \frac{M_0 \rho_{\mathrm{A,T}}}{f_{\mathrm{T}} \rho^{\mathrm{IL}}_{\mathrm{p,eff}} l_{\mathrm{mono}} \mathcal{N}_{\mathrm{b}}}, \tag{3.99}$$

where M_0 is the molar mass of the monomer, l_{mono} is the length of an extended chain per bond and $\mathcal{N}_{\mathrm{b}}$ the number of bonds per monomer (Equation 3.73). This equation fixes the value of $x_{\mathrm{T}} \cos\theta_{\mathrm{T}}$ and therefore naturally avoids density anomalies in the inter-lamellar domains.

In the current model due to the absence of tails, free chains and un-entangled loops we have $f_{\mathrm{T}} = 1$. We have already pointed out that un-entangled loops contribute negligibly to P_{c}, and their effect only amounts to a scaling factor for the volume through f_{T} (*cf.*

Equation 3.98). The local equilibrium hypothesis provides additional support to this simplification. As mentioned in Section 3.2.4, this hypothesis postulates that each chain segment in the inter-lamellar domains is in equilibrium with respect to exchange of monomers with the crystalline lamellae. Equilibrium is established when the driving force of crystallization $\mu_{\mathrm{p,mono}}$ is balanced by the variation of free energy arising from the increase of the number of monomers of each polymer segment (see Equation 3.49 and Figure 3.6).

Since at low temperatures un-entangled loops and tails have no way of resisting the driving force of crystallization, they should be almost fully incorporated in the crystalline lamellae – or at least accumulate in the boundary layer, becoming similar to tight-folds.[7,165] This suggests $f_{\mathrm{T}} \approx 1$ at low temperatures. The condition $f_{\mathrm{T}} = 1$ has been used implicitly by Mansfield[199] and later by Albrecht and Strobl[200] in order to build a model for premelting in PE; both studies assumed the local-equilibrium hypothesis and employed the Gaussian approximation for the end-to-end probability distribution of the chain segments.

Conversely, in models employing Michaels and Hausslein's theory[39,42,43,251–256] f_{T} is usually found to be much smaller than 1. Due to the aforementioned considerations, this finding seems inconsistent with the local equilibrium hypothesis at least for defect-free linear homopolymers.

Chemical potentials

Setting to zero the N_C derivatives of $\tilde{\Phi}^{\mathrm{IL},*}$ with respect to the number of solute molecules per equivalent bridge ($\tilde{n}_{\mathrm{s},i}$) leads to

$$\begin{aligned}\left(\frac{\partial\tilde{\Phi}^{\mathrm{IL},*}}{\partial\tilde{n}_{\mathrm{s},i}}\right)_{T,P,\boldsymbol{\mu}_\mathrm{s},\mu_\mathrm{p,mono},\tilde{V},\tilde{\boldsymbol{n}}_\mathrm{s}\setminus\{\tilde{n}_{\mathrm{s},i}\},n_\mathrm{T},\nu_\mathrm{T},\boldsymbol{\Gamma}_\mathrm{c}} &= \left(\frac{\partial\tilde{A}^{\mathrm{IL}}}{\partial\tilde{n}_{\mathrm{s},i}}\right)_{T,\tilde{V},\tilde{\boldsymbol{n}}_\mathrm{s}\setminus\{\tilde{n}_{\mathrm{s},i}\},n_\mathrm{T},\nu_\mathrm{T},\boldsymbol{\Gamma}_\mathrm{c}} - \mu_{\mathrm{s},i} \\ &= \mu_{\mathrm{s},i}^{(n_\mathrm{T}),\mathrm{EoS}} - \mu_{\mathrm{s},i} = 0\end{aligned}, \tag{3.100}$$

where we have used Equation 3.43 as ΔA^c does not depend on the number of solute molecules. Since in the current work the chemical potential is approximated using the reference mixture with n_0 monomers per polymer molecule, we obtain

$$\left(\frac{\partial\tilde{A}^{\mathrm{IL}}}{\partial\tilde{n}_{\mathrm{s},i}}\right)_{T,\tilde{V},\tilde{\boldsymbol{n}}_\mathrm{s}\setminus\{\tilde{n}_{\mathrm{s},i}\},n_\mathrm{T},\nu_\mathrm{T},\boldsymbol{\Gamma}_\mathrm{c}} \approx \mu_{\mathrm{s},i}^{(n_0),\mathrm{EoS}}\left(T,\frac{n_0}{n_\mathrm{T}}\tilde{V},\frac{n_0}{n_\mathrm{T}}\tilde{\boldsymbol{n}}_\mathrm{s},1\right). \tag{3.101}$$

At fixed temperature, pressure, and chemical potentials of the solutes, the combination of the two previous equations can be equivalently stated using Equation 3.44:

$$\mu_{\mathrm{s},i} = \mu_{\mathrm{s},i}^{(n_0),\mathrm{EoS}}\left(T,P+P_\mathrm{c},\frac{n_0}{n_\mathrm{T}}\tilde{\boldsymbol{n}}_\mathrm{s},1\right), \tag{3.102}$$

where P_c is a function of state via 3.92.

Lastly, setting the derivative of $\tilde{\Phi}^{\mathrm{IL},*}$ with respect to the number of monomers of the equivalent bridges (n_T) to zero yields

$$\left(\frac{\partial\tilde{\Phi}^{\mathrm{IL},*}}{\partial n_\mathrm{T}}\right)_{T,P,\boldsymbol{\mu}_\mathrm{s},\mu_\mathrm{p,mono},\tilde{V},\tilde{\boldsymbol{n}}_\mathrm{s},\nu_\mathrm{T},\boldsymbol{\Gamma}_\mathrm{c}} = \left(\frac{\partial\tilde{A}^{\mathrm{IL}}}{\partial n_\mathrm{T}}\right)_{T,\tilde{V},\tilde{\boldsymbol{n}}_\mathrm{s},\nu_\mathrm{T},\boldsymbol{\Gamma}_\mathrm{c}} - \mu_\mathrm{p,mono}. \tag{3.103}$$

By expressing $\tilde{A}^{\mathrm{IL}}$ via Equations 3.69 and 3.83 and substituting $\mathbf{\Gamma}_{\mathrm{c}}$ with δ_{T} we have

$$\left(\frac{\partial \tilde{A}^{\mathrm{IL}}}{\partial n_{\mathrm{T}}}\right)_{T,\tilde{V},\tilde{\boldsymbol{n}}_{\mathrm{s}},\nu_{\mathrm{T}},\delta_{\mathrm{T}}} \approx \mu_{\mathrm{p,mono}}^{(n_0),\mathrm{EoS}}\left(T, \frac{n_0}{n_{\mathrm{T}}}\tilde{V}, \frac{n_0}{n_{\mathrm{T}}}\tilde{\boldsymbol{n}}_{\mathrm{s}}, 1\right) - RT\left(\frac{\partial \ln p_{\mathrm{ee}}}{\partial n_{\mathrm{T}}}\right)_{V,\delta_T} \tag{3.104}$$

Performing the partial derivative of p_{ee} in the Langevin approximation (see Appendix F) leads to the following expression:

$$\begin{aligned}\left(\frac{\partial \tilde{A}^{\mathrm{IL}}}{\partial n_{\mathrm{T}}}\right)_{T,\tilde{V},\tilde{\boldsymbol{n}}_{\mathrm{s}},\nu_{\mathrm{T}},\delta_{\mathrm{T}}} &\approx \mu_{\mathrm{p,mono}}^{(n_0),\mathrm{EoS}}\left(T, \frac{n_0}{n_{\mathrm{T}}}\tilde{V}, \frac{n_0}{n_{\mathrm{T}}}\tilde{\boldsymbol{n}}_{\mathrm{s}}, 1\right) \\ &\quad - \frac{RT}{\eta}\left[\ln\left(\frac{\sinh \mathcal{L}^{-1}(x_{\mathrm{T}})}{\mathcal{L}^{-1}(x_{\mathrm{T}})}\right) - \frac{3}{2N_{\mathrm{T}}} - \frac{3}{4N_{\mathrm{T}}^2} - \frac{2}{5N_{\mathrm{T}}^3}\right]\end{aligned}. \tag{3.105}$$

Here, the constant η is the ratio of the number of monomers and the equivalent Khun monomers of the chain N_{T} (*cf.* Equation 3.72). The series in $1/N_{\mathrm{T}}$ is the result of an asymptotic expansion of the normalization constant $C(N_{\mathrm{T}})$ in Equation 3.74 and is arbitrarily truncated at third order. In both the work of Michaels and Hausslein[39] and in studies aimed at modelling premelting,[197,198,200,233] the Gaussian approximation is used, which yields ($x_{\mathrm{T}} \to 0$)

$$\left(\frac{\partial \tilde{A}^{\mathrm{IL}}}{\partial n_{\mathrm{T}}}\right)_{T,\tilde{V},\tilde{\boldsymbol{n}}_{\mathrm{s}},\nu_{\mathrm{T}},\delta_{\mathrm{T}}} \approx \mu_{\mathrm{p,mono}}^{(n_0),\mathrm{EoS}}\left(T, \frac{n_0}{n_{\mathrm{T}}}\tilde{V}, \frac{n_0}{n_{\mathrm{T}}}\tilde{\boldsymbol{n}}_{\mathrm{s}}, 1\right) - \frac{RT}{\eta}\left(\frac{3}{2}x_{\mathrm{T}}^2 - \frac{3}{2N_{\mathrm{T}}}\right). \tag{3.106}$$

Since at constant temperature and pressure the monomer chemical potential $\mu_{\mathrm{p,mono}}$ is fixed by Equation 3.48, the equilibrium condition (Equation 3.103) at fixed $T, P, \boldsymbol{n}_{\mathrm{s}}$ can therefore be restated as

$$\begin{aligned}\frac{\eta}{RT}\Bigg[M_0\Delta h_{\mathrm{m}}^0\left(1 - \frac{T}{T_{\mathrm{m}}^0}\right) + \mu_{\mathrm{p,mono}}^{(n_0),\mathrm{EoS}}\left(T, P + P_{\mathrm{c}}, \frac{n_0}{n_{\mathrm{T}}}\tilde{\boldsymbol{n}}_{\mathrm{s}}, 1\right) \\ - \mu_{\mathrm{p,mono}}^{(n_0),\mathrm{EoS}}(T, P, 0, 1)\Bigg] = \ln\left(\frac{\sinh \mathcal{L}^{-1}(x_{\mathrm{T}})}{\mathcal{L}^{-1}(x_{\mathrm{T}})}\right) - \frac{3}{2N_{\mathrm{T}}} - \frac{3}{4N_{\mathrm{T}}^2} - \frac{2}{5N_{\mathrm{T}}^3}.\end{aligned} \tag{3.107}$$

This equation determines the equilibrium number of bridge monomers n_{T} and therefore their fractional extension x_{T} at fixed $T, P, \boldsymbol{n}_{\mathrm{s}}$.

One should note that the actual "size" N_{T} of the chains enters the equation only through the asymptotic expansion in $1/N_{\mathrm{T}}$ and through the (weak) dependence of P_{loc} (Equation 3.90) on l_{a} (and therefore n_{T}, *cf.* Equation 3.98). At temperatures sufficiently below the melting point of the polymer the driving force of crystallization $M_0 \Delta h^0_{\mathrm{m}} \left(1 - T/T^0_{\mathrm{m}}\right)$ becomes significantly bigger than both of these terms. Therefore, the equilibrium fractional extension of the bridges x_{T} is determined only by the value of $M_0 \Delta h^0_{\mathrm{m}} \left(1 - T/T^0_{\mathrm{m}}\right)$ at low enough temperatures. The same arguments can be invoked to show that as long as $T << T^0_{\mathrm{m}}$ or $l_{\mathrm{a}}/b >> 1$ the properties of the bridges (i.e., x_{T} and $\cos\theta_{\mathrm{T}}$) and therefore the constraint pressure P_{c} are very weakly independent of the inter-lamellar distance (see Equations 3.92, 3.99 and 3.107).

This fact can be also used to further justify the substitution of all entangled loops with bridges performed at the beginning of this Section. As shown by Albrecht and Strobl,[200] inclusion of entangled loops in the theory leads to an equation for the equilibrium number of monomers between entanglements (n_{ES}, see Appendix E) equivalent to the one for bridges just obtained in the Gaussian approximation with the addition of a $1/N_{\mathrm{ES}}$ term on the right-hand side. Although N_{ES} is smaller than N_{T}, at low enough temperatures all the terms in $1/N_{\mathrm{ES}}$ are negligible compared to $M_0 \Delta h^0_{\mathrm{m}} \left(1 - T/T^0_{\mathrm{m}}\right)$. Therefore, at low enough temperatures bridges and entangled segments have approximately the same fractional extension as a consequence of the local-equilibrium hypothesis, possibly differing only in their average angle with respect to the normal to the lamellae. Since these angles are already averaged in the definition of the constraint pressure (see Equation 3.92), the substitution of all tie-entanglements with bridges assumed here should thus leave the qualitative features of the model unchanged.

3.3.4. Model parameters

The prior knowledge and parameters needed to perform thermodynamic calculations with the current model can be grouped in three main categories: an equation of state capable of calculating the properties of both the external fluid and polymer + solutes mixtures; a collection of polymer-specific parameters; and a few sample-specific parameters.

Equation of state parameters

The equation of state is needed to calculate the pressure and the chemical potentials of the solute and the polymer in both the free and inter-lamellar domains and in the external fluid phase. The equation of state – and related parameters – must therefore provide a reliable description of pure fluids and polymer + solutes mixtures, including their volumetric properties (namely, partial specific volumes and density) and chemical potentials. Note that in practice all calculations with the current model are made assuming that the polymer chains possess $n_0 = 1000$ main-chain monomers and no ends.

Polymer-specific parameters

The polymer-specific parameters, on the other hand, are needed in order to calculate both the properties of the equivalent freely-jointed bridges (i.e., N_T, b) and the specific Gibbs free energy of crystallization of an extended-chain crystal ($-M_0\Delta h^0_\mathrm{m}\,(1 - T/T^0_\mathrm{m})$) appearing in Equation 3.48. These parameter are readily available in the literature or can be calculated from related literature data for most common polymers.

The bond angles θ_B of all the polymers are set to the tetrahedral value of 109.47° as all the backbone atoms have sp^3 hybridisation; although the true values of their

Table 3.1.: Polymer-specific parameters for PE, isotactic PP and PEG used for all the calculations.[134,168,286–292]

Property	Symbol	PE	PP	PEG
bond angle	θ_B	109.47°	109.47°	109.47°
bond lenght	l	0.154 nm	0.154 nm	0.147 nm
main-chain bonds per monomer	$\mathcal{N}_b$	1	2	3
enthalpy of melting	Δh_m^0	293 J g^{-1}	170 J g^{-1}	205 J g^{-1}
melting temperature	T_m^0	414 K	460 K	352 K
surface stem density	ρ_A	5.50 nm^{-2}	2.86 nm^{-2}	4.66 nm^{-2}
monomer molecular weight	M_0	14.03 g mol^{-1}	42.08 g mol^{-1}	44.05 g mol^{-1}
Flory characteristic ratio	C_∞	6.9	5.9	6.7

bond angle deviate slightly from the tetrahedral angle, this difference does not impact the calculations significantly. Similarly, the bond length of both PE and PP is set to $l = 0.154$ nm – the typical length of a C-C bond between sp^3 hybridized carbons – whereas the bond length of PEG is the geometric mean of the three bonds comprising the oxyethylene repeating unit.[290]

Since in the current model $\mu_{p,mono}$ (Equation 3.48) only accounts for "bulk" crystallisation, the specific enthalpy of melting of the extended-chain polymer crystal Δh_m^0 and its respective melting temperature T_m^0 are found[168,286–289,292] by extrapolation of the highest achievable values for high-molecular weight, monodisperse samples as the crystal thickness goes to infinity (*cf.* Equation 3.6). All real polymer samples will in fact melt at temperatures lower then T_m^0 due to the finite size of the lamellae and the presence of defects such as chain ends and branching,[170,171,175,275] as discussed in Section 3.1.1.

The surface stem density ρ_A (i.e., the cross-section of the chains in the crystalline structure) is calculated using the lattice parameters of the orthorombic unit cell of crystalline PE,[293] of the monoclinic unit cell of the α form of crystalline isotactic PP[144] and the monoclinic unit cell of crystalline PEO.[291] Lastly, the Flory characteristic ratios for all the polymers are taken from Rubinstein.[134]

Sample-specific parameters

Finally, a set of sample-specific parameters is needed to characterize the morphology of a given semi-crystalline polymer sample. In order to calculate the solubility in the inter-lamellar domains $S_{\mathrm{a},i}^{\mathrm{IL}}$ we require:

- The density of the equivalent bridges on the fold surface, $\nu_{\mathrm{T}}/A_{\Sigma} = \rho_{\mathrm{A,T}}$, assumed to be equal to the surface density of tie-molecules in the sample
- The average lateral displacement of the bridges δ_{T}

In the current work the chains in the crystal are assumed to be perpendicular to the crystal amorphous interface ($\gamma = 0$). Using equation 3.10 we thus have $\rho_{\mathrm{A,T}} = p_{\mathrm{T}}\rho_{\mathrm{A}}$. We must therefore specify the fraction of stems on the lamellar surfaces attached to tie-molecules p_{T}, which is kept as a free parameters of the model.

δ_{T} can be calculated if the inter-lamellar distance l_{a}^{*} for a pure semi-crystalline sample is known at a given temperature T^{*} and pressure P^{*}. In fact, once $T^{*}, P^{*}, p_{\mathrm{T}}$ and l_{a}^{*} are specified, δ_{T} can be found by implementation of a root-finding scheme after combining Equations 3.98 and 3.107 and setting $\boldsymbol{n}_{\mathrm{s}} = 0$. p_{T} and l_{a}^{*} are therefore sufficient to fully characterize the inter-lamellar domains according to the current model.

In order to calculate sorption isotherms in a target sample, both the fraction of free amorphous mass ψ and the crystallinity of the lamellar stacks $\omega_{\mathrm{c}}^{\mathrm{LS}}$ must also be specified at each thermodynamic condition (*cf.* Equation 3.53). In this model, ψ is a constant free parameter (*cf.* Section 3.3.2). Once the overall crystallinity ω_{c}^{*} and the inter-lamellar distance l_{a}^{*} of the pure polymer are specified at given temperature T^{*} and pressure P^{*} and the constants p_{T} and ψ are fixed, by calculating $\omega_{\mathrm{c}}^{\mathrm{LS},*}$ via Equation 3.55 and finding n_{T}^{*} we can calculate $K = (1 - \omega_{\mathrm{c}}^{\mathrm{LS},*})/n_{\mathrm{T}}^{*}$ (Equation 3.79). The crystallinity of the

lamellar stacks can then be calculated at each condition of temperature, pressure, and composition via $\omega_{\mathrm{c}}^{\mathrm{LS}} = 1 - Kn_{\mathrm{T}}$.

In conclusion, each semi-crystalline polymer sample is uniquely characterized by the measurement at an arbitrary temperature T^* and pressure P^* of the crystallinity ω_{c}^* and the inter-lamellar distance l_{a}^*, and by the two free parameters ψ and p_{T}. In the following, P^* is set to 1 bar due to its negligible influence on the model's predictions. Furthermore, note that at temperatures sufficiently lower than T_{m}^0 or when $l_{\mathrm{a}}/b >> 1$ the actual value of l_{a}^* has very little influence on the sorption properties of the inter-lamellar domains. Therefore, if the inter-lamellar distance is not a property of interest l_{a}^* can be safely taken to be equal to a typical experimental value without appreciable changes in the predictions of the model.

Concluding remarks

In this Chapter we have developed a statistical mechanics framework for the description of the thermodynamic properties of semi-crystalline polymers. We have unified previous models of fluid sorption under the constraint pressure formalism, which is a natural extension of network models to compressible equations of state. We have shown that the effect of constraints (i.e., physical and/or chemical cross-links) in a polymer network is formally equivalent to the addition of a state-dependent constraint pressure P_{c} on an otherwise unconstrained polymer melt (Section 3.2.3). We have also rigorously implemented the local-equilibrium hypothesis in the theory, resulting in a model capable of describing both surface melting and the increase in solute activity at low temperatures seen in crystal-mobile polymers (Section 3.1.4).

As discussed in Section 3.2.5, the equilibrium solubility and number of chain monomers in the amorphous domains of crystal-mobile polymers can be calculated through min-

imisation of a single thermodynamic potential, $\tilde{\Phi}^*$, instead of solving $2N_C + 2$ coupled non-linear equations corresponding to the equality of pressure, solute chemical potentials and monomer chemical potential between the amorphous domains and two reservoirs (i.e., the external fluid and the crystalline lamellae). In Section 3.3 we have presented a new model of semi-crystalline polymers which incorporates three key experimental observations:

- the amorphous domains can be distinguished in constrained inter-lamellar domains and free amorphous domains[238] (Section 3.1.5);
- swelling in the inter-lamellar domains is essentially one-dimensional;[40,41,258,294]
- the chain segments in the inter-lamellar domains are highly extended[7,39,195–197,207,216] and therefore significantly at variance with Gaussian statistics.

An analytical expression for the free energy of the inter-lamellar domains is obtained by first mapping all the tie-molecules to equivalent bridges characterised by the same average properties and then performing a series of simplifying assumptions such as neglecting confinement effects – the reader is referred to the end of Section 3.3.3 for a more detailed discussion.

As discussed in Section 3.3.4, in order to perform thermodynamic calculations with our model one requires an equation of state that can accurately describe both small-molecules fluids and polymer + solutes mixtures. In the current work the SAFT-γ Mie EoS (Chapter 2) is used with the molecular models and corresponding group parameters reported in Section 2.5. Furthermore, a set of polymer-specific parameters found in the literature must be specified (Table 3.1). Lastly, each semi-crystalline sample is assigned four sample-specific parameters (ω_c^*, l_a^*, p_T and ψ) that uniquely characterise its thermodynamic properties. In Chapter 4 the model is applied to the study of three crystal-mobile semi-crystalline polymers: PE, isotactic PP and PEG/PEO. We note that crystal-fixed polymers (such as syndiotactic PP[156] and poly(ϵ-caprolactone)[232]) can be

described using the same formalism with the caveat that the number of monomers per equivalent bridge must be specified as an additional free parameter due to the absence of mass exchange at the crystal/amorphous interface.

4. Results and Discussion

In this Chapter we test the ability of the model developed in Section 3.3 to represent a number of thermodynamic properties of semi-crystalline polymers. In Section 4.1, the predictions of the model regarding properties of pure polyethylene are compared to experimental data, where available. In Section 4.2, we estimate the p_{T} and ψ parameters of six PE and PP samples by minimisation of the difference between the predicted sorption isotherms of a range of pure fluids in the polymers and experimental data at a fixed temperature. We then test the model's predictions of solubility at different temperatures. We also showcase the ability of the model to track the variation of microstructural features such as constraint pressure and the inter-lamellar distance during the sorption process, allowing comparison with nano-swelling measurements.[294]

In Section 4.3 the model is systematically benchmarked by analysing sorption isotherms of hydrocarbons in a large number of semi-crystalline PE samples analysed in the literature. ψ is estimated as a function of each sample's crystallinity using an empirical correlation of experimental data;[238] this leaves p_{T} as the only adjustable parameter, optimised to reproduce pure-component sorption isotherms at a given temperature. We then compare the model's predictions of solubility at different temperatures and of co-solubility effects (i.e., the change of solubility of a component when pure *vs.* when in mixtures). We conclude the Chapter with the analysis of moisture uptake in semi-crystalline PEG, a polymer that can undergo deliquescence[13,295] at high relative humidity. We develop

a simple model to predict the humidity at which deliquescence occurs and apply our model for semi-crystalline polymers to qualitatively describe moisture uptake at low humidity.

4.1. Prediction of pure polymer properties

In this Section, the model's calculations of constraint pressure using Gaussian and Langevin statistics for the end-to-end distribution of the tie-molecules (Equations 3.76 and 3.74, respectively) are first compared in order to justify the inclusion of the finite extensibility of the polymer chains in the theory. Next, we compare the model's predictions of the variation of the inter-lamellar distance and crystallinity with temperature in semi-crystalline PE.

4.1.1. Constraint pressure

In Figure 4.1 calculations for the temperature dependence of the constraint pressure P_{c} and the average fractional extension x_{T} of the tie-segments in the inter-lamellar amorphous domains of a hypothetical pure semi-crystalline PE sample are shown using both Langevin statistics (Equations 3.92 and 3.107) and the Gaussian approximation (Equations 3.93 and 3.106). Here, the reference measurement temperature is $T^* = 25$ °C and the corresponding inter-lamellar distance $l_{\mathrm{a}}^* = l_{\mathrm{a}}(25\ ^\circ\mathrm{C})$ is set to 10 nm due to the small influence it has on the intensive properties of the inter-lamellar domains. Furthermore, for illustration purposes p_{T} is set to 0.3, meaning that 30% of the stems on the lamellar surfaces are attached to a bridge or entangled loop. As shown later in the current work, $p_{\mathrm{T}} = 0.3$ is a typical value found for PE by comparing experimental solubility data and the model's predictions.

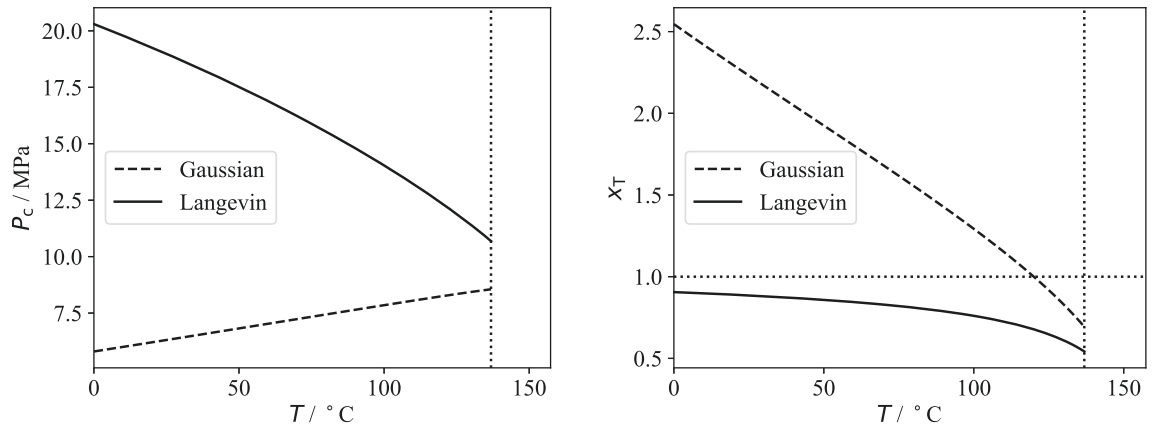

(a) (b)

Figure 4.1.: Temperature dependence of a) the constraint pressure P_c and b) the fractional extension x_T of the tie-segments in pure semi-crystalline polyethylene using Langevin statistics and the Gaussian approximation. The vertical dotted line marks the melting temperature T_m^0 of and extended-chain polyethylene crystal (see Table 3.1). Here, $l_a^* = l_a(25\ °C)$ has been fixed to 10 nm, and the surface fraction of elastically effective segments $p_T = 0.3$. The PE-specific parameters are summarized in Table 3.1. Notice that the fractional extension calculated with the Gaussian approximation needs to exceed the maximum value of 1 in order to satisfy Equation 3.106.

As expected, the fractional extension of the tie-segments is seen to increase at low temperatures as a consequence of the dependence imposed by Equations 3.107 and 3.106. The use of the Gaussian approximation is found to yield unphysical values for x_{T} at low temperatures. At room temperature, the Langevin statistics predicts $x_{\mathrm{T}} \approx 0.88$ for $p_{\mathrm{T}} = 0.3$ which indicates that tie-molecules should be extremely taut. Furthermore, while the constraint pressure increases at lower temperatures with the Langevin approximation, the contrary is true with the Gaussian approximation. In fact, P_{c} does not depend appreciably on x_{T} with the Gaussian approximation because the factor $x_{\mathrm{T}} \cos\theta_{\mathrm{T}}$ appearing in Equation 3.93 is approximately constant for $f_{\mathrm{T}} = 1$ (see Equation 3.99).

It is instructive to note that even if f_{T} were different from one and allowed to change in the Gaussian approximation, P_{c} would increase at lower temperatures only if $f_{\mathrm{T}} \to 0$ at low temperatures, as can be seen by substituting Equation 3.99 into Equation 3.93. This behaviour is, however, impossible as it would imply that either the elastically effective segments are fully incorporated in the lamellae at low temperatures or that the elastically ineffective polymer mass (tails and loops) increases at lower temperatures, which in stark contradiction with the local-equilibrium hypothesis.

As mentioned in the Introduction, Michaels and Hausslein's theory[39] implicitly predicts the presence of constraint pressure (as noted by later authors[43,44]) and manages to predict an increase of P_{c} at low temperature despite using the Gaussian approximation. This is possible because in their work the swelling in the inter-lamellar amorphous domains is assumed to be isotropic, while here it has been postulated that swelling only occurs in the direction perpendicular to the lamellar surfaces (Equation 3.88) due to the markedly one-dimensional nature of the lamellar stacks.

Since previous authors have found that P_{c} should increase at lower temperatures,[39,42,45,251] we conclude that the use of the Langevin approximation (or any chain statistics that

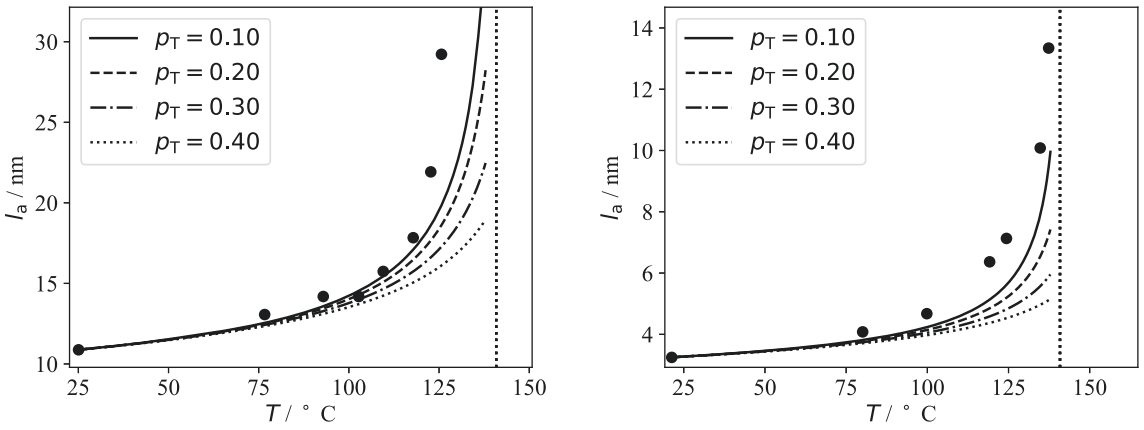

Figure 4.2.: Temperature dependence of the inter-lamellar distance l_a in semi-crystalline PE. The continuous curves represent calculations using the model developed with the Langevin approximation, and the symbols represent experimental data; the vertical dotted line denotes the melting temperature of the polymer T_m (see Table 3.1). The inter-lamellar distance at the lowest experimental temperature $l_a^* = l_a(T^*)$ is used to calculate δ_T, while p_T has been adjusted to qualitatively reflect the experimental data: a) data from Kavesh and Schultz;[155] b) Data from Tanabe *et al.*[244] The predictions of the theory close to the melting point are not reliable due to irreversible changes occurring in the lamellar stacks.[155]

accounts for the finite extensibility of the chain segments) is necessary in order to develop accurate models for the inter-lamellar domains of crystal-mobile polymers.

4.1.2. Inter-lamellar distance

In Figure 4.2, the predictions of the variations of the inter-lamellar distance l_a in semi-crystalline polyethylene obtained with our model are compared with experimental data taken from literature. In order to determine the theoretical curves, l_a^* and T^* are set to the experimental values at the lowest temperature while different values of p_T are considered.

It is apparent from Figure 4.2 that our model can be used to accurately reproduce the

experimental data for temperatures which are sufficiently lower than the melting point of an extended-chain crystal T_{m}^{0} for any value of p_{T}. The agreement is slightly worse for the data of Tanabe *et al.*[244] shown in Figure 4.2b, possibly because the inter-lamellar distance is comparable to the Khun length of polyethylene, $b \sim 1.3$ nm; approximating the real end-to-end probability distribution to that of a freely jointed chain in this limit may, in fact, lead to errors. At temperatures close to T_{m}^{0} the smaller values of p_{T} seem to fit better the experimental data and it is tempting to conclude that $p_{\mathrm{T}} \sim 0.10$ for the samples considered.

However, it must be noted that at temperatures close to the melting point irreversible transformations[39,220] and structural reorganizations[7] might change the topology of the lamellar stacks, violating the assumption inherent in the current model that p_{T} should be a constant. For example, Kavesh and Schultz[155] have noted that for the sample considered in Figure 4.2a both the inter-lamellar distance and the lamellar thickness increased at temperatures higher then about 100 °C, indicating the presence of irreversible changes to the structure which can lead to chain disentanglement and reduction in p_{T}. Furthermore, at higher temperatures neglecting fold surface free energy effects as it was done in Equation 3.48 might not be accurate.

In conclusion, the model can be safely compared to premelting data only at low temperatures compared to T_{m}^{0} where all values of p_{T} appear to provide a similar level of agreement with the experimental data.

4.1.3. Crystallinity

As discussed in Section 3.3.3, the model developed in the current work can be used to calculate the variation of the crystallinity $\omega_{\mathrm{c}}^{\mathrm{LS}}$ of the lamellar stacks. For highly crystalline samples, all of the amorphous mass should be inter-lamellar,[136] and the melting

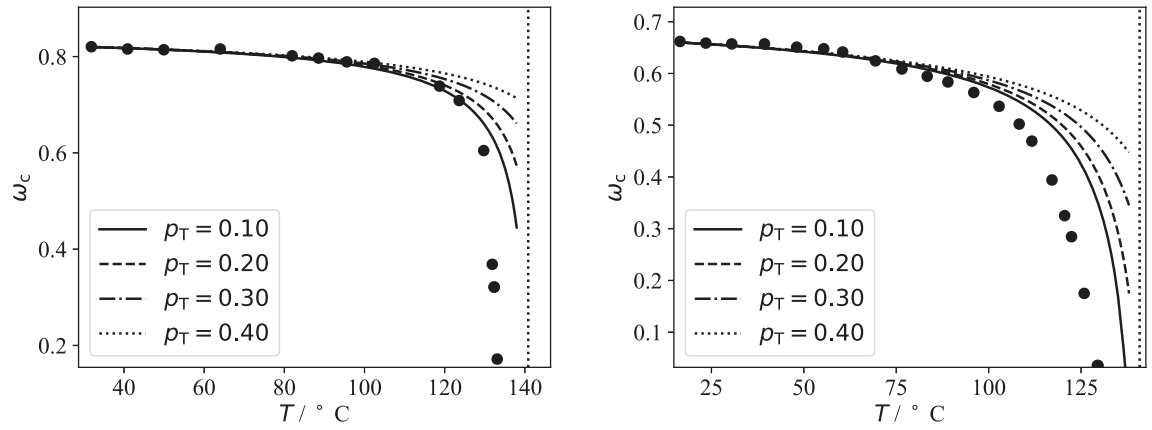

(a) Ziegler-Natta catalyst

(b) Metallocene catalyst

Figure 4.3.: Temperature dependence of the crystallinity of different highly-crystalline samples of PE. The continuous curves represent the calculations using our model developed with the Langevin approximation and assuming $\psi = 0$, while the symbols represent experimental data reported by Paricaud and coworkers.[131] The vertical dotted line marks the melting temperature of the polymer T_m^0 (see Table 3.1). For all the calculations the inter-lamellar distance at 25° C is set to 10 nm.

curves – i.e., plots of the crystallinity versus temperature – should thus be reproducible, provided that the temperature remains sufficiently lower then the melting temperature (as per the discussion in the previous section). The calculation with the current model using various values for p_T are compared to the experimental melting curves of two highly-crystalline polyethylene samples in Figure 4.3.

For all of the calculations, the crystallinity $\omega_c^{LS,*}$ of the lamellar stacks at the lowest experimental temperature T^* is set equal to the experimental crystallinity at that temperature ($\psi = 0$). For the same reasons highlighted earlier, the agreement between the model and the experimental data is satisfactory at low temperatures and deteriorates at higher temperatures. Similarly, smaller values of p_T appear to provide better agreement at higher temperatures, where the predictions are expected to be less reliable.

In order to calculate the melting curves of polymer samples with low crystallinity, the temperature dependence of ψ must be known. The total crystallinity of the sample ω_c is related to this quantity via Equation 3.55 once $\omega_c^{LS}(T)$ is known. Here, ψ is assumed to be a constant, but in reality it should change with temperature. It is therefore unlikely that the current model can describe the melting curves of low-crystallinity samples. However, for the purpose of calculating the sorption isotherms, approximating ψ with a constant is reasonable as long as the temperature is sufficiently lower than the melting temperature. The changes in the crystallinity of semi-crystalline polymer samples should in fact be small in this regime.[131]

4.2. Sorption of pure gases in semi-crystalline PE and PP

In this Section the values of the free parameters of the current model, p_T and ψ, are optimised to reproduce the sorption isotherms of pure *n*-hexane, *n*-heptane, cyclohexane and toluene in six polyethylene and polypropylene samples analysed at Imperial College London as part of a joint study.[139] Since p_T and ψ are properties of an individual polymer sample, a pair of values is assigned to each sample in order to minimize the difference between the experimental sorption isotherms at 25 ° C and the calculations obtained with the model. The predictions of the model regarding solubility at different temperatures and the variation of the properties of the inter-lamellar domain during sorption are then compared to available experimental data. Since the external fluid is here always taken to be pure, in this Section the index i and the bold notation for the solute composition is dropped.

4.2.1. Experimental

We first report the experimental details of the sorption measurements performed by Dr. J. Ramadani and Prof. D. Williams for completeness.

Materials

All the substances used for the generation of vapor isotherms – namely *n*-hexane, *n*-heptane, cyclohexane and toluene – were ordered from Sigma-Aldrich (Poole, UK) and VWR UK with a minimum of 99% purity. These reagents were used without further purification. The di-water (DI) used for all the experiments was ultra-pure Milli-Q grade. All the polyethylene samples used in the current work were ordered from Sigma-Aldrich (Poole, UK) and all the polypropylene samples were ordered from Sp2 Scientific Polymer Products Inc. (NY, USA). Isotactic polypropylene (iPP) was received as pellets, atactic polypropylene (aPP) as a waxy solid, low-density polyethylene (LDPE) and high-density polyethylene (HDPE) as pellets, and medium-density polyethylene (MDPE) as a fine powder. The commercial nonwoven (isotactic) polypropylene fibers (fPP) were kindly donated by Procter & Gamble.

Sample fabrication

Apart from aPP which was dissolved in toluene at room temperature all the other polymers were dissolved in decahydronaphthalene at 160 °C to form 2% weight/volume solutions. An alumina foil swatch (diameter 6.5 cm) was pre-cleaned with di-ionised water and isopropanol, dipped into the polymer solution for 30 seconds and then left to air dry for 30 minutes. The films obtained were then placed in a vacuum oven for 3 hours at 80 °C for aPP and 120 °C for the other samples in order to evaporate the remaining

solvents. Each alumina foil preparation was weighed before and after polymer coating to record the amount of polymer film created.

Dynamic vapour sorption (DVS) – Instrumentation

The sorption profiles of the polymer films were determined using the DVS Endeavour and Resolution (Surface Measurement Systems, London, UK). The samples, with mass ranging between 100 and 140 mg, were first directly hung on the the DVS chamber's hang-down hook, and the sample pan was removed. Before the sorption cycles the samples were dried at 0% relative humidity (RH) and 25 °C for 180 minutes to establish a dry mass. On the DVS Resolution, counterweights were used for the higher mass samples. Most samples were folded into smaller units to keep them compact. A series of experiments was then carried out using either fixed times for each experimental humidity setpoint or using a % dm/dt threshold mode. Humidity or RH here refers to the ratio between the partial pressure of the target solute and its vapour pressure at the corresponding temperature.

In the % dm/dt mode the percentage change of mass with time is measured and compared to a threshold value to determine the equilibration time at each given RH step. The % dm/dt threshold was set to 0.0005% for all experiments to ensure the sample had reached a necessary degree of equilibrium before moving on to next step. When the sample percentage change in mass was equal to or below this threshold for 10 minutes, the step stage was ended and moved onto the next programmed RH% step. Methods were run in (0–90% RH) cycles with increments of 10% RH steps. Partial pressures were generated using liquid solvent bubbling reservoirs and controlled via closed-loop speed of sound sensors. In a first series of experiments, the temperature was set to 25 °C and the sorption cycles of each individual solute were measured in all six polymer samples. The sorption cycles of n-heptane were also measured at 35, 45, and

Table 4.1.: The density ρ and mass fraction crystallinity ω_c at 25 °C and 1 bar of the dried samples obtained after solution casting on the alumina foils. The crystallinity was calculated using Equation 3.12.

	LDPE	MDPE	HDPE	aPP	fPP	iPP
ρ(25 °C) / (kg dm^{-3})	0.916	0.917	0.920	0.840	0.883	0.899
ω_c(25 °C)	0.472	0.479	0.499	0	0.435	0.586

55 °C.

Sorbed quantities were calculated using the change in mass between the ends of the current cycle's sorption and previous cycle's desorption step. A flow rate of 200 cm^3/min was used for all experiments, with the carrier gas being nitrogen in all cases. Between experiments, samples were dried at 50 °C under vacuum for 3 h to remove any residual solute or other contaminants that may influence sorption performance. The raw data was exported into Microsoft Excel ® and the analysis was undertaken using the DVS Macro Standard Analysis Suite v7.0.13 (Surface Measurement Systems, London, UK).

Density measurement: Helium pycnometry – Instrumentation

The density of the dried polymer samples was measured at 25 °C and 1 bar in order to determine their mass fraction of crystallinity ω_c using Equation 3.12. The correlated densities of fully amorphous and fully crystalline polymers appearing in Equation 3.12 were taken from the literature,[168,296] except for the density of fully amorphous PP which was taken to be equal to the density of atactic PP. At 25 °C for PE $\rho_a = 0.852$ kg dm^{-3} and $\rho_c = 1.000$ kg dm^{-3}; for isotactic PP, $\rho_a = 0.840$ kg dm^{-3} and $\rho_c = 0.946$ kg dm^{-3}. The measurements were carried out via pycnometry using an Accupyc II 1340 (Micromeritics, USA) instrument, with helium gas as the probe molecule. The densities and related crystallinity of the dried samples are reported in Table 4.1.

Since the density (and therefore crystallinity) was measured for the solution-cast samples, its value differed from the one reported by the supplier. In particular, all three polyethylene samples had similar crystallinity despite having a markedly different sorption capacity – see the Results section.

4.2.2. Evidence for the presence of free amorphous polymer: $\psi > 0$

First of all, we provide evidence to support the necessity of including the free, unconstrained amorphous polymer in the description (i.e., $\psi > 0$) in order to reproduce the experimental sorption isotherms. If all the amorphous mass is inter-lamellar, the total sorption S can be calculated from Equation 3.53 by setting $\psi = 0$. Therefore, here the amorphous solubility $S_{\rm a}$ represents the solubility in the inter-lamellar amorphous domains $S_{\rm a}^{\rm IL}$, which – provided $p_{\rm T}$ and the inter-lamellar distance $l_{\rm a}^*$ at a given temperature T^* are specified – can be calculated with the help of Equations 3.19, 3.92, 3.98, and 3.105 at each temperature T and pressure P of the external fluid. Finally, the total crystallinity $\omega_{\rm c}$ is simply the crystallinity of the lamellar stacks $\omega_{\rm c}^{\rm LS}$, and the dependence on the temperature and amount of solute dissolved can be calculated with Equation 3.79.

In Figure 4.4 predictions of the model with $\psi = 0$ (continuous curves) are compared to the experimental sorption data[139] for *n*-hexane, *n*-heptane, cyclohexane and toluene in the samples of LDPE and iPP polymers. The value of $p_{\rm T}$ is adjusted for each sample to reproduce the low-pressure sorption behaviour of the four solutes simultaneously. The optimal values of $p_{\rm T}$ are 0.23 for LDPE and 0.42 for iPP. We present additional calculations (dashed curves) assuming that the crystals are impermeable to the solute (just like in our current model, Equation 3.18) but also that all the amorphous mass is unconstrained ($\psi = 1-\omega_{\rm c}$); the equilibrium value of $S_{\rm a} = S_{\rm a}^{\rm F}$ is thus the variable defined as $S_{\rm a}^{\rm EoS}$ in Section 3.1 (see Equation 3.22).

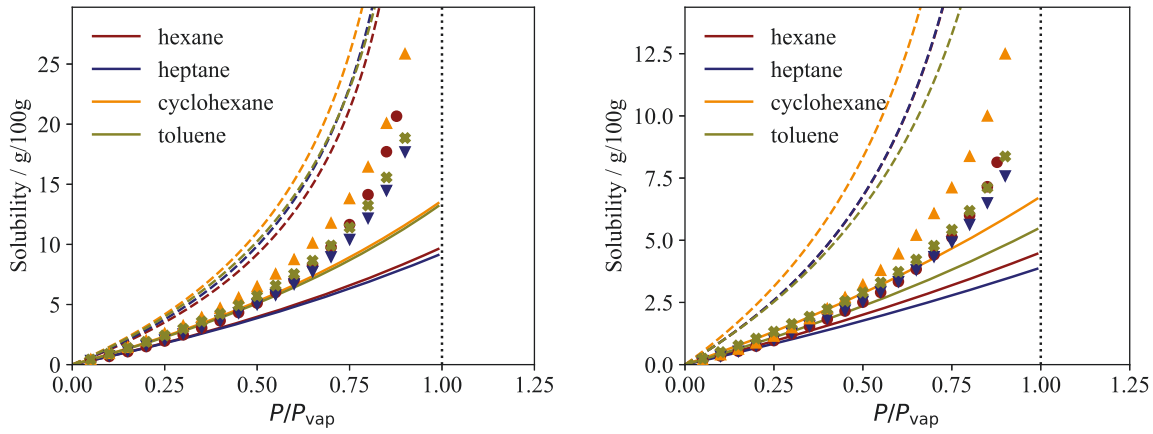

(a) LDPE, $p_T = 0.23$

(b) iPP, $p_T = 0.42$

Figure 4.4.: Sorption isotherms of *n*-hexane, *n*-heptane, cyclohexane and toluene in the LDPE and iPP samples at 25 °C. The sorption (in grams of solute per 100 grams of pure polymer) is plotted as a function of the total pressure P divided by the vapour pressure of the penetrant at that temperature. The continuous curves represent the predictions of the model assuming that all the amorphous polymer lies between crystalline lamellae ($\psi = 0$); the value of p_T has been adjusted to capture the low-pressure behaviour, while $l_a(25°C) = 10$ nm. The dashed curves represent theoretical calculations assuming that the solute cannot penetrate the crystallites (Equation 3.18) but that there are no constraints, i.e., $\psi = 1 - \omega_c$ (Equation 3.22). The symbols represent the experimental data,[139] color-coded with the calculations. Uncertainties in the data are smaller than the marker size. Not accounting for the free amorphous polymer results in a systematic underprediction of the sorption when the pressure of the external gas approaches its vapour pressure. On the other hand, not accounting for constraints at all results in a systematic overprediction of solubility.

As expected (see Figure 3.5), neglecting the presence of constraints results in a systematic overprediction of the experimental isotherms. On the other hand, if all the amorphous mass is subject to constraints – or, equivalently, if all the amorphous mass is inter-lamellar (continuous curves) – the curvature of the calculated sorption isotherms decreases significantly and the sorption at pressures close to the vapour pressure of the penetrant is systematically underestimated when the low-pressure behaviour is captured correctly. While this behaviour is found for every polymer sample, the curvature of the experimental amorphous solubility decreases with increasing crystallinity as highlighted in Figure 3.5.

This suggests that the higher the crystallinity, the more closely the morphology of the semi-crystalline sample resembles the lamellar stacks model with $\psi = 0$; conversely, the lower the crystallinity, the closer the experimental sorption isotherms are to the model calculations with $\psi = 1 - \omega_c$ (dashed curves). This finding is consistent with the experimental observation that the free amorphous content should decrease with increasing crystallinity.[238] It is thus to be expected that if ψ and p_T are simultaneously optimized to reproduce the experimental sorption isotherms, the optimal value of ψ should decrease with increasing crystallinity for all of the PE and PP samples.

4.2.3. Sorption isotherms calculated with the complete model

Model performance

The calculations obtained with the model after optimizing p_T and ψ simultaneously for each polymer sample (continuous curves) are shown together with the experimental sorption data (symbols) in Figure 4.5. The optimal parameters for each sample are listed in Table 4.4 together with the crystallinity at 25°C calculated using the density measurements (Equation 3.12). With the inclusion of the free amorphous polymer in the

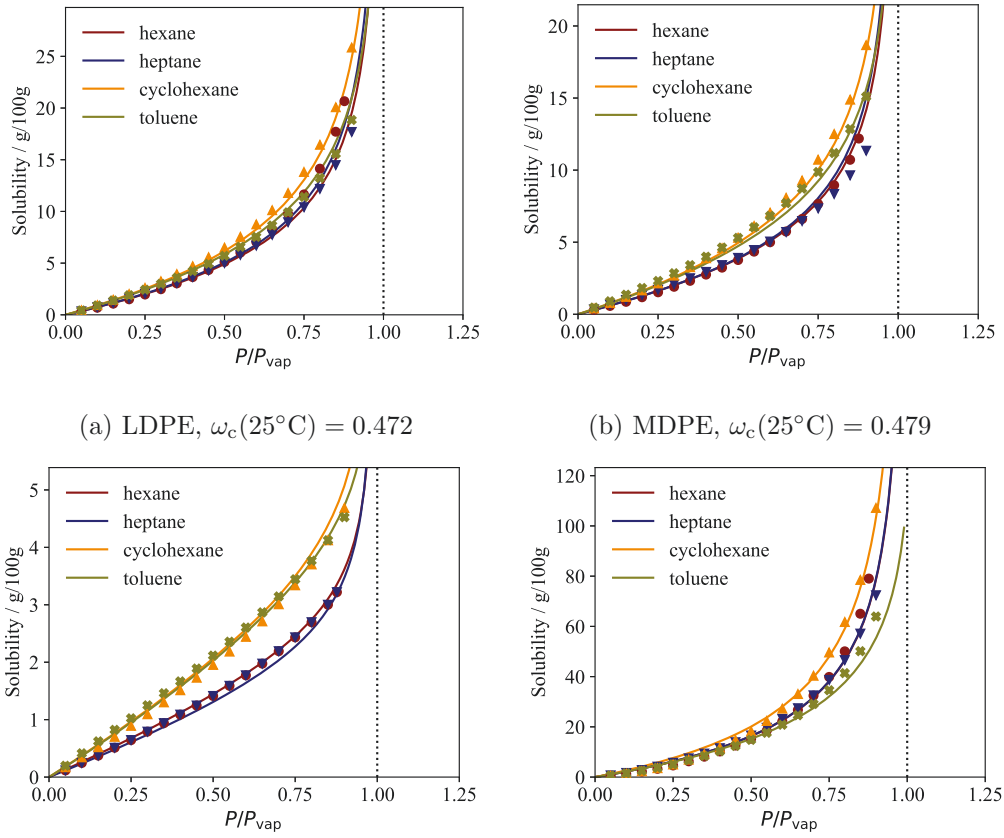

(a) LDPE, $\omega_c(25°C) = 0.472$

(b) MDPE, $\omega_c(25°C) = 0.479$

(c) HDPE, $\omega_c(25°C) = 0.499$

(d) aPP, $\omega_c = 0$

Figure 4.5.: Sorption isotherms of *n*-hexane, *n*-heptane, cyclohexane and toluene in the six polymer samples tested at 25 °C. The sorption (in grams of solute per 100 grams of pure polymer) is plotted as a function of the total pressure P divided by the vapour pressure of the penetrant at that temperature. The continuous curves represent the calculations with the model after adjusting p_T and ψ for each polymer sample to best reproduce all four sorption isotherms simultaneously; the optimal values are reported in Table 4.4. The symbols represent the experimental data,[139] whose uncertainties are smaller than the marker size.

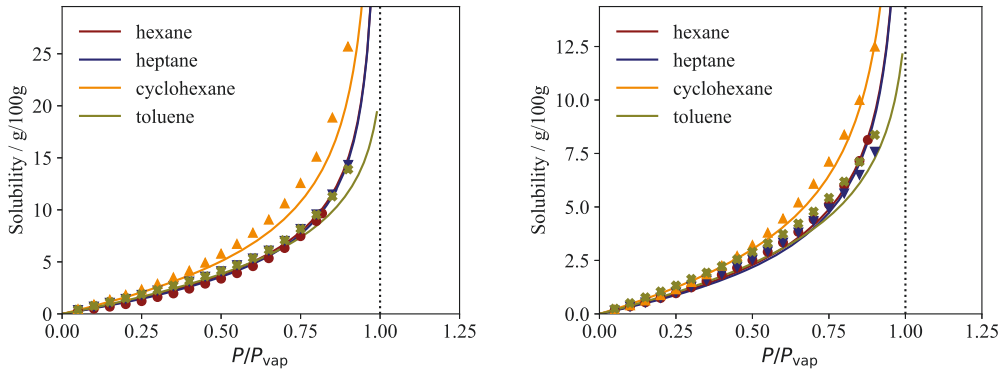

(e) PP fiber, $\omega_c(25°C) = 0.435$ (f) iPP, $\omega_c(25°C) = 0.586$

Figure 4.5.: Sorption isotherms of *n*-hexane, *n*-heptane, cyclohexane and toluene in the six polymer samples tested at 25 °C. The sorption (in grams of solute per 100 grams of pure polymer) is plotted as a function of the total pressure P divided by the vapour pressure of the penetrant at that temperature. The continuous curves represent the calculations with the model after adjusting p_T and ψ for each polymer sample to best reproduce all four sorption isotherms simultaneously; the optimal values are reported in Table 4.4. The symbols represent the experimental data,[139] whose uncertainties are smaller than the marker size.

description ($\psi \neq 0$), the agreement between the model with the optimized parameters and the experimental data is excellent for all of the samples over the entire pressure range. Since atactic polypropylene is fully amorphous, we neglect any type of constraint in the amorphous mass (i.e., all amorphous mass is free) in the calculations by setting $\psi = 1$ and $\omega_c^{LS} = 0$ in Equation 3.53.

As noted in Section 3.2.1, the sorption isotherms of different compounds in semi-crystalline samples of the same polymer are not simply re-scaled copies of one another. For example, while all the solutes have a similar solubility in LDPE at fixed P/P_{vap}, a clear difference between the solubility of the cyclic compounds (i.e., cyclohexane and toluene) and the one of the linear alkanes (*n*-hexane, *n*-heptane) is observed in HDPE. It is particularly encouraging that our model predicts this peculiar phenomenon. As shown in Section B, the solubility reduction of a solute due to the presence of constraints is a function of its partial molar volume in the polymer + solute mixture. The presence of constraints in

Table 4.2.: Sample-specific parameters for the six PE and PP samples analysed by Valsecchi *et al.*[139] The crystallinity at 25 °C is calculated with Equation 3.12 and knowledge of the density of the samples. The inter-lamellar distance of the pure polymers at 25 °C is set to 10 nm for all samples due to its negligible influence on the sorption isotherms. The values of p_T and ψ are obtained by minimizing the relative deviation of the experimental data of Figure 4.5 and the model calculations.

Polymer sample	ω_c(25°C)	l_a(25°C)	p_T	ψ
LDPE	0.472	10 nm	0.311	0.210
MDPE	0.479	10 nm	0.288	0.106
HDPE	0.499	10 nm	0.374	0.022
aPP	≈ 0	/	/	≈ 1
fPP	0.435	10 nm	0.524	0.168
iPP	0.586	10 nm	0.568	0.107

the amorphous domains thus leads to a size selection mechanism that favours solubility of components with lower partial molar volume in the mixture.

This effect has important implications for gas transport across semi-crystalline polymer. In membrane-based fluid separation, glassy polymers show remarkable selectivity – i.e., the ability to enhance permeation of one component while preventing it for another – at fixed overall permeability. This phenomenon has been explained in terms of a "molecular sieving" mechanism whereby the distribution of excess free volume in the glass selectively enhances diffusion of smaller species compared to the equilibrium "rubbery" state.[297,298] Our results suggest that in semi-crystalline polymers with rubbery amorphous domains a similar size selection must occur due to equilibrium effects related to the entropy loss of the tie-molecules upon swelling.

Optimal sample-specific parameters

As expected, for the semi-crystalline samples the optimal value of ψ decreases with increasing crystallinity.[238] Furthermore, it is apparent that the values of p_T for different samples of the same polymer are similar, with the average value of p_T being ~ 0.32 for the

PE samples and ~ 0.55 for the (semi-crystalline) PP samples. These values are higher than the estimates of previous works who attempted to predict the tie-molecule density in the inter-lamellar domains. Lacher and coworkers[206] estimated that the fraction of stems attached to tie-molecules should be in the range $\sim 0.1 - 0.2$ depending on the inter-lamellar distance. Nilsson and coworkers,[207] on the other hand, found that p_{T} should decrease with increasing inter-lamellar distance and decreasing molecular weight, remaining below approximately 0.1.

As discussed in Section 3.1.3, however, both of these estimates are based on random-walk models that do not consider entanglement segregation in the inter-lamellar domains during crystallisation[172,178] or the highly strained state of the inter-lamellar polymer chains.[217,238] The values reported by these authors should therefore be considered lower bounds for p_{T}, to which our indirect estimates conform.

An upper bound to the fraction of tie-molecules is instead provided by the fraction of tight-folds p_{TF}: since $p_{\mathrm{T}} + p_{\mathrm{TF}} + p_{\mathrm{NT}} = 1$, we must have

$$p_{\mathrm{T}} \leq 1 - p_{\mathrm{TF}}. \tag{4.1}$$

The lattice models described in Section 3.2[164,166,167,181] estimated that p_{TF} should lie in the range 0.6-0.8. The combination of these estimates and our findings implies that for PE samples there should be very few stems connected to tails and untangled loops since we find $p_{\mathrm{T}}^{\mathrm{PE}} \approx 0.32$. This is consistent with our model, since due to the local equilibrium between the lamellae and the inter-lamellar amorphous chains f_{T} is assumed to be ~ 1 – which implies $p_{\mathrm{NT}} \sim 0$.

One should note that both the bounds for p_{T} reported and the current model assume no chain tilt – i.e., that the crystalline chains are normal to the crystal/amorphous surface. In PE the chain tilt is between about 20° and 40°, which leads to a reduction in the amount of tight folds required by the aforementioned lattice models.[167] However,

the optimal value of p_{T} needed to fit the experimental sorption isotherms with our model increases for nonzero tilt angles in order to obtain the same overall tie-molecule density on the crystal/amorphous interface (Equation 3.10), suggesting that our results would predict the prevalence of tie-molecules in the inter-lamellar domains of PE (i.e., $p_{\mathrm{T}} + p_{\mathrm{TF}} \approx 1$) even if realistic chain tilts were considered.

Conversely, the very high values of p_{T} obtained for the semi-crystalline isotactic PP samples does not seem to respect the upper bounds suggested. Though this discrepancy could be due to one of the approximations employed to derive the model, the high values obtained for p_{T} in the PP samples could be explained by the absence of un-entangled loops in the inter-lamellar amorphous domains. It is apparent by substituting $\cos\theta_{\mathrm{T}}$ from Equation 3.99 in Equation 3.92 that the same constraint pressure can be obtained by reducing the value of p_{T} and allowing f_{T} to be smaller then 1.

In other words, if all of the inter-lamellar amorphous mass is either in bridges or in entangled loops at a fractional extension x_{T} (approximately fixed by Equation 3.107), the average angle of the tie-molecules with the normal to the lamellae must be closer to 90° than with the presence of some elastically ineffective mass (see Equation 3.99). As a consequence, if f_{T} is closer to 1 the tie-segments are more tilted with respect to the normal to the lamellae, and thus the component of the force normal to the lamellae (which contributes to P_{c}) is smaller.

The high values of p_{T} obtained for PP might thus be an indication that tails and free loops must be present in the inter-lamellar domains of isotactic PP. This seems at odds with the fact that isotactic PP is categorised as a crystal-mobile polymer.[156] Heuristically, however, it should be harder for PP chains to perform longitudinal sliding motion in the crystal compared to polymers such as PE and PEO that do not possess side groups.[274] Furthermore, it has been shown that metallocene-catalysed isotactic PP can include a variable amount of stereodefects[299] (i.e., defects in the regular succession of

methyl side groups). Both of these effect might lead to the persistence of un-entangled loops in the inter-lamellar domains or diminished intra-crystalline chain dynamics, leading to an overestimation of the fraction of tie-molecules with our method which assumes $f_{\mathrm{T}} < 1$.

4.2.4. Variation of solubility with temperature

In the present model both p_{T} and ψ are temperature- and composition- independent parameters: the former because the topology of the inter-lamellar domains should not change unless temperature is very close to the melting point – where structural reorganization following recrystallization may occur –, and the latter due to the simplicity of the model for the free amorphous domains – which are assumed to not exchange mass with the crystal. It is therefore necessary to test the predictions of the model at temperatures different from the ones at which the sample-specific parameters are optimised. Therefore, the sorption isotherms of *n*-heptane measured in the six polymer samples at 35, 45, and 55 °C are compared with the predictions of the model using the sample-specific parameter obtained for the isotherms of the four solutes at 25 °C. The calculations together with the experimental sorption data are reported in Figure 4.6.

The solubility predicted with the model is seen to underestimate the experimental solubility at pressures close to the vapour pressure of *n*-heptane for the six polymer samples. This might be an indication that the variations of ψ with temperature or during sorption must be accounted for in order to capture the temperature dependence of the sorption isotherms. It is important to note, however, that the fact that solubility in the atactic PP sample – i.e., the one calculated neglecting crystallinity entirely – is markedly underpredicted at higher pressures and temperatures greater than 25° C, suggests that the systematic underprediction of solubility in all of the PP samples is due to the inability

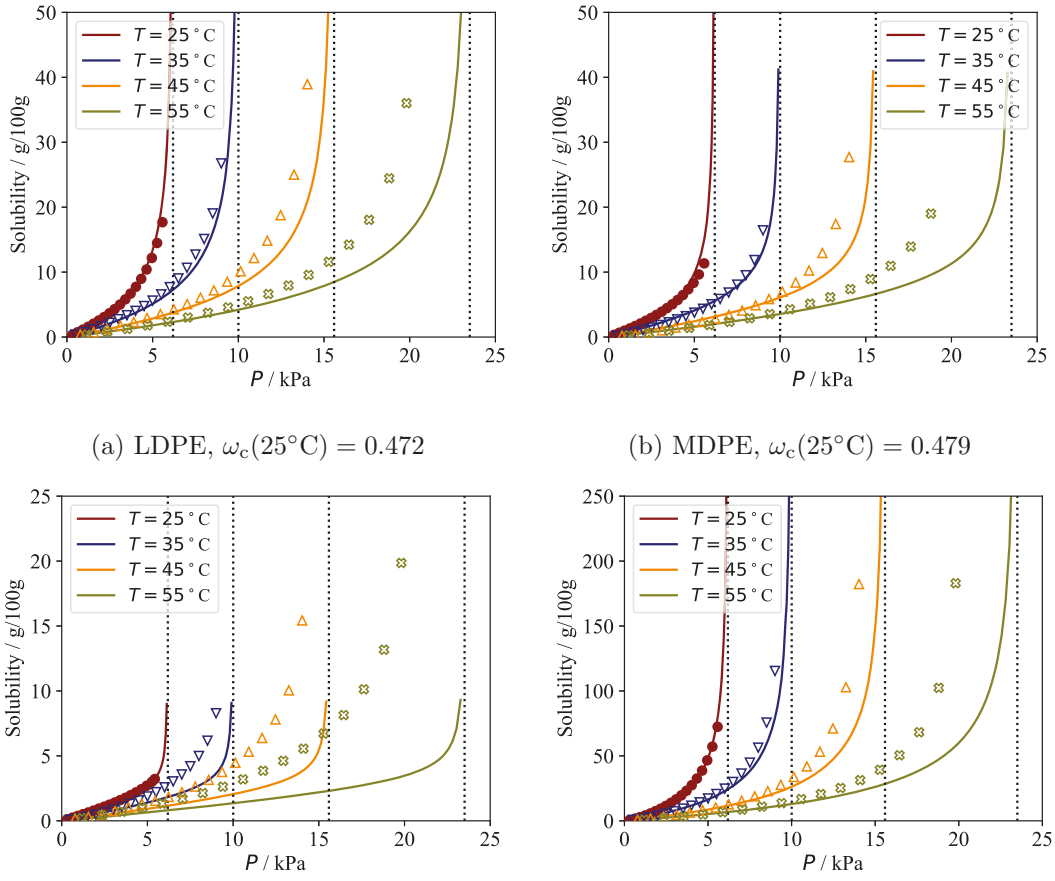

(a) LDPE, $\omega_c(25°C) = 0.472$

(b) MDPE, $\omega_c(25°C) = 0.479$

(c) HDPE, $\omega_c(25°C) = 0.499$

(d) aPP, $\omega_c(25°C) \approx 0$

Figure 4.6.: Sorption isotherms of n-heptane in the six PE and PP samples analysed at 25, 35, 45 and 55 °C. The sorption (in grams of solute per 100 grams of pure polymer) is plotted as a function of the total pressure P. The vertical dotted lines denote the vapour pressure of n-heptane at the four different temperatures. The continuous curves represent the calculations with the model after adjusting p_T and ψ for each polymer sample to best reproduce the sorption isotherms of n-hexane, n-heptane, cyclohexane and toluene at 25 °C (Figure 4.5 and Table 4.4). The symbols represent the experimental data;[139] empty symbols were not included in the optimisation of the sample-specific parameters. Uncertainty in the data points is smaller than the marker size.

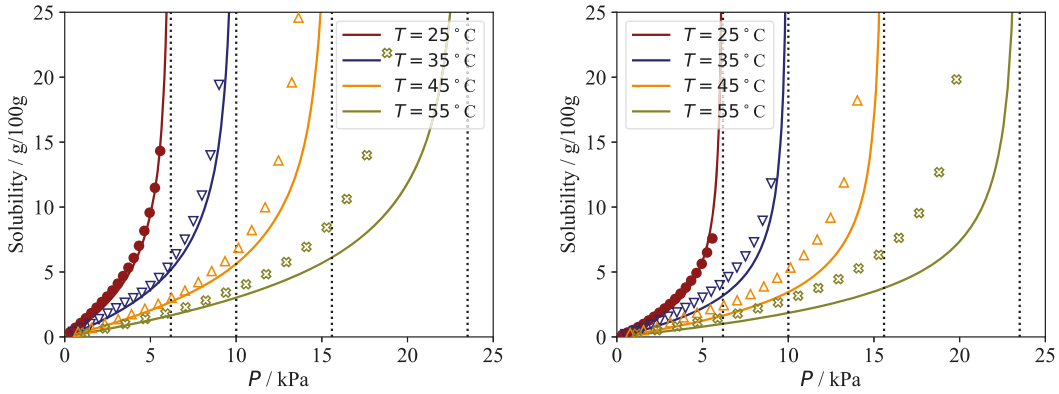

(e) PP fiber, $\omega_c(25°C) = 0.435$

(f) iPP, $\omega_c(25°C) = 0.586$

Figure 4.6.: (Continued) Sorption isotherms of n-heptane in the six PE and PP samples analysed by Valsecchi *et al.*[139] at $25, 35, 45$ and 55 °C. The sorption (in grams of solute per 100 grams of pure polymer) is plotted as a function of the total pressure P. The vertical dotted lines denote the vapour pressure of n-heptane at the four different temperatures. The continuous curves represent the calculations with the model after adjusting p_T and ψ for each polymer sample to best reproduce the sorption isotherms of n-hexane, n-heptane, cyclohexane and toluene at 25 °C (Figure 4.5 and Table 4.4). The symbols represent experimental data;[139] empty symbols were not included in the optimisation of the sample-specific parameters. Uncertainty in the data points is smaller than the marker size.

of the equation of state to describe the VLE properties of the mixture of n-heptane and PP at high pressures and temperatures.

In other words, if the equation of state alone provided accurate predictions for the solubility of n-heptane in atactic PP at all temperatures the quality of the predictions for the other two semi-crystalline samples should improve. Unfortunately, it is not possible to make the same argument for the PE samples as no fully amorphous PE exists at the temperatures investigated. Although sorption isotherms above the melting point of PE ($T_{\mathrm{m}} < 141$ °C) could be used to gauge whether the equation of state properly describes the VLE properties of the mixture of n-heptane and PE, the comparison might be misleading due to the $\sim 80 - 100$ °C temperature difference between these isotherms and the ones determined in this work.

We also note that the solubility in the HDPE sample at temperatures higher than 25 °C is under-predicted both at high and low pressures. This might indicate irreversible crystal melting at higher temperatures, possible due to an unstable microstructure obtained after solution casting of the HDPE sample (*cf.* Section 4.2.1). It is not clear, however, why this phenomenon would occur in HDPE only and not in the LDPE and MDPE samples.

4.2.5. Changes in the inter-lamellar domains during sorption

As mentioned at the end of Section 3.3.4, once the model parameters are specified all of the properties of the inter-lamellar amorphous domains are functions of state. It is then possible to track the variations of these quantities along the sorption isotherms or with temperature at a fixed composition. As an example, the predicted variation of l_{a}, P_{c}, $\omega_{\mathrm{c}}^{\mathrm{LS}}$ and x_{T} along the sorption isotherms of the four solutes in MDPE is shown in Figure 4.7.

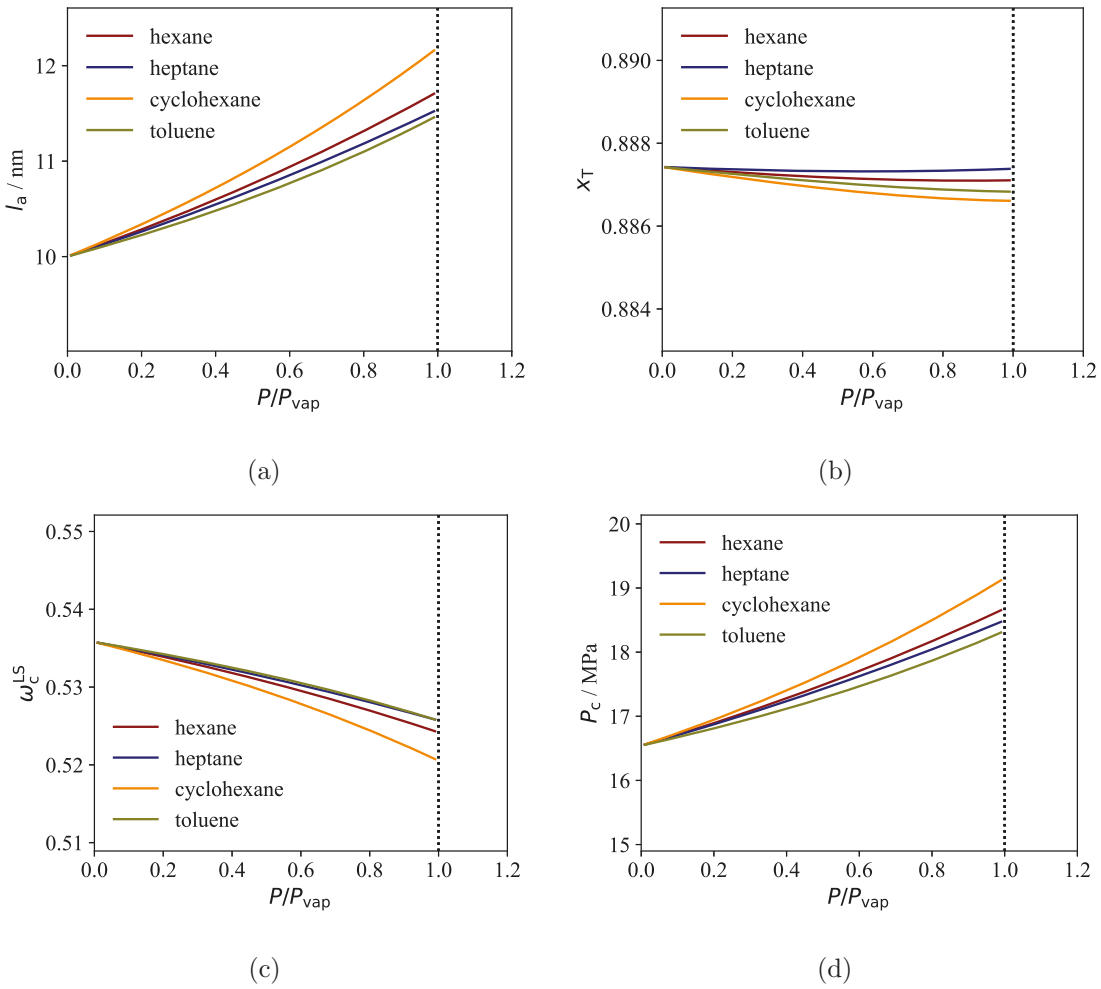

Figure 4.7.: The variation of various properties of the inter-lamellar domains during the sorption process for MDPE at 25 °C, as calculated using the model developed with the parameters of Tables 3.1 and 4.4. All of quantities are plotted as a function of the ratio between the total pressure P and the vapour pressure of the penetrant at 25 °C as for Figure 4.5: a) inter-lamellar distance l_a; b) fractional extension of the tie-segments x_T; c) crystallinity of the lamellar stacks; d) constraint pressure. We note that the fractional extension x_T is almost a constant due to Equation 3.107. The crystallinity of the lamellar stacks at zero sorption can be obtained by dividing the total crystallinity of the pure polymer by $1 - \psi$: for MDPE, $\omega_c^{LS,*} = 0.479/(1 - 0.106) \sim 0.536$.

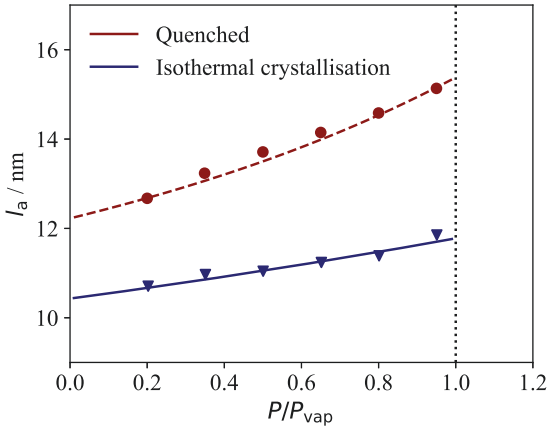

Figure 4.8.: Variation of the inter-lamellar distance during swelling of semi-crystalline PE samples with n-hexane at 21 °C. The inter-lamellar distance is plotted as a function of the ratio between pressure and the vapour pressure of n-hexane at 21 °C. Symbols are experimental data obtained by Kim and coworkers[294] for a quenched and isothermally crystallised sample using small-angle neutron scattering. The dashed and solid curves represent the model's calculations, performed by setting the inter-lamellar distance in each pure sample equal to the respective reported value and then adjusting p_T. The optimal values for the quenched and isothermally crystallised samples are, respectively, $p_T = 0.22$ and $p_T = 0.30$.

The fractional extension x_T is found to be almost constant during sorption process as can be inferred from Equation 3.107. At temperatures which are much lower than T_m^0, the lowering of the monomer chemical potential of the polymer $\mu_{p,mono}^{(n_0),EoS}$ due to the presence of the solute is insignificant compared to the driving force of crystallization, which is only a function of temperature. On the other hand, the swelling of the inter-lamellar domains (i.e., the increase of l_a) causes the angle of the tie-segments with the normal to the crystal/amorphous interface (θ_T) to become closer to 0° and thus leads $\cos\theta_T$ to increase. This explains the corresponding increase in P_c during sorption (Equation 3.92). The variation of the crystallinity of the lamellar stacks is also limited.

None of these properties was directly measured in conjunction with the sorption isotherms reported for the six PE and PP samples. Nevertheless, we can compare the model's predictions of the swelling in the inter-lamellar domains with nano-swelling measurements

of Kim and coworkers[294] (Figure 4.8). In their work, the authors prepared two semi-crystalline PE samples by quenching and isothermal crystallisation of the same PE melt. The (volume fraction) crystallinity at 21 °C for the two samples was reported as 0.54 and 0.78, respectively. The change in the long period of the lamellar stacks was then measured via in-situ small-angle neutron scattering during sorption experiments using *n*-hexane at 21 °C.

We set the inter-lamellar distance of the pure samples at 21 °C, $l_{\mathrm{a}}^{*} = l_{\mathrm{a}}(21°\mathrm{C})$, equal to the values reported by the authors (12.13 nm and 10.35 nm, respectively, for the quenched and isothermally-crystallised samples) and adjust the p_{T} value for each of the two samples to reproduce the observed swelling. Both the experimental and the theoretical nano-swelling isotherms are very linear, confirming that the dramatic increase of solubility in PE samples near condensation seen in Figure 4.5 can only be explained by including unconstrained amorphous domains in the description ($\psi \neq 0$).

The optimal values of p_{T} for the isothermally-crystallised sample is 0.30, in good agreement with the values found using sorption isotherms in Section 4.2. A lower value of $p_{\mathrm{T}} = 0.22$ is found for the quenched sample. However, it must be noted that the authors assumed the 2-domain model in order to calculate the inter-lamellar distance after measuring the long period and the sample's overall crystallinity. While assuming $\psi = 0$ is a good approximation for the isothermally crystallised sample, a non-negligible amount of free amorphous mass might be present in the quenched samples leading to a reduction in the measured inter-lamellar distance (and therefore an increase in the optimal p_{T} value for the quenched sample).

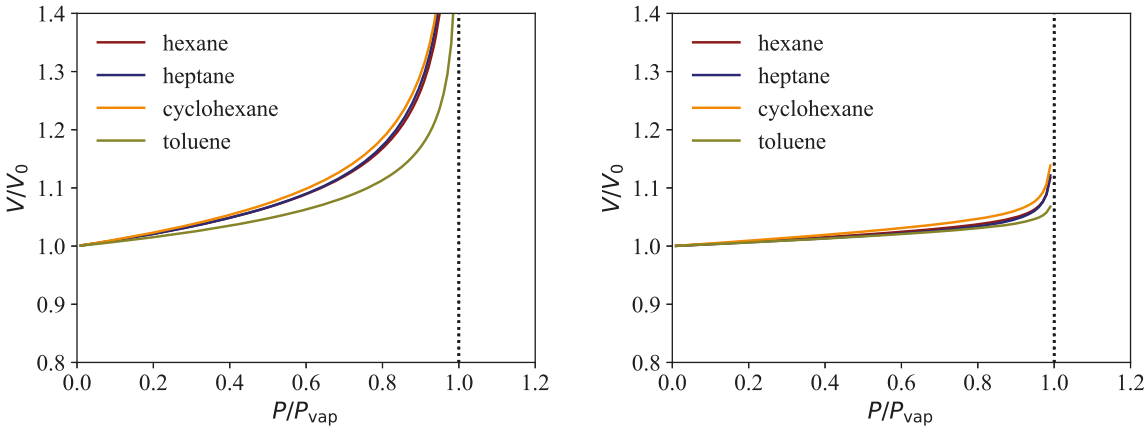

(a) LDPE

(b) HDPE

Figure 4.9.: Swelling of the LDPE and HDPE samples studied by Valsecchi *et al.*[139] during the sorption process at 25 °C as a function of the ratio between the pressure of the external gas and the vapour pressure of the penetrant at 25 °C. The continuous curves represent predictions with the model obtained using Equation 4.2. The model parameters for the two samples are listed in Tables 3.1 and 4.4. As expected, the LDPE sample swells considerably more than the HDPE sample due to the higher amount of solute dissolved in the free amorphous domains (see Figure 4.5).

4.2.6. Swelling

The model developed allows one to quantify the overall swelling of the polymer sample. As shown in Appendix G, swelling can be calculated by means of

$$\frac{V}{V_0} = \left(\frac{\omega_c}{\rho_c} + \frac{\psi}{\rho^{F}_{p,eff}} + \frac{1-\psi-\omega_c}{\rho^{IL}_{p,eff}} \right) \Big/ \left(\frac{\omega^0_c}{\rho_c} + \frac{\psi}{\rho^{F}_{a}} + \frac{1-\psi-\omega^0_c}{\rho^{IL}_{a}} \right). \tag{4.2}$$

Here, ω^0_c and V_0 are the crystallinity and the volume of the sample before sorption. Similarly, ρ^{F}_{a} and ρ^{IL}_{a} are the density of pure free amorphous and inter-lamellar domains, respectively. The effective polymer density in the free amorphous domains, $\rho^{F}_{p,eff}$, is calculated in the same way as $\rho^{IL}_{p,eff}$ (Equation 3.97) using the partial specific volumes in an unconstrained polymer + solutes mixture.

It should be noted that we assume that the free amorphous mass does not change, i.e., ψ is constant. In general, the variation of ψ during sorption, if present, should be known in order to calculate the swelling of the sample. Nonetheless, the change in free amorphous mass due to sorption should be small (this is the case at least for the inter-lamellar domains, see Figure 4.7) and the assumption that ψ is a constant during sorption (in the absence of irreversible transformations in the sample and far from the melting point) appears to be reasonable.

In Figure 4.9 the swelling of the LDPE and HDPE samples during the sorption process of the four penetrants is determined at 25 °C. Unfortunately, the swelling of the samples was not measured, preventing a direct comparison with the predictions. As expected, the LDPE sample swells significantly more then the HDPE sample because the former has a higher content of free amorphous mass and the solubility in the free amorphous domains is higher than in the inter-lamellar amorphous domains.

4.3. Estimation of the tie-molecule fraction in PE

Having looked at the theoretical predictions and experimental data of pure fluid sorption in six PE and PP samples, in this section the model developed in Chapter 3.3 is further benchmarked against a large set of experimental solubility data of hydrocarbon fluids in semi-crystalline polyethylene samples.

Just like in Section 4.2, we aim to obtain the optimal sample-specific parameters for each sample by minimizing the difference between experimental data and the model's predictions of pure-component sorption isotherms. However, optimizing p_{T} and ψ at the same time (as in Section 4.2) can lead to parameter degeneracy when the available solubility data for a given polymer sample includes measurements for only one solute in the low-pressure (Henry) regime. In this limit the solubility must increase linearly with

pressure due to the ideal gas behaviour of the external fluid and Henry's law for the polymer-solute mixture, i.e.,

$$S_i(T, P, \boldsymbol{y}) \sim k_{\mathrm{H},i}(T) P y_i, \tag{4.3}$$

as $P \to 0$. Here, $k_{\mathrm{H},i}$ is the Henry constant of solute i and y_i its mole fraction in the external gas. By looking at equation 3.53, our model predicts

$$k_{\mathrm{H},i}(T) = \psi k^{\mathrm{F}}_{\mathrm{H},i}(T) + (1-\psi)\left(1-\omega_{\mathrm{c}}^{\mathrm{LS}}\right) k^{\mathrm{IL}}_{\mathrm{H},i}(T), \tag{4.4}$$

and since the Henry constant in the inter-lamellar domains must decrease with p_{T} and $k^{\mathrm{F}}_{\mathrm{H},i} > k^{\mathrm{IL}}_{\mathrm{H},i}$ (as the inter-lamellar domains are constrained, Equation 3.44) an infinite number of pairs of p_{T} and ψ predicts the same overall Henry constant for the solute i. For example, in Section 4.2 it was shown how the linear increase in solubility at low pressures can be described accurately both by setting $\psi = 0$ and only fitting p_{T} (Figure 4.4) and by fitting both parameters (Figure 4.5).

Nonetheless, at pressures closer to the saturation point of the external fluid the degeneracy disappears as the increase in solubility in the free amorphous domains is more pronounced than in the inter-lamellar domains. In particular, it is necessary to have $\psi > 0$ to reproduce high solubilities near condensation as swelling in the inter-lamellar domains is severely restricted by the tie-molecules, as shown in Sections 4.2.2 and 4.2.5. Using solubility data of different solutes to parameterise the same sample can also help removing the degeneracy because the entity of the solubility reduction in the inter-lamellar domains (compared to the free amorphous domains) is different for each solute due to differences in the solutes' partial molar volumes (Equation B.7).

4.3.1. Making p_T the only free parameter

In this Section we adopt an *ansatz* for ψ as a function of the measured crystallinity in order to avoid degeneracy in the sample-specific parameters, as many of the sources considered (*cf.* Section 4.3.2) only reported solubility in the Henry regime or for a single solute. We remove ψ from the optimization following Chmelař and coworkers,[238] who showed that the fraction of free amorphous mass can be estimated quite precisely using only crystallinity as an input by comparing measurement from difference sources and with different techniques (see Figure 6 in their published work[238]). Here we choose the function

$$\psi(\omega_a) = \omega_a^4 \left(C(\omega_a^4 - 1) + 1\right) \tag{4.5}$$

to obtain ψ given $\omega_a = 1 - \omega_c$, where $C = -0.3673$. This functional form ensures that $\psi(0) = 0$, $\psi(1) = 1$ – which are physically sound constraints – and was selected among other low-order polynomials due to its simple form and good accuracy in the entire crystallinity range. The value of C used is obtained by minimising the mean squared error between the predictions of equation 4.5 and the data reported by Chmelař and coworkers, which refers to polyethylene samples in a wide range of crystallinity analyzed using NMR,[224,234–238] PALS[239] or a combination of DSC and WAXS.[240] A comparison between calculations using Equation 4.5 and experimental data is shown in Figure 4.10.

It is important to note that the experimental data with which we fit Equation 4.5 refers to PE samples at 25 °C, and therefore should only be applicable to PE samples at the same temperature in the absence of a model detailing the variations of crystallinity or ψ with temperature. In practice, crystallinity measurements are sometimes made at temperatures different from room temperature (*cf.* Table 4.3). For simplicity here we estimate ψ for each sample based on the crystallinity value at the reported temperature (ω_c^*) using Equation 4.5.

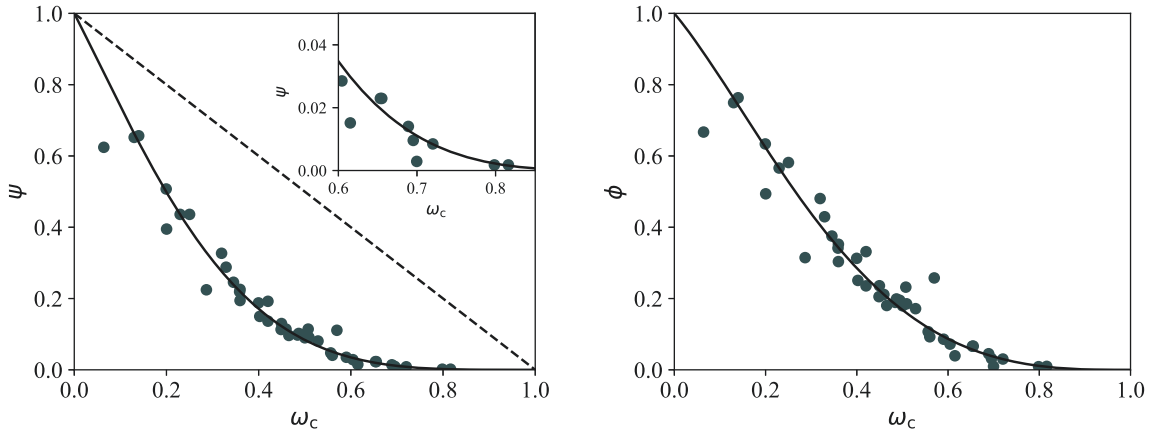

(a) ψ (b) ϕ

Figure 4.10.: Fraction of free amorphous mass over the total polymer mass (ψ) and over the amorphous mass (ϕ) as a function of the crystallinity of a semi-crystalline PE sample. Symbols are experimental data at 25 °C from a variety of sources[224, 234–240] reported by Chmelař and coworkers;[238] the solid curve is an empirical correlation of the data (Equation 4.5 with $= -0.3673$); the dashed line in a) represents the upper bound to ψ, i.e. $1 - \omega_c$. The higher crystallinity data is shown in the inset for clarity.

The only free parameter that we optimize to reproduce sorption isotherms in the current work is therefore p_T. Its value is found for each sample by minimizing the *relative* root mean squared error (RRMSE) between the model's predictions and the experimental gas solubility at a given temperature T:

$$\mathrm{RRMSE}\% = \sqrt{\frac{1}{N_s}\sum_{i}^{N_s}\frac{1}{N_{P,i}}\left[\sum_{j}^{N_{P,i}}\left(\frac{S_i^{\mathrm{exp}}(T,P_{i,j}) - S_i^{\mathrm{calc}}(T,P_{i,j})}{S_i^{\mathrm{exp}}(T,P_{i,j})}\right)^2\right]} \times 100\%. \qquad (4.6)$$

Here N_s is the number of single-solute isotherms used for each sample, $N_{P,i}$ is the number of solubility measurements for each isotherm and $P_{i,j}$ is the pressure at each measurement. The calculated solubility S_i^{calc} is here implicitly a function of the polymer- and sample-specfic parameters.

4.3.2. Sourcing crystallinity and solubility data

Table 4.3.: Crystallinity characterisation techniques employed by the sources of experimental solubility data in PE considered in the current work. The quantity T^* indicates the temperature at which the crystallinity measurement was taken (*cf.* Table 4.4).

Source	Technique	T^* / °C
Chmelař *et al.*[136]	DSC, ρ	80
Doong *et al.*[42]	ρ, DSC, SAXS	25
Dos Santos *et al.*[300]	ρ	30
Jin *et al.*[137]	ρ	25
Kiparissides *et al.*[301]	DSC	25
Lopez-Gonzalez *et al.*[302]	ρ	30
Moebus *et al.*[255]	Unknown	25
Moore *et al.*[303]	SAXS	25
Mrad *et al.*[304]	DSC, ρ	70
Novak *et al.*[138]	DSC	25
Rausch *et al.*[254]	ρ	25
Sturm *et al.*[256]	ρ	25
Valsecchi *et al.*[139]	ρ	25
von Solms *et al.*[305]	ρ	25
Yoon *et al.*[306]	ρ	25

Solubility is reported using different units across different sources; all experimental solubility data has therefore been converted in g of solute per 100 g of pure polymer to aid comparison. The data is taken directly if reported in tables in the original publications or manually extracted from plots with PlotDigitizer.[307] Unfortunately, in most cases the uncertainty of the solubility measurements was not reported.

In order to compare data between different sources, it also important to ensure that crystallinity is calculated using the same formulae and parameters consistently. Crystallinity estimated with density measurements is here re-calculated using Equation 3.12 and the correlation between crystalline and amorphous specific volumes of PE with temperature

proposed by Chiang and Flory:[168]

$$\begin{cases} v_a = 1.152 + 8.8 \times 10^{-4}(T[K] - 273.15) \quad \mathrm{cm^3 g^{-1}} \\ v_c = 0.993 + 3.0 \times 10^{-4}(T[K] - 273.15) \quad \mathrm{cm^3 g^{-1}} \end{cases}. \tag{4.7}$$

Similarly, crystallinity estimated via DSC analysis is re-scaled using the specific enthalpy of melting of extended PE crystals reported in Table 3.1, $\Delta h^0_{\mathrm{m}} = 293$ J g^{-1}.

4.3.3. Optimisation results

Optimized model parameters for polyethylene samples

In Table 4.4 the results of the optimization of the polymer sample-specific parameters for all the semi-crystalline PE samples considered are presented. For each sample we report the temperature at which the solubility used in the parameter estimation was measured, the solutes considered, the crystallinity – measured at temperature T^*, see Table 4.3 –, the source, and the denomination of the sample in the original publication. Furthermore, we report the optimal value of p_{T}, the value of ψ calculated via Equation 4.5 and the RRMSE at the optimum.

In Figure 4.11 the optimal values of p_{T} are plotted as a function of the crystallinity of the sample. The average p_{T} value across all samples is 0.297, with an average RRMSE% of 8.43%. We consider this error to be acceptable given the intrinsic uncertainty in the measurements of solubility and crystallinity. It is reassuring that approximately the same average value of p_{T} (≈ 0.32) was found for the PE samples in Section 4.2 by optimising p_{T} and ψ at the same time. As discussed in Section 4.2.3, a value of $p_{\mathrm{T}} \approx 0.3$ for PE is consistent with both upper and lower bounds estimated by theoretical models and computer simulations[164–167,206,207] and suggests that most inter-lamellar mass should belong to tie-molecules (i.e., bridges and entangled loops).

Table 4.4.: Model parameters for the semi-crystalline PE samples considered. The crystallinity ω_c^* is measured at temperature T^* as reported in Table 4.3, while ψ is calculated using Equation 4.5. The solutes used to parameterise each sample are reported in the "Solutes" column: Cn stands for n-alkanes; Cn= for linear alk-1-enes; iC4 and iC5 for isobutane and isopentane, respectively; cC6 for cyclohexane and aC6 for benzene. T is the temperature of the sorption isotherms used for each sample, and the RRMSE is the minimum relative root mean squared error calculated via Equation 4.6

Ref	Sample name	ω_c^*	p_T	ψ	Solutes	T / °C	%RRMSE
Chmelar *et al.*[136]	VLLDPE	0.272	0.015	0.728	C2=	80	0.68
	LLDPE A	0.374	0.336	0.201	C2=	80	2.61
	LLDPE B	0.401	0.370	0.170	C2=	80	1.02
	LLDPE C	0.443	0.315	0.128	C2=	80	5.22
	LLDPE D	0.475	0.224	0.102	C2=	80	2.32
	MDPE A	0.554	0.319	0.053	C2=	80	3.17
	MDPE B	0.565	0.335	0.048	C2=	80	1.26
	MDPE C	0.575	0.363	0.038	C2=	80	3.30
	HDPE A	0.592	0.356	0.017	C2=	80	1.21
	HDPE C	0.664	0.307	0.016	C2=	80	5.14
	HDPE D	0.671	0.367	0.010	C2=	80	1.90
	HDPE E	0.789	0.393	0.005	C2=	80	11.62
Doong *et al.*[42]	PE film	0.502	0.287	0.083	aC6	30	14.62
Dos Santos *et al.*[300]	DYND-3	0.481	0.308	0.097	C4, C4=, iC4	30	12.33
Jin *et al.*[137]	MTH879	0.209	0.165	0.479	C6=	50	8.17
	MTH904	0.398	0.223	0.173	C6=	50	4.29
	MTH912	0.447	0.285	0.125	C6=	50	5.18
	MTH918	0.488	0.314	0.092	C6=	50	3.13
	MTH923	0.522	0.304	0.070	C6=	50	3.19
Kiparissides *et al.*[301]	HDPE	0.681	0.330	0.014	C2=	80	11.62
Lopez-Gonzalez *et al.*[302]	LDPE87	0.231	0.413	0.433	C2=, C3=	30	20.6
	LDPE91	0.478	0.311	0.099	C2=, C3=	30	7.85
	LDPE93	0.558	0.328	0.052	C2=, C3=	30	7.20
Moebus *et al.*[255]	EH1	0.410	0.206	0.160	C2=, iC4, iC5, C6, C6=	80	11.69
	EH5	0.440	0.270	0.131	C2=, iC4, C6, C6=	85	9.18
	EB1	0.450	0.209	0.122	iC4, C4=, iC5	85	13.15
Moore *et al.*[303]	LLDPE (co-hexene)	0.185	0.015	0.532	C4=, C6=	69	12.80
	LLDPE (co-butene)	0.470	0.208	0.106	C4=, C6=	69	8.37
	LDPE	0.504	0.209	0.081	C2=, C4=, C6=	69	10.78
	HDPE	0.702	0.273	0.011	C4=, C6=	69	7.72
Mrad *et al.*[304]	LDPE	0.476	0.511	0.101	C2=	70	7.81
Novak *et al.*[138]	HDPE - Sample 1	0.601	0.399	0.034	C2=, C6=	70	4.62
	HDPE - Sample 2	0.632	0.391	0.025	C2=, C6=	70	7.75
	HDPE - Sample 3	0.710	0.362	0.010	C2=, C6=	70	4.64
Rausch *et al.*[254]	HDPE	0.754	0.337	0.005	cC6	90	3.26
Sturm *et al.*[256]	VLLDPE - Sample 5	0.450	0.279	0.122	iC5, C6=	50	9.85
	LLDPE - Sample 6	0.480	0.315	0.098	C6=	50	4.12
	LLDPE - Sample 1	0.509	0.255	0.078	iC5	50	1.16
	HDPE - Sample 3	0.700	0.283	0.011	iC5	65	1.70
	HDPE - Sample 2	0.762	0.295	0.004	iC5	50	5.27
	HDPE - Sample 4	0.771	0.270	0.004	iC5	50	3.91
Valsecchi *et al.*[139]	LDPE	0.472	0.229	0.104	C6, cC6, C7	25	11.26
	MDPE	0.479	0.283	0.099	C6, cC6, C7	25	5.98
	HDPE	0.499	0.621	0.085	C6, cC6, C7	25	36.53
von Solms *et al.*[305]	HDPE	0.731	0.238	0.007	C1	25	2.93
Yoon *et al.*[306]	LLDPE - Sample 1	0.362	0.340	0.216	C6=, C8=	70	39.89
	LLDPE - Sample 2	0.398	0.283	0.173	C6=, C8=	70	12.42
	LLDPE - Sample 3	0.487	0.292	0.093	C6=, C8=	70	14.36
	LLDPE - Sample 4	0.488	0.244	0.092	C6=, C8=	70	17.58
	LLDPE - Sample 5	0.529	0.275	0.066	C6=, C8=	70	14.74

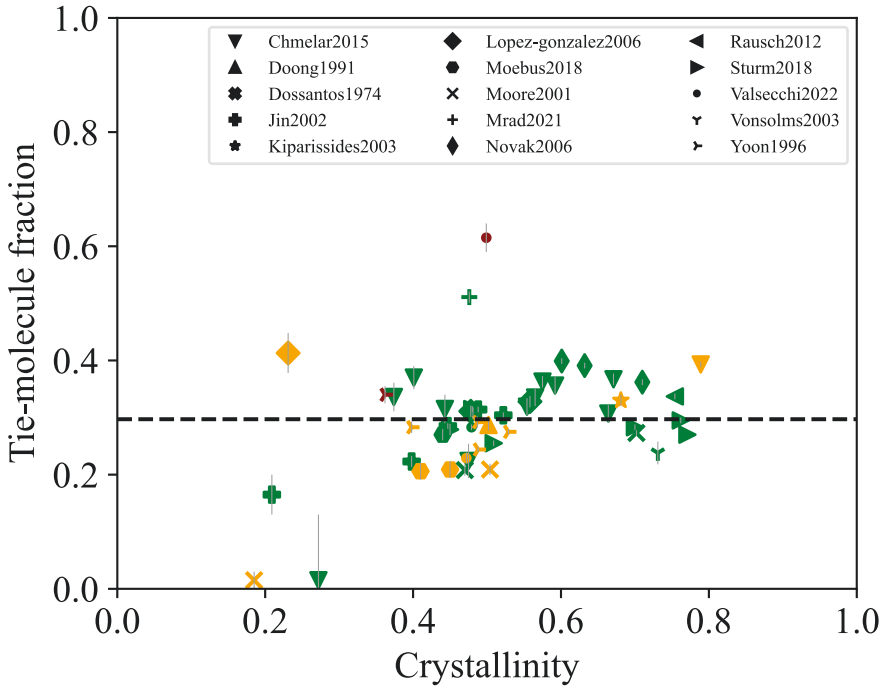

Figure 4.11.: Optimal value of p_T for each PE sample considered as a function of its measured crystallinity ω_c^*. Each marker corresponds to a different literature source (see Table 4.4), while the color represents the RRMSE % at the optimum: green if $0\% \leq \text{RRMSE}\% \leq 10\%$, yellow if $10\% < \text{RRMSE}\% \leq 30\%$ and red if $\text{RRMSE}\% > 30\%$. The horizontal dashed line indicates the average value of p_T (0.297) across all samples. The error bars indicate values of p_T that result in RRMSE % within 5 % from the optimum. Note that the solubility in the inter-lamellar domains of PE is negligible for $p_T > 0.6$. The temperature at which crystallinity was measured was 25 °C for most samples (see Table 4.3).

Various authors have argued that there could be a maximum in the tie-molecule content at intermediate crystallinity based on mechanical measurements, sorption data and theoretical calculations.[190,191,207,256] Due to the scatter in our optimal p_T values when plotted against crystallinity, we cannot confirm this hypothesis unless more experimental data at high crystallinity is analysed with the present model. Nevertheless, it is can be argued that crystallinity simply does not capture enough of the history of a sample to show strong correlation with p_T. For example, samples with same crystallinity but different average lamellar thickness should possess different tie-molecule fractions.[184,190] For accurate estimates of p_T it might thus be necessary to consider additional properties of each PE sample such as its molecular weight distribution, branching content and production history.

Finally, we note that systematic errors in the reported values of crystallinity or solubility can affect the comparison of data between different sources. For example, the LDPE sample studied by Mrad and coworkers[304] and the HDPE sample analysed in Section 4.2 are clear outliers with $p_T > 0.5$ at $\omega_c^* \approx 0.5$. These findings suggest that using crystallinity (or density) alone to estimate *a priori* ψ and p_T at the same time might result in unphysical values of some of the parameters.

Henry constants of ethylene

In Figure 4.12 the Henry constant (in (g/g) / GPa) of ethylene at 25 °C in each PE sample is plotted as a function of the sample's crystallinity. It is particularly useful to plot the calculated value of the Henry constant using the optimized model parameters instead of the experimental one since the data is not always present or smooth enough in the low-pressure regime. Ethylene is chosen here as a "probe molecule" due to its importance in polyethylene production processes. As expected, the Henry constant per total polymer mass decreases with increasing crystallinity (Figure 4.12a), remaining

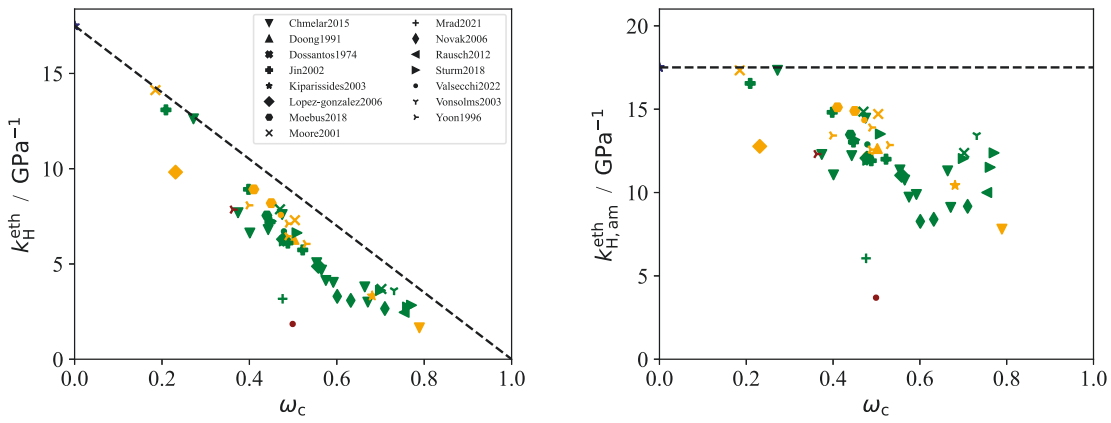

(a) (b)

Figure 4.12.: Henry constant of ethylene in the semi-crystalline PE samples studied at 25 °C calculated using the present model and the optimized sample-specific parameters (Table 4.4) in (g/g) GPa^{-1}. Symbols represent the model's calculations after optimisation of the sample-specific parameters of each sample – see Figure 4.11. The dashed lines corresponds to predictions with $\psi = 1 - \omega_c^*$, i.e. with no constraints acting on the amorphous domains. a) Henry constant per total polymer mass. b) Henry constant per amorphous polymer mass.

always below the $\psi = 1 - \omega_c^*$ line (i.e., Michaels and Bixler's model[26]). The Henry constant in the amorphous domains only (intended as the sum of free and inter-lamellar domains) is shown in Figure 4.12b). Despite the scatter in the data, the Henry constant in the amorphous domains is seen to decrease on average with crystallinity and tends to the value predicted for a subcooled polyethylene melt as $\omega_c \to 0$.

Comparison with data included in the parameterisation

In Figures 4.13 and 4.14 the model's solubility calculations are compared to experimental data for six PE samples for which sorption isotherms of multiple pure substances are available. The p_T parameter of each sample is optimised to reproduce all the isotherms at the same time. Our calculations are in excellent agreement with the experimental data, confirming that a single parameter set can be assigned to each sample to capture the solubility of different pure substances. This demonstrates that the sample-specific

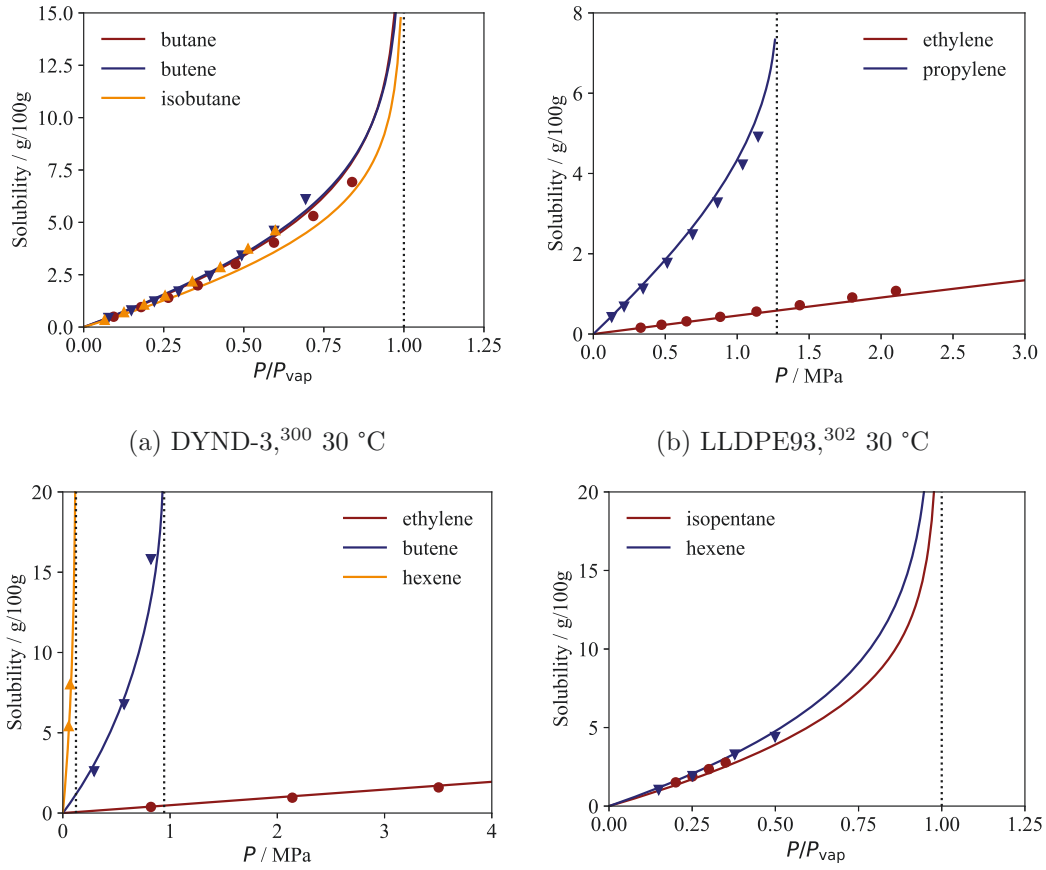

(a) DYND-3,[300] 30 °C

(b) LLDPE93,[302] 30 °C

(c) LDPE,[303] 69 °C

(d) VLLDPE,[306] 50 °C

Figure 4.13.: Solubility of various pure substances in semi-crystalline PE samples analysed in the literature. Solid curves represent the model's calculations with the sample-specific parameters found in Table 4.11; for each sample, p_T is optimised to reproduce the experimental data shown (symbols). Vertical dotted lines represent the vapour pressure of the external gas at the each temperature. The solubility is plotted as a function of total pressure if one of the solutes is supercritical at the temperature considered; otherwise, as a function of the ratio between pressure and each solute's vapour pressure at that temperature.

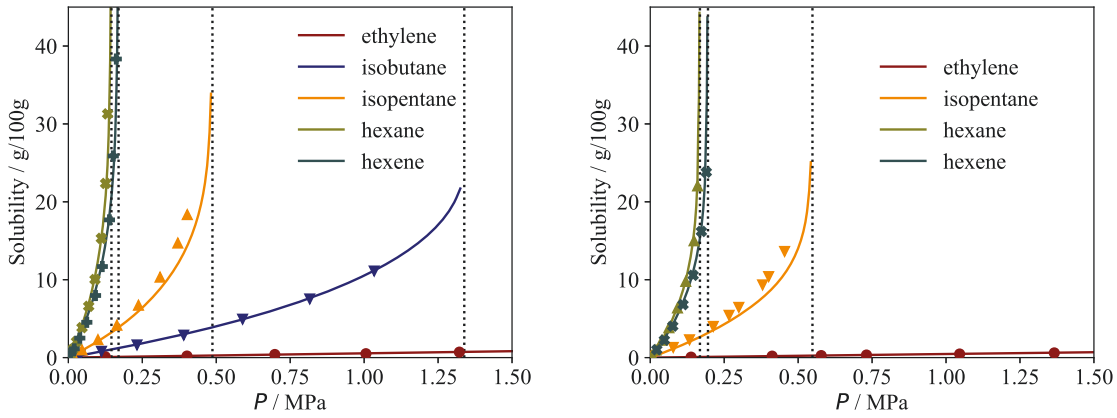

(a) EH1, $T = 80°C$ (b) EH5, $T = 85°C$

Figure 4.14.: Solubility of various pure substances in semi-crystalline PE samples analysed by Moebus and Greenhalgh[255] as a function of pressure. Solid curves represent the model's calculations, while symbols experimental data. All isotherms are plotted up to the vapour pressure of the pure fluid at the corresponding temperature, with the exception of ethylene (which is supercritical at both temperatures) a) Solubility of pure gases in the EH1 sample at 80 °C. b) Solubility of pure gases in the EH5 sample at 85 °C. The p_T parameters of the two samples (0.206 and 0.270, *cf.* Table 4.4) have been optimized to reproduce these sorption isotherms.

properties of each semi-crystalline PE sample can be effectively decoupled from the underlying equilibrium EoS, as seen in Section 4.2.

4.3.4. Prediction of co-solubility effects

The robustness of the model is showcased by predicting solubility co-solubility effects in a subset of the PE samples analyzed. The term "co-solubility effect" refers to the increase or decrease in solubility of a given compound in a sample due to the presence of other substances in the external fluid. This phenomenon is of critical importance in the production of polyolephines, as the addition induced condensing agents (ICAs) like n-hexane or co-monomers like 1-butene and 1-hexene to an ethylene reaction mixture has been shown to increase the polymerization rate of PE, presumably due to the increased ethylene solubility in the amorphous polymer near the catalyst sites.[138,255,304,308] Furthermore, in real-world applications semi-crystalline polymers are rarely in contact with pure fluids and factors such as the relative humidity can have an impact on the solubility of any given substance.

Our model naturally allows to predict the solubility of mixtures in contact with a semi-crystalline polymer, as outlined in Section 3.3. The equation of state used in the current work – i.e., SAFT-γ Mie – provides a good description of mixture properties as its parameters are usually optimized to reproduce enthalpy of mixing and/or vapour-liquid equilibrium envelopes of fluid mixtures[67,69,70,72,94,100] (*cf.* Section 2.4). In Figure 4.15 and 4.16 experimental co-solubility data of various substances in semi-crystalline PE samples reported by Moebus and Greenhalgh[255] is compared to the model's predictions. Note that the optimal p_{T} parameter for each sample (Table 4.4) has been adjusted to reproduce the single-solute isotherms reported in Figure 4.14, whereas ψ values were estimated using Equation 4.5.

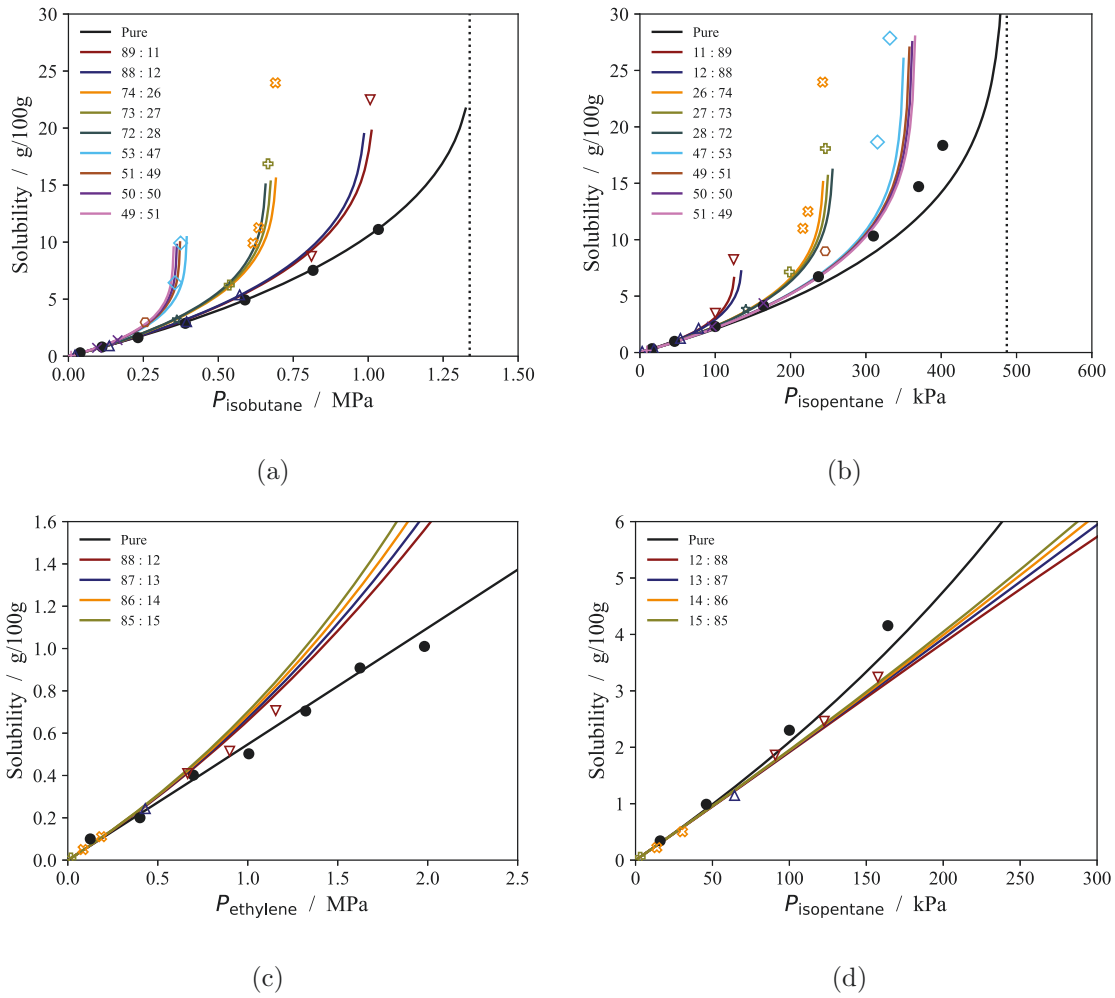

Figure 4.15.: Solubility of individual components (in grams of solute per 100 g of polymer) of fluid mixtures at 80 °C in contact with the EH1 sample analysed by Moebus and Greenhalgh[255] as a function of their partial pressure. Solid curves correspond to predictions with the present model, while symbols experimental data (colour-coded with the corresponding curves). p_T was adjusted to reproduce pure component data (black curves) The numbers in the legend refer to the composition of the two components (in % mol) in the external mixture. Vertical dotted lines, if present, indicate the vapour pressure of the pure fluids at 80 °C. a,b) Solubility of isobutane (isopentane) in the sample at varying isopentane (isobutane) concentration of an isobutane-isopentane mixture. c,d) Solubility of ethylene (isopentane) in the sample at varying isopentane (ethylene) concentration of an ethylene-isopentane mixture.

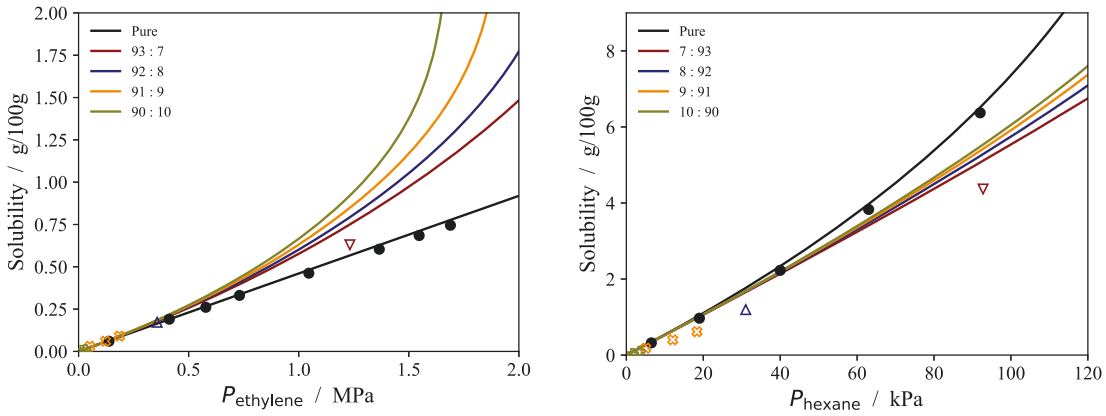

(a) Solubility of ethylene

(b) Solubility of n-hexane

Figure 4.16.: Solubility of individual components (in g of solute per 100 g of polymer) of mixtures of ethylene and n-hexane at 85 °C in the EH5 sample analysed by Moebus and Greenhalgh[255] as a function of their partial pressure. Solid curves correspond to predictions of the present model, while symbols to experimental data (colour-coded with the corresponding curves). The numbers in the legend refer to the % mole fraction of the two components in the external mixture.

The model semi-quantitatively predicts the solubility of isobutane + isopentane and ethylene + isopentane mixtures in the EH1 sample (Figure 4.15) and of ethylene + n-hexane mixtures in the EH5 sample (Figure 4.16). As expected, the solubility of a component is only a function of its partial pressure P_i (i.e., the product of the total pressure P and its mole fraction in the fluid x_i) at low partial pressures. However, at higher partial pressure different mixtures display one of two behaviours.

In the isobutane + isopentane mixture, the solubility of either component at fixed partial pressure in greatly enhanced by the presence of the other component in the external fluid. This phenomenon can be rationalized by realizing that solubility generally increases the most near saturation conditions of the external fluid (see Figure 4.14). All the isotherms in Figure 4.15a and b are calculated up to the dew pressure of the mixture at each composition. The absolute value of the dew pressure of the external fluid is not strongly influenced by composition (due to the similarity of the saturation pressure of the two

pure fluids), and therefore the partial pressure at condensation of each component is lowered as their composition in the external mixture is lowered. Isopentane's isotherms are systematically overpredicted as in Figure 4.14; this is likely a consequence of the overestimation of isopentane's vapour pressure with the SAFT-γ Mie parameters in use.[69]

Conversely, both in the case of ethylene + isopentane and of ethylene + n-hexane mixtures (Figures 4.15c and d and 4.16) the solubility of the lighter component (i.e., ethylene) is enhanced by the presence of the heavier one (i.e., isopentane or n-hexane), while the contrary is true for the solubility of the heavier components upon increasing ethylene's concentration. According to our calculations, this phenomenon is so significant that at fixed temperature and total pressure the calculated solubility of ethylene is greater if the external fluid is a mixture instead of pure ethylene, as can be seen in the figures.

A positive – albeit more modest – deviation of ethylene's solubility from Henry's law is also seen in the experimental data. Nevertheless, solubility measurements at higher pressures are needed to test the model's predictions outside of the dilute regime. A systematic over-prediction of the n-hexane solubility when mixed with ethylene is also observed, although we note the unusal behaviour of the experimental Henry constant reported for n-hexane which seems to change with the external composition.[255]

Novak and coworkers[138] reported measurements of the total solubility of ethylene + 1-hexene mixtures in three HDPE samples. In Figure 4.17 pure component and mixture solubility data in the three samples are compared with the predictions of the present model. The p_{T} parameters are optimized to provide quantitative description of the pure component isotherms (*cf.* Table 4.4), although the solubility of ethylene is slightly overestimated. The predicted total solubility of a 95.7% ethylene + 4.3 % 1-hexene mixture (in mol %) in the three samples is in good agreement with the experimental

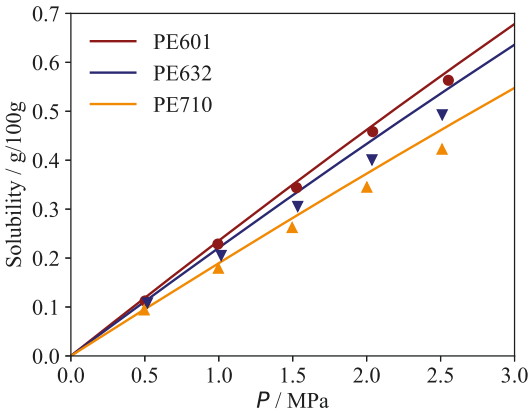

(a) Pure ethylene

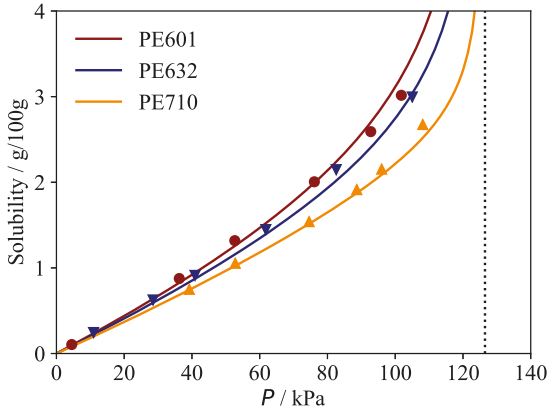

(b) Pure 1-hexene

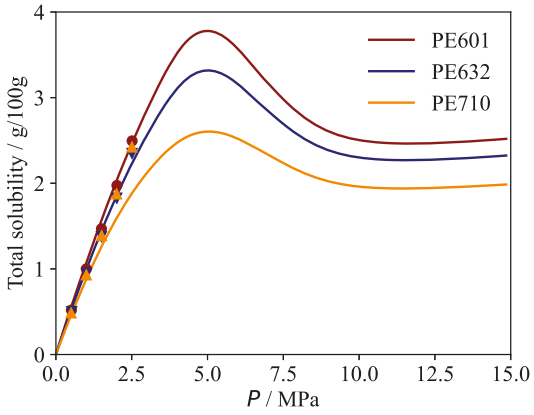

(c) 95.7% ethylene / 4.3% 1-hexene

Figure 4.17.: Solubility of ethylene, 1-hexene and a 95.7% ethylene + 4.3% 1-hexene mixture (mol %) in the semi-crystalline PE samples analysed by Novak and coworkers[138] at 70 °C as a function of pressure. Solid curves represent the calculations, while symbols the experimental data. The p_T parameters of the three polymer samples have been optimized to reproduce their respective pure component isotherms (see Table 4.4). The numbers next to PE in the legend refer to the crystallinity ω_c at 25 °C of the samples in parts per thousands.

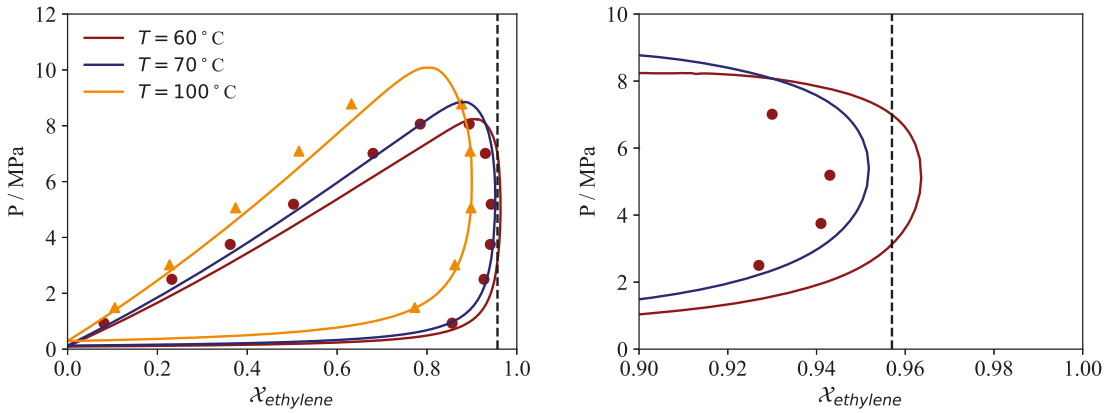

Figure 4.18.: Isothermal VLE envelope of ethylene + 1-hexene mixture. Solid curves are predictions using SAFT-γ Mie. Symbols represent experimental data from Laugier and coworkers.[309] The vertical dotted line corresponds to the composition of the mixture analyzed by Novak and coworkers,[138] i.e. $x_{\text{ethylene}} = 0.957$. a) VLE envelope b) VLE envelope for $0.9 < x_{\text{ethylene}} < 1$.

data, with the exception of the sample of highest crystallinity (PE732). Interestingly, the discrepancy seems to be due to the model predicting a decrease in solubility with increasing pressure between 5 and 10 MPa for all samples.

This artifact in the prediction is due to our SAFT-γ Mie model predicting a critical composition of 95.2% for the ethylene + 1-hexene mixture at 70 °C, just slightly below the composition of the mixture considered by Novak and coworkers (Figure 4.18). This causes the calculated partial molar volume of ethylene in the mixture to be negative for total pressures between about 5 and 10 MPa and therefore the total solubility to decrease with increasing pressure in the same range (Figure 4.17c). The actual critical composition of the mixture must be lower than the critical composition at 60 °C – i.e. about 94.3%, as seen in the experimental data by Laugier and coworkers in Figure 4.18. Since the in reality the mixture analysed by Novak and coworkers is farther away from the two-phase region of its VLE envelope, the measured total solubility data thus displays a regular Henry behaviour. This artifact in the predictions highlights the importance

of using good molecular models for the fluids studied; it is likely that a more optimized SAFT model for ethylene would result in very linear sorption isotherms for the mixture composition studied.

4.3.5. Solubility predictions at different temperatures

In Figure 4.19 the model's solubility predictions at temperatures different from the ones included in the parameterisation procedure are compared to experimental solubility data of pure substances in a subset of polymer samples. Overall, the calculations are in very good agreement with the data at all temperatures reported. It is particularly noteworthy that the solubility of cyclohexane in a LLDPE sample analysed by Sturm and coworkers[256] (Figure 4.19f) is accurately predicted at various temperatures even if cyclohexane was not included in the parameter estimation procedure (*cf.* Table 4.4).

In general, the quality of the predictions deteriorates close to saturation of the external gas. This could be due to irreversible melting and reorganisation of the smaller lamellae, a phenomenon known to occur during swelling of semi-crystalline PE at high solute activity.[258] Since irreversible transformations result in changes to the crystallinity and microstructure of a polymer sample, these effects – if present – lead to hysteresis of the sorption/desorption cycle which can be used as a measure of the degree of reversibility of the sorption process. However, desorption runs are rarely reported experimentally, preventing the direct investigation of these effects in the current work.

In some of the samples with lower crystallinity (Figure 4.19a, b and c) the model predicts greater variations of solubility with temperature than what experimental data indicates. In the absence of irreversible transformations, these findings might be evidence of partial melting at the lateral lamellar surfaces[274] leading to an increase in ψ with temperature.

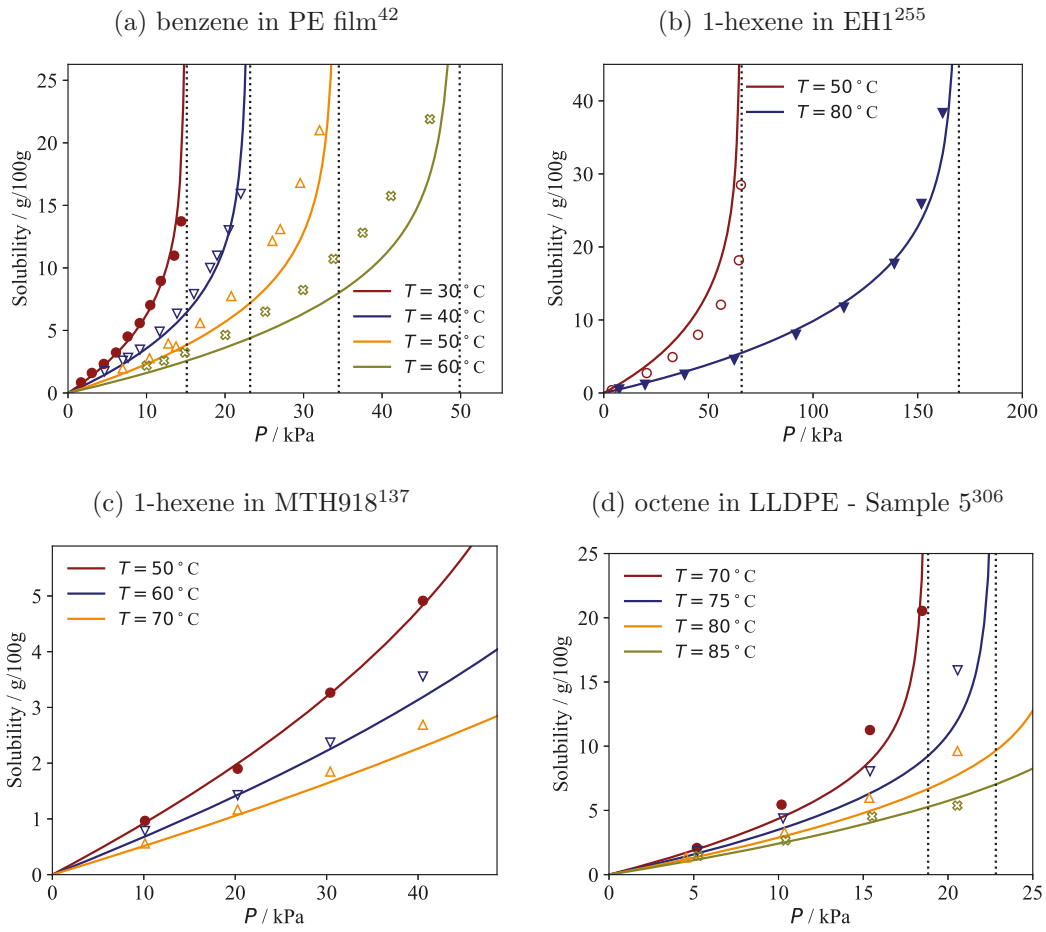

Figure 4.19.: Solubility of various pure substances in semi-crystalline PE samples at different temperatures using the optimal sample parameters found in Table 4.11. Solid curves represent the model's calculations, while symbols experimental data. Data points represented by filled symbols are included in the parameterisation procedure; empty symbols, not included. Vertical dotted lines represent the vapour pressure of the external gas at the each temperature.

(e) 1-butene in HDPE[303]

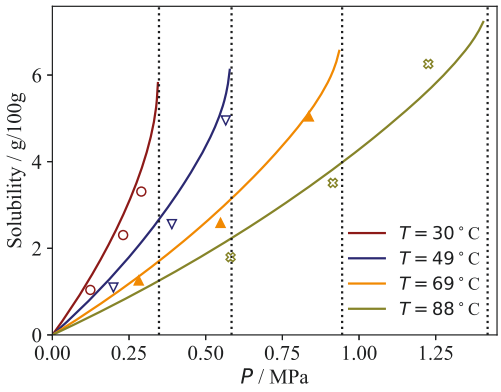

(f) cyclohexane in LLDPE - Sample 1[256]

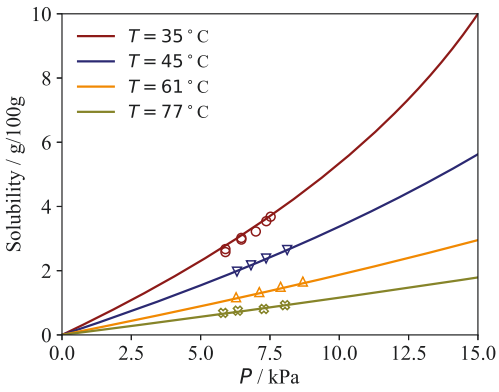

(g) isopentane in HDPE - Sample 2[256]

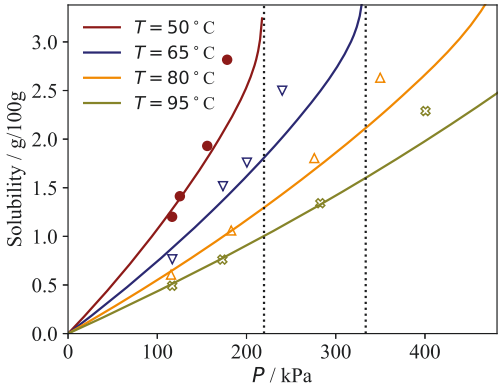

(h) 1-hexene in HDPE - Sample 3[138]

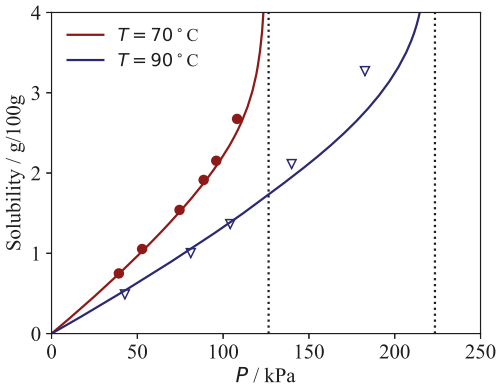

Figure 4.19.: (Continued) Solubility of various pure substances in semi-crystalline PE samples at different temperatures using the optimal sample parameters found in Table 4.11. Solid curves represent the model's calculations, while symbols experimental data. Data points represented by filled symbols are included in the parameterisation procedure; empty symbols, not included. Vertical dotted lines represent the vapour pressure of the external gas at the corresponding temperature.

It might therefore be necessary to develop models to account for the changes of ψ with temperature to characterize semi-crystalline polymers with temperature-independent sample-specific parameters over wide temperature ranges.

4.4. Moisture uptake by semi-crystalline PEG: deliquescence

We conclude this Chapter with an analysis of moisture uptake in PEG to test the ability of our methodology to reproduce equilibrium properties of hydrogen-bonding polymer + solute mixtures. The PEG polymer is semi-crystalline at room temperature, with a melting point between about 30 and 60 °C.[13,156] Semi-crystalline PEG is often used as a polymer matrix for active pharmaceutical ingredients (APIs).[310,311] Water vapour poses significant problems with the stability of such formulations, as semi-crystalline PEG is known to melt at room temperature and high relative humidity, a phenomenon known as *deliquescence*.[13] It is therefore critical to develop models which provide the capability of describing both the sorption of water in semi-crystalline PEG and the humidity at which deliquescence occurs at each temperature.

While standard vapour-liquid equilibrium (VLE) calculations can be performed to determine the sorption of water vapour in molten PEG (see Sections 2.3.5 and 2.5.2) , the presence of crystalline polymeric domains in semi-crystalline PEG warrants a more sophisticated description. The solubility of water in semi-crystalline PEG below the melting point of the fully crystalline sample should be low when a significant proportion of the crystal structure is preserved, and increase steeply once deliquescence occurs.

In this section we apply the model developed in Chapter 3 to the study of moisture

sorption in semi-crystalline PEG. A simple methodology to predict the humidity at which deliquescence should occur is also discussed, followed by a comparison with experimental data.

4.4.1. Solubility in semi-crystalline PEG

According to the methodology developed in Chapter 3, in order to perform solubility calculations in semi-crystalline PEG one requires:

- A set of sample-specific parameters, including the crystallinity ω_c, fraction of tie-molecules p_T, and fraction of free amorphous domains ψ.
- An equation of state (and corresponding parameters) describing the liquid polymer+solute mixture and the gas phase.
- A set of polymer-specific parameters.

The SAFT-γ Mie models for PEG and water are reported in Section 2.5.2. The polymer-specific parameters for PEG, on the other hand, have previously been reported in Table 3.1. The value of the inter-lamellar distance of the pure polymer ($l_a^* = l_a(25°C)$) is set to 10 nm for simplicity (as in the previous Sections) due to its small influence on the predicted moisture uptake. While the crystallinity ω_c of a sample can be measured with one of the methods highlighted in Section 3.1.6, the remaining sample-specific parameters p_T and ψ are found for each sample by minimizing the root-mean-square difference between the experimental solubility data and the model predictions.

Since semi-crystalline PEG generally has a very high crystallinity,[312] we expect the fraction of free amorphous mass to be negligible[139,238] and we can therefore set $\psi = 0$, which leaves the fraction of stems p_T as the only free sample-specifc parameter. The sorption

S of water in semi-crystalline PEG (in terms of the mass of dissolved water per mass of PEG) is therefore approximated here as (*cf.* Equation 3.53)

$$S(T,P) \approx (1-\omega_{\mathrm{c}}) S_{\mathrm{a}}^{\mathrm{IL}}(T,P;p_{\mathrm{T}},l_{\mathrm{a}}^{*}), \tag{4.8}$$

where $S_{\mathrm{a}}^{\mathrm{IL}}$ – the solubility in the inter-lamellar domains – is obtained with the methods described in Section 3.3.3. The fraction of tie-molecules p_{T} is adjusted for each sample to reproduce the water solubility in the low-humidity regime (i.e., before deliquescence occurs). At higher humidity, solubility is calculated via a standard VLE calculation (Section 2.5.2).

It must be pointed out that a great body of evidence suggests that low-molecular weight PEG crystals ($M_n < 10,000$ g/mol) consist of polymer chains either folded a small number of times or in chain-extended conformations.[148–152,310,311,313–317] This implies a very high concentration of chain ends (i.e., tails, *cf.* Section 3.2) in the inter-lamellar regions; these are neglected in the current model. Furthermore, the inter-lamellar regions of semi-crystalline PEG are very small (of the order of 1-2 nm[148]) and the amorphous polymer chains in them are very short (less than 10 repeating units[318]), implying that confinement effects (which are also neglected in our approach) and chain end-to-end distributions at variance with the Langevin statistics must be considered to accurately determine the water solubility in these regions.

Nonetheless, tie-molecules should still be present in high-molecular weight crystals based on theoretical arguments,[201,202,319] and on the experimental observation that the resistance to crack propagation of semi-crystalline PEG increases with increasing molecular weight.[187,320] Our model should therefore be able to provide one with a qualitative description of the thermodynamic properties of the inter-lamellar domains in PEG, although the adjusted values of p_{T} for each sample should not be considered accurate estimates but rather as empirical parameters.

4.4.2. Deliquescence

If we assume that no polymer is present in the external fluid phase, it is particularly useful to treat deliquescence in the osmotic ensemble. At fixed temperature T, pressure P and solute chemical potentials $\boldsymbol{\mu}_{\mathrm{s}}$, the osmotic free energy of a polymer system $\Omega_{\mathrm{s}} = G - \sum_i \mu_{\mathrm{s,i}} n_{\mathrm{s},i}$ (see Equation 2.35 for a definition for a fluid polymer system) must be at its minimum. Therefore, deliquescence of a lamella occurs when its osmotic free energy, $\Omega_{\mathrm{s}}^{\mathrm{c}}$, becomes equal to than that of a liquid polymer + solutes mixture obtained by melting all the polymer chains in the lamella, $\Omega_{\mathrm{s}}^{\mathrm{EoS}}$:

$$\Omega_{\mathrm{s}}^{\mathrm{c}}(T, P, \boldsymbol{\mu}_{\mathrm{s}}, \boldsymbol{\nu}) = \Omega_{\mathrm{s}}^{\mathrm{EoS}}(T, P, \boldsymbol{\mu}_{\mathrm{s}}, \boldsymbol{\nu}). \tag{4.9}$$

Since we assume that the lamellae are impermeable to solutes (i.e., $n_{\mathrm{s,i}}^{\mathrm{c}} \approx 0$), we have $\Omega_{\mathrm{s}}^{\mathrm{c}} \approx G_{\mathrm{lamella}}$ (Equation 3.46). On the other hand, by using the definition of monomer chemical potential (Appendix C) and assuming that the polymer molecules can be uniquely characterised by the number of repeating units n, the osmotic free energy of a liquid polymer + solutes mixture (Equation 2.35) can be rewritten as

$$\begin{aligned} \Omega_{\mathrm{s}}^{\mathrm{EoS}}(T, P, \boldsymbol{\mu}_{\mathrm{s}}, \boldsymbol{\nu}) &= \sum_i \nu_i \mu_{\mathrm{p},i}^{\mathrm{EoS}} \\ &= \sum_{n=0}^{\infty} n\nu(n) \mu_{\mathrm{p,mono}}^{(n),\mathrm{EoS}}. \\ &= n_{\mathrm{tot}} \overline{\mu_{\mathrm{p,mono}}^{\mathrm{EoS}}} \end{aligned} \tag{4.10}$$

Here, $n_{\mathrm{tot}} = \sum n\nu(n)$ is the total number of monomers in the polymer system and $\nu(n)$ the number of chains in the system with n repeating units. The quantity

$$\overline{\mu_{\mathrm{p,mono}}^{\mathrm{EoS}}} = \frac{\sum_{n=0}^{\infty} n\nu(n) \mu_{\mathrm{p,mono}}^{(n),\mathrm{EoS}}}{\sum_{n=0}^{\infty} n\nu(n)} \tag{4.11}$$

is the weight-averaged monomer chemical potential of the liquid polymer + solute mixture*. Due to the limiting properties of $\mu^{\mathrm{EoS}}_{\mathrm{p,mono}}$ at high molecular weight, we assume $\overline{\mu^{\mathrm{EoS}}_{\mathrm{p,mono}}} \approx \mu^{(n_0),\mathrm{EoS}}_{\mathrm{p,mono}}$ with $n_0 = 1000$ as was done throughout the current work.

By substituting the expressions for G_{lamella} and $\Omega^{\mathrm{EoS}}_{\mathrm{s}}$ in and Equation 4.9 and dividing both sides by the total number of monomers, for a lamella of thickness l_{c} we obtain

$$\mu^{\mathrm{l}}_{\mathrm{p,mono}} - \mu^{\mathrm{l,0}}_{\mathrm{p,mono}} + M_0 \left[\Delta h^0_{\mathrm{m}} \left(1 - \frac{T}{T^0_{\mathrm{m}}} \right) + 2 \frac{\sigma_{\mathrm{e}}}{\rho_{\mathrm{c}} l_{\mathrm{c}}} \right] = 0. \tag{4.12}$$

Here, $\mu^{\mathrm{l}}_{\mathrm{p,mono}}$ and $\mu^{\mathrm{l,0}}_{\mathrm{p,mono}}$ are the monomer chemical potential in a liquid polymer + solutes mixture at fixed $T, P, \boldsymbol{\mu}_{\mathrm{s}}$ and in a pure polymer melt at fixed T, P, respectively; both are calculated assuming the polymer monodisperse with $n_0 = 1000$ repeating units. One should note that additional terms should be considered in Equation 4.12 to account for the entropy of the chain ends on the crystal/amorphous interface,[169,171] which lead to an explicit dependence of the melting point on the polymer's molecular weight.

By defining

$$T_{\mathrm{m}} = T^0_{\mathrm{m}} - \frac{2\sigma_{\mathrm{e}} T^0_{\mathrm{m}}}{\rho_{\mathrm{c}} l_{\mathrm{c}} \Delta h^0_{\mathrm{m}}} \tag{4.13}$$

as the melting point of a lamella of thickness l_{c} (Equation 3.6) we can recast Equation 4.12 as

$$\mu^{\mathrm{l}}_{\mathrm{p,mono}} - \mu^{\mathrm{l,0}}_{\mathrm{p,mono}} + M_0 \Delta h^0_{\mathrm{m}} \left(1 - \frac{T}{T_{\mathrm{m}}} \right) = 0. \tag{4.14}$$

In Section 4.4.3, for simplicity we assume that all the crystals have an infinite extension ($T_{\mathrm{m}} = T^0_{\mathrm{m}}$); nevertheless, as shown by Equation 4.14 surface free energy effects can be taken into account approximately by using a realistic melting point $T_{\mathrm{m}}(l_{\mathrm{c}}) < T^0_{\mathrm{m}}$.

*Strictly, it is the weight-averaged monomer chemical potential only for homopolymers. Otherwise it is "monomer-averaged".

By rearranging Equation 4.12, it is apparent that at fixed temperature, pressure and solute chemical potentials a lamella with thickness l_c is stable only if

$$l_c > l_c^*(T, P, \boldsymbol{\mu}_s) = \frac{\rho_c}{2\sigma_e}\left[\Delta h_m^0\left(1 - \frac{T}{T_m^0}\right) + \mu_{p,mono}^{l} - \mu_{p,mono}^{l,0}\right]. \tag{4.15}$$

Therefore, in semi-crystalline samples with broad crystal size distributions we expect a continuous variation of the overall crystallinity due to irreversible melting (and, potentially, subsequent recrystallisation) of the smaller lamellae at varying temperature and solute chemical potentials†. However, since the lamellar thickness of melt-crystallised samples should have a finite lower bound (Section 3.1.2), this phenomenon should occur only at high temperature (relative to the melting point) and solute chemical potentials (i.e., high relative humidity in the case of water).

One should note that in the derivation of Equation 4.12 it is assumed that the lamellae can be decoupled from the surrounding amorphous domains. In reality, we expect that the stability of the lamellae should be lowered by the presence of constrained amorphous chains linked to the crystal. Furthermore, in crystal-mobile polymers such as PEG[192,219,321,322] reversible changes in lamellar thickness occur due to intra-crystalline chain dynamics, as predicted by our model (Section 3.2.4). A unified description of the lamellae and the inter-lamellar domains might therefore be necessary to capture the the interplay between such reversible and irreversible processes close to the polymer's melting point or at high relative humidity.

4.4.3. Comparison with experimental sorption isotherms

In Figure 4.20 experimental data for the water solubility in semi-crystalline PEG samples reported by Thijs *et al.*[295] and by Baird *et al.*[13] are compared to our calculations.

†The effect of pressure is once again neglected due to the high density of the systems under consideration

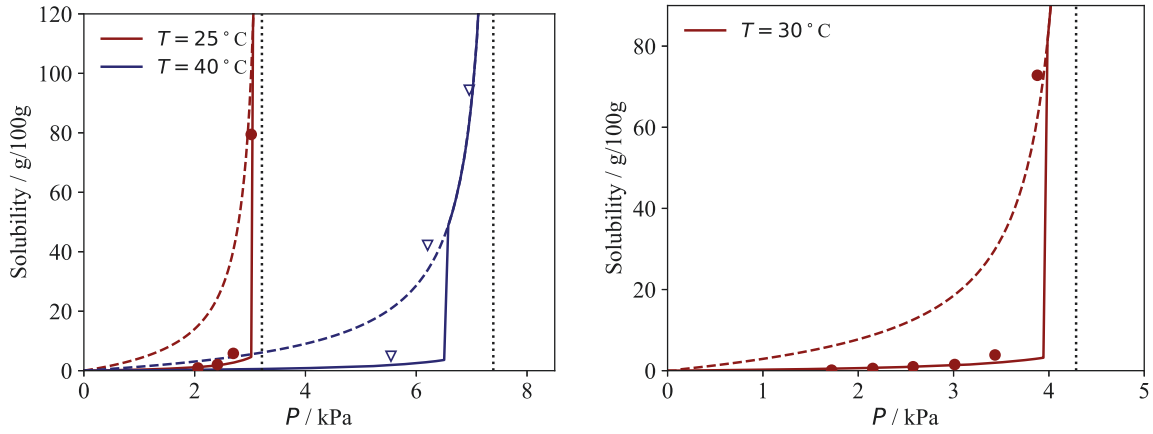

(a) (b)

Figure 4.20.: Solubility of water in semi-crystalline PEG (symbols) and the corresponding SAFT-γ Mie theoretical calculations (continuous curves) using the model outlined in Section 4.4.1. The melting of the sample is predicted to occur sharply at a limiting water pressure (P_{del}) as crystals are assumed to be infinite in extension (*cf.* Equation 4.12 with $T_{\text{m}} = T_{\text{m}}^{0}$). The vertical dotted line corresponds to the vapour pressure of water at the respective temperatures. The dashed curve, on the other hand, is the predicted water solubility in molten PEG. Comparison of the predictions for: (a) $M_n = 3350$ g/mol with the data of Baird *et al.*[13] ; and (b) $M_n = 2800$ g/mol at 30 °C with the data of Thijs *et al.*[295]

Unfortunately, the crystallinity of the samples was not reported in either study and few data points are available. For all the calculations the crystallinity ω_c of the samples at 25 °C is therefore assumed to be 90%, a typical value for low molecular weight semi-crystalline PEG,[312,318] in order to reduce the number of adjustable parameters. As a consequence and due to the inherent limitations in applying our model for semi-crystalline polymers to PEG (see Section 4.4.1), the value for the fraction of stems p_T for each sample – adjusted to reproduce solubility in the semi-crystalline, low-humidity region – should not be intended accurate estimates of the proportion of tie-molecules. All of the sample-specific parameters used for the calculations are reported in Table 4.5.

Table 4.5.: Model parameters for the semi-crystalline PEG samples considered. The crystallinity $\omega_c(25\ °C)$ is an estimate based on the typical crystallinity of low molecular weight PEG.[312,318] Similarly, ψ is set to zero due to the high crystallinity of the samples – see Figure 4.5 for PE. The reported values of p_T are adjusted to minimize the root-mean-square difference between the predicted solubility at low humidity – when the polymer is expected to be semi-crystalline – and the corresponding experimental data (*cf.* Figure 4.20)

Ref	Sample	$\omega_c(25\ °C)$	p_T	ψ	$l_a(25\ °C)$
Thijs *et al.*[295]	PEG-2800	0.9	0.51	0.00	10 nm
Baird *et al.*[13]	PEG-3350	0.9	0.38	0.00	10 nm

.

The solubility is estimated using equation 4.8 until deliquescence is found to occur – marked by a discontinuous increase in solubility – and then with VLE calculations at higher humidities. The phase transition occurs sharply at a pressure P_{del} – corresponding to a relative humidity of P_{del}/P_{vap}, with P_{vap} being the vapour pressure of water at that temperature – which is determined by solving equation 4.12. The discontinuity in the phase transition is due to our simplified model in which we assume that the polymer crystals are perfect and infinite in extension ($T_m = T_m^0$). As pointed out in

Section 4.4.1, the inclusion of surface free energy effects and realistic lamellar thickness distributions would lead to a broadening of the melting region and its shifting to lower humidity, in line with what the experimental data of Baird and coworkers suggests (Figure 4.20a).

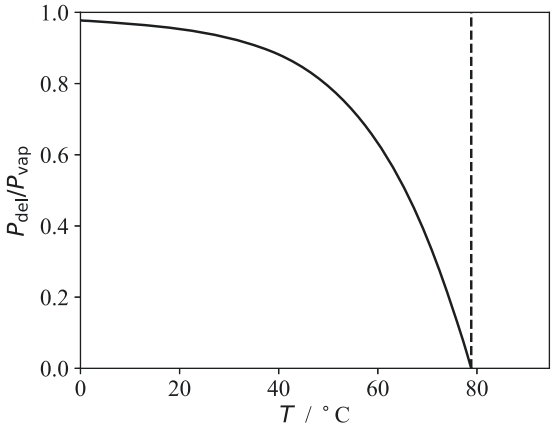

Figure 4.21.: Relative humidity $P_{\mathrm{del}}/P_{\mathrm{vap}}$ at deliquescence for semi-crystalline PEG as a function of temperature. The solid curve represents calculations with Equation 4.12 using the SAFT-γ Mie parameter set (Table 2.1, 2.2, 2.3), together with the enthalpy and temperature of melting (indicated as the vertical dashed line on the figure) for a perfect PEG crystal of infinite extension (Table 3.1). The inclusion of surface free energy effects is expected to shift the curve to lower temperatures (Equation 4.14). Calculations are made for polymer chains with $n_0 = 1000$ oxyethylene units; nevertheless, the molecular weight is not expected to have a significant impact on the deliquescence humidity except for short polymer chains.[13,295]

In Figure 4.21, we show the predicted temperature dependence of the deliquescence humidity for PEG assuming $T_{\mathrm{m}} = T_{\mathrm{m}}^0$. As expected,[13,295] the deliquescence occurs at progressively lower relative humidity with increasing temperature due to the reduction of the factor $M_0 \Delta h_{\mathrm{m}}^0 \left(1 - T/T_{\mathrm{m}}\right)$ in Equation 4.12. Calculations are only performed for $n_0 = 1000$ repeating units (corresponding to a mean molecular weight of approximately $44,000$ g/mol) due to the weak dependence of our predictions on the molecular weight. This is also seen experimentally, as Baird and coworkers[13] did not measure significant differences in the relative humidity at deliquescence of PEG samples with mean molecular weight higher than about 3000 g/mol (i.e., ~ 70 oxyethylene

units).

Concluding remarks

In this Chapter we have applied the formalism developed in Chapter 3 to the description of a range of thermodynamic properties of crystal-mobile semi-crystalline polymers. In Section 4.1 we have demonstrated that including the finite extensibility of polymer segment in the inter-lamellar domains via Langevin statistics is necessary to avoid unphysical results at low temperatures and correctly capture the increase of P_c upon decreasing temperature. We have also shown that our model can reproduce both the increase of lamellar thickness as well as the variation of crystallinity of high-crystallinity samples at low temperatures, irrespective of the value of p_T. Despite lower values of p_T appear to fit experimental data more accurately at high temperatures, irreversible transformations in the samples are likely to occur in this regime preventing direct comparison between the model and the data.

In Section 4.2 we have proven that it is necessary to assign a $\psi > 0$ to all the samples in order to reproduce solubility near saturation of the external fluid, as swelling of the inter-lamellar domains is severely restricted (Sections 4.2.2 and 4.2.5). After adjusting both p_T and ψ for each sample to reproduce pure-component sorption isotherms at 25 °C, our model can accurately reproduce the experimental data of all four compounds studied (*n*-hexane, *n*-heptane, cyclohexane and toluene) at the same time.

In Section 4.3, we have characterised 50 different PE samples using pure-component sorption isotherms reported in the literature. Here, ψ was estimated as a function of the measured crystallinity using an empirical correlation, leaving p_T as the only adjustable parameter. The resulting 1-parameter model is capable of reproducing the sorption isotherms of up to 5 compounds in the same PE sample (Figure 4.14). The average

value of p_{T} across all samples is approximately 0.3, in accordance with our findings of Section 4.2 and theoretical bounds.

The model's predictions of solubility at temperatures non included in the parameterisation procedure are in overall good agreement with experimental data. Deviations between the model's predictions and experimental data are observed mostly in low-crystallinity samples and at high pressures, possibly due to irreversible transformations in the sample or variations in ψ. The model also provides semi-quantitative predictions of co-solubility effects in PE samples, demonstrating that adding ICAs to pure ethylene enhances its solubility at fixed partial pressure.

Lastly, in Section 4.4 the model has been applied to the study of moisture uptake in PEG. We have shown with a simple model that the humidity at which semi-crystalline PEG undergoes deliquescence can be qualitatively predicted using only the Δh^0_{m} and T^0_{m} parameters,which are readily available in the literature. Finite size effect can be implemented in a straightforward fashion by tuning the melting point T_{m} in Equation 4.12, possibly leading to quantitative agreement with experimental data. The moisture uptake is quantitatively predicted with SAFT-γ Mie at humidity higher than P_{del} and qualitative reproduced at lower humidity by adjusting p_{T}.

5. Conclusions

5.1. Model development

We have presented a new thermodynamic model of semi-crystalline polymers. Each polymer sample is assumed to be composed of three distinct domains, in line with recent experimental observations:[238] crystalline lamellae; inter-lamellar amorphous domains; and free amorphous domains. In our model, the free amorphous domains are treated as a subcooled polymer melt and their mass fraction relative the total polymer mass is denoted by ψ. The lamellar stacks are treated as a sequence of alternating layers of crystalline lamellae and inter-lamellar amorphous material with a well-defined boundary with the lamellae.

A new statistical-thermodynamic model of the inter-lamellar amorphous domains has been developed Chapter 3. The presence of tie-molecules causes these domains to be (formally) subject to an additional constraint pressure P_c which makes the solubility of any given solute lower in the inter-lamellar amorphous domains compared to the free amorphous domains, and explains the experimental observation that the amorphous solubility in semi-crystalline polymer samples is lower than the one determined by assuming that all the amorphous domains are subcooled polymer melts.[37–39,44,45]

The local-equilibrium hypothesis has been implemented to explain the observed increase of P_c at low temperatures[39,45,251] and the reversible variation of the inter-lamellar dis-

tance with temperature[155,218,244] observed in crystal-mobile polymers such as PE, isotactic PP and PEO.[156,192,217] This allows one to determine the average number of monomers per tie-molecule or equivalently its fractional extension as a function of temperature, pressure, and composition of the inter-lamellar amorphous domains.

Furthermore, the Langevin approximation for the end-to-end probability distributions of the polymer chains in the inter-lamellar domains has been employed in order to account for their finite extensibility. Previous studies aimed at predicting sorption[38–41] and reversible melting[198–200] in semi-crystalline polymers almost invariably employed the Gaussian approximation, which is incompatible with the local-equilibrium hypothesis at low temperatures. Only the earliest studies of reversible melting[195,196,198] provided calculations with the Langevin approximation, although constraint pressure was neglected.

Calculations with our model also require the use of an equation of state for polymer mixtures. In this thesis the SAFT-γ Mie EoS (Chapter 2) has been chosen due to its accurate representation of both small molecule fluids and polymer mixtures, as well as for its flexible group-contribution methodology. Nevertheless, the generality of the formalism developed in Chapter 3 allows straightforward implementation of different equations of state such as the Sanchez-Lacombe EoS[49] or the PC-SAFT EoS.[64,65]

In addition to any parameter related to the selected EoS (e.g., SAFT-γ Mie here) and polymer-specific parameters (common across all polymers of any given type), each semi-crystalline polymer sample is uniquely characterised in the model by specifying four additional sample-specific parameters which embody its pseudo-equilibrium state: the crystallinity ω_{c}^{*} and inter-lamellar distance l_{a}^{*} of the pure polymer at a given temperature and pressure; the mass fraction of free amorphous domains ψ; and the fraction of stems connected to tie-molecules on the crystal/amorphous interface, p_{T}. Crystallinity can be determined experimentally with one of the techniques outlined in Section 3.1.6, and

the average inter-lamellar distance can be measured via small-angle X-ray or neutron scattering experiments[155,193,244,258] – although its value does not influence solubility calculations significantly.

As discussed in Section 3.2, there is no direct experimental evidence for p_T and other topological features of the inter-lamellar domains due to the challenge posed by resolving individual polymer strands. p_T has therefore been left as an adjustable parameter and has been optimised to reproduce experimental data. Various strategies for the estimation of ψ have been attempted in this work: while it has been adjusted in Section 4.2 to reproduce sorption isotherms, in Section 4.3 it has been estimated based on a correlation of experimental data to avoid parameter degeneracy. The model is able to accurately reproduce sorption isotherms using both parameterisation strategies.

5.2. Pure polymer properties

In Section 4.1 the model's predictions have been compared to experimental data of pure semi-crystalline PE. In Section 4.1.1 it has been shown necessary to account for the finite extensibility of the chain segments (via the Langevin approximation) in order to explain the increase in P_c at low temperatures; the Gaussian approximation has been found to yield unphysical values for the fractional extension x_T of the equivalent bridges. Our findings suggest that tie-molecules should be very taut at low temperatures in crystal-mobile polymers, as many authors have argued.[7,39,195,196,200,205,216,238,323]

We have been able to semi-quantitatively predict the variations of the inter-lamellar distance and crystallinity of PE samples with high crystallinity at temperatures sufficiently lower then the melting point T_m^0 (Figures 4.2 and 4.3), regardless of the value of p_T. Deviations between the predictions and experimental data are seen at high temperature, where irreversible transformations in the sample are expected to occur.[155,244] Inclusion

of the temperature dependence of ψ might be necessary to describe the variation of the crystallinity of the lower-crystallinity samples.

5.3. Estimation of sample-specific parameters using sorption data

In Section 4.2, the experimental sorption isotherms of pure *n*-hexane, *n*-heptane, cyclohexane and toluene in six different PE samples and PP samples have been reproduced by adjusting p_{T} and ψ simultaneously for each sample. We have found that the experimental curves always lie somewhere between the $\psi = 0$ and $\psi = 1 - \omega_{\mathrm{c}}$ theoretical curves when the low-pressure behaviour is captured (Figure 4.4). As expected,[238] the optimal value of ψ decreases with increasing crystallinity for all samples tested. The optimal value for p_{T} is around 0.32 for all the PE samples and around 0.54 for the semi-crystalline PP samples.

The model has also been benchmarked against a large set of experimental sorption data of hydrocarbons in semi-crystalline PE samples analysed in the literature. In this case, the fraction of free amorphous mass in each sample was instead estimated from the measured crystallinity using an empirical correlation[238] (Equation 4.5), whereas p_{T} was adjusted to reproduce the sorption of one or more pure substances in the sample at a fixed temperature. The average value of p_{T} across all samples (0.297 or about 30%, including the ones studied in Section 4.2) has been found to conform to theoretical bounds suggested by various authors,[164–167,201,202,206] and suggests that most polymer chains in the inter-lamellar domains of PE should be tie-molecules (bridges or entangled loops) – as it is assumed in our model.

The scatter seen in the optimal p_{T} values (Figure 4.11) suggests that factors other than

crystallinity (such as the polymer's molecular weight, co-monomer content and crystallisation conditions[7,184,190,191]) play a role in determining the chain topology in the inter-lamellar domains. A systematic investigation of these effects is therefore recommended. We note that the values of p_T obtained for semi-crystalline PP samples might be too high to be physically reasonable. As discussed in Section 4.2, we believe that this overestimation might be due to having neglected un-entangled loops and tails in the current model.

Overall, we have demonstrated that the a single pair of p_T, ψ can provide an accurate representation of sorption isotherms of multiple compounds in the same PE sample (see, e.g., Figures 4.5, 4.13 and 4.14), proving that we can effectively decouple the sample-specific features of each semi-crystalline polymer sample (due to molecular weight distribution, cooling history *etc.*) from the inter-molecular interactions between the polymer and each solute – which are here described accurately by the SAFT-γ Mie EoS.

5.4. Model predictions

5.4.1. Co-solubility

In Section 4.3.4 co-solubility effects in semi-crystalline PE samples have been predicted using the model developed using sample-specific parameters optimised to reproduce pure-component sorption isotherms. We have highlighted qualitative differences in the sorption behaviour between fluid mixtures of similar components (isobutane + isopentane) and of ethylene with heavier components (isopentane, *n*-hexane and 1-hexene). For isobutane + isopentane mixtures, the solubility of either component at constant partial pressure is enhanced when mixed compared to the pure case. This phenomenon

is due to the near-ideality of the mixture combined with the proximity of the vapour pressures of the two components.

Conversely, in mixtures of ethylene + isopentane , ethylene + n-hexane and ethylene + 1-hexene the presence of the heavier component increases the solubility of ethylene at fixed partial pressure. This phenomenon plays an important role in PE production[17,138,304,324] as the enhanced solubility of ethylene in the growing polymer increases reaction rates and yield. Our calculations have shown that even moderate amounts of n-hexane (10% mol) mixed with ethylene might lead to a twofold increase in solubility of ethylene at partial pressures of around 15 bar (total pressure $\approx$ 16.7 bar), which is just slightly above the typical range of operating pressures of fluidized bed reactors used in PE polymerisation.[17,325] We thus encourage experimental investigation at higher pressure, as the experimental data reported did not show significant variations from the Henry dilute regime.

5.4.2. Temperature

The assumption that p_{T} and ψ are temperature-independent parameters has been tested by comparing the model's predictions with experimental sorption isotherms at temperatures different from the ones at which the optimal parameters were found. Overall, the model has been found to be in very good agreement with experimental data (Figures 4.6 and 4.19). Discrepancies between data and calculations are most evident at pressures close to saturation of the external fluid, possibly due to irreversible transformations in the samples or inadequacies of the equation of state. Alternatively, it might be necessary to consider reversible changes in ψ with temperature or during sorption which could occur in the presence of mass exchange at the lateral lamellar surfaces.[274]

5.5. Moisture uptake in PEG and deliquescence

The model has also been extended to predict moisture uptake in semi-crystalline PEG. At temperatures close to the melting point, this polymer melts above a specific relative humidity – a phenomenon known as deliquescence. We have presented a simple model that predicts the water pressure P_{del} at which deliquescence should occur based on the melting point of the semi-crystalline sample (Equation 4.12). Water solubility is calculated with the model developed in Section 3.3 for $P < P_{\text{del}}$ by adjusting the fraction of tie molecules p_{T} for each sample (*cf.* Table 4.5) to reproduce the solubility at low humidity. At higher humidity, solubility can be fully predicted using SAFT-γ Mie.

The resulting model provides a semi-quantitative prediction of the water solubility in semi-crystalline PEG at all humidities except close to deliquescence (*cf.* Figure 4.20) due to the broadening of the experimental melting range, which is likely caused by the size distribution of the polymer crystals. The prediction of the temperature dependence of the humidity at deliquescence (Figure 4.21) are found to be in line with experimental observations,[13,295] suggesting that care must be taken when exposing formulations including semi-crystalline PEG at high humidity and temperatures.

One should note that the model was compared only to a handful of moisture uptake measurements, resulting in a high uncertainty on the reported optimal values of p_{T}. Furthermore, due to the low melting point of PEG irreversible transformations in the sample might occur during water sorption. Lastly, we note that for low-molecular weight PEG samples it may be necessary to account for the effects of confinement and chain ends on the free energy of the amorphous domains (*cf.* Sections 4.4.1 and 4.4.3). The reported values of p_{T} should therefore be considered only qualitative estimates.

5.6. Sorption of liquids

Although in this thesis we have only compared the model's predictions to sorption isotherms of gases and super-critical fluids, the same framework can be applied to studying the sorption isotherms of liquids (i.e. $P/P_{\text{vap}} > 1$) in semi-crystalline polymers. Some examples of our model's predictions are shown in Appendix H. It is important to note that at equilibrium the sorption of liquids can be much higher than that of gases, as seen by the rapid increase of solubility near saturation in Sections 4.2, 4.3 and 4.4. As high solute activity in the inter-lamellar amorphous domains might cause irreversible changes to the lamellar structure[258] or even dissolve the sample entirely[13] (Section 4.4.3), the model might not always be applicable in this regime.

5.7. Future work

In the current development the effects of the confinement of the amorphous material between the lamellae are neglected. Similarly, end-to-end probability distributions for the bulk polymer melt are used to approximate the probability of finding the ends of given polymer chain segment on the surfaces of two lamellae. Both of these approximations can be relaxed in order to make the theory more rigorous. For example, classical density functional theory[281,283,284,326–328] or self-consistent polymer field theory[216,262,263,329] can be used to obtain better approximations of the free energy of a polymer + solute mixture confined between the lamellae (i.e., A' in equation 3.67).

The model should be applied in temperatures ranges over which the amorphous domains of the polymer are rubbery; if the amorphous domains are glassy, the system might be trapped in a local minimum of the free energy.[30,31,33] Examples of semi-crystalline polymers with glass transition temperatures above room temperature are, e.g., PEEK[15,330]

and polyamides such as Kevlar®.[331] Out-of-equilibrium theories such as the NET-GP theory[277] might be more suitable to describe such systems. Preliminary work in collaboration with Dr. Chris Tighe (Imperial College London, Department of Chemical Engineering) shows that the implementation of the SAFT-γ Mie EoS with NET-GP can provide an accurate description of solubility in glassy polymers such as polystyrene (PS) and PEEK.

Owing to the challenge posed by investigating experimentally the properties of the inter-lamellar amorphous domains, computer simulation is necessary to test the validity of the model's assumptions. We identify a number of unresolved challenges presented by simulating such systems. Firstly, as discussed in Section 3.2, we lack detailed understanding of the mechanisms that determine the chain topology in the inter-lamellar domains after crystallisation. Therefore, in order to generate chain configurations in the simulated system it is necessary to make *a priori* assumptions on the properties of bridges, loops *etc.* which are not guaranteed to accurately represent the topology of the inter-lamellar domains.

Secondly, to our knowledge the local-equilibrium hypothesis has never been implemented in computer simulation to date. Though it is certainly possible to introduce mass exchange at the crystal/amorphous interface with a Monte Carlo scheme, the chain segments might become very taut at low temperatures (as seen in Section 4.1), preventing an effective exploration of the free energy surface. Topology-altering Monte Carlo moves such as the ones used in the studies of Rutledge and coworkers[182,208–215] might help equilibrate the system, albeit at the cost of losing the ability to directly control the chain topology.

As shown in Section 4.2.5, our model predicts the variation of microstructural properties of semi-crystalline polymers such as the inter-lamellar distance during the sorption process, allowing direct comparison with in-situ nano-swelling measurements.[193,258,294]

More experiments of this kind are needed to further test the prediction of our model for the inter-lamellar domains. It would be particularly insightful to measure both the swelling of the inter-lamellar domains and the reversible melting of lamellae at various temperatures in the same polymer sample to test the ability of the model to provide an accurate description of both properties with a single value of p_{T}. Furthermore, due to the central role of the free amorphous domains in determining the sorption behaviour in low-crystallinity samples, a systematic experimental study investigating the changes of ψ with temperature or during swelling using low-field ^{1}H NMR[238] is warranted.

5.8. Publications and conference contributions

Publications

Published contributions

- Valsecchi M., Ramadani J., Williams D., Galindo A., Jackson G. " Influence of tie-molecules and microstructure on the fluid solubility in semi-crystalline polymers". *The Journal of Physical Chemistry: Part B*, **2022**, 126, 44, 9059–9088

Submitted contributions

- Chiapasco M., Valsecchi M., Hill G., Wallis C., Porter A. E. "Spatially resolved effects of photo-oxidation of polypropylene on its microstructure". *Global Challenges*. Submitted, (2023)

Planned contributions

- Valsecchi M., Galindo A., Jackson J. "Prediction of co-solubility effects in semi-crystalline polyethylene: the role of the fluid composition and sample microstructure". *Macromolecules*. In preparation (2023)
- Valsecchi M., Galindo A., Jackson J. "Modelling the thermodynamic properties of the mixture of water and polyethylene glycol (PEG) with the SAFT-γ Mie group-contribution approach". *Fluid Phase Equilibria*. In preparation (2023)

Conference contributions

- Oral Contribution: Valsecchi M., Galindo A., Jackson J., Ramadani J., Williams D.,"The influence of tie-molecules and microstructure on the fluid solubility in semi-crystalline polymers", 2022 AIChE Annual Meeting, November 2022, Phoenix, AZ, USA.
- Oral & Poster Contribution: Valsecchi M., Galindo A., Jackson J., Ramadani J., Williams D.,"The influence of tie-molecules and microstructure on the fluid solubility sin semi-crystalline polymers", The 27$^{\text{th}}$ Thermodynamics Conference, September 2022, Bath, UK.
- Oral Contribution: Valsecchi M., Galindo A., Jackson J., Ramadani J., Williams D.,"The influence of tie-molecules and microstructure on the fluid solubility in semi-crystalline polymers", 32$^{\text{nd}}$ European Symposium on Applied Thermodynamics, July 2022, Graz, Austria.
- Poster Contribution: Valsecchi M., Galindo A., Jackson J. "Modelling the thermodynamic properties of aqueous mixtures of poly(ethylene glycol) through the

SAFT-γ Mie equation of state", 31st European Symposium on Applied Thermodynamics, July 2021, Paris (online), France.

Bibliography

[1] i. Encyclopaedia Britannica, *The New Encyclopædia Britannica: Macropædia : Knowledge in depth*. The New Encyclopædia Britannica, Encyclopaedia Britannica, 2002.

[2] E. Kvavadze, O. Bar-Yosef, A. Belfer-Cohen, E. Boaretto, N. Jakeli, Z. Matskevich, and T. Meshveliani, "30,000-year-old wild flax fibers," *Science*, vol. 325, no. 5946, pp. 1359–1359, 2009.

[3] C. Becker, N. Benecke, A. Grabundžija, H.-C. Küchelmann, S. Pollock, W. Schier, C. Schoch, I. Schrakamp, B. Schütt, and M. Schumacher, "The textile revolution. research into the origin and spread of wool production between the near east and central europe," *Space and Knowledge. Topoi Research Group Articles, eTopoi. Journal for Ancient Studies, Special Volume 6*, 2016.

[4] T. Townsend, "1B - World natural fibre production and employment," in *Handbook of Natural Fibres (Second Edition)* (R. M. Kozłowski and M. Mackiewicz-Talarczyk, eds.), Woodhead Publishing Series in Textiles, pp. 15–36, Woodhead Publishing, 2020.

[5] "Statistics for the global wool production and textile industry." `https://iwto.org/resources/statistics/`, 2021. International Wool Textile Organisation.

[6] "Plastics – the facts 2022." `https://plasticseurope.org/knowledge-hub/plastics-the-facts-2022/`, 2022. Plastics Europe.

[7] R. Seguela, "Critical review of the molecular topology of semicrystalline polymers: The origin and assessment of intercrystalline tie molecules and chain entanglements," *Journal of Polymer Science, Part B: Polymer Physics*, vol. 43, pp. 1729–1748, 2005.

[8] R. Geyer, J. R. Jambeck, and K. L. Law, "Production, use, and fate of all plastics ever made," *Science Advances*, vol. 3, no. 7, 2017.

[9] H. Jemii, A. Bahri, A. Boubakri, D. Hammiche, K. Elleuch, and N. Guermazi, "On the mechanical behaviour of industrial PVC pipes under pressure loading: experimental and numerical studies," *Journal of Polymer Research*, vol. 27, pp. 1–13, 2020.

[10] Y. Gong, S.-H. Wang, Z.-Y. Zhang, X.-L. Yang, Z.-G. Yang, and H.-G. Yang, "Degradation of sunlight exposure on the high-density polyethylene (HDPE) pipes for transportation of natural gases," *Polymer Degradation and Stability*, vol. 194, p. 109752, 2021.

[11] H. U. Khalid, M. C. Ismail, and N. Nosbi, "Permeation damage of polymer liner in oil and gas pipelines: A review," *Polymers*, vol. 12, no. 10, 2020.

[12] W. Balasooriya, C. Clute, B. Schrittesser, and G. Pinter, "A review on applicability, limitations, and improvements of polymeric materials in high-pressure hydrogen gas atmospheres," *Polymer Reviews*, vol. 62, no. 1, pp. 175–209, 2022.

[13] J. A. Baird, R. Olayo-Valles, C. Rinaldi, and L. S. Taylor, "Effect of molecular weight, temperature, and additives on the moisture sorption properties of polyethylene glycol," *Journal of pharmaceutical sciences*, vol. 99, pp. 154–168, 2010.

[14] b. Kulinski and E. Piorkowska, "Crystallization, structure and properties of plasticized poly (L-lactide)," *Polymer*, vol. 46, no. 23, pp. 10290–10300, 2005.

[15] T. Iqbal, B. Briscoe, and P. Luckham, "Surface plasticization of poly (ether ether ketone)," *European polymer journal*, vol. 47, no. 12, pp. 2244–2258, 2011.

[16] S. Yasin, A. Shakeel, M. Ahmad, A. Ahmad, and T. Iqbal, "Physico-chemical analysis of semi-crystalline PEEK in aliphatic and aromatic solvents," *Soft Materials*, vol. 17, no. 2, pp. 143–149, 2019.

[17] A. Alizadeh, J. Chmelar, F. Sharif, M. Ebrahimi, J. Kosek, and T. F. L. Mckenna, "Modeling condensed mode operation for ethylene polymerization : Part I . Thermodynamics of sorption," *Industrial and Engineering Chemistry Research*, vol. 56, pp. 1168–1185, 2017.

[18] R. F. Alves, T. Casalini, G. Storti, and T. F. McKenna, "Gas-phase polyethylene reactors—a critical review of modeling approaches," *Macromolecular Reaction Engineering*, vol. 15, pp. 1–30, 2021.

[19] Z. Shen, J. Yang, H. Lu, F. Zou, and L. Du, "Study on the effects of knitted fabric parameters on fragrance retention performance," *Fibers and Polymers*, vol. 22, no. 11, pp. 3222–3231, 2021.

[20] S. Cimilli Duru and U. K. Şahin, "Effects of yarn type, process history, softener type and concentration on wicking and drying properties of cotton plain knitted fabrics," *The Journal of The Textile Institute*, vol. 111, no. 8, pp. 1166–1175, 2020.

[21] S. Zha, H.-q. Lan, N. Lin, and T. Meng, "Degradation and characterization methods for polyethylene gas pipes after natural and accelerated aging," *Polymer Degradation and Stability*, vol. 208, p. 110247, 2023.

[22] Z. Lin, T. Jin, T. Zou, L. Xu, B. Xi, D. Xu, J. He, L. Xiong, C. Tang, J. Peng, *et al.*, "Current progress on plastic/microplastic degradation: Fact influences and mechanism," *Environmental Pollution*, p. 119159, 2022.

[23] A. Chamas, H. Moon, J. Zheng, Y. Qiu, T. Tabassum, J. H. Jang, M. Abu-Omar, S. L. Scott, and S. Suh, "Degradation rates of plastics in the environment," *ACS Sustainable Chemistry & Engineering*, vol. 8, no. 9, pp. 3494–3511, 2020.

[24] S. S. Ali, T. Elsamahy, E. Koutra, M. Kornaros, M. El-Sheekh, E. A. Abdelkarim, D. Zhu, and J. Sun, "Degradation of conventional plastic wastes in the environment: A review on current status of knowledge and future perspectives of disposal," *Science of The Total Environment*, vol. 771, p. 144719, 2021.

[25] J. G. Wijmans and R. W. Baker, "The solution-diffusion model: a review," *Journal of Membrane Science*, vol. 107, no. 1, pp. 1–21, 1995.

[26] A. S. Michaels and R. B. Parker, "Sorption and flow of gases in polyethylene," *Journal of Polymer Science*, vol. 41, pp. 53–71, 1959.

[27] M. Hedenqvist and U. Gedde, "Diffusion of small-molecule penetrants in semicrystalline polymers," *Progress in Polymer Science*, vol. 21, no. 2, pp. 299–333, 1996.

[28] J. D. Hoffman and J. I. Lauritzen, "Crystallization of bulk polymers with chain folding: theory of growth of lamellar spherulites," *Journal of Research of the National Bureau of Standards Section A: Physics and Chemistry*, vol. 65A, p. 297, 1961.

[29] R. Alamo and L. Mandelkern, "Origins of endothermic peaks in differential scanning calorimetry," *Journal of Polymer Science Part B: Polymer Physics*, vol. 24, pp. 2087–2105, 1986.

[30] J. H. Gibbs and E. A. DiMarzio, "Nature of the glass transition and the glassy state," *Zeitschrift für Physik B Condensed Matter*, vol. 28, pp. 373–383, 1957.

[31] G. Adam and J. H. Gibbs, "On the temperature dependence of cooperative relaxation properties in glass-forming liquids," *The Journal of Chemical Physics*, vol. 43, pp. 139–146, 1965.

[32] P. G. Debenedetti and F. H. Stillinger, "Supercooled liquids and the glass transition," *Nature*, vol. 410, pp. 259–267, 2001.

[33] J. Dudowicz, K. F. Freed, and J. F. Douglas, "Generalized entropy theory of polymer glass formation," in *Advances in Chemical Physics* (S. A. Rice, ed.), vol. 137, pp. 125–222, John Wiley & Sons, Inc., 2008.

[34] R. Rangappa and S.-K. Yeh, "Effect of N_2 plasticization on the crystallization of different hardnesses of thermoplastic polyurethanes," *The Journal of Supercritical Fluids*, vol. 189, p. 105726, 2022.

[35] R. K. Arya, D. Thapliyal, J. Sharma, and G. D. Verros, "Glassy polymers—diffusion, sorption, ageing and applications," *Coatings*, vol. 11, no. 9, p. 1049, 2021.

[36] G. C. Sarti and F. Doghieri, "Predictions of the solubility of gases in glassy polymers based on the nelf model," *Chemical Engineering Science*, vol. 53, pp. 3435–3447, 1998.

[37] R. B. Richards, "The phase equilibria between a crystalline polymer and solvents," *Transactions of the Faraday Society*, vol. 42, pp. 10–28, 1946.

[38] C. E. Rogers, V. Stannett, and M. Szwarc, "The sorption of organic vapors by polyethylene," *Journal of Physical Chemistry*, vol. 63, pp. 1406–1413, 1959.

[39] A. S. Michaels and R. W. Hausslein, "Elastic factors controlling sorption and transport properties of polyethylene," *Journal of Polymer Science Part C: Polymer Symposia*, vol. 10, pp. 61–86, 1965.

[40] H. Brown, "Flory–Huggins–Rehner theory and the swelling of semicrystalline polymers by organic fluids," *Journal of Polymer Science*, vol. 16, pp. 1887–1889, 1978.

[41] C. P. Liu and P. Neogi, "Sorption of benzene and n-hexane in polyethylene," *Journal of Membrane Science*, vol. 35, pp. 207–215, 1988.

[42] S. J. Doong and W. S. Ho, "Sorption of organic vapors in polyethylene," *Industrial and Engineering Chemistry Research*, vol. 30, pp. 1351–1361, 1991.

[43] B. J. Banaszak, D. Lo, T. Widya, W. H. Ray, J. J. D. Pablo, A. Novak, and J. Kosek, "Ethylene and 1-hexene sorption in LLDPE under typical gas phase reactor conditions: A priori simulation and modeling for prediction of experimental observations," *Macromolecules*, vol. 37, pp. 9139–9150, 2004.

[44] P. Memari, V. Lachet, and B. Rousseau, "Molecular simulations of the solubility of gases in polyethylene below its melting temperature," *Polymer*, vol. 51, pp. 4978–4984, 2010.

[45] M. Minelli and M. G. D. Angelis, "An equation of state (EoS) based model for the fluid solubility in semicrystalline polymers," *Fluid Phase Equilibria*, vol. 367, pp. 173–181, 2014.

[46] P. J. Flory, "Themodynamics of high polymer solutions," *The Journal of Chemical Physics*, vol. 10, pp. 51–61, 1942.

[47] M. L. Huggins, "Some properties of solutions of long-chain compounds," *Journal of Physical Chemistry*, vol. 46, pp. 151–158, 1942.

[48] A. J. Staverman, "The entropy of high polymer solutions. generalization of formulae," *Recueil des Travaux Chimiques des Pays-Bas*, vol. 69, pp. 163–174, 1950.

[49] I. C. Sanchez and R. H. Lacombe, "Statistical thermodynamics of polymer solutions," *Macromolecules*, vol. 11, pp. 1145–1156, 1978.

[50] J. Dudowicz and K. F. Freed, "Effect of monomer structure and compressibility on the properties of multicomponent polymer blends and solutions: 1. Lattice cluster theory of compressible systems," *Macromolecules*, vol. 24, no. 18, pp. 5076–5095, 1991.

[51] J. D. van der Waals, *Over de Continuiteit van den Gas-en Vloeistoftoestand*. PhD thesis, University of Leiden, 1873.

[52] R. W. Zwanzig, "High-temperature equation of state by a perturbation method. I. Nonpolar gases," *Journal of Chemical Physics*, vol. 22, pp. 1420–1426, 1954.

[53] W. G. Chapman, G. Jackson, and K. E. Gubbins, "Phase equilibria of associating fluids chain molecules with multiple bonding sites," *Molecular Physics*, vol. 65, pp. 1057–1079, 1988.

[54] W. G. Chapman, K. E. Gubbins, G. Jackson, and M. Radosz, "New reference equation of state for associating liquids," *Industrial and Engineering Chemistry Research*, vol. 29, pp. 1709–1721, 1990.

[55] M. S. Wertheim, "Fluids with highly directional attractive forces. I. statistical thermodynamics," *Journal of Statistical Physics*, vol. 35, pp. 19–34, 1984.

[56] M. S. Wertheim, "Fluids with highly directional attractive forces. II. thermodynamic perturbation theory and integral equations," *Journal of Statistical Physics*, vol. 35, pp. 35–47, 1984.

[57] M. Wertheim, "Fluids with highly directional attractive forces. III. Multiple attraction sites," *Journal of statistical physics*, vol. 42, no. 3-4, pp. 459–476, 1986.

[58] M. S. Wertheim, "Fluids with highly directional attractive forces. IV. equilibrium polymerization," *Journal of Statistical Physics*, vol. 42, pp. 477–492, 1986.

[59] M. S. Wertheim, "Thermodynamic perturbation theory of polymerization," *The Journal of Chemical Physics*, vol. 87, pp. 7323–7331, 1987.

[60] P. T. Cummings and D. J. Evans, "Nonequilibrium molecular dynamics approaches to transport properties and non-newtonian fluid rheology," *Industrial & engineering chemistry research*, vol. 31, no. 5, pp. 1237–1252, 1992.

[61] P. T. Cummings, "Molecular dynamics simulation of realistic systems," *Fluid Phase Equilibria*, vol. 116, no. 1, pp. 237–248, 1996.

[62] A. Gil-Villegas, A. Galindo, P. J. Whitehead, S. J. Mills, G. Jackson, and A. N. Burgess, "Statistical associating fluid theory for chain molecules with attractive potentials of variable range," *The Journal of Chemical Physics*, vol. 106, pp. 4168–4186, 1997.

[63] F. J. Blas and L. F. Vega, "Prediction of binary and ternary diagrams using the statistical associating fluid theory (saft) equation of state," *Industrial and Engineering Chemistry Research*, vol. 37, pp. 660–674, 1998.

[64] J. Gross and G. Sadowski, "Perturbed-chain SAFT: An equation of state based on a perturbation theory for chain molecules," *Industrial and Engineering Chemistry Research*, vol. 40, pp. 1244–1260, 2001.

[65] J. Gross and G. Sadowski, "Application of the perturbed-chain SAFT equation of state to associating systems," *Industrial and Engineering Chemistry Research*, vol. 41, pp. 5510–5515, 2002.

[66] T. Lafitte, A. Apostolakou, C. Avendaño, A. Galindo, C. S. Adjiman, E. A. Müller, and G. Jackson, "Accurate statistical associating fluid theory for chain molecules formed from mie segments," *The Journal of Chemical Physics*, vol. 139, 2013.

[67] V. Papaioannou, T. Lafitte, C. Avendaño, C. S. Adjiman, G. Jackson, E. A. Müller, and A. Galindo, "Group contribution methodology based on the statistical

associating fluid theory for heteronuclear molecules formed from mie segments," *Journal of Chemical Physics*, vol. 140, 2014.

[68] S. Dufal, V. Papaioannou, M. Sadeqzadeh, T. Pogiatzis, A. Chremos, C. S. Adjiman, G. Jackson, and A. Galindo, "Prediction of thermodynamic properties and phase behavior of fluids and mixtures with the SAFT-γ Mie group-contribution equation of state," *Journal of Chemical and Engineering Data*, vol. 59, pp. 3272–3288, 2014.

[69] S. Dufal, T. Lafitte, A. J. Haslam, A. Galindo, G. N. Clark, C. Vega, and G. Jackson, "The A in SAFT: Developing the contribution of association to the Helmholtz free energy within a Wertheim TPT1 treatment of generic mie fluids," *Molecular Physics*, vol. 113, pp. 948–984, 2015.

[70] J. Burger, V. Papaioannou, S. Gopinath, G. Jackson, A. Galindo, and C. S. Adjiman, "A hierarchical method to integrated solvent and process design of physical CO_2 absorption using the SAFT-γ Mie approach," *AlChE Journal*, vol. 61, pp. 3249–3269, 2015.

[71] M. Wehbe, A. J. Haslam, G. Jackson, and A. Galindo, "Phase behaviour and pH-solubility profile prediction of aqueous buffered solutions of ibuprofen and ketoprofen," *Fluid Phase Equilibria*, vol. 560, p. 113504, 2022.

[72] A. J. Haslam, A. González-Pérez, S. Di Lecce, S. H. Khalit, F. A. Perdomo, S. Kournopoulos, M. Kohns, T. Lindeboom, M. Wehbe, S. Febra, G. Jackson, C. S. Adjiman, and A. Galindo, "Expanding the applications of the SAFT-γ Mie group-contribution equation of state: Prediction of thermodynamic properties and phase behavior of mixtures," *Journal of Chemical & Engineering Data*, vol. 65, no. 12, pp. 5862–5890, 2020.

[73] M. Fayaz-Torshizi and E. A. Müller, "Coarse-grained molecular simulation of polymers supported by the use of the SAFT-γ Mie equation of state," *Macromolecular Theory and Simulations*, vol. 31, 2022.

[74] C. C. Walker, J. Genzer, and E. E. Santiso, "Development of a fused-sphere SAFT-γ Mie force field for poly(vinyl alcohol) and poly(ethylene)," *The Journal of Chemical Physics*, vol. 150, no. 3, 2019.

[75] F. London, "The general theory of molecular forces," *Transactions of the Faraday Society*, vol. 33, pp. 8b–26, 1937.

[76] A. Lymperiadis, C. S. Adjiman, A. Galindo, and G. Jackson, "A group contribution method for associating chain molecules based on the statistical associating fluid theory (SAFT- γ)," *Journal of Chemical Physics*, vol. 127, 2007.

[77] J. A. Barker and D. Henderson, "Perturbation theory and equation of state for fluids. II. a successful theory of liquids," *The Journal of Chemical Physics*, vol. 47, pp. 4714–4721, 1967.

[78] J. A. Barker and D. Henderson, "Perturbation theory and equation of state for fluids: The square-well potential," *The Journal of Chemical Physics*, vol. 47, pp. 2856–2861, 1967.

[79] K. Gubbins, W. Smith, M. Tham, and E. Tiepel, "Perturbation theory for the radial distribution function," *Molecular Physics*, vol. 22, no. 6, pp. 1089–1105, 1971.

[80] J. A. Barker and D. Henderson, "What is "liquid"? understanding the states of matter," *Reviews of Modern Physics*, vol. 48, pp. 587–664, 1976.

[81] L. Ornstein and F. Zernike, "Accidental deviations of density and opalescence at the critical point of a single substance," *Proc. Akad. Sci.(Amsterdam)*, vol. XVII, pp. 793–806, 1914.

[82] J. K. Percus and G. J. Yevick, "Analysis of classical statistical mechanics by means of collective coordinates," *Physical Review*, vol. 110, pp. 1–13, 1958.

[83] N. F. Carnahan and K. E. Starling, "Equation of state for nonattracting rigid spheres," *The Journal of Chemical Physics*, vol. 51, pp. 635–636, 1969.

[84] T. Boublík, "Hard-sphere equation of state," *The Journal of Chemical Physics*, vol. 53, pp. 471–472, 1970.

[85] G. A. Mansoori, N. F. Carnahan, K. E. Starling, and T. W. Leland, "Equilibrium thermodynamic properties of the mixture of hard spheres," *The Journal of Chemical Physics*, vol. 54, pp. 1523–1525, 1971.

[86] M. S. Wertheim, "Theory of polar fluids: V. thermodynamics and thermodynamic perturbation theory," *Molecular Physics*, vol. 37, pp. 83–94, 1979.

[87] W. Zmpitas and J. Gross, "Detailed pedagogical review and analysis of Wertheim's thermodynamic perturbation theory," *Fluid Phase Equilibria*, vol. 428, pp. 121–152, 2016.

[88] W. Zmpitas and J. Gross, "A new equation of state for linear hard chains: Analysis of a third-order expansion of Wertheim's thermodynamic perturbation theory," *Fluid Phase Equilibria*, vol. 416, pp. 18–26, 2016.

[89] W. Chapman, K. Gubbins, G. Jackson, and M. Radosz, "SAFT: Equation-of-state solution model for associating fluids," *Fluid Phase Equilibria*, vol. 52, pp. 31–38, 1989.

[90] P. Paricaud, S. Varga, and G. Jackson, "Study of the demixing transition in model athermal mixtures of colloids and flexible self-excluding polymers using the thermodynamic perturbation theory of wertheim," *Journal of Chemical Physics*, vol. 118, pp. 8525–8536, 2003.

[91] P. Paricaud, A. Galindo, and G. Jackson, "Examining the effect of chain length polydispersity on the phase behavior of polymer solutions with the statistical associating fluid theory (wertheim tpt1) using discrete and continuous distributions," *Journal of Chemical Physics*, vol. 127, 2007.

[92] N. Pedrosa, L. F. Vega, J. A. Coutinho, and I. M. Marrucho, "Modeling the phase equilibria of poly(ethylene glycol) binary mixtures with soft-saft eos," *Industrial and Engineering Chemistry Research*, vol. 46, pp. 4678–4685, 2007.

[93] H. S. Byun and B. S. Lee, "Liquid-liquid equilibrium of hydrogen bonding polymer solutions," *Polymer*, vol. 121, pp. 1–8, 2017.

[94] M. Valsecchi, A. Galindo, and G. Jackson, "Modelling the thermodynamic properties of the mixture of water and polyethylene glycol (PEG) through the SAFT-γ Mie group-contribution approach." In preparation, 2023.

[95] P. J. Walker, H.-W. Yew, and A. Riedemann, "Clapeyron.jl: an extensible, open-source fluid thermodynamics toolkit," *Industrial & Engineering Chemistry Research*, vol. 61, no. 20, pp. 7130–7153, 2022.

[96] J. Bezanson, A. Edelman, S. Karpinski, and V. B. Shah, "Julia: A fresh approach to numerical computing," *SIAM review*, vol. 59, no. 1, pp. 65–98, 2017.

[97] F. E. Pereira, G. Jackson, A. Galindo, and C. S. Adjiman, "The HELD algorithm for multicomponent, multiphase equilibrium calculations with generic equations of state," *Computers & chemical engineering*, vol. 36, pp. 99–118, 2012.

[98] P. J. Walker, T. Zhao, A. J. Haslam, and G. Jackson, "Ab initio development of generalized Lennard-Jones (Mie) force fields for predictions of thermodynamic properties in advanced molecular-based saft equations of state," *The Journal of Chemical Physics*, vol. 156, no. 15, 2022.

[99] S. Dufal, T. Lafitte, A. Galindo, G. Jackson, and A. J. Haslam, "Developing intermolecular-potential models for use with the SAFT-VR mie equation of state," *AIChE Journal*, vol. 61, pp. 2891–2912, 2015.

[100] V. Papaioannou, F. Calado, T. Lafitte, S. Dufal, M. Sadeqzadeh, G. Jackson, C. S. Adjiman, and A. Galindo, "Application of the SAFT-γ Mie group contribution equation of state to fluids of relevance to the oil and gas industry," *Fluid Phase Equilibria*, vol. 416, pp. 104–119, 2016.

[101] P. Hutacharoen, S. Dufal, V. Papaioannou, R. M. Shanker, C. S. Adjiman, G. Jackson, and A. Galindo, "Predicting the solvation of organic compounds in aqueous environments: From alkanes and alcohols to pharmaceuticals," *Industrial and Engineering Chemistry Research*, vol. 56, pp. 10856–10876, 2017.

[102] A. J. Haslam, A. González-Pérez, S. Di Lecce, S. H. Khalit, F. A. Perdomo, S. Kournopoulos, M. Kohns, T. Lindeboom, M. Wehbe, S. Febra, *et al.*, "Expanding the applications of the SAFT-γ mie group-contribution equation of state: Prediction of thermodynamic properties and phase behavior of mixtures," *Journal of Chemical & Engineering Data*, vol. 65, no. 12, pp. 5862–5890, 2020.

[103] T. W. De Loos, W. Poot, and R. N. Lichtenthaler, "Fluid phase equilibria in binary ethylene + *n*-alkane systems," *Berichte der Bunsengesellschaft für physikalische Chemie*, vol. 88, no. 9, pp. 855–859, 1984.

[104] J. D. Gómez-Ibáñez and F. T. Wang, "The excess Gibbs energy of mixtures of cyclohexane with *n*-eicosane and with two other *n*-alkanes. a relation of congruence," *The Journal of Chemical Thermodynamics*, vol. 3, no. 6, pp. 811–817, 1971.

[105] R. R. Mallepally, V. S. Gadepalli, B. A. Bamgbade, N. Cain, and M. A. McHugh, "Phase behavior and densities of propylene + hexane binary mixtures to 585 k and

70 mpa," *Journal of Chemical & Engineering Data*, vol. 61, no. 8, pp. 2818–2827, 2016.

[106] I. Thoedtmann, H. Preuss, and D. Pape, "Determination of the vapor-liquid equilibria in binary systems formed by *n*-heptane, but-1-ene, and ethene," *Leuna-Protokoll*, p. 12011, 1989.

[107] S. Febra, *Ring formation in a statistical associating fluid theory framework*. PhD thesis, Imperial College London, 2018.

[108] C. Wohlfarth, "Vapour-liquid equilibrium data of binary polymer solutions: Vapour pressures, Henry-constants and segment-molar excess Gibbs free energies," in *Physical Science Data 44*, Elsevier, Amsterdam, Netherlands, 1994.

[109] M. L. Sherrill, "An investigation of a series of derivatives of normal heptane. I. preparation, identification and physical constants," *Journal of the American Chemical Society*, vol. 52, no. 5, pp. 1982–1992, 1930.

[110] L. Deffet, "The freezing points of organic compounds XIII. Compounds with seven, eight, nine or ten carbon atoms," *Bulletin des Sociétés Chimiques Belges*, vol. 40, pp. 385–402, 1931.

[111] E. S. Guenther and E. E. Langenau, "An investigation of the chemical constituents of distilled lime oil (citrus medica, l., var. acida, brandis)(citrus aurantifolia, swingle)," *Journal of the American Chemical Society*, vol. 65, no. 5, pp. 959–963, 1943.

[112] P. Foote and R. Z. Gelpi, "Florida volatile oils IV. sweet orange," *Journal of the American Pharmaceutical Association*, vol. 32, no. 6, pp. 145–148, 1943.

[113] M. Stoll and A. Rouve, "Étude des réactions secondaires de l'ozonolyse d'une liaison éthylénique," *Helvetica Chimica Acta*, vol. 27, no. 1, pp. 950–961, 1944.

[114] J. N. Friend and W. D. Hargreaves, "LXXI. viscosities and rheochors of aldehydes, nitrites and of secondary and tertiary amines," *The London, Edinburgh, and Dublin Philosophical Magazine and Journal of Science*, vol. 35, no. 248, pp. 619–631, 1944.

[115] F. McKenna, H. Tartar, and E. Lingafelter, "Studies of hemiacetal formation in alcohol-aldehyde systems. I. cryoscopic studies," *Journal of the American Chemical Society*, vol. 71, no. 2, pp. 729–732, 1949.

[116] T. E. Smith and R. F. Bonner, "Acetaldehyde, propionaldehyde, and *n*-butyraldehyde," *Industrial & Engineering Chemistry*, vol. 43, no. 5, pp. 1169–1173, 1951.

[117] C. T. Kyte, G. H. Jeffery, and A. I. Vogel, "864. physical properties and chemical constitution. Part XXVIII. Pyridine derivatives," *Journal of the Chemical Society (Resumed)*, pp. 4454–4472, 1960.

[118] J. G. Wojtasinski, "Measurement of total pressures for determining liquid-vapor equilibrium relations of the binary system isobutyraldehyde *n*-butyraldehyde.," *Journal of Chemical and Engineering Data*, vol. 8, no. 3, pp. 381–385, 1963.

[119] G. Geiseler and M. Rätzsch, "Bildungsenthalpien stellungsisomerer *n*-Alkanderivate 1. Mitteilung: Bildungsenthalpien des Octanals und der drei isomeren Octanone," *Berichte der Bunsengesellschaft für physikalische Chemie*, vol. 69, no. 6, pp. 485–488, 1965.

[120] M. Mamedov, K. Guseinov, and A. Kerimov, "Experimental observation of PVT dependence of liquid aldehydes," *Izvestiya Vysshikh Uchebnykh Zavedenii, Neft' i Gaz*, vol. 18, no. 6, pp. 70–80, 1975.

[121] Q. Wang and K.-C. Chao, "Vapor-liquid equilibria for binary mixtures of butylene oxide + *n*-butyraldehyde, butylene oxide + isobutyraldehyde and methyl acetate + butylene oxide," *AIChE Symposium Series*, vol. 86, pp. 26–32, 1990.

[122] M. Antosik, Z. Fraś, and S. K. Malanowski, "Vapor- liquid equilibrium in 2-ethoxyethanol+ valeraldehyde and propyl ether at 313.15 to 333.15 k," *Journal of Chemical & Engineering Data*, vol. 47, no. 4, pp. 757–760, 2002.

[123] S. P. Verevkin, E. L. Krasnykh, T. V. Vasiltsova, B. Koutek, J. Doubsky, and A. Heintz, "Vapor pressures and enthalpies of vaporization of a series of the linear aliphatic aldehydes," *Fluid phase equilibria*, vol. 206, no. 1-2, pp. 331–339, 2003.

[124] H. Djojoputro and S. Ismadji, "Density and viscosity of several aldehydes fragrance compounds in their binary mixtures with ethanol at (298.15 k, 308.15 k, and 318.15 k)," *Journal of Chemical & Engineering Data*, vol. 50, no. 6, pp. 2003–2007, 2005.

[125] V. H. Alvarez, S. Mattedi, and M. Aznar, "Isobaric (vapor+ liquid) equilibria of 1-ethyl-3-methylimidazolium ethylsulfate plus (propionaldehyde or valeraldehyde): Experimental data and prediction," *The Journal of Chemical Thermodynamics*, vol. 43, no. 6, pp. 895–900, 2011.

[126] D. A. Meneses, A. Bejarano, and J. C. de la Fuente, "Vapor pressure data for ethyl-2-methylbutyrate, hexanal and (e)-2-hexenal at a pressure range of (25 to 190) kpa," *The Journal of Chemical Thermodynamics*, vol. 74, pp. 16–21, 2014.

[127] R. Eng and S. I. Sandler, "Vapor-liquid equilibria for three aldehyde/hydrocarbon mixtures," *Journal of Chemical and Engineering Data*, vol. 29, no. 2, pp. 156–161, 1984.

[128] A. A. Polyakov, T. N. Tyvina, V. V. Fokina, and A. A. Naumova, "Compositions and molar volumes of solutions of ethylene, ethane, and carbon-dioxide in propionaldehyde," *Journal of Applied Chemistry of the USSR*, vol. 59, no. 6, pp. 1261–1263, 1986.

[129] I. I. Vasileva, A. A. Naumova, A. A. Polyakov, T. N. Tyvina, and V. V. Fokina, "Compositions and molar volumes of solutions of hydrogen, nitrogen, propane,

and isobutylene in butyraldehyde," *Journal of Applied Chemistry of the USSR*, vol. 62, no. 8, pp. 1755–1757, 1989.

[130] D. P. Maloney and J. M. Prausnitz, "Solubilities of ethylene and other organic solutes in liquid, low-density polyethylene in the region 124° to 300°C," *AIChE Journal*, vol. 22, pp. 74–82, 1976.

[131] P. Paricaud, A. Galindo, and G. Jackson, "Modeling the cloud curves and the solubility of gases in amorphous and semicrystalline polyethylene with the SAFT-VR approach and flory theory of crystallization," *Industrial and Engineering Chemistry Research*, vol. 43, pp. 6871–6889, 2004.

[132] P. Paricaud, S. Varga, P. T. Cummings, and G. Jackson, "Effect of polymer chain-length polydispersity on the phase behavior of model athermal mixtures of colloids and flexible self-excluding polymers," *Chemical Physics Letters*, vol. 398, no. 4, pp. 489–494, 2004.

[133] J. D. Moore, S. T. Cui, H. D. Cochran, and P. T. Cummings, "Transient rheology of a polyethylene melt under shear," *Phys. Rev. E*, vol. 60, pp. 6956–6959, 1999.

[134] M. Rubinstein and R. Colby, *Polymer Physics*. Oxford University Press, 2003.

[135] W. Hu, "The physics of polymer chain-folding," *Physics Reports*, vol. 747, pp. 1–50, 2018.

[136] J. Chmelař, K. Smolná, K. Haškovcová, M. Podivinská, J. Maršálek, and J. Kosek, "Equilibrium sorption of ethylene in polyethylene: Experimental study and PC-SAFT simulations," *Polymer*, vol. 59, pp. 270–277, 2015.

[137] H. joon Jin, S. Kim, and J. san Yoon, "Solubility of 1-hexene in LLDPE synthesized by (2-MeInd)$_2$ZrCl2/MAO and by Mg(OEt)2/DIBP/TiCl$_4$–TEA," *Journal of Applied Polymer Science*, vol. 84, pp. 1566–1571, 2002.

[138] A. Novak, M. Bobak, J. Kosek, B. J. Banaszak, D. Lo, T. Widya, W. H. Ray, and J. J. D. Pablo, "Ethylene and 1-hexene sorption in LLDPE under typical gas-phase reactor conditions : Experiments," *Journal of Applied Polymer Science*, vol. 100, pp. 1124–1136, 2006.

[139] M. Valsecchi, J. Ramadani, D. Williams, A. Galindo, and G. Jackson, "Influence of tie-molecules and microstructure on the fluid solubility in semicrystalline polymers," *Journal of Physical Chemistry B*, vol. 126, pp. 9059–9088, 2022.

[140] F. Malcolm and J. Rowlinson, "The thermodynamics properties of aqueous solutions of polyethylene glycol, polypropylene glycol and dioxane," *Transactions of the Faraday Society*, vol. 53, pp. 921–931, 1957.

[141] M. Herskowitz and M. Gottlleb, "Vapor-liquid equilibrium in aqueous solutions of various glycols and poly(ethylene glycols). 3. poly(ethylene glycols)," *Journal of Chemical and Engineering Data*, vol. 30, pp. 233–234, 1985.

[142] J. D. Hoffman and R. L. Miller, "Kinetics of crystallization from the melt and chain folding in polyethylene fractions revisited: theory and experiment," *Polymer*, vol. 38, pp. 3151–3212, 1997.

[143] M. C. Zhang, B. H. Guo, and J. Xu, "A review on polymer crystallization theories," *Crystals*, vol. 7, pp. 1–37, 2017.

[144] G. Natta and P. Corradini, *Structure and Properties of Isotactic Polypropylene*. Pergamon Press Ltd, 1967.

[145] P. H. Geil, F. R. Anderson, B. Wunderlich, and T. Arakawa, "Morphology of polyethylene crystallized from the melt under pressure," *Journal of Polymer Science Part A: General Papers*, vol. 2, no. 8, pp. 3707–3720, 1964.

[146] M. Hikosaka, "Unified theory of nucleation of folded-chain crystals and extended-chain crystals of linear-chain polymers," *Polymer*, vol. 28, no. 8, pp. 1257–1264, 1987.

[147] M. Hikosaka, "Unified theory of nucleation of folded-chain crystals (FCCs) and extended-chain crystals (ECCs) of linear-chain polymers: 2. Origin of FCC and ECC," *Polymer*, vol. 31, no. 3, pp. 458–468, 1990.

[148] J. P. Arlie, P. A. Spegt, and A. E. Skoulios, "Etude de la cristallisation des polymères I. structure lamellaire de polyoxyéthylènes de faible masse moléculaire," *Die Makromolekulare Chemie*, vol. 99, pp. 160–174, 1966.

[149] P. J. P. Arlie, P. Spegt, and A. Skoulios, "Etude de la cristallisation des polymères. II. structure lamellaire et repliement des chaînes du polyoxyéthylène," *Die Makromolekulare Chemie*, vol. 104, pp. 212–229, 1967.

[150] A. J. Kovacs, A. Gonthier, and C. Straupe, "Isothermal growth, thickening, and melting of poly(ethylene oxide) single crystals in the bulk," *Journal of Polymer Science: Polymer Symposia*, vol. 50, pp. 283–325, 1975.

[151] A. J. Kovacs, C. Straupe, and A. Gonthier, "Isothermal growth, thickening, and melting of polyethylene oxide) single crystals in the bulk. II," *Journal of Polymer Science: Polymer Symposia*, vol. 59, pp. 31–54, 1977.

[152] A. J. Kovacs and C. Straupe, "Isothermal growth, thickening and melting of poly(ethylene oxide) single crystals in the bulk. part 4.—dependence of pathological crystal habits on temperature and thermal history," *Faraday Discussions of the Chemical Society*, vol. 68, pp. 225–238, 1979.

[153] L. Melillo and B. Wunderlich, "Extended-chain crystals VIII. morphology of polytetrafluoroethylene," *Kolloid-Zeitschrift und Zeitschrift für Polymere*, vol. 250, pp. 417–425, 1972.

[154] J. Lu, R. Huang, L. Li, and J. Luo, "Growth of large polymer extended-chain single crystals in a poly(ethylene terephthalate)/bisphenol a polycarbonate blend under high pressure," *Macromolecular Rapid Communications*, vol. 26, no. 18, pp. 1478–1482, 2005.

[155] S. Kavesh and J. M. Schultz, "Lamellar and interlamellar structure in melt-crystallized polyethylene. II. Lamellar spacing, interlamellar thickness, interlamellar density, and stacking disorder," *Journal of Polymer Sience Part A-2*, vol. 9, pp. 85–114, 1971.

[156] G. Strobl, "Crystallization and melting of bulk polymers: New observations, conclusions and a thermodynamic scheme," *Progress in Polymer Science (Oxford)*, vol. 31, pp. 398–442, 2006.

[157] A. Keller, "A note on single crystals in polymers: evidence for a folded chain configuration," *The Philosophical Magazine: A Journal of Theoretical Experimental and Applied Physics*, vol. 2, no. 21, pp. 1171–1175, 1957.

[158] P. H. Till Jr., "The growth of single crystals of linear polyethylene," *Journal of Polymer Science*, vol. 24, no. 106, pp. 301–306, 1957.

[159] E. W. Fischer, "Notizen: Stufen- und spiralförmiges kristallwachstum bei hochpolymeren," *Zeitschrift für Naturforschung A*, vol. 12, no. 9, pp. 753–754, 1957.

[160] P. J. Flory, "On the morphology of the crystalline state in polymers," *Journal of the American Chemical Society*, vol. 84, pp. 2857–2867, 1962.

[161] A. Keller and H. H. Wills, "Polymer crystals," *Reports on Progress in Physics*, vol. 31, pp. 623–704, 1968.

[162] J. I. Lauritzen and J. D. Hoffman, "Extension of theory of growth of chain-folded polymer crystals to large undercoolings," *Journal of Applied Physics*, vol. 44, pp. 4340–4352, 1973.

[163] V. Petraccone, G. Allegra, and P. Corradini, "Calculation of minimum potential energy of folds and kinks in polyethylene crystals," *Journal of Polymer Science*, vol. 38, pp. 419–427, 1972.

[164] M. L. Mansfield, "Monte carlo study of chain folding in melt-crystallized polymers," *Macromolecules*, vol. 16, no. 6, pp. 914–920, 1983.

[165] P. J. Flory, D. Y. Yoon, and K. A. Dill, "The interphase in lamellar semicrystalline polymers," *Macromolecules*, vol. 17, pp. 862–868, 1984.

[166] J. A. Marqusee and K. A. Dill, "Chain configurations in lamellar semicrystalline polymer interphases," *Macromolecules*, vol. 19, pp. 2420–2426, 1986.

[167] S. K. Kumar and D. Y. Yoon, "Lattice model for crystal-amorphous interphases in lamellar semicrystalline polymers: Effects of tight-fold energy and chain incidence density," *Macromolecules*, vol. 22, pp. 3458–3465, 1989.

[168] R. Chiang and P. J. Flory, "Equilibrium between crystalline and amorphous phases in polyethylene," *Journal of the American Chemical Society*, vol. 83, pp. 2857–2862, 1961.

[169] P. J. Flory and A. Vrij, "Melting points of linear-chain homologs. the normal paraffin hydrocarbons," *Journal of the American Chemical Society*, vol. 85, pp. 3548–3553, 1963.

[170] I. C. Sanchez and R. K. Eby, "Thermodynamics and crystallization of random copolymers," *Macromolecules*, vol. 8, pp. 638–641, 1975.

[171] C. P. Buckley and A. J. Kovacs, "Melting behaviour of low molecular weight poly (ethylene-oxide) fractions 2. Folded chain crystals," *Colloid and Polymer Science*, vol. 254, pp. 695–715, 1976.

[172] K. Iwata, "Role of entanglement in crystalline polymers 1. Basic theory," *Polymer*, vol. 43, pp. 6609–6626, 2002.

[173] W. Thomson, "4. On the equilibrium of vapour at a curved surface of liquid," *Proceedings of the Royal Society of Edinburgh*, vol. 7, pp. 63–68, 1872.

[174] J. W. Gibbs, "On the equilibrium of heterogeneous substances," *American Journal of Science*, vol. 3, no. 96, pp. 441–458, 1878.

[175] P. J. Flory, "Theory of crystallization in copolymers," *Transactions of the Faraday Society*, vol. 51, pp. 848–857, 1955.

[176] C. Schick, R. Androsch, and J. W. Schmelzer, "Homogeneous crystal nucleation in polymers," *Journal of Physics Condensed Matter*, vol. 29, 2017.

[177] C. Ruan, C. Liu, and G. Zheng, "Monte carlo simulation for the morphology and kinetics of spherulites and shish-kebabs in isothermal polymer crystallization," *Mathematical Problems in Engineering*, vol. 2015, 2015.

[178] P. J. Flory and D. Y. Yoon, "Molecular morphology in semi-crystalline polymers," *Nature*, vol. 272, pp. 226–229, 1978.

[179] G. Hauser, J. Schmidtke, and G. Strobl, "The role of co-units in polymer crystallization and melting: new insights from studies on syndiotactic poly (propene-co-octene)," *Macromolecules*, vol. 31, no. 18, pp. 6250–6258, 1998.

[180] B. Crist, "Equilibrium aspects of folded chain polymer crystals," *Macromolecules*, vol. 39, pp. 1971–1980, 2006.

[181] D. Y. Yoon and P. J. Flory, "Chain packing at polymer interface," *Macromolecules*, vol. 17, pp. 868–871, 1984.

[182] S. Gautam, S. Balijepalli, and G. C. Rutledge, "Molecular simulations of the interlamellar phase in polymers: Effect of chain tilt," *Macromolecules*, vol. 33, no. 24, pp. 9136–9145, 2000.

[183] H. D. Keith, F. J. Padden, and R. G. Vadimsky, "Intercrystalline links in polyethylene crystallized from the melt," *Journal of Polymer Science Part A-2: Polymer Physics*, vol. 4, pp. 267–281, 1966.

[184] S. Adhikari and M. Muthukumar, "Theory of statistics of ties, loops, and tails in semicrystalline polymers," *Journal of Chemical Physics*, vol. 151, 2019.

[185] A. Makke, O. Lame, M. Perez, and J. L. Barrat, "Influence of tie and loop molecules on the mechanical properties of lamellar block copolymers," *Macromolecules*, vol. 45, pp. 8445–8452, 2012.

[186] S. Jabbari-Farouji, O. Lame, M. Perez, J. Rottler, and J. L. Barrat, "Role of the intercrystalline tie chains network in the mechanical response of semicrystalline polymers," *Physical Review Letters*, vol. 118, pp. 1–5, 2017.

[187] R. Seguela and F. Rietsch, "Molecular topology in ethylene copolymers studied by means of mechanical testing," *Journal of Materials Science*, vol. 23, pp. 415–421, 1988.

[188] J. T. Yeh and J. Runt, "Fatigue crack propagation in high-density polyethylene," *Journal of Polymer Science Part B: Polymer Physics*, vol. 29, pp. 371–288, 1991.

[189] J. Runt and M. Jacq, "Effect of crystalline morphology on fatigue crack propagation in polyethylene," *Journal of Materials Science*, vol. 24, pp. 1421–1428, 1989.

[190] Y. Huang and N. Brown, "Dependence of slow crack growth in polyethylene on butyl branch density: morphology and theory," *Journal of Polymer Science Part B: Polymer Physics*, vol. 29, pp. 129–137, 1991.

[191] R. M. Patel, K. Sehanobish, P. Jain, S. P. Chum, and G. W. Knight, "Theoretical prediction of tie-chain concentration and its characterization using postyield response," *Journal of Applied Polymer Science*, vol. 60, pp. 749–758, 1996.

[192] W. Hu, T. Albrecht, and G. Strobl, "Reversible surface melting of PE and PEO crystallites indicated by TMDSC," *Macromolecules*, vol. 32, pp. 7548–7554, 1999.

[193] M. Polińska, A. Rozanski, A. Galeski, and J. Bojda, "The modulus of the amorphous phase of semicrystalline polymers," *Macromolecules*, vol. 54, pp. 9113–9123, 2021.

[194] M. Polinska, A. Rozanski, M. Kozanecki, and A. Galeski, "Elastic modulus of the amorphous phase confined between lamellae: The role of crystalline component," *Polymer*, vol. 269, p. 125753, 2023.

[195] R. J. Roe, K. J. Smith, and W. R. Krigbaum, "Equilibrium degrees of crystallization predicted for "single pass" and folded chain crystallite models," *The Journal of Chemical Physics*, vol. 35, pp. 1306–1311, 1961.

[196] W. R. Krigbaum, R. J. Roe, and K. J. Smith, "A theoretical treatment of the modulus of semi-crystalline polymers," *Polymer*, vol. 5, pp. 533–542, 1964.

[197] E. W. Fischer, "Das grenzflächenschmelzen der kristallite in teilkristallisierten hochpolymeren - teil i: Theoretische grundlagen," *Kolloid-Zeitschrift & Zeitschrift für Polymere*, vol. 218, pp. 97–114, 1967.

[198] H. G. Zachmann and A. Peterlin, "Influence of the surface morphology on the melting of polymer crystals. I. Loops of random length and adjacent reentry," *Journal of Macromolecular Science, Part B*, vol. 3, pp. 495–517, 1969.

[199] M. L. Mansfield, "Temperature-dependent changes in the structure of the amorphous domains of semicrystalline polymers," *Macromolecules*, vol. 22, pp. 3810–3812, 1989.

[200] T. Albrecht and G. Strobl, "Temperature-dependent crystalline-amorphous structures in linear polyethylene: surface melting and the thickness of the amorphous layers," *Macromolecules*, vol. 28, pp. 5827–5833, 1995.

[201] C. M. Guttman, E. A. DiMarzio, and J. D. Hoffman, "Modelling the amorphous phase and the fold surface of a semicrystalline polymer – the Gambler's Ruin method," *Polymer*, vol. 22, pp. 1466–1479, 1981.

[202] E. A. DiMarzio and C. M. Guttman, "Three statistical mechanical arguments that favour chain folding in polymer systems of lamellar morphology," *Polymer*, vol. 21, pp. 733–744, 1980.

[203] S. F. Edwards, "The statistical mechanics of polymers with excluded volume," *Proceedings of the Physical Society*, vol. 85, pp. 613–624, 1965.

[204] S. F. Edwards, "The statistical mechanics of polymers with excluded volume," *Proceedings of the Physical Society*, vol. 85, pp. 613–624, 1965.

[205] M. Schulz, A. Seidlitz, R. Kurz, R. Bärenwald, A. Petzold, K. Saalwächter, and T. Thurn-Albrecht, "The underestimated effect of intracrystalline chain dynamics on the morphology and stability of semicrystalline polymers," *Macromolecules*, vol. 51, pp. 8377–8385, 2018.

[206] R. C. Lacher, J. L. Bryant, and L. N. Howard, "A model for the asymptotic behavior of loop entanglement in a constrained liquid region," *The Journal of Chemical Physics*, vol. 85, no. 10, pp. 6147–6152, 1986.

[207] F. Nilsson, X. Lan, T. Gkourmpis, M. S. Hedenqvist, and U. W. Gedde, "Modelling tie chains and trapped entanglements in polyethylene," *Polymer*, vol. 53, pp. 3594–3601, 2012.

[208] S. Balijepalli and G. C. Rutledge, "Simulation study of semi-crystalline polymer interphases," *Macromolecular Symposia*, vol. 133, pp. 71–99, 1998.

[209] P. J. in 't Veld and G. C. Rutledge, "Temperature-dependent elasticity of a semicrystalline interphase composed of freely rotating chains," *Macromolecules*, vol. 36, pp. 7358–7365, 2003.

[210] P. J. in 't Veld, M. Hütter, and G. C. Rutledge, "Temperature-dependent thermal and elastic properties of the interlamellar phase of semicrystalline polyethylene by molecular simulation," *Macromolecules*, vol. 39, pp. 439–447, 2006.

[211] G. C. Rutledge, "Implications of metastability for the crystal/amorphous interface from molecular simulation," *Journal of Macromolecular Science, Part B: Physics*, vol. 41 B, pp. 909–922, 2007.

[212] S. Lee and G. C. Rutledge, "Plastic deformation of semicrystalline polyethylene by molecular simulation," *Macromolecules*, vol. 44, pp. 3096–3108, 2011.

[213] P. Yi, C. R. Locker, and G. C. Rutledge, "Molecular dynamics simulation of homogeneous crystal nucleation in polyethylene," *Macromolecules*, vol. 46, pp. 4723–4733, 2013.

[214] A. Ghazavizadeh, G. C. Rutledge, A. A. Atai, S. Ahzi, Y. Rémond, and N. Soltani, "Hyperelastic characterization of the interlamellar domain and interphase layer in semicrystalline polyethylene," *Journal of Polymer Science, Part B: Polymer Physics*, vol. 51, pp. 1692–1704, 2013.

[215] V. Kumar, C. R. Locker, P. J. in 't Veld, and G. C. Rutledge, "Effect of short chain branching on the interlamellar structure of semicrystalline polyethylene," *Macromolecules*, vol. 50, no. 3, pp. 1206–1214, 2017.

[216] T. Uneyama, T. Miyata, and K. H. Nitta, "Self-consistent field model simulations for statistics of amorphous polymer chains in crystalline lamellar structures," *The Journal of Chemical Physics*, vol. 141, p. 164906, 2014.

[217] M. Schulz, M. Schäfer, K. Saalwächter, and T. Thurn-Albrecht, "Competition between crystal growth and intracrystalline chain diffusion determines the lamellar thickness in semicrystalline polymers," *Nature Communications 2022 13:1*, vol. 13, pp. 1–10, 2022.

[218] J. Petermann and H. Gleiter, "Observation of interface melting in polyethylene," *Journal of Polymer Science: Polymer Physics Edition*, vol. 14, pp. 555–558, 1976.

[219] T. Albrecht, S. Armbruster, S. Keller, and G. Strobl, "Dynamics of surface crystallization and melting in polyethylene and poly(ethylene oxide) studied by Temperature-Modulated DSC and heat wave spectroscopy," *Macromolecules*, vol. 34, 2001.

[220] R. Androsch and B. Wunderlich, "Specific reversible melting of polyethylene," *Journal of Polymer Science, Part B: Polymer Physics*, vol. 41, pp. 2157–2173, 2003.

[221] R. Androsch, B. Wunderlich, and H. J. Radusch, "Analysis of reversible melting in polytetrafluoroethylene," *Journal of Thermal Analysis and Calorimetry*, vol. 79, pp. 615–622, 2005.

[222] R. H. Boyd, "Relaxation processes in crystalline polymers: Molecular interpretation - a review," *Polymer*, vol. 26, pp. 1123–1133, 1985.

[223] W.-G. Hu and K. Schmidt-Rohr, "Polymer ultradrawability: the crucial role of alpha-relaxation chain mobility in the crystallites," *Acta Polymerica*, vol. 50, pp. 271–285, 1999.

[224] K. Kuwabara, H. Kaji, F. Horii, D. C. Bassett, and R. H. Olley, "Solid-state $_{13}$C NMR analyses of the crystalline-noncrystalline structure for metallocene-catalyzed linear low-density polyethylene," *Macromolecules*, vol. 30, pp. 7516–7521, 1997.

[225] K. Kuwabara, H. Kaji, and F. Horii, "Solid-state ^{13}C NMR analyses for the structure and molecular motion in the α relaxation temperature region for metallocene-catalyzed linear low-density polyethylene," *Macromolecules*, vol. 33, pp. 4453–4462, 2000.

[226] C. Hedesiu, D. E. Demco, R. Kleppinger, A. A. Buda, B. Blümich, K. Remerie, and V. M. Litvinov, "The effect of temperature and annealing on the phase composition, molecular mobility and the thickness of domains in high-density polyethylene," *Polymer*, vol. 48, pp. 763–777, 2007.

[227] R. Bärenwald, Y. Champouret, K. Saalwächter, and K. Schäler, "Determination of chain flip rates in poly(ethylene) crystallites by solid-state low-field ^{1}H NMR for two different sample morphologies," *Journal of Physical Chemistry B*, vol. 116, pp. 13089–13097, 2012.

[228] R. Bärenwald, S. Goerlitz, R. Godehardt, A. Osichow, Q. Tong, M. Krumova, S. Mecking, and K. Saalwächter, "Local flips and chain motion in polyethylene crystallites: A comparison of melt-crystallized samples, reactor powders, and nanocrystals," *Macromolecules*, vol. 47, pp. 5163–5173, 2014.

[229] V. Litvinov and Y. Men, "Time-domain NMR in polyolefin research," *Polymer*, vol. 256, p. 125205, 2022.

[230] V. Litvinov, R. Deblieck, C. Clair, W. V. D. Fonteyne, A. Lallam, R. Kleppinger, D. A. Ivanov, M. E. Ries, and M. Boerakker, "Molecular structure, phase composition, melting behavior, and chain entanglements in the amorphous phase of high-density polyethylenes," *Macromolecules*, vol. 53, pp. 5418–5433, 2020.

[231] B. Heck, G. Strobl, and M. Grasruck, "Characteristic variations in the effect of diluents on polymer crystallization and melting observed for a sample of poly

(ethylene-co-octene)," *The European Physical Journal E*, vol. 11, pp. 117–130, 2003.

[232] R. Kurz, M. Schulz, F. Scheliga, Y. Men, A. Seidlitz, T. Thurn-Albrecht, and K. Saalwächter, "Interplay between crystallization and entanglements in the amorphous phase of the crystal-fixed polymer poly(ϵ-caprolactone)," *Macromolecules*, vol. 51, pp. 5831–5841, 2018.

[233] J. Rieger and M. L. Mansfield, "Comments on "Temperature-dependent changes in the structure of the amorphous domains of semicrystalline polymers"," *Macromolecules*, vol. 22, pp. 3810–3812, 1989.

[234] E. W. Hansen, P. E. Kristiansen, and B. Pedersen, "Crystallinity of polyethylene derived from solid-state proton NMR free induction decay," *Journal of Physical Chemistry*, vol. 102, pp. 5444‘–5450, 1998.

[235] C. Hertlein, K. Saalwächter, and G. Strobl, "Low-field NMR studies of polymer crystallization kinetics: changes in the melt dynamics," *Polymer*, vol. 47, pp. 7216–7221, 2006.

[236] M. Wang, G. M. Bernard, R. E. Wasylishen, and P. Choi, "A solid-state ^{13}C NMR investigation of the morphology of single-site and ziegler-natta linear low-density polyethylenes with varying branch contents," *Macromolecules*, vol. 40, pp. 6594–6599, 2007.

[237] X. Shi, J. Wang, S. Stapf, C. Mattea, W. Li, and Y. Yang, "Effects of thermo-oxidative aging on chain mobility, phase composition, and mechanical behavior of high-density polyethylene," *Polymer Engineering & Science*, vol. 51, pp. 2171–2177, 2011.

[238] J. Chmelař, R. Pokorný, P. Schneider, K. Smolná, P. Bělský, and J. Kosek, "Free and constrained amorphous phases in polyethylene: Interpretation of ^{1}H NMR

and SAXS data over a broad range of crystallinity," *Polymer*, vol. 58, pp. 189–198, 2015.

[239] D. Kilburn, D. Bamford, T. Lüpke, G. Dlubek, T. J. Menke, and M. A. Alam, "Free volume and glass transition in ethylene/1-octene copolymers: positron lifetime studies and dynamic mechanical analysis," *Polymer*, vol. 43, pp. 6973–6983, 2002.

[240] S. Martín, J. F. Vega, M. T. Expósito, A. Flores, and J. Martínez-Salazar, "A three-phase microstructural model to explain the mechanical relaxations of branched polyethylene: A DSC, WAXD and DMTA combined study," *Colloid and Polymer Science*, vol. 289, pp. 257–268, 2011.

[241] Y. Kong and J. N. Hay, "The enthalpy of fusion and degree of crystallinity of polymers as measured by DSC," *European Polymer Journal*, vol. 39, pp. 1721–1727, 2003.

[242] S. Rabiej and A. Wlochowicz, "SAXS and WAXS investigations of the crystallinity in polymers," *Die Angewandte Makromolekulare Chemie*, vol. 175, no. 1, pp. 81–97, 1990.

[243] A. J. Ryan, W. Bras, G. R. Mant, and G. E. Derbyshire, "A direct method to determine the degree of crystallinity and lamellar thickness of polymers: application to polyethylene," *Polymer*, vol. 35, no. 21, pp. 4537–4544, 1994.

[244] Y. Tanabe, G. R. Strobl, and E. W. Fischer, "Surface melting in melt-crystallized linear polyethylene," *Polymer*, vol. 27, pp. 1147–1153, 1986.

[245] A. S. Michaels and H. J. Bixler, "Flow of gases through polyethylene," *Journal of Polymer Science*, vol. 50, pp. 413–439, 1961.

[246] A. S. Michaels and H. J. Bixler, "Solubility of gases in polyethylene," *Journal of Polymer Science*, vol. 50, pp. 393–412, 1961.

[247] D. Larobina, L. Sanguigno, V. Venditto, G. Guerra, and G. Mensitieri, "Gas sorption and transport in syndiotactic polystyrene with nanoporous crystalline phase," *Polymer*, vol. 45, pp. 429–436, 2004.

[248] G. Mensitieri, D. Larobina, G. Guerra, V. Venditto, M. Fermeglia, and S. Pricl, "Chloroform sorption in nanoporous crystalline and amorphous phases of syndiotactic polystyrene," *Journal of Polymer Science Part B: Polymer Physics*, vol. 46, pp. 8–15, 2008.

[249] M. Galizia, C. Daniel, G. Fasano, G. Guerra, and G. Mensitieri, "Gas sorption and diffusion in amorphous and semicrystalline nanoporous poly(2,6-dimethyl-1,4-phenylene)oxide," *Macromolecules*, vol. 45, pp. 3604–3615, 2012.

[250] C. E. Rogers, V. Stasnett, and M. Szwarc, "The sorption, diffusion, and permeation of organic vapors in polyethylene," *Journal of Polymer Science*, vol. 45, pp. 61–82, 1960.

[251] E. F. Castro, E. E. Gonzo, and J. C. Gottifredi, "The analysis of sorption data of organic vapors in polymeric membranes through novel theories," *Journal of Membrane Science*, vol. 113, pp. 57–64, 1996.

[252] W. Yao, X. Hu, and Y. Yang, "Modeling solubility of gases in semicrystalline polyethylene," *Journal of Applied Polymer Science*, vol. 103, pp. 1737–1744, 2007.

[253] L. Serna, J. Becker, J. Galdamez, R. Danner, and J. Duda, "Elastic effects on solubility in semicrystalline polymers," *Journal of Applied Polymer Science*, vol. 107, pp. 138–146, 2008.

[254] J. L. Rausch, T. C. Schulz, and R. P. Danner, "Solubility and diffusivity of cyclohexane in high density polyethylene," *Journal of Applied Polymer Science*, vol. 124, pp. 4315–4321, 2012.

[255] J. A. Moebus and B. R. Greenhalgh, "Modeling vapor solubility in semicrystalline polyethylene," *Macromolecular Reaction Engineering*, vol. 12, pp. 1–17, 2018.

[256] D. R. Sturm, K. J. Caputo, S. Liu, and R. P. Danner, "Solubility of solvents in polyethylene below the melt temperature," *Fluid Phase Equilibria*, vol. 470, pp. 68–74, 2018.

[257] O. Atiq, E. Ricci, M. G. Baschetti, and M. G. D. Angelis, "Modelling solubility in semi-crystalline polymers: a critical comparative review," *Fluid Phase Equilibria*, vol. 556, p. 113412, 2022.

[258] A. G. McDermott, P. J. Deslauriers, J. S. Fodor, R. L. Jones, and C. R. Snyder, "Measuring tie chains and trapped entanglements in semicrystalline polymers," *Macromolecules*, vol. 53, pp. 5614–5626, 2020.

[259] P. J. Flory, "Statistical mechanics of swelling of network structures," *The Journal of Chemical Physics*, vol. 18, pp. 108–111, 1950.

[260] L. R. G. Treloar, *The physics of rubber elasticity*. Oxford University Press, USA, 1975.

[261] P. J. Flory, "Theory of elasticity of polymer networks. the effect of local constraints on junctions," *The Journal of Chemical Physics*, vol. 66, pp. 5720–5729, 1977.

[262] S. F. Edwards and T. Vilgis, "The effect of entanglements in rubber elasticity," *Polymer*, vol. 27, pp. 482–492, 1986.

[263] S. F. Edwards and T. A. Vilgis, "The tube model theory of rubber elasticity," *Reports on Progress in Physics*, vol. 51, pp. 243–297, 1988.

[264] P. J. Flory and J. Rehner, "Statistical mechanics of cross-linked polymer networks I. Rubberlike elasticity," *The Journal of Chemical Physics*, vol. 11, pp. 512–520, 1943.

[265] P. J. Flory, *Principles of polymer chemistry*. Cornell University Press, 1953.

[266] H. M. James and E. Guth, "Theory of the elastic properties of rubber," *The Journal of Chemical Physics*, vol. 11, pp. 455–481, 1943.

[267] P. J. Flory, "Molecular theory of rubber elasticity," *Polymer Journal*, vol. 17, pp. 1–12, 1985.

[268] M. Rubinstein and S. Panyukov, "Nonaffine deformation and elasticity of polymer networks," *Macromolecules*, vol. 30, pp. 8036–8040, 1997.

[269] B. Bonavoglia, G. Storti, and M. Morbidelli, "Modeling of the sorption and swelling behavior of semicrystalline polymers in supercritical CO_2," *Industrial and Engineering Chemistry Research*, vol. 45, pp. 1183–1200, 2006.

[270] M. A. Bashir, V. Monteil, V. Kanellopoulos, M. A. H. Ali, and T. McKenna, "Partial molar volumes and thermal expansion coefficients as an explanation for cosolvent effect of penetrants in multicomponent polymer mixtures," *Macromolecular Chemistry and Physics*, vol. 216, pp. 2129–2140, 2015.

[271] P. Memari, V. Lachet, M. H. Klopffer, B. Flaconnèche, and B. Rousseau, "Gas mixture solubilities in polyethylene below its melting temperature: Experimental and molecular simulation studies," *Journal of Membrane Science*, vol. 390-391, pp. 194–200, 2012.

[272] P. Memari, V. Lachet, and B. Rousseau, "Gas permeation in semicrystalline polyethylene as studied by molecular simulation and elastic model," *Oil and Gas Science and Technology*, vol. 70, pp. 227–235, 2015.

[273] M. Fischlschweiger, A. Danzer, and S. Enders, "Predicting gas solubility in semicrystalline polymer solvent systems by consistent coupling of Sanchez-Lacombe EoS with a continuum mechanics approach," *Fluid Phase Equilibria*, vol. 506, p. 112379, 2020.

[274] R. Androsch and B. Wunderlich, "Reversible crystallization and melting at the lateral surface of isotactic polypropylene crystals," *Macromolecules*, vol. 34, pp. 5950–5960, 2001.

[275] J. des Cloizeaux, "A theory of the influence of branching on the crystallinity of bulk polyethylene," *Journal of Polymer Science Part A-2: Polymer Physics*, vol. 8, pp. 1773–1786, 1970.

[276] E. F. Casassa, "Equilibrium distribution of flexible polymer chains between a macroscopic solution phase and small voids," *Journal of Polymer Science Part B: Polymer Letters*, vol. 5, pp. 773–778, 1967.

[277] F. Doghieri and G. C. Sarti, "Nonequilibrium lattice fluids: a predictive model for the solubility in glassy polymers," *Macromolecules*, vol. 29, pp. 7885–7896, 1996.

[278] F. Doghieri, M. Quinzi, D. G. Rethwisch, and G. C. Sarti, "Predicting gas solubility in glassy polymers through nonequilibrium EOS," *Advanced Materials for Membrane Separations*, pp. 74–90, 2004.

[279] E. A. DiMarzio and R. J. Rubin, "Adsorption of a chain polymer between two plates," *The Journal of Chemical Physics*, vol. 55, pp. 4318–4336, 1971.

[280] A. Vrij, "Polymers at interfaces and the interactions in colloidal dispersions," *Pure and applied chemistry*, vol. 48, no. 4, pp. 471–483, 1976.

[281] Y.-X. Yu and J. Wu, "Density functional theory for inhomogeneous mixtures of polymeric fluids," *The Journal of chemical physics*, vol. 117, no. 5, pp. 2368–2376, 2002.

[282] S.-C. Kim and P. T. Cummings, "Adsorption properties of a colloid-polymer mixture confined in a slit pore," *Phys. Rev. E*, vol. 64, p. 041507, 2001.

[283] B. J. Schindler, L. A. Mitchell, C. McCabe, P. T. Cummings, and M. D. LeVan, "Adsorption of chain molecules in slit-shaped pores: Development of a SAFT–FMT–DFT approach," *The Journal of Physical Chemistry C*, vol. 117, no. 41, pp. 21337–21350, 2013.

[284] L. A. Mitchell, B. J. Schindler, G. Das, M. C. dos Ramos, C. McCabe, P. T. Cummings, and M. D. LeVan, "Prediction of n-alkane adsorption on activated carbon using the SAFT–FMT–DFT approach," *The Journal of Physical Chemistry C*, vol. 119, no. 3, pp. 1457–1463, 2015.

[285] C. Panayiotou and I. C. Sanchez, "Swelling of network structures," *Polymer*, vol. 33, pp. 5090–5093, 1992.

[286] F. J. Lanyi, N. Wenzke, J. Kaschta, and D. W. Schubert, "On the determination of the enthalpy of fusion of α-crystalline isotactic polypropylene using differential scanning calorimetry, X-ray diffraction, and Fourier-Transform Infrared Spectroscopy: An old story revisited," *Advanced Engineering Materials*, vol. 22, 2020.

[287] B. Wunderlich and G. Czornyj, "A study of equilibrium melting of polyethylene," *Macromolecules*, vol. 10, pp. 906–913, 1977.

[288] H. Asakawa, K. Nishida, T. Kanaya, and M. Tosaka, "Giant single crystal of isotactic polypropylene showing near-equilibrium melting temperature," *Polymer Journal*, vol. 45, pp. 287–292, 2013.

[289] K. Yamada, M. Hikosaka, A. Toda, S. Yamazaki, and K. Tagashira, "Equilibrium melting temperature of isotactic polypropylene with high tacticity: 1. Determination by differential scanning calorimetry," *Macromolecules*, vol. 36, pp. 4790–4801, 2003.

[290] J. E. Mark and P. J. Flory, "The configuration of the polyoxyethylene chain," *Journal of the American Chemical Society*, vol. 87, pp. 1415–1423, 1965.

[291] S. Yang, Z. Liu, Y. Liu, and Y. Jiao, "Effect of molecular weight on conformational changes of PEO: an infrared spectroscopic analysis," *Journal of Materials Science*, vol. 50, pp. 1544–1552, 2015.

[292] A. A. Krauskopf, A. M. Jimenez, E. A. Lewis, B. D. Vogt, A. J. Müller, and S. K. Kumar, "Mechanisms of directional polymer crystallization," *ACS Macro Letters*, vol. 9, pp. 1007–1012, 2020.

[293] J. Kleis, B. I. Lundqvist, D. C. Langreth, and E. Schröder, "Towards a working density-functional theory for polymers: First-principles determination of the polyethylene crystal structure," *Physical Review B - Condensed Matter and Materials Physics*, vol. 76, pp. 2–5, 2007.

[294] M. H. Kim and C. J. Glinka, "Correlation between structure and vapor sorption in semicrystalline linear polyethylene: one dimensional nano-swelling measured using in situ vapor sorption small angle neutron scattering (iVSANS)," *Macromolecules*, vol. 42, pp. 2618–2625, 2009.

[295] H. M. Thijs, C. R. Becer, C. Guerrero-Sanchez, D. Fournier, R. Hoogenboom, and U. S. Schubert, "Water uptake of hydrophilic polymers determined by a thermal gravimetric analyzer with a controlled humidity chamber," *Journal of Materials Chemistry*, vol. 17, pp. 4864–4871, 2007.

[296] J. R. Isasi, L. Mandelkern, M. J. Galante, and R. G. Alamo, "The degree of crystallinity of monoclinic isotactic poly(propylene)," *Journal of Polymer Science, Part B: Polymer Physics*, vol. 37, pp. 323–334, 1999.

[297] L. M. Robeson, "Correlation of separation factor versus permeability for polymeric membranes," *Journal of membrane science*, vol. 62, no. 2, pp. 165–185, 1991.

[298] B. D. Freeman and I. Pinnau, "Gas and liquid separations using membranes: an overview," *ACS Symposium Series*, vol. 876, 2004.

[299] C. De Rosa, F. Auriemma, O. Ruiz de Ballesteros, L. Resconi, and I. Camurati, "Crystallization behavior of isotactic propylene- ethylene and propylene- butene copolymers: effect of comonomers versus stereodefects on crystallization properties of isotactic polypropylene," *Macromolecules*, vol. 40, no. 18, pp. 6600–6616, 2007.

[300] M. L. D. Santos, N. F. Correa, and D. M. Leitao, "Interaction of polyethylene with isobutane, isobutylene, l-butene and normal butane," *Journal of Colloid and Interface Science*, vol. 47, pp. 621–627, 1974.

[301] C. Kiparissides, V. Dimos, T. Boultouka, A. Anastasiadis, and A. Chasiotis, "Experimental and theoretical investigation of solubility and diffusion of ethylene in semicrystalline PE at elevated pressures and temperatures," *Journal of Applied Polymer Science*, vol. 87, pp. 953–966, 2003.

[302] M. Lopez-Gonzalez, V. Compan, and E. Riande, "Gas sorption in semicrystalline rubbery polymers revisited," *Journal of Applied Polymer Science*, vol. 105, pp. 903–907, 2007.

[303] S. J. Moore and S. E. Wanke, "Solubility of ethylene, 1-butene and 1-hexene in polyethylenes," *Chemical Engineering Science*, vol. 56, pp. 4121–4129, 2001.

[304] A. B. Mrad, S. Norsic, N. Sheibat-Othman, and T. F. McKenna, "Multicomponent solubility of vapors in polyethylene: An experimental and theoretical analysis," *Industrial and Engineering Chemistry Research*, vol. 60, pp. 10791–10806, 2021.

[305] N. V. Solms, J. K. Nielsen, O. Hassager, A. Rubin, A. Y. Dandekar, S. I. Andersen, and E. H. Stenby, "Direct measurement of gas solubilities in polymers with a high-pressure microbalance," *Journal of Applied Polymer Science*, vol. 91, pp. 1476–1488, 2003.

[306] J. san Yoon, H.-S. Yoo, and K.-S. Kang, "Solubility of alpha-olefins in linear low density polyethylenes," *European Polymer Journal*, vol. 32, pp. 1333–1336, 1996.

[307] "PlotDigitizer: Version 3.1.5." `https://plotdigitizer.com`, 2023.

[308] R. F. Alves and T. F. McKenna, "Estimation of diffusion coefficients for multiple penetrant/polyolefin systems based on sorption data," *Chemical Engineering Journal*, vol. 383, p. 123114, 2020.

[309] S. Laugier, D. Richon, and H. Renon, "Ethylene + olefin binary systems: Vapor-liquid equilibrium experimental data and modeling," *Journal of Chemical & Engineering Data*, vol. 39, no. 2, pp. 388–391, 1994.

[310] T. V. Duong, G. Reekmans, A. Venkatesham, A. V. Aerschot, P. Adriaensens, J. V. Humbeeck, and G. V. D. Mooter, "Spectroscopic investigation of the formation and disruption of hydrogen bonds in pharmaceutical semicrystalline dispersions," *Molecular Pharmaceutics*, vol. 14, pp. 1726–1741, 2017.

[311] T. V. Duong, B. Goderis, J. V. Humbeeck, and G. V. D. Mooter, "Microstructure of pharmaceutical semicrystalline dispersions: The significance of polymer conformation," *Molecular Pharmaceutics*, vol. 15, pp. 629–641, 2018.

[312] K. Pielichowski and K. Flejtuch, "Differential scanning calorimetry studies on poly(ethylene glycol) with different molecular weights for thermal energy storage materials," *Polymers for Advanced Technologies*, vol. 13, pp. 690–696, 2002.

[313] A. J. Kovacs, "Isothermal growth, thickening and melting of poly(ethylene-oxide) single crystals in the bulk: III. bilayer crystals and the effect of chain ends," *Journal of Crystal Growth*, vol. 48, pp. 210–226, 1980.

[314] S. Z. Cheng and B. Wunderlich, "Study of crystallization of low molecular mass poly(ethylene oxide) from the melt," *Macromolecules*, vol. 22, pp. 1866–1873, 1989.

[315] S. Z. Cheng, A. Zhang, J. Chen, and D. P. Heberer, "Nonintegral and integral folding crystal growth in low-molecular mass poly(ethylene oxide) fractions. I. Isothermal lamellar thickening and thinning," *Journal of Polymer Science Part B: Polymer Physics*, vol. 29, pp. 287–297, 1991.

[316] S. Z. Cheng, J. Chen, A. Zhang, and D. P. Heberer, "Nonintegral and integral folding crystal growth in low-molecular mass poly (ethylene oxide) fractions. II. End-group effect: α,ω-methoxy-poly (ethylene oxide)," *Journal of Polymer Science Part B: Polymer Physics*, vol. 29, pp. 299–310, 1991.

[317] S. Z. Cheng and J. Chen, "Nonintegral and integral folding crystal growth in low-molecular mass poly (ethylene oxide) fractions. III. Linear crystal growth rates and crystal morphology," *Journal of Polymer Science Part B: Polymer Physics*, vol. 29, pp. 311–327, 1991.

[318] J. Spěváček and J. Baldrian, "Solid-state ^{13}C NMR and SAXS characterization of the amorphous phase in low-molecular weight poly(ethylene oxide)s," *European Polymer Journal*, vol. 44, pp. 4146–4150, 2008.

[319] S. H. Huang and M. Radosz, "Equation of state for small, large, polydisperse, and associating molecules," *Industrial and Engineering Chemistry Research*, vol. 29, pp. 2284–2294, 1990.

[320] M. A. Al-Nasassrah, F. Podczeck, and J. M. Newton, "The effect of an increase in chain length on the mechanical properties of polyethylene glycols," *European Journal of Pharmaceutics and Biopharmaceutics*, vol. 46, pp. 31–38, 1998.

[321] K. Ishikiriyama and B. Wunderlich, "Crystallization and melting of poly(oxyethylene) analyzed by temperature-modulated calorimetry," *Journal of Polymer Science Part B: Polymer Physics*, vol. 35, pp. 1877–1886, 1997.

[322] L. G. Beekmans, D. W. V. der Meer, and G. J. Vancso, "Crystal melting and its kinetics on poly(ethylene oxide) by in situ atomic force microscopy," *Polymer*, vol. 43, pp. 1887–1895, 2002.

[323] G. Strobl, "A thermodynamic multiphase scheme treating polymer crystallization and melting," *European Physical Journal E*, vol. 18, pp. 295–309, 2005.

[324] A. J. Haslam, N. von Solms, C. S. Adjiman, A. Galindo, G. Jackson, P. Paricaud, M. L. Michelsen, and G. M. Kontogeorgis, "Predicting enhanced absorption of light gases in polyethylene using simplified PC-SAFT and SAFT-VR," *Fluid Phase Equilibria*, vol. 243, pp. 74–91, 2006.

[325] J. M. Jenkins, R. L. Jones, T. M. Jones, and S. Beret, "Method for fluidised bed polymerisation," 1985. US4588790.

[326] R. Evans, "The nature of the liquid-vapour interface and other topics in the statistical mechanics of non-uniform, classical fluids," *Advances in physics*, vol. 28, no. 2, pp. 143–200, 1979.

[327] J. Liu, L. Wang, S. Xi, D. Asthagiri, and W. G. Chapman, "Adsorption and phase behavior of pure/mixed alkanes in nanoslit graphite pores: an iSAFT application," *Langmuir*, vol. 33, no. 42, pp. 11189–11202, 2017.

[328] P. Rehner, T. V. Westen, and J. Gross, "Equation of state and helmholtz energy functional for fused heterosegmented hard chains," *Physical Review E*, vol. 105, 2022.

[329] P. G. de Gennes, "Conformations of polymers attached to an interface," *Macromolecules*, vol. 13, pp. 1069–1075, 1980.

[330] S. Z. Cheng, M. Cao, and B. Wunderlich, "Glass transition and melting behavior of poly (oxy-1, 4-phenyleneoxy-1, 4-phenylenecarbonyl-1, 4-phenylene)(PEEK)," *Macromolecules*, vol. 19, no. 7, pp. 1868–1876, 1986.

[331] J. R. Brown and B. C. Ennis, "Thermal analysis of Nomex® and Kevlar® fibers," *Textile Research Journal*, vol. 47, no. 1, pp. 62–66, 1977.

A. SAFT Combining Rules

In SAFT the segment size and hard-sphere diameters follow the Lorentz (arithmetic mean) combining rule, i.e.

$$\begin{aligned} \sigma_{kl} &= \frac{\sigma_{kk} + \sigma_{ll}}{2} \\ d_{kl} &= \frac{d_{kk} + d_{ll}}{2} \end{aligned}. \tag{A.1}$$

If we postulate a geometric combining rule for the (unmodified) van der Waals constants this assumption determines[66] the form of the combining rule for the unlike interaction energies ϵ_{kl} and the unlike repulsive exponents λ^r_{kl}:

$$\begin{aligned} \epsilon_{kl} &= \frac{\sqrt{\sigma^3_{kk}\sigma^3_{ll}}}{\sigma^3_{kl}}\sqrt{\epsilon_{kk}\epsilon_{ll}} \\ \lambda^r_{kl} &= 3 + \sqrt{\left(\lambda^r_{kk} - 3\right)\left(\lambda^r_{ll} - 3\right)} \end{aligned}. \tag{A.2}$$

Last, the combining rules for the association parameters (which weren't used in our work) are given by

$$\begin{aligned} \epsilon^{HB}_{kl} &= \sqrt{\epsilon_{kk}\epsilon_{ll}} \\ K^{HB}_{kl,ab} &= \left(\frac{\sqrt[3]{K^{HB}_{kk,aa}} + \sqrt[3]{K^{HB}_{ll,bb}}}{2}\right)^3 \end{aligned} \tag{A.3}$$

B. Solubility Reduction Under Constraint Pressure

We are interested the variation of the equilibrium solubility as P_c is increased at constant $T, P, \boldsymbol{\mu}_\mathrm{s}$. By inversion of the relationship between between $\boldsymbol{S}_\mathrm{a}$ and $\boldsymbol{\mu}_\mathrm{s}$ defined by Equation 3.35* and using the implicit function theorem we obtain in matrix representation

$$\left(\frac{\partial \boldsymbol{S}_\mathrm{a}}{\partial P_\mathrm{c}}\right)_{T,P,\boldsymbol{\mu}_\mathrm{s}} = -\left[\left(\frac{\partial \boldsymbol{\mu}_\mathrm{s}}{\partial \boldsymbol{S}_\mathrm{a}}\right)_{T,P,P_\mathrm{c}}\right]^{-1}\left(\frac{\partial \boldsymbol{\mu}_\mathrm{s}}{\partial P_\mathrm{c}}\right)_{T,P,\boldsymbol{S}_\mathrm{a}}. \tag{B.1}$$

The first term on the right hand side is the inverse of the jacobian of the transformation $\boldsymbol{S}_\mathrm{a} \to \boldsymbol{\mu}_\mathrm{s}$ in Equation 3.35, given by

$$\left[\left(\frac{\partial \boldsymbol{\mu}_\mathrm{s}}{\partial \boldsymbol{S}_\mathrm{a}}\right)_{T,P,P_\mathrm{c}}\right]^{-1} = \begin{bmatrix} \frac{\partial \mu^{\mathrm{EoS}}_{\mathrm{s},1}}{\partial S_{\mathrm{a},1}}(T, P+P_\mathrm{c}, \boldsymbol{S}_\mathrm{a}) & \dots & \frac{\partial \mu^{\mathrm{EoS}}_{\mathrm{s},1}}{\partial S_{\mathrm{a},N_\mathrm{C}}}(T, P+P_\mathrm{c}, \boldsymbol{S}_\mathrm{a}) \\ \vdots & \ddots & \vdots \\ \frac{\partial \mu^{\mathrm{EoS}}_{\mathrm{s},N_\mathrm{C}}}{\partial S_{\mathrm{a},1}}(T, P+P_\mathrm{c}, \boldsymbol{S}_\mathrm{a}) & \dots & \frac{\partial \mu^{\mathrm{EoS}}_{\mathrm{s},N_\mathrm{C}}}{\partial S_{\mathrm{a},N_\mathrm{C}}}(T, P+P_\mathrm{c}, \boldsymbol{S}_\mathrm{a}) \end{bmatrix}^{-1}. \tag{B.2}$$

*This can always be done in a neighborhood of each $(\boldsymbol{S}_\mathrm{a}, \boldsymbol{\mu}_\mathrm{s})$ solution of equation 3.35 at fixed T, P as long as the determinant of the Jacobian of the transformation $\boldsymbol{S}_\mathrm{a} \leftrightarrow \boldsymbol{\mu}_{\mathrm{s},i}$ and the derivatives with respect to constraint pressure are defined and different from zero.

This matrix multiplies the column vector

$$\left(\frac{\partial \boldsymbol{\mu}_{\mathrm{s}}}{\partial P_{\mathrm{c}}}\right)_{T,P,\boldsymbol{S}_{\mathrm{a}}} = \begin{pmatrix} \frac{\partial \mu^{\mathrm{EoS}}_{\mathrm{s},1}}{\partial P}\left(T, P+P_{\mathrm{c}}, \boldsymbol{S}_{\mathrm{a}}\right) \\ \vdots \\ \frac{\partial \mu^{\mathrm{EoS}}_{\mathrm{s},N_{\mathrm{C}}}}{\partial P}\left(T, P+P_{\mathrm{c}}, \boldsymbol{S}_{\mathrm{a}}\right) \end{pmatrix} \tag{B.3}$$

to yield the vector of derivatives on the left-hand side of B.1. Since $\boldsymbol{\mu}^{\mathrm{EoS}}_{\mathrm{s}}$ is the vector of solute chemical potentials of an equilibrium polymer + solutes mixture at temperature T, pressure $P + P_{\mathrm{c}}$ and composition $\boldsymbol{S}_{\mathrm{a}}$, by using a Maxwell relation and denoting with $\boldsymbol{n}_{\mathrm{s}}$ the (vector of) moles of solutes in the amorphous domains we find that

$$\frac{\partial \mu^{\mathrm{EoS}}_{\mathrm{s},i}}{\partial P}\left(T, P+P_{\mathrm{c}}, \boldsymbol{S}_{\mathrm{a}}\right) = \frac{\partial V^{\mathrm{EoS}}}{\partial n_{\mathrm{s},i}}\left(T, P+P_{\mathrm{c}}, \boldsymbol{S}_{\mathrm{a}}\right) = \bar{V}^{\mathrm{EoS}}_{\mathrm{s},i}\left(T, P+P_{\mathrm{c}}, \boldsymbol{S}_{\mathrm{a}}\right), \tag{B.4}$$

where $\bar{V}^{\mathrm{EoS}}_{\mathrm{s},i}$ is the partial molar volume of solute i in the polymer + solutes mixtures and V^{EoS} the equilibrium volume of the mixture calculated through the equation of state (*cf.* Equation 3.33).

In the infinite dilution (Henry) regime, we expect

$$\mu^{\mathrm{EoS}}_{\mathrm{s},i}(T, P+P_{\mathrm{c}}, \boldsymbol{S}_{\mathrm{a}}) \sim \mu^{\mathrm{H,EoS}}_{\mathrm{s},i}(T, P+P_{\mathrm{c}}) + RT \ln S_{\mathrm{a},i} \tag{B.5}$$

asymptotically as $\boldsymbol{S}_{\mathrm{a}} \to \boldsymbol{0}$. Here $\mu^{\mathrm{H,EoS}}_{\mathrm{s},i}$ is the Henry chemical potentials of solute i in the polymer calculated using the fluid EoS at infinite dilution[†]. In this limit the matrix in Equation B.2 is diagonal as for $i = j$ we obtain

$$\left(\frac{\partial \mu^{\mathrm{EoS}}_{\mathrm{s},i}}{\partial S_{\mathrm{a},i}}\right)\left(T, P+P_{\mathrm{c}}, \boldsymbol{S}_{\mathrm{a}}\right) \sim RT/S_{\mathrm{a},i}, \tag{B.6}$$

[†]To be precise, this a the *definition* of the Henry chemical potential which depends on the fact that $S_{\mathrm{a},i}$ was chosen as a variable instead of, e.g., the number of solute molecules $n_{\mathrm{s},i}$

whereas the $i \neq j$ derivatives are zero. Combining Equations B.1, B.4 and B.5 yields

$$\left(\frac{\partial \ln S_{\mathrm{a},i}}{\partial P_{\mathrm{c}}}\right)_{T,P,\boldsymbol{\mu}_{\mathrm{s}}} \sim -\frac{\bar{V}_{\mathrm{s},i}^{\mathrm{EoS}}}{RT} \tag{B.7}$$

asymptotically as $\boldsymbol{S}_{\mathrm{a}} \to \mathbf{0}$. In particular, in the Henry regime (which is valid for low to moderate pressures – see Chapter 4) the equilibrium solubility decreases at increasing constraint pressure since the partial molar volume is generally positive for molecules of non-ionic mixtures[‡].

[‡]To be precise, mixtures of nonionic species near the critical point can display negative partial molar volumes – see for example the ethylene + 1-hexene mixture giving rise to unique sorption isotherms (Figure 4.17)

C. Monomer Chemical Potential

In order to simplify derivatives with respect to the number of chain monomers, in this work we exploit the intuitive notion that for long polymer chains certain properties of a polymer + solute mixture should only depend on temperature, pressure and the mass fraction of solute, regardless of the molecular weight n of the polymer. For example, the polymer chemical potential *per monomer* – i.e., the "monomer chemical potential" – in a monodisperse polymer mixture is here defined as follows:

$$\mu_{\mathrm{p,mono}}^{(n),\mathrm{EoS}} := \frac{1}{n}\mu_{\mathrm{p}}^{(n),\mathrm{EoS}}. \tag{C.1}$$

In this equation n is the number of monomers comprising the polymer chains and $\mu_{\mathrm{p}}^{(n),\mathrm{EoS}}$ is the "standard" chemical potential of the polymer in the mixture (*cf.* Section 2.3). For polydisperse mixtures, the monomer chemical potential can be calculated for each distinct polymer molecule by dividing its chemical potential in the mixture by its number of monomers.

As anticipated, $\mu_{\mathrm{p,mono}}^{(n),\mathrm{EoS}}$ is independent of n as $n \to \infty$ at fixed temperature, pressure and mass fraction of solute. In Figure C.1 we show that at fixed temperature and pressure, using the SAFT-γ Mie model of Papaioannou and coworkers[67] for a mixture of n-hexane and polyethylene the dependence of $\mu_{\mathrm{p}}^{(n),\mathrm{EoS}}/n$ on the weight fraction ω_{s} of n-heptane is not significantly influenced by the number of polymer repeat units for $n > 100$.

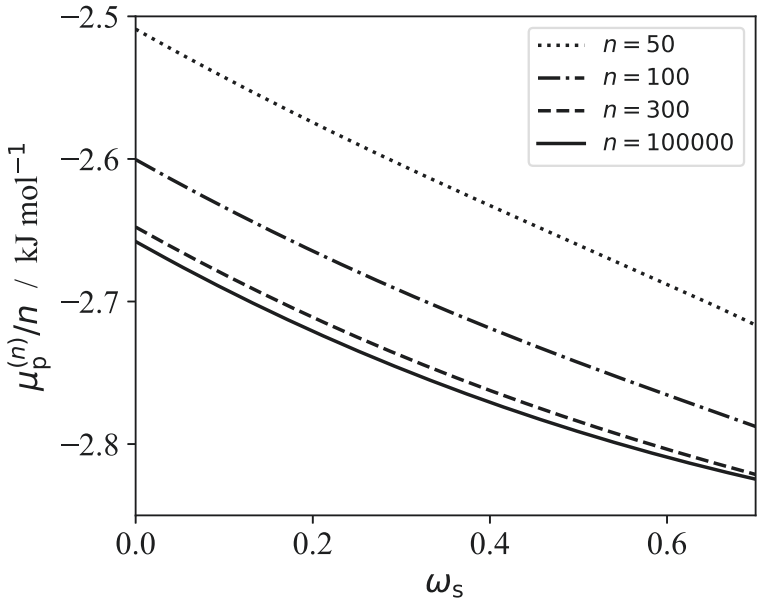

Figure C.1.: The dependence of $\mu_{\mathrm{p}}^{(n)}/n$ in a mixture of n-heptane and polyethylene (see Equation C.1) on the mass fraction ω_{s} of n-heptane as a function of the number n of methylene monomers in the polymer, as calculated using the SAFT-γ Mie model of Papaioannou and co-workers[67] at 300K and 1 bar. We note that $\mu_p^{(n)}/n$ approaches the continuous curve ($n = 100,000$) very rapidly for $n > 100$.

D. Mass Balances in the Inter-Lamellar Domains

The inter-lamellar amorphous polymer mass $m_{\mathrm{p}}^{\mathrm{IL}}$ can in general be divided into two contributions: the mass of elastically ineffective molecules (tails and un-entangled loops) $m_{\mathrm{p,NT}}^{\mathrm{IL}}$; and the mass of tie-molecules $m_{\mathrm{p,T}}^{\mathrm{IL}}$. In our model, $m_{\mathrm{p,T}}^{\mathrm{IL}}$ can be expressed as

$$m_{\mathrm{p,T}}^{\mathrm{IL}} = M_0 A_{\Sigma} \rho_{\mathrm{A,T}} n_{\mathrm{T}}, \tag{D.1}$$

where M_0 is the molar mass of the monomer characterizing the polymer. Since $x_{\mathrm{T}} = R_{\mathrm{ee,T}}/R_{\max}$ and $R_{\max} = \mathcal{N}_{\mathrm{b}} n_{\mathrm{T}} l \cos(\theta_B/2) = \mathcal{N}_{\mathrm{b}} n_{\mathrm{T}} l_{\mathrm{mono}}$ due to Equation 3.72, the average number of bridge monomers n_{T} satisfies $n_{\mathrm{T}} = R_{\mathrm{ee,T}}/(x_{\mathrm{T}} l_{\mathrm{mono}} \mathcal{N}_{\mathrm{b}})$. By substituting for n_{T}, using $R_{\mathrm{ee,T}} = l_{\mathrm{a}}/\cos\theta_{\mathrm{T}}$ and $\rho_{\mathrm{A,T}} = p_{\mathrm{T}}\rho_{\mathrm{A}}$ (neglecting chain-tilt, i.e. $\gamma = 0$) we can write

$$m_{\mathrm{p,T}}^{\mathrm{IL}} = \frac{l_{\mathrm{a}} M_0 A_{\Sigma} \rho_{\mathrm{A}} p_{\mathrm{T}}}{x_{\mathrm{T}} \cos\theta_{\mathrm{T}} l_{\mathrm{mono}} \mathcal{N}_{\mathrm{b}}}. \tag{D.2}$$

If the polymer segments in the lamellae are chain-extended (as in PE), $\rho_{\mathrm{c}}^{*} = M_0 \rho_{\mathrm{A}}/(\mathcal{N}_{\mathrm{b}} l_{\mathrm{mono}})$ is simply the mass density ρ_{c} of the lamellae. By combining this expression with Equation 3.97, using $V = A_{\Sigma} l_{\mathrm{a}}$ and $m_{\mathrm{p}}^{\mathrm{IL}} = m_{\mathrm{p,NT}}^{\mathrm{IL}} + m_{\mathrm{p,T}}^{\mathrm{IL}}$ the following expression is obtained:

$$1 = \frac{m_{\mathrm{p,NT}}^{\mathrm{IL}}}{m_{\mathrm{p}}^{\mathrm{IL}}} + \frac{p_{\mathrm{T}} \rho_{\mathrm{c}}^{*}}{\rho_{\mathrm{p,eff}}^{\mathrm{IL}} x_{\mathrm{T}} \cos\theta_{\mathrm{T}}}. \tag{D.3}$$

After defining $f_{\mathrm{T}} = 1 - (m_{\mathrm{p,NT}}^{\mathrm{IL}}/m_{\mathrm{p}}^{\mathrm{IL}})$ as the fraction of elastically effective polymer mass in the inter-lamellar domains (i.e., the free parameter in the Michaels and Hausslein theory, not to be confused with the average force $f_{\mathrm{ee,T}}$), Equation D.3 implies that

$$f_{\mathrm{T}} = \frac{p_{\mathrm{T}}\rho_{\mathrm{c}}^{*}}{\rho_{\mathrm{p,eff}}^{\mathrm{IL}} x_{\mathrm{T}} \cos\theta_{\mathrm{T}}} \rightarrow x_{\mathrm{T}} \cos\theta_{\mathrm{T}} = \frac{p_{\mathrm{T}}\rho_{\mathrm{c}}^{*}}{f_{\mathrm{T}}\rho_{\mathrm{p,eff}}^{\mathrm{IL}}}, \tag{D.4}$$

or equivalently

$$l_{\mathrm{a}}(T, P, \boldsymbol{n}_{\mathrm{s}}, n_{\mathrm{T}}; \nu_{\mathrm{T}}, \delta_{\mathrm{T}}) = \frac{M_0 \rho_{\mathrm{A,T}} n_{\mathrm{T}}}{f_{\mathrm{T}}\rho_{\mathrm{p,eff}}^{\mathrm{IL}}}. \tag{D.5}$$

E. Loops and Entanglements

In this Appendix the model for the inter-lamellar domains developed in Section 3.3.3 is extended to include entangled and un-entangled loops.

E.1. Free energy

Let us assume that the inter-lamellar domains are composed of ν_{BR} bridges, ν_{L} un-entangled loops and ν_{EL} entangled loops. The free energy difference due to formation of bridges has been derived in Section 3.3.3 (Equation 3.69).

The contribution of un-entangled loops ($\Delta A_{\mathrm{L}}^{\mathrm{c}}$) can be obtained in the same way as that of the bridges:

$$\Delta A_{\mathrm{L}}^{\mathrm{c}} \approx -k_{\mathrm{B}}T\left(\nu_{\mathrm{L}} \ln\left(p_{\mathrm{ee}}\left(R_{\mathrm{ee,L}}\right)\Delta\tau\right) + \nu_{\mathrm{L}} \ln\left(\frac{\Delta\tau}{V}\right)\right), \tag{E.1}$$

where $R_{\mathrm{ee,L}}$ is their average end-to-end distance and terms that are only temperature dependent have here been neglected.

The other term that has to be evaluated is the Helmholtz free energy of formation of the entangled loops in the inter-lamellar domains, $\Delta A_{\mathrm{EL}}^{\mathrm{c}}$. Following Mansfield[199] and Albrecht and Strobl,[200] we assume that the entanglements between different loops

can be treated as network junctions that on average subdivide each entangled loop in m entangled segments (ES). With this approximation, $\Delta A^{\mathrm{c}}_{\mathrm{EL}}$ is the free energy of formation of a tetrafunctional network which Flory[259] gave as:

$$\Delta A^{\mathrm{c}}_{\mathrm{EL}} \approx -k_{\mathrm{B}}T\left(\nu_{\mathrm{ES}} \ln\left(p_{\mathrm{ee}}\left(R_{\mathrm{ee,ES}}\right)\Delta\tau^{'}\right) + \frac{3\nu_{\mathrm{ES}}}{2}\ln\left(\frac{\Delta\tau^{'}}{V}\right)\right), \tag{E.2}$$

In Equation E.2, $\Delta\tau^{'}$ is a hypothetical volume in which the ends of the entangled segments are confined assuming they maintain a point of contact. Furthermore, $\nu_{\mathrm{ES}} = m\nu_{\mathrm{EL}}$ is the number of entangled segments and $R_{\mathrm{ee,ES}}$ their average end-to-end distance. The factor $\nu_{\mathrm{ES}} \ln\left(p_{\mathrm{ee}}\left(R_{\mathrm{ee,ES}}\right)\Delta\tau^{'}\right)$ in Equation E.2 is not present in Flory's original work since it was assumed that the average end-to-end distance of the chain segments in the melt is unchanged upon cross-linking.

This expression is derived for chemically cross-linked networks, and thus neglects the fact that the junctions in the entangled network are actually slip-links[200] that can change the length of the corresponding entangled segments due to their motion. Using a mean-field argument and a simplified expression, Albrecht and Strobl[200] proposed that a combinatorial term should be added to the network term in order to account for the number of ways the junctions in the network can be arranged; if n_{ES} is the average number of monomers per entangled segment, they obtained an entropic contribution in the form $\Delta S \approx mk_{\mathrm{B}} \ln n_{\mathrm{ES}} + C$ where C is a function of the number of entangled segments per loop (m). Here, these considerations are neglected: if the polymer is crystal-fixed, m or n_{ES} should not change and thus the term of Albrecht and Strobl is a constant in the free energy of the inter-lamellar amorphous domains. If the polymer is crystal-mobile, on the other hand, the addition of such a term does not impact the local equilibrium at low temperatures significantly, as is briefly discussed in Section 3.3.3.

E.2. Constraint pressure

With the addition of the free energy of formation of loops, the constraint pressure is obtained like in Section 3.3.3:

$$\begin{aligned} P_{\mathrm{c}} &= \left(\frac{\partial \Delta A^{\mathrm{c}}}{\partial V}\right)_{T,\boldsymbol{n}_{\mathrm{s}},n_{\mathrm{T}},\nu_{\mathrm{T}},\boldsymbol{\Gamma}_{\mathrm{c}}} \\ &= \sum_{i\in\{\mathrm{BR,L,ES}\}} \left(\nu_i \frac{\partial R_{\mathrm{ee},i}}{\partial V}\right)_{\boldsymbol{\Gamma}_{\mathrm{c}}} f_{\mathrm{ee},i} + \frac{k_{\mathrm{B}}T\left(\nu_{\mathrm{BR}} + \nu_{\mathrm{L}} + \frac{3}{2}\nu_{\mathrm{ES}}\right)}{V}. \\ &= P_{\mathrm{el}} + P_{\mathrm{loc}} \end{aligned} \tag{E.3}$$

Here, the subscript "BR" indicates the bridges and $f_{\mathrm{ee},i} = -k_{\mathrm{B}}T\left(\partial \ln p_{\mathrm{ee}}/\partial R_{\mathrm{ee},i}\right)_{T,\boldsymbol{n}_{\mathrm{s}},n_{\mathrm{T}},\nu_{\mathrm{T}}}$. The partial derivative for the bridge terms has been performed in Section 3.92. For unentangled loops, on the other hand, $\left(\partial R_{\mathrm{ee,L}}/\partial V\right)_{\boldsymbol{\Gamma}_{\mathrm{c}}} = 0$.

In order to obtain an expression for the elastic contribution of the entangled loops, we assume for simplicity that all polymer segments between entanglements are identical and that the entanglement points move affinely with the inter-lamellar mass upon swelling.[199,200] By calling δ_{ES} the projection of the end-to-end vector of the entangled segments on the lamellar surface and θ_{ES} the angle with the normal to the lamellar surface, the following holds:

$$\begin{aligned} \cos\theta_{\mathrm{ES}} &\approx (l_{\mathrm{a}}/m)/\sqrt{(l_{\mathrm{a}}/m)^2 + \delta_{\mathrm{ES}}^2} \\ \left(\frac{\partial R_{\mathrm{ee,ES}}}{\partial V}\right)_{\boldsymbol{\Gamma}_{\mathrm{c}}} &= \frac{1}{A_\Sigma}\left(\frac{\partial R_{\mathrm{ee,ES}}}{\partial l_{\mathrm{a}}}\right)_{A_\Sigma} \\ &= \frac{1}{mA_\Sigma}\cos\theta_{\mathrm{ES}} \end{aligned} \quad . \tag{E.4}$$

Therefore, entangled loops gives rise to an additional term to P_{el}:

$$P_{\mathrm{el}} = \rho_{\mathrm{A,BR}} f_{\mathrm{ee,BR}} \cos\theta_{\mathrm{BR}} + \rho_{\mathrm{A,EL}} f_{\mathrm{ee,ES}} \cos\theta_{\mathrm{ES}}. \tag{E.5}$$

Here $\rho_{\mathrm{A,BR}}$ and $\rho_{\mathrm{A,EL}}$ are the surface density of stems connected to bridges and entangled loops, respectively (defined in a similar way as the surface densities of equation 3.10). Note that the surface density of tie-molecules $\rho_{\mathrm{A,T}}$ is given by $\rho_{\mathrm{A,T}} = \rho_{\mathrm{A,BR}} + \rho_{\mathrm{A,EL}}$.

Due to the symmetry between the contribution of bridges and entangled loops to P_{el}, it is apparent that a system made of bridges and entangled loops with total surface density $\rho_{\mathrm{A,T}}$ can be functionally represented by an equivalent system made only of bridges with surface density $\rho_{\mathrm{A,T}}$.

Similarly, inclusion of loops in the theory gives rise to additional "ideal gas" terms to P_{loc} (Equation E.3):

$$P_{\mathrm{loc}} \approx \frac{RT\left(\nu_{\mathrm{BR}} + \nu_{\mathrm{L}} + \frac{3}{2}\nu_{\mathrm{ES}}\right)}{V} = \frac{RT}{l_{\mathrm{a}}}\rho_{\mathrm{A,BR+L+EL}} + \frac{RT\nu_{\mathrm{EL}}}{V}\left(\frac{3m}{2} - 1\right). \tag{E.6}$$

Now, $(m-1)\nu_{\mathrm{EL}}/2$ is the total number of entanglements (or "knots") ν_{e}, as each entanglement is shared among two entangled loops and there are $m-1$ entanglements per entangled loop (since m is the number of entangled segments per entangled loop). Hence, P_{loc} can be expressed in terms of the entanglement density $\rho_{\mathrm{e}} = \nu_{\mathrm{e}}/V$ as

$$P_{\mathrm{loc}} = \frac{RT}{l_{\mathrm{a}}}\left(\rho_{\mathrm{A,BR+L+EL}} + \frac{1}{2}\rho_{\mathrm{A,EL}}\right) + 3RT\rho_{\mathrm{e}}. \tag{E.7}$$

Since most stems on the lamellar surface are expected to perform a tight-fold back into the lamella,[160,201,265] $\left(\rho_{\mathrm{A,BR+L+EL}} + \frac{1}{2}\rho_{\mathrm{A,EL}}\right)$ should be smaller than ρ_{A}, the maximum amount of stems per unit surface on the lamellae (*cf.* Section 3.1.3). In PE the

maximum value of ρ_{A} can be inferred from the crystalline structure[293] corresponding to ~ 5.5 stems/nm^2; on the other hand, the typical value of inter-lamellar distance is $l_{\mathrm{a}} \sim 10$ nm.[155] Inserting these values into Equation E.7 yields at room temperature $RT\left(\rho_{\mathrm{A,BR+L+EL}} + \frac{1}{2}\rho_{\mathrm{A,EL}}\right)/l_{\mathrm{a}} < 2.5$ MPa.

Furthermore, if ρ_{mono} is the monomer density in the amorphous domains, the entanglement density satisfies $\rho_{\mathrm{e}} \leq \rho_{\mathrm{mono}}/(2n_{\mathrm{ES}})$, with the equality holding if there are only entangled loops in the inter-lamellar domains. Since the density of the amorphous domains of PE[168] is ~ 850 kg m^{-3} and the molecular weight of the methylene monomer is ~ 14 g mol^{-1}, $\rho_{\mathrm{mono}}^{\mathrm{PE}} \approx 6 \times 10^4$ mol m^{-3}. Additionally, although different estimates for n_{ES} have suggested,[230] when $n_{\mathrm{ES}} \approx 50$ is considered the upper bound $3RT\rho_{\mathrm{e}} \leq 4.5$ MPa is obtained at room temperature. Consequently, $P_{\mathrm{loc}} < 7$ MPa at room temperature, although its actual value is expected to be significantly smaller than the upper bound due to the nature of the approximations used to obtain this estimate.

Furthermore, we note that these results were obtained by assuming a chemically cross-linked network. P_{loc} should be reduced even further by treating the network junctions as slip-links (as done by Albrecht and Strobl[200]). Since the values of P_{c} found indirectly in the literature[44,45] are of the order of tens of MPa, we conclude that in our model $P_{\mathrm{el}} >> P_{\mathrm{loc}}$ and the approximation $P_{\mathrm{loc}} \approx \nu_{\mathrm{T}} k_{\mathrm{B}} T/V$ – which neglects the contribution of loops and substitutes every entangled loop with a bridge – should thus not affect the model significantly.

F. Derivatives of p_{ee} in the Langevin Approximation

In this Section the derivative of the end-to-end distribution in the Langevin approximation,

$$\left(\frac{\partial \ln p_{ee}}{\partial n_T}\right)_V = \left(\frac{\partial \ln p_{ee}^{FJ}}{\partial n_T}\right)_V, \tag{F.1}$$

appearing in Equation 3.104 is computed. In the following the subscript "T" of the tie-molecules will be dropped for clarity. Taking the derivative at constant volume and δ_T translates in a constant end-to-end distance due to Equation 3.61:

$$\left(\frac{\partial \ln p_{ee}^{FJ}}{\partial n}\right)_{R_{ee}}, \tag{F.2}$$

with p_{ee}^{FJ} given by Equation 3.74. Since $p_{ee}^{FJ} = p_{ee}^{FJ}(R_{ee}, N; b)$, with N being the number of equivalent Khun monomers, we have

$$\begin{aligned}\left(\frac{\partial \ln p_{ee}^{FJ}}{\partial n}\right)_{R_{ee}} &= \frac{dN}{dn}\left(\frac{\partial \ln p_{ee}^{FJ}}{\partial N}\right)_{R_{ee}} \\ &= \frac{1}{\eta}\left(\frac{\partial \ln p_{ee}^{FJ}}{\partial N}\right)_{R_{ee}}\end{aligned}. \tag{F.3}$$

Here $\eta = n/N = C_\infty / \left(\mathcal{N}_b \cos^2((\pi - \theta_B)/2)\right)$ (Equation 3.73).

Let's thus concentrate on the derivative with respect to N. Using the properties of logarithms and Equation 3.74, we have

$$\left(\frac{\partial \ln p_{\mathrm{ee}}^{\mathrm{FJ}}}{\partial N}\right)_{R_{\mathrm{ee}}} = \frac{d \ln C}{dN} - \frac{\partial}{\partial N}\left(N \int_0^{R_{\mathrm{ee}}/Nb} \mathcal{L}^{-1}(x)\mathrm{d}x\right). \tag{F.4}$$

We will first look at the second term on the right hand side of this equation. By using the fundamental theorem of calculus, the properties of derivatives and remembering that the derivative is taken at constant R_{ee} we obtain

$$\frac{\partial}{\partial N}\left(N \int_0^{\frac{R_{\mathrm{ee}}}{Nb}} \mathcal{L}^{-1}(x)\mathrm{d}x\right) = \int_0^{\frac{R_{\mathrm{ee}}}{Nb}} \mathcal{L}^{-1}(x)\mathrm{d}x - \frac{R_{\mathrm{ee}}}{Nb}\mathcal{L}^{-1}\left(\frac{R_{\mathrm{ee}}}{Nb}\right). \tag{F.5}$$

Let us define the fractional extension $x = R_{\mathrm{ee}}/Nb$ and change the dummy integration variable to x' to avoid confusion. Now, if $f(y)$ is a continuous invertible function on an interval $[a, b]$, $f^{-1}(y)$ is its inverse and $F(y)$ its primitive, we have

$$\int f^{-1}(y)dy = yf^{-1}(y) - F\left(f^{-1}(y)\right) + c, \tag{F.6}$$

where c is the integration constant. If we apply this lemma to equation F.5 and note that the primitive $F(y)$ of the Langevin function is

$$F(y) = \ln\left(\frac{\sinh y}{y}\right), \tag{F.7}$$

we obtain

$$\begin{aligned}\frac{\partial}{\partial N}\left(N \int_0^{\frac{R_{\mathrm{ee}}}{Nb}} \mathcal{L}^{-1}(x)\mathrm{d}x\right) &= \int_0^{x} \mathcal{L}^{-1}(x')\mathrm{d}x' - x\mathcal{L}^{-1}(x) \\ &= -\ln\left(\frac{\sinh \mathcal{L}^{-1}(x)}{\mathcal{L}^{-1}(x)}\right).\end{aligned} \tag{F.8}$$

Let's now evaluate the derivative $d\ln C/dN$ of Equation F.4. Since $C(N)$ is the normalization constant of $p_{\text{ee}}^{\text{FJ}}$, by performing a change of variables we can rewrite $C^{-1}(N)$ as follows:

$$\begin{aligned} C^{-1}(N) &= \int_0^{R_{\max}} 4\pi R^2 e^{-N\int_0^{R/Nb}\mathcal{L}^{-1}(x)\mathrm{d}x}\mathrm{d}R \\ &= 4\pi\,(Nb)^3 \int_0^1 x^2 e^{-N\int_0^x \mathcal{L}^{-1}(x')\mathrm{d}x'}\mathrm{d}x. \\ &= 4\pi\,(Nb)^3\, I(N) \end{aligned} \tag{F.9}$$

Differentiating, we obtain

$$\frac{d\ln C}{dN} = -\frac{3}{N} - \frac{d\ln I(N)}{dN}. \tag{F.10}$$

Let us then define the function $g(x)$ as

$$g(x) = \int_0^x \mathcal{L}^{-1}(x')\mathrm{d}x'. \tag{F.11}$$

Its MacLaurin series is given by

$$\begin{aligned} g(x) &= \frac{3}{2}x^2 + \frac{9}{20}x^4 + \frac{99}{350}x^6 + O(x^8) \\ &= c_2x^2 + c_4x^4 + c_6x^6 + O(x^8) \end{aligned}. \tag{F.12}$$

The term of lowest order in the expansion, $3x^2/2$, is the only one accounted for in the Gaussian approximation. Now we use the properties of exponentials to perform the factorization

$$e^{-N\int_0^x \mathcal{L}^{-1}(x')\mathrm{d}x'} = e^{-Ng(x)} = e^{-c_2Nx^2}e^{-N(c_4x^4+c_6x^6+c_8x^8+O(x^{10}))}. \tag{F.13}$$

By using the Maclaurin series of the exponential function,

$$e^y = 1 + y + \frac{1}{2}y^2 + \frac{1}{3!}y^3 + \cdots, \tag{F.14}$$

we obtain

$$e^{-N(c_4x^4+c_6x^6+c_8x^8+O(x^{10}))} = 1 - Nc_4x^4 - Nc_6x^6 + \left(\frac{N^2c_4^2}{2} - Nc_8\right)x^8 + \cdots \tag{F.15}$$

Here we have grouped the terms with the same power in x. In order to obtain the term of power n, the procedure is as follows:

- List all the possible ways in which you can obtain the number n by summing the degrees of the powers in x appearing in the MacLaurin expansion of $g(x)-c_2x^2$. For example, since the Maclaurin expansion of $g(x) - c_2x^2$ features only even powers greater or equal than 4, we can obtain the number $n = 12$ in four different ways: $12 = 4 + 4 + 4$, $12 = 8 + 4$, $12 = 6 + 6$, $12 = 12$.
- For each possible decomposition, write down a term obtained by multiplying factors c_i with multiplicity given by the decomposition. For example, write $c_4 \cdot c_4 \cdot c_4 = c_4^3$ for $12 = 4 + 4 + 4$ and $c_4 \cdot c_8$ for $12 = 8 + 4$
- Multiply each term by $(-N)$ to the power given by the total number of terms in the decomposition. For example, we multiply c_4^3 by $(-N)^3$ and c_4c_8 by $(-N)^2$
- Divide each term by a combinatorial factor obtained as follows: for each different c_i appearing in the term, multiply the factor by $k_i!$, where k_i is the multiplicity of that c_i factor in the term. For example, we divide the term $c_4^3c_6^2$ appearing in the decomposition of $n = 24$ by $(3! \cdot 2!) = 12$
- Sum all the terms

Now, since $I(N)$is given by

$$I(N) = \int_0^1 x^2 e^{-Ng(x)} \mathrm{d}x, \tag{F.16}$$

using the expansion just obtained we have

$$\begin{aligned} I(N) &= \int_0^1 x^2 e^{-c_2 N x^2} e^{-N(c_4 x^4 + c_6 x^6 + c_8 x^8 + \cdots)} \mathrm{d}x \\ &= \int_0^1 x^2 \left(1 - N c_4 x^4 - N c_6 x^6 + \left(\frac{N^2 c_4^2}{2} - N c_8\right) x^8 + \cdots\right) e^{-c_2 N x^2} \mathrm{d}x \\ &= \int_0^1 \left(x^2 - N c_4 x^6 - N c_6 x^8 + \left(\frac{N^2 c_4^2}{2} - N c_8\right) x^{10} + \cdots\right) e^{-c_2 N x^2} \mathrm{d}x \\ &= \int_0^1 x^2 e^{-c_2 N x^2} \mathrm{d}x - N c_4 \int_0^1 x^6 e^{-c_2 N x^2} \mathrm{d}x - N c_6 \int_0^1 x^8 e^{-c_2 N x^2} \mathrm{d}x + \cdots \end{aligned} . \tag{F.17}$$

All the integrals appearing in the final line of the equation above can be related as follows. Using Leibniz integral rule to differentiate under the integral and calling $\alpha = c_2 N$, we have

$$Q_k(\alpha) = \int_0^1 x^{2k} e^{-\alpha x^2} \mathrm{d}x = (-1)^k \frac{\partial^k}{\partial \alpha^k} \int_0^1 e^{-\alpha x^2} \mathrm{d}x = (-1)^k \frac{\partial^k}{\partial \alpha^k} Q_0(\alpha). \tag{F.18}$$

The integral $Q_0(\alpha)$ can be further split into the sum of two integrals:

$$\begin{aligned} Q_0(\alpha) &= \int_0^{+\infty} e^{-\alpha x^2} \mathrm{d}x - \int_1^{+\infty} e^{-\alpha x^2} \mathrm{d}x \\ &= A_0(\alpha) + B_0(\alpha) \end{aligned} . \tag{F.19}$$

The second integral in the equation above is related to the error function and it can be shown that both the integral and its derivatives in α decay exponentially as $\alpha \to +\infty$. Furthermore, exploiting the parity of $e^{-\alpha x^2}$ we get

$$A_0(\alpha) = \int_0^{+\infty} e^{-\alpha x^2} \mathrm{d}x = \frac{1}{2} \left(\frac{\pi}{\alpha}\right)^{\frac{1}{2}}. \tag{F.20}$$

Combining the equations above, we then have

$$\begin{aligned} Q_k(\alpha) &= (-1)^k \frac{\partial^k}{\partial \alpha^k} Q_0(\alpha) \\ &= \frac{(2k-1)!!}{2^{k+1}} \pi^{\frac{1}{2}} \alpha^{-\frac{1}{2}-k} + (-1)^k \frac{\partial^k}{\partial \alpha^k} \left(- \int_1^{+\infty} e^{-\alpha x^2} \mathrm{d}x \right) \\ &= \frac{(2k-1)!!}{2^{k+1}} \pi^{\frac{1}{2}} \left(c_2 N\right)^{-\frac{1}{2}-k} + B_k(c_2 N) \\ &= A_0(c_2 N) \frac{(2k-1)!!}{3^k} N^{-k} + B_k(c_2 N) \\ &= A_0(c_2 N) \left(a_k N^{-k} + \tilde{B}_k(c_2 N) \right) \end{aligned} \quad . \tag{F.21}$$

Here we have defined $\tilde{B}_k(\alpha) = (-1)^k \left(\frac{\partial^k}{\partial \alpha^k} B_0(\alpha) \right) / A_0(\alpha)$, $a_k = (2k-1)!!/3^k$ and we have used the fact that $c_2 = 3/2$. The two exclamation marks represent the double factorial (e.g., $5!! = 5 \cdot 3 \cdot 1$).

We can now use this expression to evaluate the series in Equation F.17. Since some terms are multiplied by powers of N, we need a little bit of care to group the terms according to their power in N. After performing this operation and stopping at third order in the expansion we have

$$I(N) = A_0(c_2 N) \left(a_1 N^{-1} - c_4 a_3 N^{-2} + \left(\frac{c_4^2 a_5}{2} - c_6 a_4 \right) N^{-3} + o(N^{-3}) \right). \tag{F.22}$$

Here we have used the little-o notation $o(N^{-3})$ to indicate a term that is vanishingly small with respect to N^{-3} as $N \to +\infty$. Notice that this quantity includes all the $\tilde{B}_k(c_2 N)$ terms generated by each integral in the series; all these terms decay exponentially as $N \to +\infty$, and will thus always be included in the little-o regardless of the order at which we decide to stop the expansion.

Substituting the values for c_k, a_k, writing $A_0(c_2 N)$ explicitly and regrouping we finally

have

$$I(N) = \left(\frac{\pi}{54}\right)^{\frac{1}{2}} N^{-\frac{3}{2}} \left(1 - \frac{3}{4}N^{-1} + \frac{13}{160}N^{-2} + o(N^{-2})\right). \tag{F.23}$$

Since we have to calculate $d\ln I/dN = I'(N)/I(N)$, we should perform the same operation for $I'(N)$ in order to find its asymptotic expansion in powers of N^{-1}. Here we note that we can obtain the expression for $I'(N)$ by formally differentiating the asymptotic expansion of Equation F.23 with respect to N:

$$\begin{aligned} I'(N) &= \frac{dI}{dN} \\ &= \left(\frac{\pi}{54}\right)^{\frac{1}{2}} N^{-\frac{3}{2}} \left(-\frac{3}{2}N^{-1} + \frac{15}{8}N^{-2} - \frac{91}{320}N^{-3} + o(N^{-3})\right). \end{aligned} \tag{F.24}$$

We finally obtain

$$\begin{aligned} \frac{d\ln I}{dN} &= \frac{I'(N)}{I(N)} \\ &= \frac{-\frac{3}{2}N^{-1} + \frac{15}{8}N^{-2} - \frac{91}{320}N^{-3} + o(N^{-3})}{1 - \frac{3}{4}N^{-1} + \frac{13}{160}N^{-2} + o(N^{-2})}. \\ &= -\frac{3}{2N} + \frac{3}{4N^2} + \frac{2}{5N^3} + o(N^{-3}) \end{aligned} \tag{F.25}$$

Combining this equation with Equations F.4, F.8 and F.10 we finally obtain Equation 3.107:

$$\left(\frac{\partial \ln p_{\text{ee}}^{\text{FJ}}}{\partial n}\right)_V = \frac{1}{\eta}\left(\ln\left(\frac{\sinh \mathcal{L}^{-1}(x)}{\mathcal{L}^{-1}(x)}\right) - \frac{3}{2N} - \frac{3}{4N^2} - \frac{2}{5N^3} + o\left(\frac{1}{N^3}\right)\right). \tag{F.26}$$

Notice that the expansion in Equation F.25 doesn't converge to the actual value of $d\ln I/dN$ for any value of N, as we have placed all the terms that are exponentially decaying in N (i.e., the $\tilde{B}_k(c_2 N)$ terms) in the little-o symbol. The series must then be intended as an asymptotic series in N^{-1} for $d\ln I/dN$:

$$\frac{d\ln I}{dN} + \frac{3}{2N} - \frac{3}{4N^2} - \frac{2}{5N^3} = o\left(\frac{1}{N^3}\right) \text{ as } N \to \infty. \tag{F.27}$$

Higher order expansions are thus not guaranteed to reduce the error in the approximation for $d \ln I/dN$ if N is small. The procedure can be generalized to any functional form for the end-to-end probability distribution, provided that the function multiplying N in Equation 3.74 is only a function of the fractional extension x and is analytic in x around $x = 0$.

G. Swelling

The total volume of a semi-crystalline sample is the sum of the volume of the crystalline lamellae, the free and inter-lamellar amorphous domains:

$$V = V_{\mathrm{c}} + V^{\mathrm{F}} + V^{\mathrm{IL}}. \tag{G.1}$$

The volume of the inter-lamellar amorphous domains and of the free amorphous domains can be obtained using the properties of the partial specific volume (*cf.* Section 3.3.3):

$$\begin{aligned} V^{\mathrm{IL}} &= \bar{v}_{\mathrm{p}}^{\mathrm{IL}} m_{\mathrm{p}}^{\mathrm{IL}} + \sum_{i=1}^{N_{\mathrm{c}}} \bar{v}_{\mathrm{s},i}^{\mathrm{IL}} m_{\mathrm{s},i}^{\mathrm{IL}} \\ V^{\mathrm{F}} &= \bar{v}_{\mathrm{p}}^{\mathrm{F}} m_{\mathrm{p}}^{\mathrm{F}} + \sum_{i=1}^{N_{\mathrm{c}}} \bar{v}_{\mathrm{s},i}^{\mathrm{F}} m_{\mathrm{s},i}^{\mathrm{F}} \end{aligned} . \tag{G.2}$$

At each temperature T and total pressure P, the partial specific volumes in the inter-lamellar amorphous domains are calculated using the equation of state at T and $P + P_{\mathrm{c}}$ for a polymer-solute mixture at composition $\boldsymbol{S}_{\mathrm{a}}^{\mathrm{IL}}(T, P)$. On the other hand, the partial specific volumes in the free amorphous domains are calculated at T, P and $\boldsymbol{S}_{\mathrm{a}}^{\mathrm{F}} = \boldsymbol{S}_{\mathrm{a}}^{\mathrm{EoS}}(T, P)$ (Equation 3.22). Since the crystallites are assumed to be impermeable to the solute, the volume of the crystalline polymer can be expressed as $V_{\mathrm{c}} = m_{\mathrm{p}}^{\mathrm{c}}/\rho_{\mathrm{c}}$. By factoring out $m_{\mathrm{p}}^{\mathrm{tot}}$ (the total polymer mass) in Equation G.1 and using Equation G.2,

the following expression is obtained:

$$\begin{aligned} V/m_{\mathrm{p}}^{\mathrm{tot}} &= \frac{m_{\mathrm{p}}^{\mathrm{c}}}{\rho_{\mathrm{c}} m_{\mathrm{p}}^{\mathrm{tot}}} + \frac{m_{\mathrm{p}}^{\mathrm{F}}}{\rho_{\mathrm{p,eff}}^{\mathrm{F}} m_{\mathrm{p}}^{\mathrm{tot}}} + \frac{m_{\mathrm{p}}^{\mathrm{IL}}}{\rho_{\mathrm{p,eff}}^{\mathrm{IL}} m_{\mathrm{p}}^{\mathrm{tot}}} \\ &= \frac{\omega_{\mathrm{c}}}{\rho_{\mathrm{c}}} + \frac{\psi}{\rho_{\mathrm{p,eff}}^{\mathrm{F}}} + \frac{1-\psi-\omega_{\mathrm{c}}}{\rho_{\mathrm{p,eff}}^{\mathrm{IL}}} \end{aligned} . \tag{G.3}$$

Here, the effective polymer density in the free amorphous domains $\rho_{\mathrm{p,eff}}^{\mathrm{F}}$ is given by

$$\rho_{\mathrm{p,eff}}^{\mathrm{F}} = \left(\bar{v}_{\mathrm{p}}^{\mathrm{F}} + \sum_{i=1}^{N_{\mathrm{c}}} \bar{v}_{\mathrm{s},i}^{\mathrm{F}} S_{\mathrm{a},i}^{\mathrm{F}} \right)^{-1} , \tag{G.4}$$

mirroring the definition of $\rho_{\mathrm{p,eff}}^{\mathrm{IL}}$ in Equation 3.97. Since the total polymer mass $m_{\mathrm{p}}^{\mathrm{tot}}$ does not change, by taking V_0 and ω_{c}^0 as the volume and the crystallinity, respectively, of the pure semi-crystalline polymer ($\boldsymbol{n}_{\mathrm{s}} = 0$ in both amorphous domains), we obtain Equation 4.2.

H. Solubility of Liquids in Semi-crystalline PE

In the current work only sorption isotherms of gases and supercritical fluids have been shown. As seen throughout this thesis, the solubility of most hydrocarbons in PE, PP and of water in PEG diverges near condensation of the external fluid. This phenomenon is due to the full miscibility of the polymer and the external fluid at pressures higher than the saturation (dew) point. In particular, these divergences occur due to the presence of free amorphous domains in the sample, as pointed out in Section 4.2.2. A divergent solubility implies that the osmotic free energy of the molten polymer + solute mixture at equilibrium must become smaller than that of the crystals (*cf.* Section 4.4.3), inevitably leading to deliquescence.

Nevertheless, deliquescence does not necessarily occur in the presence of fluids that are near-critical or not fully miscible with the polymer. For example, in Figure H.1 we show the predicted solubility of ethylene and water at 20, 30, 40 and 50 °C in the EH1 sample analysed by Moebus and Greenalgh.[255] The SAFT-γ Mie models for all the components are reported in Tables 2.1, 2.2 and 2.3, whereas the sample-specific parameters of the EH1 sample can be found in Table 4.3.3.

Since the critical temperature of ethylene predicted with SAFT-γ Mie is $T_{\mathrm{c}}^{\mathrm{eth}} = 23.7$ °C, we observe a transition from a subcritical to supercritical regime in the tempera-

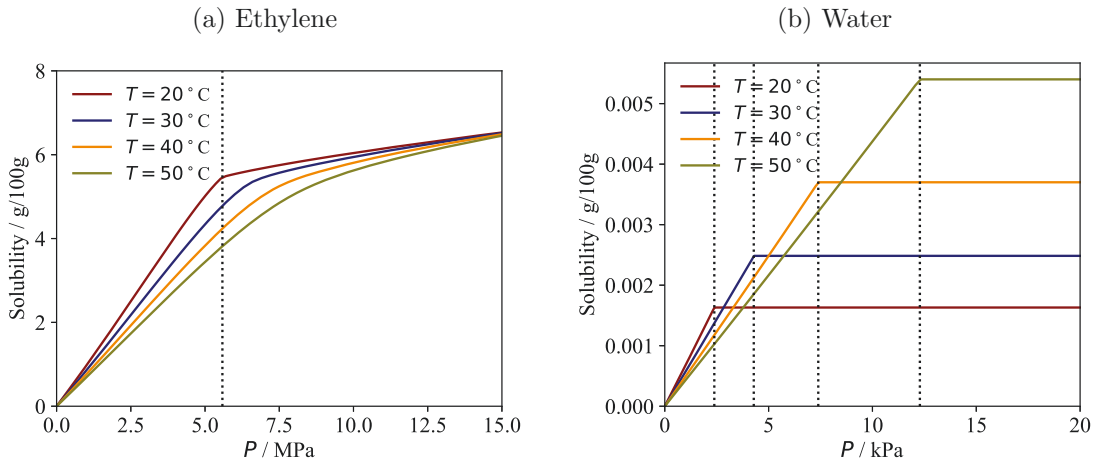

Figure H.1.: Predicted solubility of water and ethylene at 20, 30, 40 and 50 °C in the EH1 semi-crystalline PE sample analysed by Moebus and Greenalgh.[255] Calculations are performed with the model developed in Section 3.3 using the PE, water and ethylene SAFT-γ Mie models reported in Tables 2.1, 2.2 and 2.3 together with the sample-specific parameters reported in Table 4.4. Vertical dotted lines, if present, represent the vapour pressure of the solutes at the corresponding temperature. Note that the critical temperature of ethylene predicted with SAFT-γ Mie is $T_c^{eth} = 23.7$ °C.

ture range considered. While solubility at fixed pressure is higher in the low-pressure regime at low temperatures, the contrary is true at pressures higher than approximatly 15 MPa due to the lower compressibility of liquid ethylene compared to supercritical ethylene. Conversely, the critical temperature of water predicted with SAFT-γ Mie is $T_c^{water} = 400.8$ °C, meaning that the fluid remains subcritical at all temperatures considered. Due to the immiscibility of water and PE, solubility is extremely low. After saturation, solubility does not increase with pressure significantly due to the high density and low compressibility of liquid water at the corresponding temperatures.

List of Symbols

a	Subscript indicating the amorphous domains
a	Reduced Helmholtz free energy (Section 2.2)
$a^{\mathrm{c}}_{\mathrm{s},i}$	Excess activity of a solute in a swollen polymer network with respect to the unconstrained polymer + solutes mixture
A	Helmholtz free energy
$A^{(n)}$	Helmholtz free energy of a system in which polymer chains have n monomers
$\tilde{A}$	Helmholtz free energy per polymer chain
$A^{'}$	Helmholtz free energy of a confined fluid
A_{Σ}	Area of one of the two major surfaces of a lamella (i.e., the fold surfaces)
ΔA^{c}	Helmholtz free energy difference between a constrained and unconstrained polymer mixture (Equation 3.37)
b	Khun length of a polymer
BR	Subscript indicating bridges (Appendix E)
$B_{n,l}$	Incomplete Bell polynomial of degree n, l
c	Subscript/superscript indicating the crystalline domains or the constraints acting on the amorphous domains
C_{kl}	Numerical factor appearing in Mie potentials
C_{∞}	Flory characteristic ratio
d_{kl}	Barker and Henderson unlike hard-sphere diameter between group k and l
EL	Subscript indicating entangled loops
ES	Subscript indicating polymer segments between entanglements
EoS	Superscript indicating a quantity calculated with an equation of state for bulk fluids
f	Superscript indicating the external fluid phase
F	Superscript indicating free amorphous domains
f_{ee}	Thermodynamic force acting on the ends of a polymer chain

f_{N}	Functionality of a polymer network (i.e., number of chains meeting at junctions
f_{obj}	Objective function
f_{T}	Mass fraction of tie-molecules (bridges + entangled loops)
$g_{kl}(r)$	Radial distribution function for the pair of groups k and l
Δg_{crys}	Specific Gibbs free energy of crystallisation of an extended-chain crystal
G, G^*	Gibbs free energy. G is the minimum of G^* at varying V (Section 2.3.3)
h	Planck constant
Δh^0_{m}	Specific enthalpy of melting of an extended-chain crystal
H	Enthalpy
$\boldsymbol{H}_A$	Hessian matrix of the Helmholtz free energy
HS	Superscript indicating the hard-sphere reference system (Section 2.2)
i	Index referring do distinct components of a system
$I_{kl,ab}$	Association integral appearing in SAFT-γ Mie
IL	Superscript indicating inter-lamellar domains
j	Index
k	Index. in Chapter 2 it refers to individual groups
k_{B}	Boltzmann constant
$k_{\mathrm{H},i}$	Henry constant of solute i in the polymer sample (Equation 4.3)
K	Proportionality constant between $\omega_{\mathrm{c}}^{\mathrm{LS}}$ and n_{T} (Equation 3.79)
$K_{kl,ab}$	Bonding volume for the association interaction between sites a and b on groups k and l
$K^0_{\boldsymbol{X}}$	Cumulant-generating function for the random variable $\boldsymbol{X}$ in the purely repulsive system (Section 2.2)
l	Bond length of a polymer (or its geometric average along the backbone as with PEO/PEG, see Section 3.3.4)
l_{a}	Inter-lamellar distance
l^*_{a}	Inter-lamellar distance of a pure sample measured at temperature T^* and pressure P^*
l_{c}	Lamellar thickness
$l^*_{\mathrm{c}}(T)$	Lamellar thickness of the smallest stable lamella at temperature T
LP	Long period ($l_{\mathrm{a}} + l_{\mathrm{c}}$)
LS	Superscript indicating the inter-lamellar domains
$\mathcal{L}, \mathcal{L}^{-1}$	Langevin function and its inverse
m	Mass. In Appendix E, it indicates the average number of monomers between entanglements
$\tilde{m}_i$	Effective number of segments of component i (Section 2.2)
$M_{\mathrm{s},i}$	Molar mass of solute i
M_0	Molar mass of the polymer's repeating unit (i.e., per monomer)

$M^0_{\boldsymbol{X}}$	Moment-generating function for the random variable $\boldsymbol{X}$ in the purely repulsive system (Section 2.2)
Mie	Superscript indicating the Mie potential or a Mie momnomer fluid
n	Number of monomers per polymer chain. In Section 2.3, number of molecules of a pure component system
(n)	Superscript indicating that the polymer chains in the system described have n monomers
n_{T}, n_0	Number of monomers per equivalent bridge and of the reference polymer + solutes mixture used for the calculations ($n_0 = 1000$)
$n_{\mathrm{s,i}}$	Number of solute molecules of type i
$\tilde{n}_{\mathrm{s,i}}$	Number of solute molecules of type i per polymer chain
$\boldsymbol{n}_{\mathrm{s}}$	Vector of the $n_{\mathrm{s,i}}$
$\tilde{\boldsymbol{n}}_{\mathrm{s}}$	Vector of the $\tilde{n}_{\mathrm{s,i}}$
$n_{k,a}$	Number of sites of type a on group k (Section 2.2)
N	In Section 2.2, total number of molecules. Otherwise, equivalent number of Khun monomers of a polymer chain
N_{C}	Number of distinct solutes. In Section 2.2, number of components (solutes + polymers)
N_{G}	Number of SAFT groups
$N_{\mathrm{ST,k}}$	Number of types of association sites on group k
$\mathcal{N}_{\mathrm{b}}$	Number of main-chain bonds per monomer
$\mathcal{N}_{\mathrm{p}}$	Number of phases in a system
p_{ee}, p'_{ee}	Distribution of the end-to-end vectors of polymer chain segments in a bulk fluid (p_{ee}) or in a fluid confined between lamellae (p'_{ee})
p_{T}, p_{TF}, p_{NT}	Fraction of stems in on the crystal/amorphous interface connected to tie-molecules (p_{T}), tight folds (p_{TF}) and un-entangled loops and tails (p_{NT}) – Figure 3.2
P	Pressure
P^*	Pressure at which crystallinity and inter-lamellar distance of a polymer are measured
P_{c}	Constraint pressure
P_{vap}	Vapour pressure of a component
P_{del}	Pressure at which deliquescence occurs
r	Euclidean distance between two points
$r^c_{kl,ab}$	Cut-off radius for the SAFT association potential between sites a, b on groups k, l
$r^d_{kl,ab}$	Cut-off radius for the SAFT association potential between sites a, b on groups k, l
R	Universal gas constant

S_i, $S_{\mathrm{a},i}$	Solubility of solute i in mass of solute per total polymer mass and amorphous mass only, respectively
S_k	Shape factor of the SAFT group k (Section 2.2)
T	Temperature
T_m	Melting point of a lamella or more generally of a polymer sample
T_m^0	Melting point of an extended-chain crystal
T^*	Temperature at which crystallinity and inter-lamellar distance of a pure polymer are measured
u_{kl}	Dispersion potential between two monomers
U_0, U_1	Repulsive and attractive parts, respectively, of the Mie force field (Equation 2.9)
V	Volume
$\tilde{V}$	Volume per polymer chain
V_0	Volume of a pure polymer sample
$\bar{V}_{\mathrm{s},i}$	Partial molar volume of solute i (Equation 3.33)
$\bar{V}_\mathrm{p}$	Partial molar volume of the polymer (Equation 3.33)
$\bar{v}_{\mathrm{s},i}$	Partial specific volume of solute i (Equation 3.95)
$\bar{v}_\mathrm{p}$	Partial specific volume of the polymer (Equation 3.95)
v_a	Specific volume of pure amorphous domains intended as a homogeneous mass (Equation 3.12)
v_c	Specific volume of pure crystalline polymer (Equation 3.12)
w_k	Molar mass of the SAFt group k
x_i	Mole fraction of component i
x_T, x_ES	Fractional extension of equivalent bridges and polymer segments between entanglements (Equation 3.75)
$X_{i,k,a}$	Fraction of groups k on component i not bonded at site a
y_i	Mole fraction of component i. Used for polymer-free systems
$\boldsymbol{y}$	Vector of the y_i
α, $\alpha^{'}$	Index used to refer to individual monomers in Section 2.2
β	Defined as $1/k_\mathrm{B}T$
γ	Chain-tilt angle between the [001] crystallographic axis and the crystal/amorphous interface
$\mathbf{\Gamma}_\mathrm{c}$	Set of constraints acting on a system of polymer chains
δ_T	Projection of the end-to-end vector of an equivalent bridge on the crystal/amorphous interface
Δ	When placed before another symbol, it indicates the difference of the relative quantity between two systems
$\Delta_{ij,kl,ab}$	Association strength (Section 2.2)
ϵ	Energy well-depth for the Mie potential between groups k and l (ϵ_{kl}) or for the square-well association potential ($\epsilon^{\mathrm{HB}}_{kl,ab}$) (Section 2.2)

ζ	Function representing Helmholtz combinatorial terms that only depend on the number of chains in Section 3.3
ζ_m	m^{th} density moment (Section 2.2)
η	Ratio between the number of bonds in a real chain and the equivalent number of Khun bonds (Equation 3.73)
θ_B	Bond angle along the polymer's backbone
θ_{T}	Angle between the end-to-end vector of an equivalent bridge (Section 3.3.3) and the normal to the crystal/amorphous interface. Extended to bridges (BR) and entangled segments (ES) in Appendix E
$\kappa_n^0, \kappa_n^{\text{HS}}$	n^{th} cumulant of the attractive potential V_1 in the repulsive and equivalent hard-sphere system (Section 2.2)
λ_{kl}^a	Attractive exponent of the Mie potential
λ_{kl}^r	Repulsive exponent of the Mie potential
Λ_i	Thermal de Broglie wavelength of component i
$\mu_{\text{s},i}$	Chemical potential of solute i
$\boldsymbol{\mu}_{\text{s}}$	Vector of the $\mu_{\text{s},i}$
$\mu_{\text{p},i}$	Chemical potential of polymer i
μ_{p}	Chemical potential of the polymer in a monodisperse mixture
$\mu_{\text{p,mono}}$	Monomer chemical potential. Defined in Equation 3.47 for the lamellae and in Appendix C for a bulk polymer + solute mixture
μ_m^0	m^{th} moment of the attractive potential in the purely repulsive system (Section 2.2)
ν_i	Number of polymer chains of type i
$\boldsymbol{\nu}$	Vector of the ν_i – i.e., molecular weight distribution of a polymer sample
$\nu_{k,i}$	Number of SAFT groups of type k on component i
ν_k^*	Number of identical segments a group is made of (Section 2.2)
$\nu_{k,\text{p}}^{\text{R}}$, $\nu_{k,\text{p}}^{\text{E}}$	Number of group of type k on the polymer's repeating unit and on the chain ends
ρ	Particle density (Section 2.2)
ρ_{a}	Density (in mass) of amorphous polymer
ρ_{c}	Density (in mass) of the crystal structure of a polymer
$\rho_{\text{p,eff}}$	Polymer density (polymer mass divided by volume)
ρ_{A}	Cross-section of a polymer chain in its crystal structure. I.e., number of chains per unit area on the (001) crystal plane
$\rho_{\text{A,T}}$	Surface density of tie-molecules (in our model, equivalent bridges) on the crystal/amorphous interface (Equation 3.10)
σ_{e}	Gibbs free energy of the fold surface per unit area
σ_{kl}	Diameter of the Mie potential between groups k and l

$\tau_{\mathrm{D}}, \tau_{\mathrm{ICD}}, \tau_{\mathrm{R}}$	Respectively, characteristic time of solute diffusion in a semi-crystalline sample, of intra-crystalline chain dynamics and of irreversible recrystallisation
$\Delta\tau$	Thermal volume in which the ends of a bridge are confined due to bonding with the crystalline stems
$\Delta\tau'$	Hypothetical volume in which entangled segments meet to form an entanglements
ϕ	Mass fraction of free amorphous mass over the total amorphous mass
$\phi_{\mathrm{s},i}$	Volume fraction of solute i in the polymer mixture
ϕ_{p}	Volume fraction of the polymer in the polymer mixture
Φ, Φ^*	Thermodynamic potential of constrained amorphous domains in the $T, P, \boldsymbol{\mu}_{\mathrm{s}}, \mu_{\mathrm{p,mono}}$ ensemble. Φ is the minimum of Φ^* at varying $V, \boldsymbol{n}_{\mathrm{s}}, n$
$\tilde{\Phi}, \tilde{\Phi}^*$	Obtained dividing Φ, Φ^* by the number of polymer chains
χ	Interaction parameter in the FHS theory
ψ	Mass fraction of free amorphous polymer (MAF)
ω_{c}	Crystallinity (Equation 3.8)
ω_{a}	Amorphous mass fraction $(1 - \omega_{\mathrm{c}})$
ω_{c}^*	Crystallinity measured for the pure polymer at temperature T^* and pressure P^*
$\omega_{\mathrm{c}}^{\mathrm{LS}}$	Crystallinity of the lamellar stacks only
$\omega_{\mathrm{c}}^{\mathrm{LS},*}$	Crystallinity of the lamellar stacks only measured for the pure polymer at temperature T^* and pressure P^*
$\omega_{\mathrm{s},i}$	Mass fraction of solute i. The index is removed if there is only one solute
$\Omega_{\mathrm{s}}, \Omega_{\mathrm{s}}^*$	Osmotic free energy of a polymer + solute mixture in the $T, P, \boldsymbol{\mu}_{\mathrm{s}}$ ensemble. Ω is the minimum of Ω^* at varying $V, \boldsymbol{n}_{\mathrm{s}}$ (Section 2.3.3)

List of Acronyms

aPP	Atactic polypropylene
BH	Barker and Henderson
CG	Coarse-grained
DSC	Differential scanning calorimetry
EoS	Equation of state
FHS	Flory-Huggins-Staverman
fPP	Polypropylene fibre
FR	Flory-Rehner
GC	Group-contribution
GR	Gambler's Ruin
HB	Huang and Brown / hydrogen-bonding
HDPE	High-density polyethylene
HL	Hoffman and Lauritzen
iPP	Isotactic polypropylene
ICD	Intra-crystalline chain dynamics
LDPE	Low-density polyethylene
LLDPE	Linear low-density polyethylene
LLE	Liquid-liquid equilibrium
MAF	Mobile amorphous fraction
MDPE	Medium-density polyethylene
MH	Michaels and Hausslein
NMR	Nuclear magnetic resonance
PA	Polyamide
PBD	Polybutadiene
PE	Polyethylene
PEEK	Polyether ether ketone

PEO/PEG	Polyethylene glycol/oxide
PP	Polypropylene
PTFE	Polytetrafluoroethylene
PVC	Polyvinyl chloride
PVDF	Polyvinylidine fluoride
RAF	Rigid amorphous fraction
sPPcO	Syndiotactic polypropylene-co-octene
SAFT	Statistical associating fluid theory
SAXS, SANS	Small-angle X-ray (respectively, neutron) scattering
TD-NMR	Time-domain NMR
UA	United-atom
VLE	Vapour-liquid equilibrium
WAXS	Wide-angle X-ray scattering